Journal of Applied Mechanics

(Contributions of the ASME Applied Mechanics Division)

A Critical Examination of Procedures Used in Britain and the United States to Determine Creep Stresses for the Design of Power Plant for Long Life at High Temperatures . . . *R. W. Bailey* 389

Polynomial Stress-Strain Relations of a Strain-Hardening Metal . . . . . *S. R. Bodner and Bernard Budiansky* 385

The Existence and Stability of Ultraharmonics and Subharmonics in Forced Nonlinear Oscillations . . . . . *T. K. Caughey* 327

Rigid-Plastic Analysis of Symmetrically Loaded Cylindrical Shells . . . . . *P. G. Hodge, Jr.* 336

Boundary-Value Problems of the Thin-Walled Circular Cylinder . . . . . *N. J. Hoff* 343

The Anticlastic Curvature of a Strip With Lateral Thickness Variation . . . . . *Y. C. Fung and W. H. Wittrick* 351

Steady-State Vibrations of Beam on Elastic Foundation for Moving Load . . . *J. T. Kenney, Jr.* 359

Vibration of Triangular Cantilever Plates by the Ritz Method . . . . . *R. W. Anderson* 365

Prediction and Evaluation of Sensitivity to Transient Accelerations . . . . . *M. Kornhauser* 371

Torsional Vibrations of Beams of Thin-Walled Open Section . . . . . *J. M. Gere* 381

Wave Groups in the Flexural Motion of Beams Predicted by the Timoshenko Theory . . . . . *R. A. Anderson* 388

Tensile Corrosion of Mild Steel in Air and in Nitrogen . . . . *I-Ming Feng and H. H. Uhlig* 395

Mechanism of Pressure Corrosion . . . . . *H. H. Uhlig* 401

Brief Notes

On the Signs in the Mathematical Expression of the Second Law of Thermodynamics . . . . . *S. J. Kline* 406

Discussion on previously published papers by *J. E. Brady, R. P. N. Jones, and H. Kolsky* . . . 408

Book Reviews 416

DECEMBER, 1954

VOL. 21, NO. 4

Transactions of The American Society of Mechanical Engineers

Journal of Applied Mechanics

Papers Contributed to the Transactions by the ASME Applied Mechanics Division

EXECUTIVE COMMITTEE OF THE APPLIED MECHANICS DIVISION

N. M. Newmark, *Chairman* — N. J. Hoff, *Secretary*

Jesse M. Lemmon, *Technical Editor*

Published Quarterly by

The American Society of Mechanical Engineers

Publication Office, 20th and Northampton Streets, Easton, Pa.
Editorial Department at the Headquarters of the Society, 29 West Thirty-Ninth Street, New York 18, N. Y.

OFFICERS OF THE SOCIETY

Lewis E. Seaton, *President*

Joseph L. Kopf, *Treasurer* — C. B. Davis, *Secretary*
E. J. Kates, *Assistant Treasurer*

PUBLICATIONS COMMITTEE

Paul T. Norton, Jr., *Chairman*

Gregory A. Stanton, *Editor*
K. W. Cunningham, *Mgr. Editor*

By-Law: The Society shall not be responsible for statements or opinions advanced in papers or . . . printed in its publications (B13, Par. 4).

Published quarterly by The American Society of Mechanical Engineers. Publication office at 20th and Northampton Streets, Easton, Pa. The editorial department is located at the headquarters of the Society, 29 West Thirty-Ninth Street, New York 18, N. Y. Cable address, "Dynamic," New York. Price $1.25 a copy, $5.00 a year; to members $2.50 a year; single copy price to members, $1.00. Add 25c for postage to all countries outside the United States, Canada, and Pan-American Union. Changes of address must be received at Society headquarters seven weeks before they are to be effective on the mailing list. Please send old as well as new address. . . . By-Law: The Society shall not be responsible for statements or opinions advanced in papers or . . . printed in its publications (B13, Par. 4). . . . Entered as second-class matter March 14, 1933, at the Post Office at Easton, Pa., under the act of August 24, 1912. . . .
Copyright, 1954, by The American Society of Mechanical Engineers. Reprints from this publication may be made on condition that full credit be given the JOURNAL OF APPLIED MECHANICS and the author, and that date of publication be stated.

A Critical Examination of Procedures Used in Britain and the United States to Determine Creep Stresses for the Design of Power Plant for Long Life at High Temperatures

By R. W. BAILEY,[1] MANCHESTER, ENGLAND

The operating life of land power plant being far longer than allowable testing times for the constructional metals, the selection of a material, or the determination of its appropriate working stress, is dependent in an important degree upon the procedure followed in utilizing the creep-test results obtained. Different procedures practiced both in Britain and in the United States can result in different views regarding the potentialities of a material, and also about the working stress allowable. The paper examines the more commonly used procedures and focuses attention upon the factors present which would operate to introduce uncertainty and error as between the probable behavior in the long time of actual service, and as yielded by a test procedure. The principal disturbing factor in altering the resistance to creep of the material is thermal action. In some procedures, especially where the creep tests are made at working temperatures, the influence of this factor may be small or negligible in the procedure, compared with its magnitude in service. The need is emphasized for thermal action to be taken adequately into account by the test procedure. Next in importance as a possible source of error is the method of extrapolation beyond the test times to the time of the operating life. The factor of thermal action and of its representation in the several procedures examined is considered. The circumstances of extrapolation are similarly investigated, especially in regard to whether the result would overestimate or underestimate the safe working stress. Satisfying comparisons of working stresses using different procedures cannot at present be made. The position is therefore disappointing and one which it is very desirable should be rectified.

[1] Consulting Research Engineer to Metropolitan-Vickers Electrical Company, Ltd.; D.Sc. (Eng.), Wh. Sc. (Vice-President, The Institution of Mechanical Engineers), F.R.S.

Presented at a General Meeting of The Institution of Mechanical Engineers, London, England, December 4, 1953; also presented at a joint session of the Petroleum and Power Divisions, Research Committee on High Temperature Steam Generation, and the Joint ASTM-ASME Committee on the Effect of Temperature on Properties of Metals, at the Annual Meeting, New York, N. Y., November 29–December 4, 1953, of The American Society of Mechanical Engineers.

Discussion of this paper should be addressed to the Secretary, ASME, 29 West 39th Street, New York, N. Y., and will be accepted until January 10, 1955, for publication at a later date. Discussion received after the closing date will be returned.

Note: Statements and opinions advanced in papers are to be understood as individual expressions of their authors and not those of the Society. The manuscript of this paper was received at the Institution, July 29, 1953. Paper No. 53—A-196.

Introduction

THE paper by Messrs. Bardgett and Clark[2] has shown satisfactory correspondence between creep behavior of the same steels when tested in Britain and the United States. In addition, it has shown that steels of the same nominal composition, made in the two countries, exhibit only small but admissible differences of behavior and these the authors attribute to manufacturing differences which could be eliminated. The information presented by the paper is both timely and valuable, in view of British interest in American practice, and because it makes clear the urgent need for both countries to review critically different methods used by laboratories in providing the creep-test data and the guidance which engineers and designers accept trustingly from these laboratories. Engineers and designers will, therefore, have a vital interest in the magnitudes of the design stresses which result from different test procedures, and in their degrees of reliability. The situation in the important case of long-life requirements, where the operating period far exceeds possible testing times, is, however, very unsatisfactory and extremely disappointing, considering the enormous volume and cost of the associated testing done during the last fifteen years and more.

The position concerning high-temperature power plant in Britain, vis-à-vis the United States, is that during the 1939–1945 war, progress in the development of steam power plant was suspended in the former country because of war needs, and attention was diverted to gas-turbine development, especially for aircraft, in which Britain achieved a leading position. This lead Britain has maintained as a result of the continuing research upon materials and of progress in design and development in this field. In the United States progress in the development of steam power plant was not similarly arrested; the trend toward higher operating temperatures continued, and was manifested by development in design, and the acquisition of operating experience under the more advanced conditions adopted.

Naturally, both of these, as also the resulting trends in design, are of considerable interest to engineers and designers in Britain. A critical review of the methods of testing for design stresses adopted in the United States, and of the procedures followed in deriving them, is consequently needed. The matter should also be of equal interest to engineers and designers in the United States, either with a view to justifying what has already been done there, or by leading to improved practice in the future.

Stress values should, of course, be directly comparable for similar materials, and without ambiguity. So far as similar tests

[2] "Comparative High-Temperature Properties of British and American Steels," by W. E. Bardgett and C. L. Clark, Paper No. 53—A-195, presented at the Annual Meeting, New York, N. Y., November 29–December 4, 1953, of The American Society of Mechanical Engineers, pp. 2–6.

on similar materials are concerned, the paper by Messrs. Bardgett and Clark shows the position to be satisfactory in the two countries. Long time of service, however, is the source of possible differences in derived working stresses because, for practical purposes, tests to determine design stresses can never approach in duration the operating period for which the working stresses are needed. An extrapolation procedure using data given by tests having a duration rarely one tenth, and frequently less than one hundredth, of the operating period has, therefore, to be adopted. Apart from differences in the permissible total deformation, which can readily be allowed for when specified, it is the period over which extrapolation has to be made that can be the source of so much uncertainty and error, leading to large differences in derived working stresses.

The author's purpose is to examine different procedures critically in the hope that their limitations may be seen by engineers, who would then be able to require that design stresses were determined by a procedure in which they could have full confidence. At present this is not so, and much has to be taken on trust, the means which would enable its validity to be questioned being lacking.

There is a commercial aspect of differences in stress values arising from the adoption of different procedures in using creep-test data which may be mentioned. If by one procedure higher design stresses are obtained than by another and better-founded procedure, advantage in tendering for overseas contracts is conferred upon the country sanctioning the first, over another country whose practice, other things being equal, should be the more reliable. Ability to make dependable comparisons would therefore be an aid to judgment when weighing the merits of competing tenders.

Uncertainties concerning stress values arise, as already indicated, when a considerable extrapolation is inevitable. With equal test and operating periods, however, the same stress values would be reached by different means. When this is not so, as is generally the case with power plant of long operating life, the position as a rule is complex, and if different stress values result the cause is likely to be incompatible and questionable procedures. All procedures should be called in question until critical examination has resulted in evidence of reliability.

Notation

A = a coefficient, constant
$\mathbf{A}, a$ = constants
B = a coefficient, constant
b = a constant
c = a constant
E = activation energy
f = stress
$\bar{f}$ = stress corresponding to $\bar{l}$
i = slope of curve
k = Boltzmann constant
m = a constant
n = index, assumed constant in analysis
p = index, assumed constant in analysis
q = index relating to thermal action
T = absolute temperature of heating
T_1, T_2 = absolute temperatures of heating for a specific change
t = time
t' = creep test time to produce a specific creep strain after heating for time t'' at temperature $\bar{\theta}$
$\bar{l}$ = working-life period, time to rupture
$\mathbf{t}$ = time to fracture under stress
X = a steel, unstressed during heating prior to test
x = tensile creep strain
$\bar{x}$ = elongation of fracture
$\dot{x}$ = creep rate
Y = a steel, different from X, unstressed during heating prior to test
α = index representing $E \div k$
θ = test temperature
$\bar{\theta}$ = temperature of heating, working temperature
ρ = a constant
τ = time for a particular change by thermal action
τ_1, τ_2 = times corresponding to T_1 and T_2

Thermal-Action Effect

The influence of thermal action in service in changing the behavior of a material under stress is of fundamental significance and, unless the procedure for arriving at design stress values and the assessment of a material correctly allows for this, the risk of error and unreliability is present from the outset. Nevertheless, much testing in both Britain and the United States, directed ostensibly to producing stress values for design, or to offering guidance in the choice of a material, takes negligible account, or no account at all, of this most important factor.

In both countries, accelerated creep tests in simple tension are recognized as the only practical means of obtaining test data. And such data, plotted with log (time) as a co-ordinate, and the plotted relations extrapolated to the operating life, yield a result, either stress for a particular temperature, or temperature for a particular stress—according to whether temperature, or stress, respectively, is constant in the tests of the series. If then several series of tests are made, each at a specific temperature (regarded as a working temperature), a stress-temperature relation suitable for design is obtained. Correspondingly, if several series of tests are made each for a specific stress, a stress-temperature relation for the same purpose would then be obtained. With reliable extrapolation the two stress-temperature relations would coincide if the material were unaltered by the stress or temperature imposed, or if the testing period equaled the life period, but not otherwise. Hence difference in stress values can be expected from different test procedures where their purpose is to provide design stresses for long operating life. There must, of course, be a unique relation between stress and temperature for a given material, specific creep strain, and life period. This paper directs attention to the factors which affect the approach by different procedures to the unique relation.

The powerful influence of thermal action in affecting creep behavior and, therefore, in contributing to difference of stress values resulting from a difference in test procedure is illustrated in Fig. 1 which shows the influence of heating two unstressed steels X and Y for different periods at 650 deg C (1202 deg F) prior to making a creep test under a stress and temperature common to the two steels. Ordinates of the curves give the times for 0.001 creep strain for the abscissas times of the prior heating at 650 deg C (1202 deg F).

Fig. 1 shows that for no prior heating the creep test places the two steels in an order of creep resistance which is altered radically by the thermal action imposed by the prior heating. Fig. 1 indicates that if the assumption, in support of which there is much evidence, were made that the thermal action of heating in service would have an equivalent in a period of prior heating at 650 deg C (1202 deg F) or at other temperatures below the lower critical temperature, steels would differ considerably in their "staying-power" and, in addition, that tests made without allowing for the thermal-action factor—both in the testing and as imposed by service—would be likely to lead to uncertainty and error in the design stresses resulting from the test procedure adopted, particularly with higher operating temperatures and longer operating periods where thermal action would be greater.

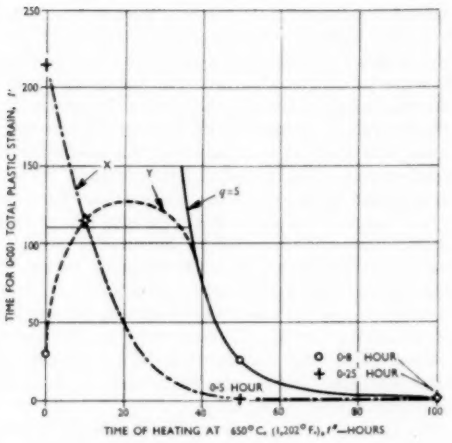

+ Test points for steel X
o Test points for steel Y

FIG. 1 EFFECT OF PRELIMINARY HEATING AT 650 DEG C (1202 DEG F) UPON CREEP OF TWO STEELS X AND Y
(Tests at 550 deg C [1022 deg F] and 16,000 lb per sq in.)

For the present, Fig. 1 sufficiently demonstrates the importance of the thermal-action factor.

Apart from change attributable to thermal action, the other factor which accounts for difference in derived stress values is, as has been noticed, error accompanying extrapolation of test data from the test periods to the operating period. At present the position is most unsatisfactory and little serious attention appears to have been given to the question of reliable or safe extrapolation.

Scatter of ascertained values hampers satisfactory extrapolation, and the choice of co-ordinate scales is likely to affect the result because of the natural tendency to extrapolate linearly. A case can be made for adopting co-ordinate scales which would allow a linear relation between the plotted quantities, or which would cause linear extrapolation to give the result on the safe side. Errors may be minimized by generalization and analysis to provide a rational pattern for the relation plotted, and its extrapolation. Indeed, without this aid when comparing test procedures, the volume of testing needed to establish a relation would be quite impracticable, and the data no less confusing. In addition, the analytical approach enables a feature revealed by a test procedure to be identified and associated with its cause. Attention is therefore given in this paper to this aspect, taking first the case where temperature is constant for a series of tests at different stresses.

ANALYTICAL REPRESENTATION OF THE CREEP CURVE INCLUDING A FACTOR FOR THERMAL ACTION

The form of creep curve connecting the tensile creep strain x with time t, is now widely known, and may be conveniently generalized for a particular stress f and constant temperature, by the relation

$$\frac{dx}{dt} = Af^n x^{-p} \quad \ldots\ldots [1]$$

in which, with an unchanging material, A, n, and p are treated as constants, and have values depending upon the stage of creep represented, p being, respectively, positive, zero, and negative, for the corresponding primary, secondary, and tertiary stages. Often the secondary stage is little more than a brief transition from primary to tertiary, or the point of inflection marking this. Values of A, n, and p can be obtained readily from the creep curves given by tests, and it is found that both n and p vary with the stress in a way that must be determined for a given material; but commonly n has values which increase with the stress, whereas p has a tendency to diminish with stress, and may be more influenced by temperature, being, for primary-stage creep, smaller at higher temperatures.

The relation between x, f, and t from Equation [1], when x and t are zero together, is

$$x = [A(p+1)]^{\frac{1}{p+1}} f^{\frac{n}{p+1}} t^{\frac{1}{p+1}} \quad \ldots\ldots [2]$$

Judged by the time t', in the creep test of Fig. 1 at 550 deg C (1022 deg F), to produce a creep strain of 0.001, thermal action changes the creep behavior of different materials in different ways.

If thermal action does not significantly alter n and p, as it seems reasonable to believe, the coefficient A will embrace the thermal-action effect as represented by the curves of Fig. 1. Generally, for a specific creep strain x, the time t would be inversely proportional to A, and vice versa. Applied to the creep tests made at 16,000 lb per sq in. and 550 deg C (1022 deg F), the inverse of t' would be proportional to, and may be taken to represent, the coefficient A. Fig. 2 gives values of $1/t'$ for the experimental times t'' of heating at the temperature $\bar{\theta}$ of 650 deg C (1202 deg F) for the chromium-molybdenum steel Y. The tests represented by Fig. 1 give a measure of the thermal-action factor as it affects the two steels, or its "pattern." But many more test points, to define the curve for the range of heating temperatures, are needed. Tests after heating at more than one temperature $\bar{\theta}$ are necessary for the factor to be given representative expression. Appendix 2 considers in more detail the factor of thermal action, particularly in connection with a procedure which makes a definite provision for thermal action.

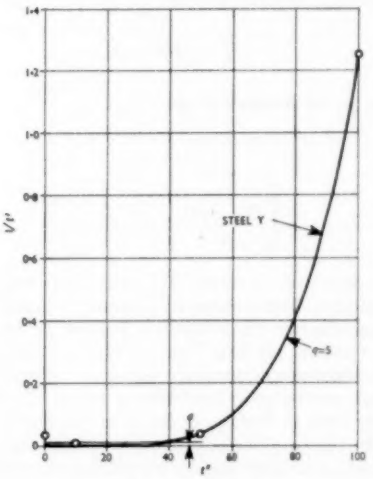

o Test points of Fig. 1

FIG. 2 VALUES OF INCREASE OF $1/t'$ FOR EXPERIMENTAL TIMES t''

Referring to procedures first to be considered in which stress is varied to alter creep strain or creep rate, Equation [1] can be extended by the addition of the index q as shown by Equation [3] so as to take thermal action into account.

Briefly, this conclusion is reached by considering that $1/t'$ as a function of the time of heating t'' at the temperature $\bar{\theta}$, or absolute temperature $T(650 + 273 = 923$ deg K for the curves of Fig. 1) may be treated, by simple approximation, as consisting of two

separate parts, a first part represented by an average ordinate $1/t'$, treated as constant, and a second part in which $1/t'$ increases with increase in t''. For both parts $1/t' \propto t''^q$, the index q being zero for the first part, and having a positive value, integral or fractional, for the second part. Writing for the first part $1/t' = a$, and for the second part $1/t' = bt''^q$, the time t'' marking the end of the first part and the beginning of the second part, is given by $bt''^q = a$, or $t'' = (a/b)^{1/q}$.

The times t'' relate to the heating temperature T. The thermal action in service, or in the creep tests, would occur at a temperature $\theta + 273$ and in a time t, proportional to the equivalent time t'', the proportionality for a metastable change (Appendix 2) being expressed by the relation

$$t/t'' = e^{a\left(\frac{1}{\theta+273} - \frac{1}{T}\right)} = \rho, \text{ say, or } t'' = t/\rho$$

For the second part $1/t' = b(t/\rho)^q$ and is proportional to A. A of the first part may, therefore, be replaced by Bt^q to represent the second part when the temperature is constant, which is often the case when making creep tests. Introducing this value of A in Equation [1], Equation [3] results. This reduces to Equation [1] for the first part of Fig. 1, if a constant average value of $1/t'$ can be accepted as an approximation applicable to this part.

The following relations may now be given

$$\frac{dx}{dt} = Bt^q f^n x^{-p} \quad \ldots\ldots [3]$$

Equation [3] by integration gives

$$x^{p+1} = B(p+1)f^n t^{q+1}/(q+1)$$

or

$$x = \left[\frac{B(p+1)}{q+1}\right]^{\frac{1}{p+1}} f^{\frac{n}{p+1}} t^{\frac{q+1}{p+1}} \quad \ldots\ldots [4]$$

As was done with Equation [2], x and t have both been taken as zero initially. This is not strictly correct, but must be regarded as an approximation which becomes increasingly justified as the time t is taken to the large values which extrapolation entails, especially when temperatures are high.

Although testing procedure making use of the creep rate is not widely used in Britain, it has been popular in the United States. It will be useful, therefore, to obtain the relation connecting creep rate and time, by introducing the value of x given by Equation [4] into Equation [3], thus giving

$$\frac{dx}{dt} = Bt^q f^n \left[\frac{B(p+1)}{q+1}\right]^{-\frac{p}{p+1}} f^{-\frac{np}{p+1}} t^{-p\frac{q+1}{p+1}}$$

or

$$\frac{dx}{dt} = B^{\frac{1}{p+1}} \left(\frac{p+1}{q+1}\right)^{-\frac{p}{p+1}} f^{\frac{n}{p+1}} t^{\frac{q-p}{p+1}} \quad \ldots\ldots [5]$$

which for $q = 0$, i.e., the case of Equations [1] and [2] where there is no thermal-action effect, gives

$$\frac{dx}{dt} = A^{\frac{1}{p+1}} (p+1)^{-\frac{p}{p+1}} f^{\frac{n}{p+1}} t^{-\frac{p}{p+1}} \quad \ldots\ldots [6]$$

Extrapolation of Test Data (Test Varied, Temperature Constant)

Widespread failure to recognize the significance and importance of thermal-action effect, and the fact that it is simpler and easier to conduct a series of tests by keeping a common temperature, merely altering the load and stress, than by altering temperature, probably account for the fact that most testing to determine design stresses has been carried out in Britain and the United States at a series of stresses at a common temperature, which is usually regarded as a possible working temperature. From the consideration already given to thermal-action effect, it will be appreciated that the results of this practice may be expected to be in error, whatever extrapolation procedure is adopted to obtain the design stress for long life and high temperature. Nevertheless, attention should be given to extrapolation procedure so that, so far as this factor is concerned, the circumstances of reliable extrapolation may be insured, and the direction of possible error—whether by overestimating or underestimating—of the allowable working stress may be made known and understood.

Procedure 1. The commonest procedure appears to have been to plot the relation between the test stress f and the time t to produce a specific creep strain, either with $\log f$, or f, as ordinate, and with $\log t$ as abscissa, and to extrapolate to the working life period $\bar{t}$ to obtain the corresponding stress $\bar{f}$.

It will be seen from Equation [4] that, for the same creep strain x, $f^n t^{q+1}$ is constant and that, therefore, $nf^{n-1}t^{q+1}df + (q+1) \times f^n t^q dt = 0$ giving

$$ntdf + (q+1)fdt = 0 \text{ and } \frac{df}{dt} = -\frac{(q+1)}{n}\frac{f}{t}$$

Case (a): log f and log t plotted. The slope i of the curve is given by

$$i = \frac{d(\log f)}{d(\log t)} = \frac{t}{f}\frac{df}{dt} = -\frac{q+1}{n} \quad \ldots\ldots [7]$$

Case (b): f and log t plotted. In this instance, the slope i of the curve is given by

$$i = \frac{df}{d(\log t)} = t\frac{df}{dt} = -\frac{q+1}{n} f \quad \ldots\ldots [8]$$

Equations [7] and [8] do not involve the index p and can, therefore, be regarded as not being dependent to any important degree upon the stage of creep.

The slope is, of course, negative at all stresses. In both cases the index q, operating when the thermal-action effect is present producing weakening, acts to increase the negative slope, and hence if the tests have not taken place at a temperature at which significant thermal weakening is occurring—as will almost certainly be so when tests are made at possible working temperatures—extrapolation of the plotted data will overestimate the working stress safely allowable.

But another question is involved. It is most probable that linear extrapolation would be employed, the slope of the curve at the longest times being continued. The question is whether this practice would overestimate or underestimate the working stress. To answer this question the stress dependence of n needs to be examined. In the author's experience, when this has been done it has been found that n decreases as the test stress is reduced, so that, if the tests have been made at stresses higher than the allowable stress as must be the case where extrapolation has to be employed, a diminishing n over the extrapolated region would be expected, unless experimental evidence, specifically directed to determining n, indicated otherwise.

In Case (a), a diminishing n would signify an increasing negative slope of the $\log f$, $\log t$ curve and, therefore, linear extrapolation would overestimate the working stress safely allowable.

In Case (b), the position is not immediately apparent because a diminishing n in the denominator of the expression for i in Equation [8] would be accompanied by the diminishing f in the numerator; therefore the variation of f/n should be examined. As examples the author would refer to the cases of a molybdenum-

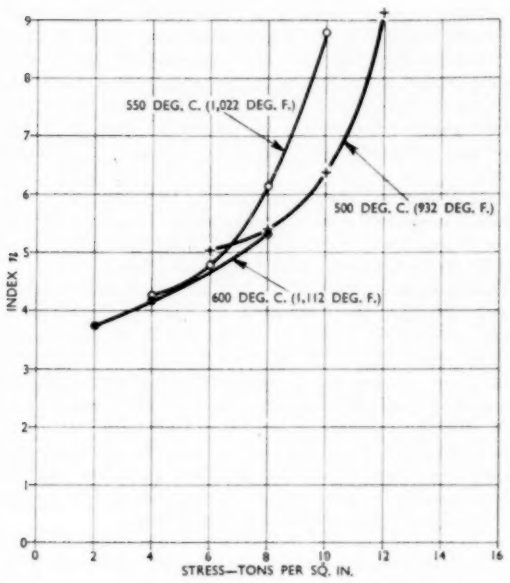

FIG. 3 VALUES OF n FOR MOLYBDENUM-VANADIUM STEEL PIPE

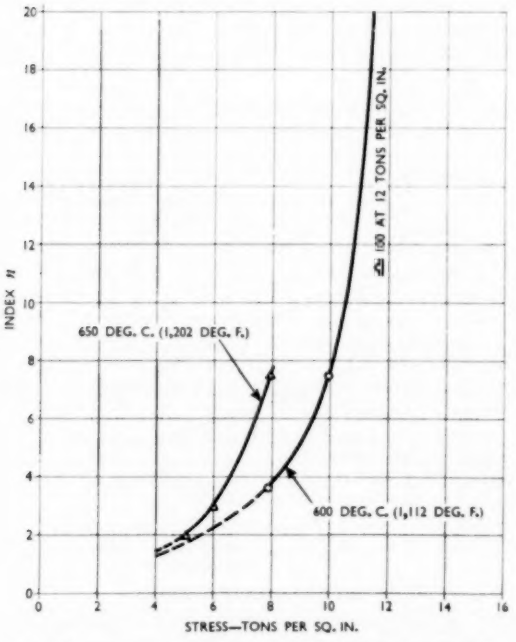

FIG. 4 VALUES OF n FOR CHROMIUM-NICKEL-COLUMBIUM STEEL

vanadium ferritic steel, and a nickel-chromium-columbium austenitic steel, dealt with by Bailey (1951)[3] from which source Figs. 3 and 4 of the present paper are reproduced. Figs. 5 and 6 show the corresponding variations of f/n for these steels. With the molybdenum-vanadium steel there is very clear evidence that at stresses less than 7 tons per sq in. f/n diminishes with the stress.

[3] An alphabetical list of references is given in Appendix 3.

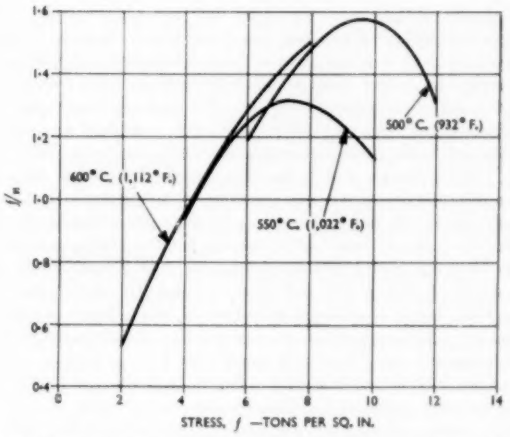

FIG. 5 VARIATION OF f/n FOR MOLYBDENUM-VANADIUM STEEL PIPE

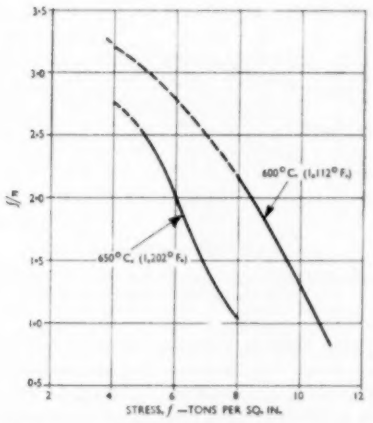

FIG. 6 VARIATION OF f/n FOR CHROMIUM-NICKEL-COLUMBIUM STEEL

Similar evidence is not provided by the experimental values of Fig. 6 and only a guess can be made. This would be that the value of f/n would pass through maxima values at stresses less than 4 tons per sq in. and decline as occurs with the molybdenum-vanadium steel, since the values of f/n and f must approach zero together as is found for the molybdenum-vanadium steel.

The definitely diminishing value of f/n for the molybdenum-vanadium steel, with but small variation of n, indicates that the undetermined f-log t curve in the extrapolated region for this steel would be convex to the log t-axis and that, therefore, linear extrapolation would be on the safe side in underestimating the safe allowable working stress.

With the nickel-chromium-columbium steel it seems very probable that extrapolation would similarly be on the safe side for stresses of 3 tons per sq in. and less, but with diminishing stress from above, say, 4 tons per sq in., f/n would increase and so extrapolation would then tend to overestimate the allowable working stress.

Summing up, the double-log method of plotting stress and time—Case (a)—must be expected to result in a relation always concave to the log t-axis, and linear extrapolation must be expected to give an overestimate of the safe working stress. For this reason it is, in the author's view, an unreliable method and stresses

for design obtained by this procedure are questionable. The single log method of plotting, i.e., f and log t—Case (b)—can be taken to yield a curve convex to the log t-axis at the lower stresses, and longer times and normal extrapolation may be expected not to overestimate the safe allowable working stress.

Procedure 2. As previously mentioned, a method making use of the creep rate, dx/dt, appears to have been used considerably in the United States, and it seems probable that it has been responsible for an appreciable quantity of design stress data from that source. A series of creep tests are made at the same temperature and at a number of stresses, each test being carried out for the same period of time, frequently 1000 hours, at the end of which the creep rate $\dot{x}$ is measured and the relation between log f and log $\dot{x}$, as ordinate and abscissa, respectively, is plotted. From this, by interpolation or extrapolation, the stress is obtained for a specific creep rate, commonly expressed as 0.01 or 0.1 per cent per 1000 hours, or strains of 0.0001, or 0.001, per 1000 hours, respectively, representing corresponding creep rates of 10^{-7}, or 10^{-6}, strain per hr. An example of this method and form of plotting for a $2^1/_4$ per cent chromium—1 per cent molybdenum steel is shown in Fig. 7 which is reproduced from a publication of

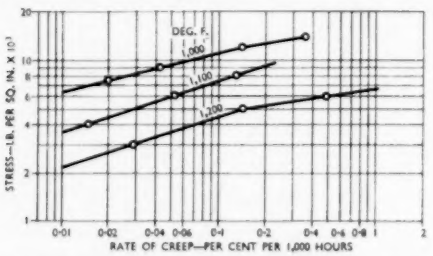

FIG. 7 STRESS-CREEP RATE CURVES FOR $2^1/_4$ PER CENT CHROMIUM—1 PER CENT MOLYBDENUM STEEL

Timken Roller Bearing Company (1939). Since the time at temperature is only 1000 hours, and the temperatures are regarded as possible working temperatures, the thermal-action effect, compared with service operation, must in many instances be virtually absent or quite inadequate. However, this does not concern the question of extrapolation procedure now under review.

The slope i of the log f, log $\dot{x}$ relation for the test data is given

$$i = \frac{d(\log f)}{d(\log \dot{x})} = \frac{\dot{x}}{f}\frac{df}{d\dot{x}}$$

by differentiating with respect to f. From Equation [5], since the time t of the tests is constant, and $\dot{x}$ and f are the only variables

$$\dot{x} f^{-\frac{n}{p+1}} = \text{constant}$$

Consequently

$$\frac{d\dot{x}}{df} f^{-\frac{n}{p+1}} - \frac{n\dot{x}}{p+1} f^{-\frac{n}{p+1}-1} = 0 \quad \text{and} \quad \frac{d\dot{x}}{df} f - \frac{n\dot{x}}{p+1} = 0$$

giving

$$\frac{df}{d\dot{x}} = \frac{p+1}{n}\frac{f}{\dot{x}} \quad \text{and} \quad i = \frac{p+1}{n} \qquad [9]$$

Equation [9] is illuminating and offers explanation of features commonly exhibited by log f, log $\dot{x}$ plottings according to the present method. Clearly, if the tests at a specific temperature involve first-stage or primary creep at the lower stresses, but run into third-stage or tertiary creep at the higher stresses, there would be a marked reduction in the slope i, because p is positive for primary creep and negative for tertiary creep. This feature is noticeable in Fig. 7 at the largest creep rates and at the higher test temperatures. However, at the moment the point is only of passing interest, as the present inquiry is concerned with extrapolation to low creep rates where creep is unlikely to be in the tertiary stage and, therefore, the important cause of change in the slope i, would arise from the index n owing to its dependence upon f.

Since n may be expected to diminish with f the slope will be expected to increase over the extrapolation range and, therefore, linear extrapolation to creep rates below the experimental values is likely to overestimate the safe allowable stress.

Thermal-action effect, if it became significant, would not directly influence the features of the log f, log $\dot{x}$ curve for a specific temperature, because, assuming that the influence upon thermal action of the stress present could be neglected, the duration of the test being the same throughout, the thermal-action effect would be the same for all tests at the same temperature. But the thermal-action effect in 1000 hours could not approach the effect of service, which would arise from at least 100 times the test period, and weakening from this cause would result in lowering the whole log f, log $\dot{x}$ relation, and hence in increasing the overestimation of the allowable safe stress.

An important aspect of Procedure 2, which should be noted, is that it is likely to overestimate the promise of austenitic steels for long-life high-temperature service. As will be seen from Fig. 11, a substantial superiority of the austenitic steel over the ferritic steel is shown by the 1000-hour tests. This advantage falls off with increase in time, making the 1000-hour tests unrepresentative for long-time service. The position is very different with ferritic steels as a class, as is made evident by Fig. 8

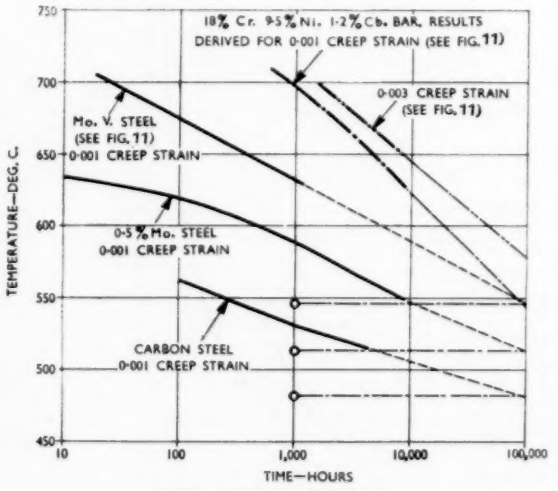
18% Cr. 9·5% Ni. 1·2% Cb. BAR. RESULTS DERIVED FOR 0·001 CREEP STRAIN (SEE FIG. 11)
0·003 CREEP STRAIN (SEE FIG. 11)
Mo. V. STEEL (SEE FIG. 11) 0·001 CREEP STRAIN
0·5% Mo. STEEL 0·001 CREEP STRAIN
CARBON STEEL 0·001 CREEP STRAIN
TEMPERATURE—DEG. C.
TIME—HOURS

o Temperature, Procedure 2

FIG. 8 CREEP-TEST RESULTS FOR STRESSES OF 3 TONS PER SQ IN. ON THREE FERRITIC STEELS AND ONE AUSTENITIC STEEL

which refers to several ferritic steels and shows that the 1000-hour test times give a relative order much more representative of their promise for the long-time service period.

Another feature, but one of general significance, is that there may be a wide disparity between the creep strain involved by the stress found by Procedure 2 and the creep strain it would be necessary to allow in practice for economic design. From Equations [4] and [5] it will be found generally that

$$x \Big/ \frac{dx}{dt} = \frac{p+1}{q+1}\,t, \quad \text{or} \quad x = \left(\frac{p+1}{q+1}\right) t\,\frac{dx}{dt}$$

Since q may be taken as zero, because of the virtual absence of thermal-action effect, and p also would frequently not have a larger magnitude than 2, x would commonly not be greater than $3t\,dx/dt$, and since for the Procedure t = 1000 hours and dx/dt = 10^{-7} strain per hour, the creep strain for the extrapolated stress would not usually exceed 3×10^{-4} or 0.03 per cent extension. In some cases it may be noticeably less.

For example, in the case of the chromium-nickel-columbium steel a value of p was found not exceeding 0.5, and averaging 0.33 (Bailey, 1951, Appendix 1). For this case, taking p = 0.5, the creep strain x would not exceed 1.5×10^{-4}. The extrapolated stress would depend, of course, upon test data involving larger strains and creep rates, but probably effective creep strains not greater than five times the extrapolated magnitude, or, say, less than 0.001. Economic design using this steel for high temperatures and pressures may demand allowable creep strains ten times this amount, and involve creep almost wholly of tertiary stage kind, whereas, in effect, the small creep strains concerned in the Procedure would fall within the primary stage and give results based upon the characteristics of this stage.

Stress-Rupture Tests

Procedure 3. Stress-rupture creep tests enjoy a measure of popularity in both countries, perhaps less so in Britain than in the United States. The attractiveness of the test may be due in part to the fact that it is about the simplest and cheapest of any of the tests in cost of equipment and staff time, requiring for a test only constant load, constant temperature, and little attention from start to fracture.

In the United States instances are found of both Procedure 2 and stress-rupture tests being conducted upon the same material, at the same temperature, to assist in the selection of a stress which would have a creep rate not exceeding a specific figure at 1000 hours, and which would also be safe against fracture for a specified life. Several examples where both tests have been made, have been given by the Timken Roller Bearing Company (1939). In their stress-rupture tests, and also in examples given by Thielemann (1940), of which Fig. 9 (reproduced from the latter

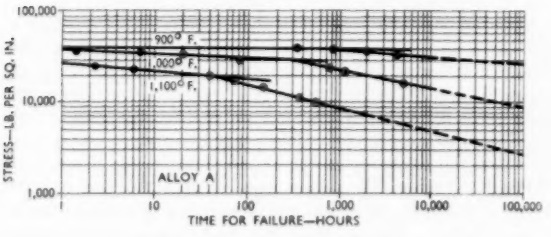

⊙ Indicates intergranular fracture

Fig. 9 Stress-Time-for-Failure Curves for Carbon-Molybdenum Steel

source) is typical, the log f, log t relation where t is the time for fracture under the stress, is composed of two linear segments of different slope, the steeper segment applying to the longer fracture times and higher temperatures.

By interpolation and extrapolation there may be obtained the stresses for specific fracture times, including for a nominal long-life time of 100,000 hours by extrapolation. Rarely, however, has the fracture time by test exceeded 10,000 hours, whereas the service life of present-day high-temperature power plant may be as much as 150,000 hours. Consequently, the thermal-action effect operating in stress-rupture tests would not as a rule approach that of service. Generally, this factor, therefore, must be regarded as virtually absent, or only partially operative. Because the test period under Procedure 2 is only 1000 hours, while that in stress-rupture test procedure is variable, and probably much greater, strict comparison of results is likely to be misleading. Nevertheless, apart from the uncertain influence of thermal action, it is of interest to make the same analytical approach to the question of extrapolation as has been made already in dealing with other procedures.

Since extrapolation concerns long times as well as the lower range of stresses which goes with them, it is probable that in most instances fractures would be intercrystalline for most good creep-resistant steels and alloys and, therefore, that elongation to fracture would be small but would not necessarily be taken as constant as in Procedure 1.

An abrupt change from transcrystalline to intercrystalline rupture is hardly to be expected, but rather a stage of transition from rupture wholly of the one to that wholly of the other type, during which the elongation to failure would diminish. Results of creep tests given by Robinson (1940) and reproduced in Fig. 10 for

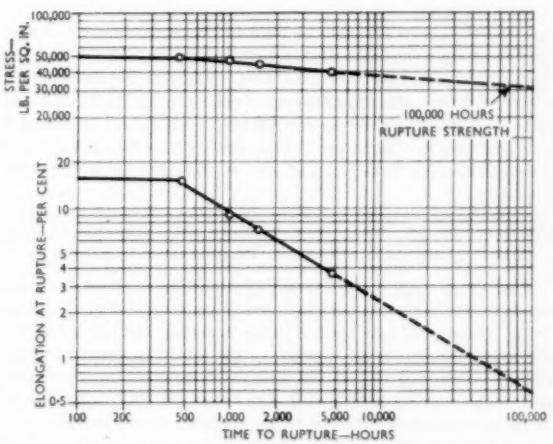

Fig. 10 Rupture Tests at 900 Deg F, Normalized Carbon-Molybdenum Steel Pipe

material from a carbon-molybdenum steel pipe (0.44 per cent molybdenum) showed that when tested at 900 deg F the elongation $\bar{x}$ to fracture fell from about 15 per cent to approximately 3.5 per cent, the corresponding times $\bar{t}$ to rupture being 500 hours and 5000 hours, respectively. The results plotted as log $\bar{x}$ and log $\bar{t}$ gave a linear relation represented by $\log \bar{x} = \log c - m \log \bar{t}$, c and m being constants. Thus the relation between $\bar{x}$ and $\bar{t}$ was of the form $\bar{x} = c\bar{t}^{-m}$. It is probable that when there is intercrystalline fracture of other materials, the relation between $\bar{x}$ and $\bar{t}$ could be similarly represented, employing appropriate constants c and m. Assuming this would be admissible, introduction of this value of $\bar{x}$ in Equation [4] gives a relation between $\bar{f}$ and $\bar{t}$ for rupture as follows

$$c\bar{t}^{-m} = \left\{\frac{B(p+1)}{q+1}\right\}^{\frac{1}{p+1}} \bar{f}^{\frac{n}{p+1}}\, \bar{t}^{\frac{q+1}{p+1}}$$

Rupture would be characterized by

$$\bar{f}^{n}\bar{t}^{q+1+m(p+1)} = \text{constant}$$

With steels of high creep resistance it is probable that fracture

would occur in the first or second stages of creep and unimportant error would be made by considering fracture to occur in the second stage for which p is zero. The slope i of the $\log \bar{f}$, $\log \bar{t}$ relation is determined as in Procedure 1, Case (a), except that $q + 1$ is replaced by $q + 1 + m$ making

$$i = -\frac{q + 1 + m}{n} \quad [10]$$

Equation [10] offers a ready interpretation of the features usually exhibited by the $\log \bar{f}$, $\log \bar{t}$ diagram. For the shorter fracture times, or lower temperatures, where the effect of thermal action is not appreciable in producing weakening, q would be negligible or zero and the slope would be expressed by $-(1 + m)/n$. It is possible, however, that at the shorter times and lower temperatures the constant m may not have begun to operate, in which case the slope would be expressed by $-(1/n)$, and there would be good ductility and transcrystalline fracture. There appears to be a possibility of two changes of slope, one associated with m and the other associated with thermal-action effect and with q. The two factors might, of course, act together and make separate identification difficult. It is probable that, if a steel showing good ductility and transcrystalline fracture exhibited definite change of slope, this would have arisen from thermal action.

A basis has been found to account for the segments of the $\log \bar{f}$, $\log \bar{t}$ diagram as usually drawn, but the question arises whether the segments are straight lines. This would be substantially so if n were constant, but as has already been stated, n has been found to become less as the stress is reduced, as in the cases represented by Figs. 3 and 4. This would cause concavity to the $\log \bar{t}$-axis and extrapolation to overestimate the rupture stress for the life period.

Comparison of Stresses Obtained by Different Test Procedures (Test Varied, Temperature Constant)

The test procedures so far dealt with all make stress the independent variable, and also the means for accelerating the creep tests. No specific provision is made to ascertain, or to allow for, the important factor of thermal action, and this omission must vitiate in varying degree the results at different temperatures, and render extremely doubtful, if not unprofitable, a comparison of stresses obtained by different procedures. When the profound and different influence of this factor upon the behavior of steel and alloys is appreciated, no satisfactory comparison of different test procedures can be offered without taking this factor into account, nor can there be confidence in the reliability of the stresses obtained. As remarked at the beginning, the situation generally regarding stresses for long-time high-temperature service is most disappointing, especially after so much testing. Henceforward a critical attitude to test procedures is required in both Britain and the United States for this unfortunate situation to be rectified.

So far as test procedures have been considered, little can usefully be done at the moment beyond giving general expressions which include provision for thermal action and other factors, enabling a comparison of stresses for different procedures to be made when the factors concerned are sufficiently known, and then applying these expressions, omitting thermal weakening, to procedures in common use in the two countries. Appendix 1 presents information of this kind relating to Procedures 1 and 2.

A highly important aspect of stress values as influenced by the procedures used to determine them concerns extensive tables of recommended stresses published in the United States. These are of considerable interest to engineers in Britain but their value would be increased if the procedures by which the stresses have been determined were to be given, so that the magnitudes could be judged from the standpoint of the technical approach and practice in Britain.

A guide is given as to the basis used in arriving at stresses recently issued by the ASME Committee dealing with the Code for Pressure Piping. The following statement has been published (*Mechanical Engineering*, 1951).

"The maximum allowable working stresses shall be established as the lowest of the following stresses: (A) 1/4 of the minimum specified tensile strength; (B) 1/4 of the tensile strength at temperatures as reported by test data; (C) 62 1/2 per cent of the yield strength at temperature as reported by test data; (D) A conservative average of the stress to give a creep rate of 0.01 per cent in 1000 hours as reported by test data."

The author understands from a British engineer in touch with American design practices on steam piping, where creep is significant, that it is usual in the United States to allow 100 per cent of the stress according to requirement (D), subject to a limitation of 60 per cent of the average stress, and 80 per cent of the minimum stress, whichever is the lower, estimated to produce rupture in 100,000 hours.

It is understood that the published stress is for insertion in a formula for pipe-wall thickness, and that the equivalent stress in the pipe would be somewhat less.

It appears, therefore, that for high temperatures requirement (D) is likely to be the most common requirement determining stress, and Procedure 2 the most probable basis of the published stresses. It has been found that extrapolation in Procedure 2 involves the possibility of overestimating the stress required, and the certainty of doing so if the composition of the material and the operating temperature and life period are such that weakening by thermal action would occur.

This is the most serious defect of Procedure 2, the more so if its action can be anticipated, because it is progressive and the results of weakening would become most manifest in the later stages of the operating life, and it might even have important consequences in middle age. To the author, therefore, it is disturbing that the recently published stresses referred to represent considerable increases in some instances on the allowable stresses previously in operation, and it can only be assumed that, guided, perhaps, by experience gained so far, satisfactory performance in early life has been mistakenly accepted as evidence for allowing an increased burden without first inquiring whether such burden can be carried satisfactorily if weakening sets in later in life.

A case of particular interest in allowing investigation is that of the austenitic steel 18 per cent chromium—8 per cent nickel-columbium because it has been introduced in Britain for steam piping in one of the latest electric generating stations. The stress given by ASME Tables P-5 and P-7 for this steel at 1050 deg F is 13,100 lb per sq in. Previously, the highest temperature for which the stress was given was 1000 deg F, the figure being 10,000 lb per sq in. The recent figure given for this steel for 1000 deg F is 13,500 lb per sq in., which affords a measure of the increase allowed. Bailey (1951) in reply to discussion mentioned that he had found this type of steel to be subject to substantial weakening by thermal action, the relevant sentence being: "Tests made for himself suggested that heating at 750 deg C (1382 deg F) for 100 hours prior to testing would reduce the time for 0.003 strain to about 40 per cent of the time for the material not preheated." The significance of the preheating at 750 deg C (1382 deg F) in relation to the operating temperature 566 deg C (1050 deg F) is referred to under Procedure 4. In the weakened condition the average creep rate is increased 2.5 times. If the index p remained the same and the index n were about 2, as suggested by Fig. 4, the stress acting on unaltered material, which would produce the higher creep rate, would need to be increased $\sqrt{2.5}$, or 1.58, times. The weakening effect would thus be repre-

sented by a reduction in stress to 1/1.58 or to 63 per cent of that for the unweakened material. This case justifies concern regarding stresses derived by Procedure 2 in cases where there is evidence that important weakening by thermal action may be expected with operating temperatures and times.

Extrapolation of Test Data (Test Temperature Varied, Stress Constant)

Procedure 4. The reliability—when testing to determine design stresses for long-time service (many times the testing periods)—of adopting a working stress as the test stress and of using temperature to accelerate creep has always been urged by the author who has also discouraged methods, e.g., Procedures 1 and 2, which make working temperature the test temperature, as well as the use of stress to accelerate creep. The method advocated was described by Bailey (1935) when attention was also directed to the thermal-action factor. Failure by many engineers and testing authorities to appreciate the significance of the principles involved, particularly in connection with long-life high-temperature plant, has resulted in the publication of much unreliable data relating to design stress, and in many unsound conclusions as to the comparative merits of steels of different compositions and as to the influence of particular elements which, because of thermal-action effect, can only be judged correctly in relation to the life period and working temperature to be borne. This may appear to be a sweeping and disturbing statement, but to support it it is only necessary to refer to the curves of Fig. 1 and to similar curves by Glen (1948).

Development of plant to higher temperatures and longer life caused the author to consider whether the method advocated and since used by him might stand in need of some refinement in extrapolation. This would arise if the thermal-action effect operating during the actual creep tests influenced the results from which extrapolation would be made in such a way that the effect which might operate during the very much longer time of the period covered by extrapolation would be different. A difference was assumed, greater or less than the thermal-action effect present in the tests made, and a correction was estimated to give the time that was to be expected had the thermal effect been correct. A second extrapolation using the corrected times was intended, but when applied, for example, in the case of a 2¼ per cent chromium-1 per cent molybdenum steel it was found that the correction was very small.

The question of thermal action as it concerns Procedure 4 is examined in Appendix 2 and the following conclusion arrived at relating to plant for long life at high temperatures.

It is rational and correct in principle to test at temperatures above the working temperature using the working stress. It is to be noted that Dickenson (1922) in his pioneer investigation showed commendable foresight in testing at a working stress and in adopting temperature as the means for accelerating creep.

Following recognition of this principle, shortened rational methods of test can be chosen, of a suitable degree of approximation for any given purpose. In view of the probability that the need will arise for making a number of tests taking thermal action into account, the matter is referred to in Appendix 2.

Returning to the case of the chromium-nickel-columbium steel and the tests already mentioned in which thermal action was measured by the result of heating for 100 hours at 750 deg C (1382 deg F), Fig. 11 reproduces a figure from Bailey (1951). The points A and B record data obtained by Kirkby and Sykes (1951) for this steel. BA is extended to the left (not shown) to mark log (time) for 100 hours using the magnitude of α derivable from the points B and A (α = 31,000), and giving the temperature 790 deg C (1454 deg F), which in 100 hours would approach the thermal action present at A and B. Thus the thermal

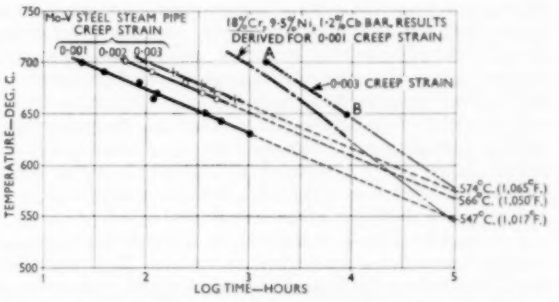

Fig. 11 Creep-Test Results for Stresses of 3 Tons Per Sq In. on Molybdenum-Vanadium Steel Pipe and Chromium-Nickel-Columbium Steel Bar

action applied by the heating was less than that present at A and B. The time at 750 deg C (1382 deg F), which would be approximately equivalent, would be 310 hours.

It was estimated earlier that the weakening effect, which, it is now seen, occupied about one third of the period corresponding to the normal life of the thermal action applied at 750 deg C (1382 deg F) would account for a reduction in stress to 63 per cent of that for the unweakened material. In Appendix 1 Procedures 1 and 2 were applied to chromium-nickel-columbium steel, on the basis of 0.003 creep strain in 100,000 hours for Procedure 1, and 0.01 per cent in 1000 hours for Procedure 2, and the creep strain determined by Procedure 2 was estimated to be 1.168 times that obtained by Procedure 1, but with no thermal-action effect included. Allowing for the estimated influence of the thermal-action effect, the stress by Procedure 1 would be 63/1.168 or 55 per cent of that found for Procedure 2 without thermal-action effect present. The latter should correspond with the stress determined by the requirement (D) of the ASME Committee referred to previously, and the former approximately with what should be found by using Procedure 4. It is significant that 55 per cent of the ASME recommended stress at 1050 deg F of 13,500 lb per sq in., i.e., 7420 lb per sq in., compares with 3 tons per sq in., or 6720 lb per sq in., which is the stress applying to AB in Fig. 11.

The thermal-action effect is by far the largest factor found to account for the wide difference of the stress values of 6720 lb per sq in. and 13,500 lb per sq in., as given by Procedure 4, and Fig. 11, and as recently recommended in the United States (presumably based upon Procedure 2). The disparity is at first alarming, but the low value of the index n at working-stress values possessed by this steel (Fig. 4) is a circumstance providing relief, minimizing the action of the higher stress in producing more creep. The creep, from what has been seen, would probably be not less than 2½ times that represented by Fig. 11, or the creep strain would be 0.0075 instead of 0.003. The matter is, of course, one which should be more fully examined, but the information considered is sufficient to emphasize the importance of thermal-action effect and the need for both the United States and Britain to give attention to the question of allowable creep strains, with the purpose of securing agreement upon magnitudes. In addition, there should be common interest in the associated question of deciding on the test procedure calculated to produce the most reliable estimate of creep in the operating life.

Creep-Relaxation Tests

Although outside the field of the present paper, it is worth referring to creep-relaxation tests which, when made at working temperatures, are open to criticism similar to that made of constant-load tests, when the tests apply to materials required for

long life and high temperatures. In this instance the influence of thermal action is likely to be a factor. It is recommended that tests be made at a series of temperatures above the working temperature with a specific initial strain, and the times determined for the stress to relax by specific amounts, i.e., to specific stresses. For each specific relaxed stress, the corresponding temperatures and times would be plotted on an abscissa of log (time), and extrapolation made to the life period to give the temperature at which the specific relaxed stress would be reached in the life period. Thus, for the material, and specific initial strain, a working stress-working temperature relation would be derived, which would embody the influence of thermal action.

To compare materials on the basis of creep-relaxation tests at working temperatures can be most misleading. The comparison should be made on the basis of tests at an elevated temperature and time embodying thermal action representative of the anticipated service effect. When this is done the element chromium in particular will in a ferritic steel frequently be found disappointing for service at the higher temperatures because of its apparent influence in inducing increased weakening by thermal action, which can more than offset the advantage it has shown by tests at working temperatures.

Conclusions

The most important conclusions to be drawn—apart from the examinations made of the different Procedures—relate to the direction which investigation should take so as to be most profitable for practical and scientific purposes, in the case of the materials with which the paper is particularly concerned, namely, materials for long-life plant operating at high temperatures. These are:

1 That, in the author's view, Procedure 4 is the most rational and reliable for determining dependable working stresses.

2 That for reliably assessing the potentialities of a composition, the influence of a particular element or combination of elements, or the influence of a thermal treatment, it is essential that thermal action should be correctly taken into account. The principle of Procedure 4 provides for this.

3 That metallurgical investigation of creep phenomena of metals generally, and of the complex industrial metals, in particular, whether fundamental or technological in character, has to be regarded as incomplete if attention has not been given to the factor of thermal action.

The author would have been highly gratified if his examination of test procedures had resulted in useful comparative British and American data, instead of considerable disappointment with the present position in both countries.

Unfortunately, the practice of making tests at the working temperature, and applying extrapolation on a stress basis, has been so extensively and mistakenly followed in both countries, in the particular case investigated, that a general state of unreliability and uncertainty regarding design-stress values has been found to exist where materials and their behavior for long life at high temperatures are concerned, and where thermal action plays an important part.

Procedure 4, advocated by the author, which takes the influence of thermal action into account and leads to the most dependable stresses and reliable assessment of materials, has only been applied in a comparatively few instances to yield published information. So far as the author is aware, such instances have been where his influence upon investigations carried out for a committee has been responsible, and investigations in which, on behalf of his company, he has had a personal interest. Few useful comparisons of satisfactory data, not vitiated by the absence, or inadequate influence, of the thermal-action factor, or not open to doubt because of extrapolation, can therefore be made. Nevertheless if, by its critical approach to test practices and procedures, the paper results both in Britain and the United States in practice of greater reliability, and leads to common working-stress values, an important object will have been achieved.

Acknowledgments

The author wishes to record his indebtedness to the directors of the Metropolitan-Vickers Electrical Company, Ltd., for permission to publish this paper, and to Mr. N. Elce, MSc, director and chief mechanical engineer, for his particular interest in its subject matter.

Appendix 1

Comparison of Stresses and Creep Strains Resulting From Procedures 1 and 2

Identifying the several quantities employed in a relation by the suffixes 1 and 2, corresponding with Procedures 1 and 2[4] respectively, the following rearrangements of Equations [4] and [5] apply:

Procedure 1

$$f_1 = B^{-\frac{1}{n_1}} \left(\frac{q_1 + 1}{p_1 + 1}\right)^{\frac{1}{n_1}} x_1^{\frac{p_1+1}{n_1}} t_1^{-\frac{q_1+1}{n_1}}$$

Procedure 2

$$f_2 = B^{-\frac{1}{n_2}} \left(\frac{p_2 + 1}{q_2 + 1}\right)^{\frac{p_2}{n_2}} \left(\frac{dx_2}{dt}\right)^{\frac{p_2+1}{n_2}} t_2^{-\frac{q_2-p_2}{n_2}}$$

giving

$$\frac{f_2}{f_1} = B^{\frac{1}{n_1} - \frac{1}{n_2}} \frac{\left(\frac{p_2 + 1}{q_2 + 1}\right)^{\frac{p_2}{n_2}} \left(\frac{dx_2}{dt}\right)^{\frac{p_2+1}{n_2}} t_2^{-\frac{q_2-p_2}{n_2}}}{\left(\frac{q_1 + 1}{p_1 + 1}\right)^{\frac{1}{n_1}} x_1^{\frac{p_1+1}{n_1}} t_1^{-\frac{q_1+1}{n_1}}} \quad \ldots . [11]$$

The coefficient B, as taken above, is the same for the two procedures, since difference in thermal action for the two would be taken into account by the respective values for q. The times t_1 and t_2 are greatly different. Thus it is common practice in Britain to adopt a nominal life of 100,000 hours and extrapolation to this time, therefore t_1 = 100,000 hours; and it seems to be common American practice to employ the creep rate at the end of 1000 hours, therefore, t_2 = 1000 hours. In addition, x_1 is frequently 0.001 strain, but may, of course, be more, e.g., 0.003. In American practice the creep rate dx_2/dt is 0.01 per cent in 1000 hours, or 10^{-7} strain per hour, and extrapolation to this of the log (stress), log (creep rate) relation gives the stress f_2.

To obtain an idea of stress ratio f_2/f_1 some approximations can be made. The thermal-action effect in both procedures, as practiced, can be regarded as negligible, since in Procedure 1, although extrapolation is carried to 100,000 hours, the actual duration of the tests is unlikely to be more than several thousand hours. Since the stresses obtained in the two cases are unlikely to be widely different, n_1 and n_2 may be assumed, as an approximation, to be equal, and similarly with p_1 and p_2. Putting $q_1 = q_2 = 0$, making $n_1 = n_2 = n$, and $p_1 = p_2 = p$, and putting $x_1 = 0.001$, $dx_2/dt = 10^{-7}$, t_1 = 100,000, t_2 = 1000, the stress ratio becomes

$$\frac{f_2}{f_1} = \frac{(p + 1)^{\frac{p+1}{n}} \, 10^{-7\left(\frac{p+1}{n}\right)} \, 10^{3\frac{p}{n}}}{10^{-3\left(\frac{p+1}{n}\right)} \, 10^{-\frac{5}{n}}}$$

$$= (p + 1)^{\frac{p+1}{n}} \, 10^{\frac{1-p}{n}} = (p + 1)^{\frac{p+1}{n}} \, 10^{-\frac{p+1}{n} + \frac{2}{n}}$$

[4] Procedure 1 is practiced in both Britain and the United States, and Procedure 2 principally in the latter country.

or

$$\frac{f_2}{f_1} = \left(\frac{p+1}{10}\right)^{\frac{p+1}{n}} 10^{\frac{2}{n}} \quad [12]$$

If creep is substantially of the second-stage type, i.e., $p = 0$, $f_2/f_1 = 10^{1/n}$, which would exceed unity for all values of n.

Perhaps the most useful approach to make when comparing the procedures is to determine what creep strain x_1 of Procedure 1 would make the stresses f_1 and f_2 equal. For this condition

$$(x_1)^{\frac{p+1}{n}} 10^{-\frac{5}{n}} = (p+1)^{\frac{p+1}{n}} 10^{-7\left(\frac{p+1}{n}\right)} 10^{3\frac{p}{n}}$$

$$x_1 = (p+1)10^{-7} 10^{\frac{3p+5}{p+1}} \quad [13]$$

It will be noticed that x_1 is independent of n and depends only on the stage of creep involved. If creep were substantially of second-stage kind, i.e., $p = 0$, $x_1 = 0.01$ strain, or 1.0 per cent. This is more than practice in Britain would allow, or correspondingly, the allowable stress would be less than that arrived at by Procedure 2 on the basis of a creep rate of 0.01 per cent in 1000 hours.

If, using steels of high creep resistance, where the intercrystalline mode of fracture can be expected, a creep strain x_1 of 0.003 were allowed, the stress ratio f_2/f_1 would be given by

$$\frac{f_2}{f_1} = \frac{(p+1)^{\frac{p+1}{n}} 10^{-7\left(\frac{p+1}{n}\right)} 10^{3\frac{p}{n}}}{3^{\frac{p+1}{n}} 10^{-3\left(\frac{p+1}{n}\right)} 10^{-\frac{5}{n}}} = \left(\frac{p+1}{3}\right)^{\frac{p+1}{n}} 10^{\frac{1-p}{n}}$$

$$= \left(\frac{p+1}{30}\right)^{\frac{p+1}{n}} 10^{\frac{2}{n}} \quad [14]$$

With second-stage creep, $p = 0$, $f_2/f_1 = 3.33^{1/n}$.

In order to give numerical value to the stress ratio represented by Equation [14] the magnitudes of n and p need to be known, and it is desirable for f_2 to have been determined for the same steel on the basis of 0.01 per cent creep in 1000 hours. Values of n and p of a chromium-nickel-columbium austenitic steel were given by Bailey (1951). For a working temperature of 1050 deg F and an appropriate working stress, approximate values were $n = 2$, and $p = 0.3$–0.5, say, 0.4. If these values could be taken to apply to an 18 per cent chromium-8 per cent nickel austenitic steel, for which a value of f_2 for 0.01 per cent creep in 1000 hours at 1050 deg F has been given as approximately 9000 lb per sq in. (Timken Roller Bearing Company, 1939), a value of f_2/f_1 can be determined using Equation [14]. Thus

$$\frac{f_2}{f_1} = \left(\frac{1.4}{30}\right)^{0.7} \times 10 = 1.168, \text{ making } f_1 = 9000/1.168$$

$$= 7700 \text{ lb per sq in.}$$

or, f_1 in this case for a creep strain of 0.003 is approximately 85 per cent of f_2.

Weakening of the steel by thermal action because of long operating life at high temperature, as in modern steam power plant, is probable. If this occurs, values of both f_1 and f_2 would be lower than those given.

Appendix 2

Thermal Action, Creep, and Procedure 4

Procedure 4 embodies thermal action, but the question arises as to whether the thermal action present in the tests would represent substantially that which would operate over the long time in service at the working temperature. There are grounds for thinking that it would not be the same and that, more commonly, it would be less than thermal action in service in the case of carbon and low-alloy ferritic steels, and perhaps also in the case of steels and metals generally.

Evidence upon which to found belief is limited, but fortunately there are examples which offer exact information on thermal action and comparable creep test data, namely, on carbon steel, and carbon-molybdenum steel (Bailey and Roberts, 1932) and (Bailey, 1935). Before considering the evidence, the physical basis of the subject should first be stated.

It is assumed that the changes which occur arise from a metastable condition, and that temperatures used do not involve a constitutional change, e.g. from ferritic to austenitic in steels, and derive therefore at the atomic or molecular level from the operation of the Maxwell-Boltzmann distribution law of energies, whereby the time τ for a particular change would be connected with the temperature T (absolute) of heating by the relation $\tau = \mathbf{A}e^{E/kT}$, where k is the Boltzmann constant, E is the activation energy characterizing the change, and $\mathbf{A}$ is a constant. For present purposes the relation may be written $\tau = \mathbf{A}e^{\alpha/T}$ already referred to. Considering the same change at different temperatures T_1 and T_2 occupying times τ_1 and τ_2, respectively

$$\frac{\tau_1}{\tau_2} = e^{\alpha\left(\frac{1}{T_1} - \frac{1}{T_2}\right)}$$

and taking common logarithms

$$\log \tau_1 - \log \tau_2 = 0.4343\,\alpha\left(\frac{1}{T_1} - \frac{1}{T_2}\right)$$

and

$$\alpha = \frac{\log \tau_1 - \log \tau_2}{0.4343\left(\frac{1}{T_1} - \frac{1}{T_2}\right)} \quad [15]$$

The experimental work on carbide spheroidization in carbon steels (Bailey and Roberts, 1932) gave, for a specific structural change, remarkably consistent and reliable results in showing the same value of α (i.e., 33,000) for steels of different carbon content, whether cast, forged, annealed, normalized, or cold rolled. A carbon-molybdenum steel, 0.5 per cent molybdenum, was similarly examined by the author (data not published) but in the normalized condition only. Identification of the same degree of structural change was more difficult than with the carbon steels, and the heating times at different temperatures for a specific structural change, could only be identified by ranges of time. But these ranges when plotted gave a linear band of the same slope as was found for carbon steel, thereby signifying the same magnitude of α.

Approximately linear relations can be found connecting $\log \tau$ and $1/T$ for creep test results according to Procedure 4. The magnitudes of α obtained for creep tests upon the carbon and 0.5 per cent molybdenum steels are, however, found to be substantially greater than the figure of 33,000 applicable to the structural change in these steels. Table 1 gives the values of α applicable to the creep test results, including results of tests upon two carbon steels, 0.15 per cent carbon and 0.4 per cent carbon, both initially normalized and spheroidized before testing. In these particular tests creep was defined by the minimum creep rate, strain per hour (i.e., second-stage creep), and thus τ for a specific creep strain during this stage would be inversely proportional to the minimum creep rate, and when so plotted gave the values of α recorded in Table 1. It is noteworthy that, over the temperature range 480–540 deg C (896–1004 deg F) for the 0.15 per cent carbon steel, and 500–540 deg C (932–1004 deg F) for the 0.4 per cent carbon steel, the value of α for the initially

TABLE 1 VALUES OF α

Reference	Type of steel	Initial condition	Stress, tons per sq in.	Temperature range, Deg C	Temperature range, Deg F	α from creep tests
Bailey (1935)	0.4 per cent carbon	Normalized	1.0	550–600	1022–1112	50500
Bailey (1935)	0.4 per cent carbon	Normalized	2.0	500–550	932–1022	64500
Bailey (1935)	0.4 per cent carbon	Normalized	6.0	450–500	842– 932	63000
Bailey (1935)	0.4 per cent carbon	Normalized	10.0	400–425	752– 797	47600
Bailey (1935)	0.5 per cent molybdenum	Normalized	2.0	536–595	997–1103	54700
Bailey (1935)	0.5 per cent molybdenum	Normalized	6.0	508–549	946–1020	72000
Bailey and Roberts (1932)	0.15 per cent carbon	Normalized	6.0	480–526	896– 979	60200[a]
Bailey and Roberts (1932)	0.15 per cent carbon	Spheroidized	6.0	480–526	896– 979	60200[a]
Bailey and Roberts (1932)	0.4 per cent carbon	Normalized	7.0	506–565	943–1049	51000[a]
Bailey and Roberts (1932)	0.4 per cent carbon	Spheroidized	7.0	506–565	943–1049	51000[a]

[a] Based upon creep tests determining minimum creep rate.

normalized and spheroidized conditions was the same, although of course, for the spheroidized condition the creep resistance was substantially smaller than for the normalized condition.

The values of α fall substantially in the range 50,000–65,000, in marked contrast to the value of 33,000 found for the thermal-action change of carbide spheroidization. Creep-test results from Mr. P. Whitaker for a $2^1/_4$ per cent chromium-1 per cent molybdenum steel, at a stress of 3 tons per sq in. and 0.3 per cent strain, have given $\alpha = 51{,}200$ for the temperature range 616–653 deg C (1141–1207 deg F); and for a 0.5 per cent molybdenum-0.25 per cent vanadium steel tested for the author under the same conditions and temperature range 600–650 deg C (1112–1202 deg F), gave $\alpha = 47{,}000$. Thus creep tests upon all the steels considered yield values of α 50 per cent or more greater than α for carbide spheroidization found for carbon steels initially normalized or spheroidized, and for normalized 0.5 per cent molybdenum steel.

Structural change tests to determine values of α were not made with the $2^1/_4$ per cent chromium—1 per cent molybdenum, and 0.5 per cent molybdenum—0.25 per cent vanadium, steels, but, because the creep tests give values of α comparable in magnitude with those of Table 1, by inference it is not unlikely that structural change by thermal action would yield magnitudes comparable with those found for carbide spheroidization.

It is possible, and indeed probable, that the visible change of comparatively massive carbides merely serves as an indicator of a change associated with the invisible carbide in solution in the ferrite, upon which creep resistance most likely depends. However, it would not necessarily follow that the α for massive carbide spheroidization would be the same as for the changes associated with the carbide in solution in the ferrite. Nevertheless, it is an important fact to bear in mind, that the same magnitude of α is found by creep tests for the same carbon steel, whether initially normalized or spheroidized by preheating without stress for 24 hours at 650 deg C (1202 deg F), or 2000 hours at 560 deg C (1008 deg F), before testing. The two preheating treatments were chosen to produce the same degree of carbide spheroidization. It may be concluded that the fundamental mechanism of creep remained unaffected by the thermal action applied, although the rate of creep was increased. A more complete view of the mechanism of thermal action and of creep is needed to increase understanding of what has occurred.

An effort was made by Bailey and Roberts (1932) to obtain a fundamental view of structural change of the metastable kind, which assumed the change might involve several stages of the kind here considered, each of an atomic or molecular character, and governed by its own value of α. The several stages were considered as being in series in the sense that the proportion of atoms or molecules participating in the first stage provided operating material for the second stage, the product of which provided operating material for the third stage, and so on. The result suggested that thermal action for the complete change would be subject to the same type of law as for a single stage, but with an index α equal to the sum of the α's of the stages. The author suggests that the creep mechanism would constitute a separate stage additional to the stage, or stages, involved by the structural change, so that if α' applied to the structural change and α'' to the creep mechanism, the combined result of thermal action and creep would be represented by the index α, where $\alpha = \alpha' + \alpha''$.

Regarding the legitimacy of creep as a stage, creep depends upon thermal softening of strain-hardened material, and this is subject basically to the same exponential law as the other stages, whether strain hardening is given an explanation upon an atomic, molecular, or dislocation-theory basis, and therefore the fundamental view referred to would equally apply to the combined result of thermal action and creep action, which is manifested by creep as ordinarily understood.

The foregoing tentative suggestion, if correct, has interesting consequences. It at once provides an explanation of the α found by creep tests upon the carbon, and 0.5 per cent molybdenum, steels being greater than the magnitude of this index for structural change alone, and suggests its general applicability, although it does not answer the question whether the α for massive carbide spheroidization would apply to changes associated with dissolved carbides in the ferrite. It can account for normalized and spheroidized carbon steels having the same index α as given by creep tests, although the creep rates are different. A similarity is to be found—and for a like reason—in the thermal softening of a strain-hardened metal, where the index α is independent of the degree of strain hardening, but the rate of softening can vary widely, being greater the higher the degree of initial strain hardening.

The circumstances of the problem of accelerating Procedure 4, and of reliable extrapolation of its test data, are aided by Fig. 12 which shows a temperature (θ), log time (τ) diagram with two curves AB and AC drawn for values of α of 33,000 and 50,000, respectively, and having the common point A marking the service temperature $\bar{\theta} = 500$ deg C (932 deg F), and the service life $\tau = 100{,}000$ hours. AB would represent well the temperature, log time relation for structural change of a normalized or annealed carbon steel, and AC the temperature, time relation in an application of Procedure 4. The curves A′B′ and A′C′ are similar to AB and AC, respectively, but refer to A′ marking $\bar{\theta} = 550$ deg C (1022 deg F) and a life of 100,000 hours. Referring to AB and AC, the thermal-action effect present in the test data would always be less than that corresponding with 100,000 hours at 500 deg C (932 deg F) represented by the point A, but the lower the test temperature the larger is the proportion of the thermal-action effect represented by A which is present in the creep test and, therefore, referring to Fig. 1 for illustration, the greater would be the proportion of the abscissa of the curve equivalent to 100,000 hours at 500 deg C (932 deg F).

If thermal action caused little variation of creep resistance over the operating period, as represented by the time of heating in Fig. 1, there would be no counterpart evident in AC. But if, as the test temperatures are taken lower, thus, as pointed out, bringing into the tests a larger proportion of the thermal action represented by the point A, a substantial decline in creep resistance were involved, then the time for a specific creep strain

would be less than that given by AC at the temperatures concerned, thereby increasing the slope of AC at the region and affecting extrapolation. Correspondingly, if the thermal-action effect increased creep resistance, the slope of AC would be decreased. Clearly, therefore, the shape of Fig. 1, particularly the proportion that is embraced by the abscissa representing the working life—which depends upon the working temperature and life as defined by the point A—is a factor in the shape of AC as determined by the data of Procedure 4 and therefore also in its extrapolation. The values of α given by Table 1, depending as they do upon the features of Fig. 1, would be subject to variation.

The difficulties and uncertainties of Procedure 4 can now be seen, as well as ways of dealing with them.

A fundamental and major problem is the determination of AB to represent the true thermal-action effect as it affects creep behavior, which may not be the same as for a particular structural change. With carbon steels the evidence of the behavior of the 0.15 per cent carbon and 0.4 per cent carbon steels, normalized and spheroidized, suggests that for this case the behavior of the massive carbide does reflect the action of the carbide dissolved in the ferrite, since if they were different, the two thermal treatments chosen to produce the same degree of carbide spheroidization as determined by $\alpha = 33{,}000$ would result in different creep behavior. But, taking the evidence of the two steels together, it may be concluded that the effect as shown by the creep test results was substantially the same. This justifies AB in Fig. 12 as satisfactorily representing thermal-action effect. As indicated earlier, however, general sanction should not be assumed for structural change as a criterion of thermal-action effect upon creep. Reason was given, however, for believing that AB would generally be to the right of AC as in Fig. 12. The question is where AB should fall, or what the magnitude of the index α should be.

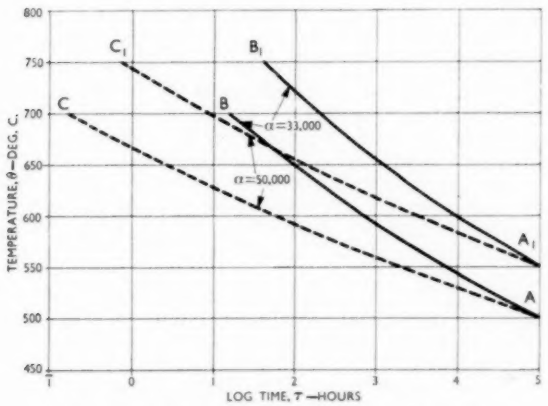

FIG. 12 TEMPERATURE θ, LOG TIME (τ) DIAGRAM

If structural change as a criterion is uncertain, a more satisfactory one is needed, and as it is also necessary to foresee the probable influence of thermal action upon creep, as is shown, for example, by Fig. 1, a magnitude of α can be found by determining the effect of thermal action by heating at two or more temperatures, and by determining the α from the corresponding heating times and temperatures to produce the same change in the time t' given by the creep test used to represent creep behavior. This may appear to be a simple and direct method but its features need consideration. The creep test itself, at temperature $\theta + 273$ deg C, adds thermal-action effect to that of the prior heating, and it will be assumed that α would be the same for both stages. The thermal action of the creep test can be expressed as a corresponding time at each temperature T_1 and T_2 used for heating, but as this addition varies between zero at the beginning of the test and the full value at the end, a mean value of one half may be taken for the test, or the time at the test temperature $\theta + 273$ deg C would be taken as $^1/_2t'$.

Let

τ_1' = time at temperature T_1 equivalent in thermal action to that of the creep test for time $^1/_2t'$ at the temperature $\theta + 273$

τ_2' = time at temperature T_2 equivalent in thermal action to that of the creep test for time $^1/_2t'$ at the temperature $\theta + 273$

τ_1 = time for the prior heating without stress at the temperature T_1

τ_2 = time for the prior heating without stress at the temperature T_2

$\bar{\tau}_1 = \tau_1 + \tau_1'$, total equivalent time of heating at the temperature T_1

$\bar{\tau}_2 = \tau_2 + \tau_2'$, total equivalent time of heating at the temperature T_2

$$\tau_1' = \tfrac{1}{2}\, t' e^{\alpha\left(\frac{1}{T_1} - \frac{1}{\theta + 273}\right)};\quad \tau_2' = \tfrac{1}{2} t' e^{\alpha\left(\frac{1}{T_2} - \frac{1}{\theta + 273}\right)}$$

$$\tau_1'/\tau_2' = e^{\alpha\left(\frac{1}{T_1} - \frac{1}{T_2}\right)};\quad \bar{\tau}_1/\bar{\tau}_2 = e^{\alpha\left(\frac{1}{T_1} - \frac{1}{T_2}\right)} = \frac{\tau_1 + \tau_1'}{\tau_2 + \tau_2'} = \frac{\tau_1'}{\tau_2'}$$

and corresponding times are proportional, or

$$\tau_1/\tau_1'/\bar{\tau}_1 = \tau_2/\tau_2'/\bar{\tau}_2$$

Therefore the value of α obtained for the preheating times τ_1 and τ_2 at temperatures T_1 and T_2 to produce the same time t' by the creep test at temperature $\theta + 273$ deg C would not be modified by taking into account the thermal action added during the creep test. The reliability of this conclusion depends, of course, upon the validity of the assumption that the same magnitude of α would apply to the thermal-action process during the heating period and during the creep test. In the event of difference the error should be minimized by choosing the creep test to minimize the thermal-action effect during the creep test. The value of α obtained would determine AB in Fig. 12.

As mentioned, it is desirable to accelerate the creep tests to minimize a possible error of an assumption, and also to shorten the times t' of testing, determining the pattern of creep behavior shown by Fig. 1, as dependent upon thermal action. The thermal-action effect introduced by the creep test can be minimized by making the test temperature lower than the temperatures at which heating is applied, and also by increasing stress, or by employing both means. The function of the test is that of a comparator to measure, with creep as the criterion, a specific change produced by thermal action.

Having arrived at a value of α for AB, and assumed an approximate temperature for A, perhaps the most satisfactory way of incorporating an appropriate measure of thermal-action effect into the procedure, because of the difference between AC and AB, would be to determine in the usual way the first point at the high-temperature end of AC and to repeat the test with material heated prior to testing to give it the thermal-action effect corresponding with the difference between the test time and the corresponding time given by AB. Thereby, the full thermal action would be reached in the repeat test, approximately by the end of the test. If there were appreciable weakening because of the added thermal action, the second test time would be less than the first and the total thermal-action effect would be less than the full service amount. On the other hand, the reduced test time would most probably be less than it would have been had the thermal-action effect been spread over the whole period of the test, and in this

respect the resulting time would most probably be on the safe side.

This preliminary testing would have given some idea of the importance of thermal-action effect for the case concerned. A second point in AB at a lower temperature could similarly be determined, and if it appeared to be of consequence an alteration could be made in the temperature of A and a corresponding adjustment in the position of AB. A check test made at the first temperature, with preheating modified to correspond with the new position of AB, would show whether any significant change in the time had been caused by the change. The tests at the highest temperature might be chosen to occupy about 100 hours and the next, say, 500–1000 hours. Extrapolated time for the test at the next lower temperature could be used in conjunction with AB to determine the preheating to be applied, which for time saving would be made at a suitable high temperature, the time of heating being the same proportion of the time given by AB, as is suggested by the extrapolation of the test time. Obtaining corrected test points of AC in this way, a much more reliable extrapolation can be made where there is important thermal action present, which may produce its major effects over the period 10,000–100,000 hours, and which may thus be inadequately represented by the test data of Procedure 4 without correction. But this correction depends upon a reliable and satisfactory criterion being found for measuring thermal-action effect to enable the position of AB in Fig. 12 to be determined.

Experimental investigation of different alloys would probably establish approximate values of α for different classes, just as it was found that $\alpha = 33{,}000$ applied to carbon steels generally, and to a 0.5 per cent molybdenum steel as judged by carbide spheroidization. It is most probable, however, that α would have different values for ferritic and austenitic steels. But, having an approximate idea of α to determine AB, the higher temperature tests of Procedure 4, with time corrected as suggested in the foregoing, would provide a comparatively short-time procedure for assessing the potentialities of a material taking into account thermal-action effect.

Appendix 3

References

Bailey, R. W. 1935 Proc. I. Mech. E., vol. 131, p. 131, "The Utilization of Creep Test Data in Engineering Design."
1951 Proc. I. Mech. E., vol. 164, p. 324, "Steam Piping for High Pressures and High Temperatures."

Bailey, R. W., and Roberts, A. M. 1932 Proc. I. Mech. E., vol. 122, p. 209, "Testing of Materials for Service in High-Temperature Steam-Plant."

Dickenson, J. H. S. 1922 Jl. Iron and Steel Inst., vol. 106, p. 103, "Some Experiments on the Flow of Steels at a Low Red Heat, With a Note on the Scaling of Heated Steels."

Glen, J. 1948 Jl. Iron and Steel Inst., vol. 158, p. 37, "Creep Properties of Molybdenum, Chromium-Molybdenum, and Molybdenum-Vanadium Steels."

Kirkby, H. W., and Sykes, C. 1952 Iron and Steel Inst. Special Report No. 43, Symposium on High-Temperature Steels and Alloys for Gas Turbines, "Properties of Chromium Nickel Niobium Austenitic Steel."

Mechanical Engineering 1951, vol. 73, p. 867, "Interpretations of Code for Pressure Piping."

Robinson, E. L. 1940 Proc. Am. Soc. Testing Materials, vol. 40, p. 811, "High Temperature Rupture and Creep Tests."

Thielemann, R. H. 1940 Proc. Am. Soc. Testing Materials, vol. 40, p. 788, "Some Effects of Composition and Heat Treatment on the High-Temperature Rupture Properties of Ferrous Alloys."

Timken Roller Bearing Co. 1939 "Digest of Steels for High Temperature Service," fourth edition, p. 83.

Polyaxial Stress-Strain Relations of a Strain-Hardening Metal[1]

By S. B. BATDORF[2] and BERNARD BUDIANSKY[3]

The authors assess a plastic stress-strain law of anisotropic strain-hardening type which they previously developed on the basis of explicit consideration of the polycrystalline nature of metals and the mechanism of plastic deformation. The assumptions made are reviewed, together with the successes and limitations of the theory. The authors indicate the lines along which they feel that improvement of the theory is to be sought.

Introduction

WITHIN the elastic range the stress-strain relations for isotropic structural materials are remarkably simple. The equations are linear, and the differences between various materials are completely characterized (to engineering accuracy) by two parameters, usually chosen to be Young's modulus and Poisson's ratio.

Beyond the elastic limit, a wide variation in behavior is exhibited, and a number of different formulations approximating different types of physical behavior encountered in practice have been developed and explored analytically. The simplest of these formulations is the so-called ideal plasticity, which neglects not only viscous effects (as do also all other theories to be discussed in this paper) but also any strain-hardening effects. This theory is useful for the analysis of problems involving materials having a rather flat stress-strain curve and is so well developed as to have reached the textbook stage (1, 2).[4]

Stress-strain laws for strain-hardening materials were investigated initially on the assumption of isotropic strain hardening. The theory underlying this type of stress-strain law was perfected during the 1940's largely by Prager and his associates (see references 3 to 5 for review of this work). The approach used was to make assumptions regarding the general form of the stress-strain law and then extract as much information as possible about the specific form of the law by exploiting such fundamental concepts as the tensor character of stress and strain, continuity, work hardening, uniqueness, and so on.

It was soon recognized that the existence of the Bauschinger effect implies that strain hardening must, in reality, be anisotropic (6) and, consequently, very general theories, admitting any kind of anisotropy, have been proposed (7, 8, 9). Unfortunately, these general theories have not as yet been particularly fruitful from a practical point of view, for when the assumption of isotropic strain hardening is relinquished, the stress-strain law becomes too vague to be of much use. For lack of something better, isotropic strain-hardening laws have continued to be used, especially since there was reason to feel that the actual anisotropy might not be sufficient to impair their accuracy seriously. Support for this view could be found in the classic yield-point experiments of Taylor and Quinney (10) and in the more recent variable stress-ratio experiments reported by Morrison and Shepherd (11). The latter authors conclude, in fact, that the discrepancy between the simplest isotropic strain-hardening theory of incremental type (sometimes called Laning's law) and experimental data was no greater than the discrepancy that reasonably might be expected to occur in data from different specimens of nominally identical material.

On the other hand, experiments by Dow and his associates (12), Shaw and Wycherly (13), and Marin and Hu (14) tend to discredit the view that the assumption of isotropic strain hardening is an acceptable one. Without going into detail with respect to these various experiments, it may be noted in passing that those tending to support isotropic strain hardening were carried out at considerably higher values of plastic strain than those tending to discredit it. The significance of this observation will become evident from the following discussion of the Bauschinger effect.

A small plastic tensile prestrain results in a decrease in compression yield stress; whereas a large plastic tensile prestrain results in an increase in compression yield (15). This suggests that the plastic behavior is different at low strain from what it is at high strain, and, in particular, that the assumption of isotropic strain hardening might prove to be quite satisfactory at high strain and yet not be acceptable at low strain. A clue is afforded for a fresh attempt to develop a stress-strain law for anisotropic strain hardening by the explanation generally given for the Bauschinger effect (see for example reference 16). According to this explanation, at low plastic tensile strain some of the grains in the material suffer plastic extension while the rest remain elastic. When the external stress is removed, the extended grains are compressed and the remaining grains remain in tension. When external compression is applied, premature yielding occurs in those grains which already were in compression, resulting in a lowering of the compression yield stress for the material.

Therefore it would appear reasonable to base a theory for the anisotropic strain-hardening behavior of structural metals in the low strain range on an explicit consideration of their polycrystalline nature and of the differences in plastic response of the various grains to the applied stress. Such a theory was proposed by the authors in 1949 (17). The purpose of the present paper is to review the underlying assumptions of this theory, outline its principal successes and failures, and indicate the lines along which, in the opinion of the authors, improvement of the theory is to be sought.

Physical Assumptions and Theoretical Analysis

It is assumed, in the following, that a metal that is isotropic in the gross mechanical sense can be sufficiently approximated theoretically by an aggregation of randomly oriented crystals

---

[1] Most of the contributions of the first author reported in this paper were made while he was at the Langley Aeronautical Laboratory.

[2] Materials Engineering Department, Westinghouse Electric Corporation, East Pittsburgh, Pa. Mem. ASME.

[3] Langley Aeronautical Laboratory, Langley Field, Va.

[4] Numbers in parentheses refer to the Bibliography at the end of the paper.

Presented at the West Coast Meeting of the Applied Mechanics Division, San Francisco, Calif., June 21–23, 1954, of The American Society of Mechanical Engineers.

Discussion of this paper should be addressed to the Secretary, ASME, 29 West 39th Street, New York, N. Y., and will be accepted until January 10, 1955, for publication at a later date. Discussion received after the closing date will be returned.

Note: Statements and opinions advanced in papers are to be understood as individual expressions of their authors and not those of the Society. Manuscript received by ASME Applied Mechanics Division, July 1, 1953. Paper No. 54—APM-2.

which will be regarded as identical except for orientation; that is, effects of variations in grain size and shape will be ignored. Further, it will be assumed that the grain is the smallest structural unit requiring consideration so that local variations of stress within the grain can be neglected. It is felt that, without some such simplifications, the problem would be completely intractable. An additional simplifying assumption is that the material is elastically homogeneous, or alternatively that within the elastic range variations in stress from grain to grain can be neglected so that the local stress is equal to the average stress. This is not a bad assumption for metals having crystals which are fairly isotropic elastically, such as aluminum.

Next, the nature of the plastic deformation must be considered. A number of different mechanisms of plastic deformation exist, and opinions differ as to their relative importance. It is generally felt, however, that for structural metals at room temperature and normal rates of straining, and for strains not exceeding a few per cent, slip is the principal mechanism. Moreover, slip is probably the only mechanism sufficiently understood to be made the basis of a quantitative analysis, and, consequently, it is the sole mechanism considered in what follows.

In simple slip in single crystals, sliding occurs along certain parallel crystallographic planes in a crystallographically determined direction of easy slip, resulting in a permanent shear deformation of the crystal as a whole. The amount of this deformation depends upon the component in the slip direction of the shear stress on the slip plane. It is assumed that these same remarks apply to the slip in the grains of a polycrystal, but that the relation between resolved shear stress and resulting plastic shear strain differs in the polycrystal because of the impeding influence of the neighboring grains. For this reason, the theory is not constructed around single-crystal data, but rather around the plastic strain produced in an element of volume as a whole by the slip which takes place in grains having a particular orientation within the element.

Consider first a tiny sample of all the crystals in the volume, namely, those with slip planes having normals within the solid angle $d\Omega$ about the direction $\bar{n}_\Omega$, and slip directions within the element of angle $d\beta$ about the direction $\bar{n}_\beta$, Fig. 1. The number

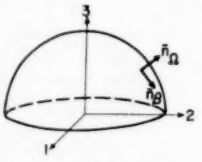

FIG. 1 SLIP-PLANE AND SLIP-DIRECTION ORIENTATION

of such grains per unit volume is proportional to the product $d\Omega d\beta$. It is plausible that the strain produced in the volume element by the plastic yielding of these grains will be a shear strain of the same orientation as that in the yielding grains, that it will be proportional to the number of such grains, and that it will depend in some fashion on the component of stress causing the plastic deformation. These assumptions lead to the following equation for the plastic strain in the volume element as a whole due to slip in the grains under consideration

$$d\gamma^P{}_{\Omega\beta} = F(\hat{\tau}_{\Omega\beta})d\Omega d\beta \quad \ldots\ldots [1]$$

Here, $d\gamma^P{}_{\Omega\beta}$ is a differential element of plastic shear strain referred to the axes $\bar{n}_\Omega$ and $\bar{n}_\beta$, $\tau_{\Omega\beta}$ is the corresponding shear stress and $\hat{\tau}_{\Omega\beta}$ is the largest value of $\tau_{\Omega\beta}$ in the history of loading. $F(\tau)$ is an odd, monotonically increasing function that is zero for τ less than the value at which yielding begins. The use in the equation of $\hat{\tau}_{\Omega\beta}$, rather than $\tau_{\Omega\beta}$, acts to preserve the plastic strain when $\tau_{\Omega\beta}$ is decreased in absolute value.

If each set of slipped grains makes an independent contribution to the deformation of the volume element as a whole, the total plastic strain in the 1,2,3-system of axes can be found by summing componentwise, just as in the case of resolution and addition of vectors. Thus

$$\left.\begin{aligned} \epsilon_{11}{}^P &= \int_H d\Omega \int_S d\beta F(\hat{\tau}_{\Omega\beta}) l_{1\Omega} l_{1\beta} \\ \gamma_{12}{}^P &= \int_H d\Omega \int_S d\beta F(\hat{\tau}_{\Omega\beta})(l_{1\Omega} l_{2\beta} + l_{2\Omega} l_{1\beta}) \end{aligned}\right\} \quad \ldots\ldots [2]$$

where (see Fig. 1) H denotes a hemisphere swept by $\bar{n}_\Omega$ and S a semicircle swept out by $\bar{n}_\beta$. The l are direction cosines corresponding to the pairs of directions denoted by their subscripts. Analogous expressions can be written for the remaining strain components; in fact, the stress-strain law can be written compactly in tensor notation as

$$\epsilon_{ij}{}^P = \frac{1}{2} \int_H d\Omega \int_S d\beta F(\hat{\tau}_{\Omega\beta})(l_{i\Omega} l_{j\beta} + l_{j\Omega} l_{i\beta}) \quad \ldots\ldots [3]$$

It is evident that these equations furnish a basis for finding the strain in a volume element resulting from any stress history, provided that the function $F(\tau)$ is known for the material. Fortunately, this function can be determined readily from a simple tensile test. A simple approximate method for accomplishing this purpose is to expand F as a Taylor series, integrate the first of Equations [2], and determine the desired number of coefficients in the series by fitting a corresponding number of points in the stress-strain curve (17). A better method may be to solve an integrodifferential equation for F, which was derived by Cicala (18) as one of several elegant contributions to the theory.

While it is evident that the stress-strain law written permits a unique calculation of strain at a point in terms of stress history at the same point, the questions arise whether our "slip theory" satisfies the various mathematical and physical requirements demanded of all plasticity theories, and whether it constitutes a theory that is applicable to the solution of boundary-value problems. These questions have been explored in detail (19) and it has turned out that the slip theory is indeed a bona fide mathematical theory in all respects, notwithstanding the fact that some of its mathematical features (such as nonlinearity between stress and strain increments) were decidedly unconventional at the time of its original promulgation. It has been shown further that, in connection with boundary-value problems, the slip theory obeys the Hodge-Prager minimum principle that holds (20) for a large class of linear incremental plasticity theories, of which the slip theory is not a member.

It appears, then, that the development outlined leads to an anisotropic strain-hardening plasticity theory applicable in principle, at least, to the solution of practical problems. It is not quite complete in that it does not predict explicitly the Bauschinger effect, and it rests upon a number of simplifying assumptions, some of which conform with the present state of knowledge while others are definitely limitations. These limitations constitute "dirt" in the theory. However, owing to the circumstance that the function F is determined empirically from a tensile test, the theory has considerable dirt-hiding capacity. The tensile stress-strain curve itself will be given correctly by the theory, of course, and if the actual behavior of the grains bears the same relation to the assumptions for other stress paths that it does for simple tension, it is possible that the theory may be reasonably accurate in spite of any limitations in its underlying assumptions. This possibility is best investigated by comparison with experiment.

Comparison With Experimental Data

One of the simplest experiments to analyze is that of biaxial tension with stress ratios kept constant. One such experiment was conducted by Osgood (21) with ratios of circumferential to axial stress equal to 0, 1/2, 1, 2, and ∞. For isotropic material, stress ratios 0 and ∞ are equivalent, and similarly 1/2 and 2 are equivalent. Moreover, the case of stress ratio 1 differs from uniaxial compression only by a hydrostatic pressure. Thus, the data for ratios 0, 1, and ∞ ideally should be equivalent and should serve as a basis for predicting the (ideally equivalent) data for stress ratios 1/2 and 2.

As it turned out, the experimental results for stress ratios 1/2 and 2 were not equivalent, indicating either anisotropy or a difference in material properties between specimens. However, the data fell generally in between the results for maximum-shear theory and octahedral-shear theory, as did also the prediction of the slip theory.

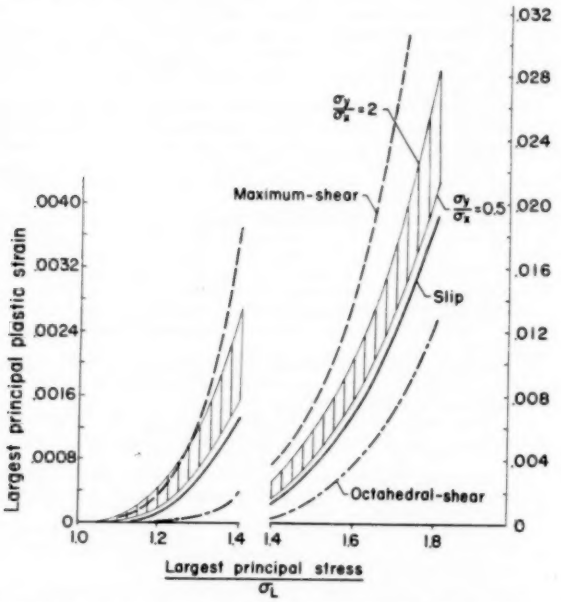

Fig. 2 Comparison of Plastic-Strain Theories With Experimental Data

A comparison of these results is shown in Fig. 2, taken from reference (22). The plastic strain in the direction of the smaller stress is not shown because it was essentially zero in accord with the predictions of all the theories. The general conclusion to be drawn from the comparison is that, for constant stress-ratio biaxial tension, the slip theory is rather satisfactory. Indeed, the theory illustrates its dirt-hiding capacity by giving good agreement with experiment at strains far above those for which the model employed reasonably could be expected to be valid.

A more severe test of theory is provided by the case of variable-stress ratios.

Consider the case in which the specimen is loaded in tension (or compression) into the plastic region and then shear stress is added. According to the slip theory, the elastic-plastic boundary before the addition of shear stress has a pointed corner, as shown in Fig. 3. (This feature, characteristic of the slip theory, is in sharp contrast to the smooth loading surfaces that, until recently, were the only kind assumed in other theories.) Cicala has shown that, at the stress σ_{x_0}, according to the slip theory, the initial shear stiffness G_{eff} deviates from the elastic value G_0 in the following fashion, depending on the ratio $(d\sigma/(d\tau)$

$$(a)\ \text{For all } \frac{d\sigma}{d\tau} > m, \quad G_{eff} = \frac{G_0}{1 + 3G_0\left(\frac{1}{E_s} - \frac{1}{E}\right)}$$

$$(b)\ \text{For all } \frac{d\sigma}{d\tau} < -m, \quad G_{eff} = G_0$$

while in the intermediate region, for

$$-m < \frac{d\sigma}{d\tau} < m$$

G_{eff} varies continuously between these two extreme values. (Here E_s is the secant modulus at the stress σ_{x_0}.) In contrast, Drucker's work (9) shows that all consistent plasticity theories embodying a smooth elastic plastic boundary after loading to σ_{x_0} imply that the initial G_{eff} equals G_0 for all subsequent loading paths.

In experiments conducted at the NACA (23), the initial shear stiffness and the subsequent plastic strains were explored systematically throughout the intermediate region. The initial shear stiffnesses were found to be G_0 throughout, in contradiction to the prediction of the slip theory. On the other hand, the subsequent plastic deformations themselves in the two tests performed with $(d\sigma)/(d\tau) < 0$ were in better accord with the slip theory than with other theories investigated.

It appears then, that in spite of a number of successes, the slip theory is not a satisfactory formulation of the polyaxial stress-strain relations of a polycrystalline aggregate. In the opinion of the authors, its limitations are due primarily to two causes: the neglect of the interaction between grains and the tacit assumption that only one slip system occurs in any one grain.

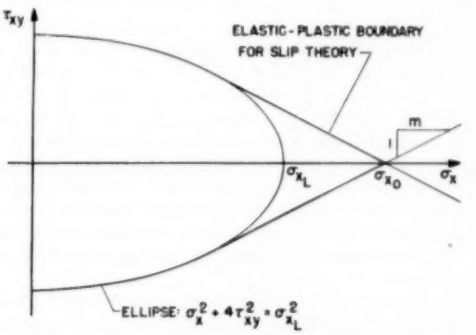

Fig. 3 Elastic-Plastic Boundary After Application of Compressive Stress σ_{x_0}

In an effort to assess the validity of some of the assumptions of the slip theory, a tensile specimen of commercially pure aluminum was polished, etched, and stretched plastically (24). A statistical analysis was then made of the angular distribution of slip lines observed in the various grains and compared with the assumptions of the slip theory (25).

The results are shown in Fig. 4 taken from reference (26). In this figure, the probability that a slip line will make an angle with the normal to the direction of tension equal to or less than θ is plotted against θ. The discrepancy between the experimental data and the prediction of the slip theory, labeled "single mode" in the figure, is quite large at high values of slip angle. The calculation of slip-angle distribution was revised in reference (26) to take into account the fact that aluminum has not one but 12 slip systems,

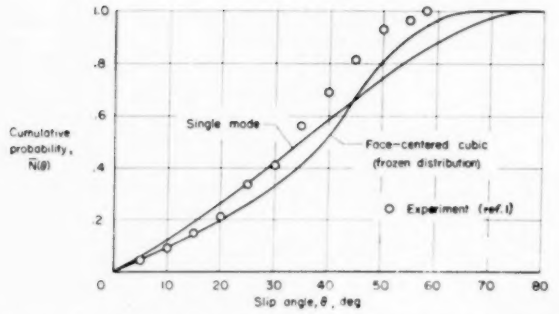

FIG. 4 THEORETICAL AND EXPERIMENTAL SLIP-ANGLE DISTRIBUTIONS, $\left(\frac{\sigma}{\sigma_{yield}} = 2\right)$

but the interaction between grains was still neglected. The angular distribution of slip lines found on this basis, labeled "face-centered cubic" in the figure, reduces the discrepancy between theory and experiment. The authors are inclined to feel that most of the discrepancy remaining probably could be eliminated by taking account of the interaction between grains, but a feasible method for accomplishing this result has not yet come to their attention.

CONCLUSION

The foregoing discussion shows that it is possible to develop a complete and self-consistent theory for the polyaxial stress-strain relations in the plastic range based on the physical mechanism of plastic deformation. In any theory of this type, a number of simplifying assumptions are required. Those used in the present paper have led to a theory (17) which is successful in a number of respects but unsatisfactory in others. It is felt that the principal sources of error are the neglect of the interaction between neighboring grains and the assumption that each grain has only a single slip system. At the present time, it is not clear whether a phenomenological theory such as some kind of generalized incremental theory, or a physical theory, i.e., one based on a physical model of the plastically deforming material, will first achieve success in correlating polyaxial-flow phenomena properly.

The authors do not wish to urge the merits of either type of approach as intrinsically superior. They do, however, wish to emphasize that the partial success of the present attempt encourages the view that reasonable prospects of success are associated with the physical approach.

BIBLIOGRAPHY

1 "Theory of Perfectly Plastic Solids," by William Prager and Philip G. Hodge, Jr., John Wiley & Sons, Inc., New York, N. Y., 1951.

2 "The Mathematical Theory of Plasticity," by R. Hill, Oxford University Press, London, England, 1950.

3 "The Stress-Strain Laws of the Mathematical Theory of Plasticity—A Survey of Recent Progress," by W. Prager, Trans. ASME, vol. 71, 1949, pp. 226–233.

4 "Stress-Strain Relations in the Plastic Range—A Survey of Theory and Experiment," by D. C. Drucker, Rep. A11-S1, Graduate Division of Applied Mathematics, Brown University, Providence, R. I., December, 1950.

5 "On the Stress-Strain Relations of Plastic Deformation," by J. P. Benthem, Report S. 398, National Luchtvaartlaboratorium, Amsterdam, 1951.

6 "Relation of Experiments to Mathematical Theories of Plasticity," by D. C. Drucker, Trans. ASME, vol. 71, 1949, pp. 349–357.

7 "Recent Developments in the Mathematical Theory of Plasticity," by W. Prager, *Journal of Applied Physics*, vol. 20, 1949, pp. 235–241.

8 "Some Implications of Work Hardening and Ideal Plasticity," by D. C. Drucker, *Quarterly of Applied Mathematics*, vol. 7, January, 1950, pp. 411–418.

9 "A More Fundamental Approach to Plastic Stress-Strain Relations," by D. C. Drucker, Proceedings of the First U. S. National Congress for Applied Mechanics, Chicago, Ill., 1951.

10 "The Plastic Distortion of Metals," by G. I. Taylor and H. Quinney, Philosophical Transactions of the Royal Society of London, England, series A, vol. 230, 1931, pp. 323–362.

11 "An Experimental Investigation of Plastic Stress-Strain Relations," by J. L. M. Morrison and W. M. Shepherd, Proceedings of the Institution of Mechanical Engineers, vol. 163, 1950, pp. 1–9.

12 "Preliminary Experiments for Testing Basic Assumptions of Plasticity Theories," by R. W. Peters, N. F. Dow, and S. B. Batdorf, Proceedings of the Society of Experimental Stress Analysis, vol. 7, 1950, pp. 127–140.

13 "Experiments on the Plasticity of Metals 1. The Octahedral Shear Stress Loading Criterion," by F. S. Shaw and G. W. Wycherly, Structures and Materials, Note 181, Aero. Res. Labs., Australia, 1950.

14 "On the Validity of Assumptions Made in Theories of Plastic Flow of Metals," by Joseph Marin and L. W. Hu, Trans. ASME, vol. 75, 1953, pp. 1181–1190.

15 "Some Stress-Strain Studies of Metals," by R. L. Templin and R. G. Sturm, *Journal of the Aeronautical Sciences*, vol. 7, 1940, pp. 189–198.

16 "The Physics of Metals," by Fredrick Seitz, McGraw-Hill Book Company, Inc., New York, N. Y., 1943.

17 "A Mathematical Theory of Plasticity Based on the Concept of Slip," by S. B. Batdorf and Bernard Budiansky, NACA TN 1871, April, 1949.

18 "Sobre la teoría de Batdorf y Budiansky de la deformación plástica," by P. Cicala, Revista de la Universidad de Córdoba (Argentina), Ano XII, no. 2, 1950.

19 "Fundamental Theorems and Consequences of the Slip Theory of Plasticity," by B. Budiansky, PhD thesis, Brown University, 1950.

20 "On the Variational Principles of Plasticity," by H J. Greenberg, Rep. A11-S4, Graduate Division of Applied Mathematics, Brown University, March, 1949.

21 "Combined-Stress Tests on 24S-T Aluminum Alloy Tubes," by W. R. Osgood, JOURNAL OF APPLIED MECHANICS, Trans. ASME, vol. 69, 1947, p. A-147.

22 "The Interpretation of Biaxial-Tension Experiments Involving Constant Stress Ratios," by S. B. Batdorf, NACA TN 2029, February, 1950.

23 "Experimental Studies of Polyaxial Stress-Strain Laws of Plasticity," by B. Budiansky, N. F. Dow, R. W. Peters, and R. P. Shepherd, Proceedings of the First U. S. National Congress of Applied Mechanics, Chicago, Ill., 1951.

24 "A Study of Slip Formation in Polycrystalline Aluminum," by A. E. Johnson, Jr., and S. B. Batdorf, NACA TN 2576, 1951.

25 "On the Angular Distribution of Slip Lines in Polycrystalline Aluminum Alloy," by J. M. Hedgepeth, S. B. Batdorf, and J. Lyell Sanders, Jr., NACA TN 2577, 1951.

26 "Theoretical Distribution of Slip Angles in an Aggregate of Face-Centered Cubic Crystals," by J. M. Hedgepeth, NACA TN 2777, August, 1952.

The Existence and Stability of Ultraharmonics and Subharmonics in Forced Nonlinear Oscillations

By T. K. CAUGHEY,[1] PASADENA, CALIF.

A study is made of the forced oscillations of a second-order system having a small cubic nonlinearity in the restoring force. It is shown that under suitable conditions ultraharmonic or subharmonic motion exists in addition to the harmonic motion which a linearized theory would predict. By studying the stability of such motions it is shown that at points on the amplitude frequency-response curves having vertical tangents, instability and consequently "jumps" occur. A study of the dependence of the motion on the initial conditions reveals that while ultraharmonic and harmonic motions are rather insensitive to initial conditions, the existence of subharmonic motion can be achieved only for a restricted set of initial conditions.

Nomenclature

The following nomenclature is used in the paper:

- A = amplitude of harmonic motion
- ϕ = phase angle between harmonic motion and forcing function
- U = amplitude of predominant component of ultraharmonic motion
- β = phase angle between ultraharmonic motion and harmonic motion
- S = amplitude of predominant component of subharmonic motion
- γ = phase angle between subharmonic and harmonic motion
- P = amplitude of forcing function
- A_o, ϕ_o, etc. = steady-state values of A, ϕ, etc.
- ξ, η = small perturbations on the steady-state amplitude and phase
- λ = exponent of ξ, η in perturbation equations
- $\Omega' = 3\Omega$
- $\Omega'' = \frac{1}{3}\Omega$
- $0(\mu)$ = a quantity of order μ
- K = damping factor
- ω = linear natural frequency of system
- μ = small parameter indicating magnitude of nonlinearity

[1] Instructor in Applied Mechanics, Division of Engineering, California Institute of Technology.

Presented at the West Coast Conference of the Applied Mechanics Division, University of California, Berkeley, Calif., June 21–23, 1954, of The American Society of Mechanical Engineers.

Discussion of this paper should be addressed to the Secretary, ASME, 29 West 39th Street, New York, N. Y., and will be accepted until January 10, 1955, for publication at a later date. Discussion received after the closing date will be returned.

Note: Statements and opinions advanced in papers are to be understood as individual expressions of their authors and not those of the Society. Manuscript received by ASME Applied Mechanics Division, March 5, 1954. This paper was not preprinted.

Ultraharmonics and Subharmonics in Forced Nonlinear Oscillations

In essence, all problems encountered in mechanics are nonlinear in nature, and the linearizations commonly used are only approximations, though in many cases they are quite satisfactory for all practical purposes. However, there are also many cases in which a linearized theory fails completely to explain phenomena which occur in a nonlinear system. The aim of this paper is to focus attention on some features of the problem in which nonlinearity results in essentially new phenomena; no attempt is made to improve on those phenomena which can be predicted by linear theory. Unfortunately, no exact method exists for solving nonlinear problems and recourse must be made to approximate techniques, and in using such techniques one must be guided by the physics of the problem.

A differential equation of the following form occurs in many different physical problems

$$\frac{d^2y}{dt^2} + K\frac{dy}{dt} + \omega^2 y + \mu F\left(y, \frac{dy}{dt}\right) = P\cos(\Omega t + \alpha) \quad [1]$$

$$\mu F\left(y, \frac{dy}{dt}\right) \ll \omega^2 y,\ P \ll \omega^2,\ K\frac{dy}{dt} \ll \omega^2 y$$

where $F[y, (dy)/(dt)]$ is a nonlinear function of y and $(dy)/(dt)$.

From the theory of differential equations it is known that an equation such as Equation [1] possesses solutions $y(t)$ which are determined uniquely once the initial conditions are specified. In the case of a linear system, $\mu = 0$, there is only one periodic solution after transients have died out. Nonlinear systems possess the distinctive characteristic that various types of periodic solutions may exist depending on the initial conditions in the system and on the relative values of ω and Ω.

If the discussion is restricted to force oscillations of a system having a nonlinear restoring force, then there are three essentially new phenomena which are introduced:

(a) Predominantly harmonic solutions—such solutions have a period equal to that of the forcing function. Harmonic nonlinear solutions may exhibit jump phenomena—a feature which distinguishes them from linear harmonic solutions.

(b) Predominantly ultraharmonic motion—under suitable conditions a system may exhibit ultraharmonic solutions, in which the main component of the motion occurs at some integral multiple of the frequency of the forcing function. Ultraharmonic solutions exhibit jump phenomena similar to that which occurs in (a), the existence of such phenomena cannot be predicted on the basis of a linear theory.

(c) Predominantly subharmonic motion—a nonlinear system under suitable conditions may exhibit subharmonic motion in which the main component of the motion has a frequency which is a rational fraction of the forcing frequency.

The analysis which follows can be shown to hold for any anti-

symmetric nonlinearity, but for simplicity, only the cubic nonlinearity will be considered.

Predominantly Harmonic Solutions

Predominantly harmonic motion has received considerable attention in the literature on nonlinear mechanics,[2] and there is little new that can be added to the first-order theory. However, it has been thought desirable to include the harmonic case both for the sake of completeness and for comparison with the other two cases.

Consider the case in which $\mu F(y, (dy)/(dt))$ of Equation [1] is given by μy^3, then

$$\frac{d^2y}{dt^2} + K\frac{dy}{dt} + \omega^2 y + \mu y^3 = P\cos(\Omega t + \alpha) \quad [2]$$

In the case of predominantly harmonic motion, a solution of Equation [2] may be taken of the form[3]

$$y = A\cos(\Omega t + \phi), \quad \alpha = 0 \quad [3]$$

where A and ϕ are slowly varying functions of time. Substituting Equation [3] into Equation [2] and separately equating the terms containing $\sin(\Omega t + \phi)$ and $\cos(\Omega y + \phi)$ to zero, gives

$$-2\Omega\frac{dA}{dt} = \Omega AK + P\sin\phi \quad [4]$$

$$-2\Omega A_1\frac{d\phi}{dt} = (\Omega^2 - \omega^2)A - \frac{3}{4}\mu A^3 + P\cos\phi \quad [5]$$

where all second-order terms have been neglected.

Steady-State Conditions. The steady-state harmonic solutions corresponding to $(dA)/(dt) = 0$ and $(d\phi)/(dt) = 0$ are

$$\left.\begin{aligned} \Omega A_o K + P\sin\phi_o &= 0 \\ (\Omega^2 - \omega^2)A_o - \frac{3}{4}\mu A_o^3 + P\cos\phi_o &= 0 \end{aligned}\right\} \quad [6]$$

Eliminating ϕ_o gives

$$(\Omega K)^2 A_o^2 + \left[(\omega^2 - \Omega^2)A_o + \frac{3}{4}\mu A_o^3\right]^2 = P^2 \quad [7]$$

from which

$$\sin\phi_o = \frac{\pm\Omega A_o K}{\sqrt{(\Omega K)^2 A_o^2 + \left[(\omega^2 - \Omega^2)A_o + \frac{3}{4}\mu A_o^3\right]^2}} \quad [8]$$

As later analysis will show that the points at which the amplitude/frequency-response curve possesses vertical tangents are points of instability, for this reason the loci of vertical tangency play an important role in determining the stability of the system.

From Equation [7] the loci of vertical tangency are readily obtained; they are

$$(\Omega K)^2 + \left(\omega^2 - \Omega^2 + \frac{3}{4}\mu A_o^2\right)\left(\omega^2 - \Omega^2 + \frac{9}{4}\mu A_o^2\right) = 0 \quad [9]$$

if $\Omega K \ll \omega^2$ the upper branch being given by

$$\omega^2 - \Omega^2 + \frac{3}{4}\mu A_o^2 = 0$$

the lower branch by

$$\omega^2 - \Omega^2 + \frac{9}{4}\mu A_o^2 = 0$$

From Equation [8] it will be observed that on the upper loci

$$\sin\phi_o \doteq \pm 1, \quad \phi_o \doteq \frac{\pi}{2}, \frac{3\pi}{2}, \text{ etc.} \quad [10]$$

Stability of Steady-State Solutions. Let $A = A_o + \xi$ and $\phi = \phi_o + \eta$; then writing perturbations on Equations [4] and [5]

$$\left.\begin{aligned} -2\Omega\frac{d\xi}{dt} &= \Omega K\xi + P\cos\phi_o\eta \\ -2\Omega A_o\frac{d\eta}{dt} &= (\Omega^2 - \omega^2)\xi - \frac{9}{4}\mu A_o^2\xi - P\sin\phi_o\eta \end{aligned}\right\} \quad [11]$$

Assuming solutions of the form $e^{\lambda t}$, and replacing $P\cos\phi_o$ and $P\sin\phi_o$ from Equation [6]

$$\left.\begin{aligned} -(2\Omega\lambda + \Omega K)\xi &= \left[(\omega^2 - \Omega^2)A_o + \frac{3}{4}\mu A_o^3\right]\eta \\ \left[(\omega^2 - \Omega^2) + \frac{9}{4}\mu A_o^2\right]\xi &= (2\Omega\lambda + \Omega K)\eta \end{aligned}\right\} \quad [12]$$

From which, if $A_o \neq 0$

$$(2\Omega\lambda)^2 + (2\Omega\lambda)(\Omega K) + (\Omega K)^2 + \left[(\omega^2 - \Omega^2) + \frac{3}{4}\mu A_o^2\right]\left[(\omega^2 - \Omega^2) + \frac{9}{4}\mu A_o^2\right] = 0 \quad [13]$$

For stability, $\Omega K > 0$, a condition which is always satisfied for $K > 0$, and

$$(\Omega K)^2 + \left[(\omega^2 - \Omega^2) + \frac{3}{4}\mu A_o^2\right]\left[(\omega^2 - \Omega^2) + \frac{9}{4}\mu A_o^2\right] \geqslant 0 \quad [14]$$

The last condition is simply the requirement that A_o lie outside the region enclosed by the loci of vertical tangency, as defined by Equation [9].

Fig. 1 shows a typical amplitude/frequency-response curve for the case of predominantly harmonic motion; at points P and Q where $|A_o|$ enters the region of instability, vertical jumps PR, QS occur. The general features of Fig. 1 have been described by many authors so there is no need to repeat them here.

So far, it has been shown that in the region $\omega' < \Omega < \omega''$ two stable solutions may exist; the conditions which determine the existence of a particular solution will now be examined.

Effect of Initial Conditions on Steady-State Solutions. In order to study the effect of initial conditions on the steady-state conditions, it is necessary to obtain the integral curves for the motion; this can be done by eliminating time between Equations [4] and [5]

$$\frac{dA}{d\phi} = \frac{(\Omega K + P\sin\phi)A}{A(\Omega^2 - \omega^2) - \frac{3}{4}\mu A^3 + P\cos\phi} \quad [15]$$

The simplest case to discuss is that in which $K = 0$, then

$$\frac{dA}{d\phi} = \frac{PA\sin\phi}{A(\Omega^2 - \omega^2) - \frac{3}{4}\mu A^3 + P\cos\phi} \quad [16]$$

[2] References (1, 2, 3) contain extensive bibliographies on harmonic solutions. Numbers in parentheses refer to the Bibliography at the end of the paper.

[3] E. Trefftz (4) points out that if a solution of Equation [2] is stable, it ultimately must lead to a periodic solution whose period is equal to that of the forcing function, or to some integral multiple of that period.

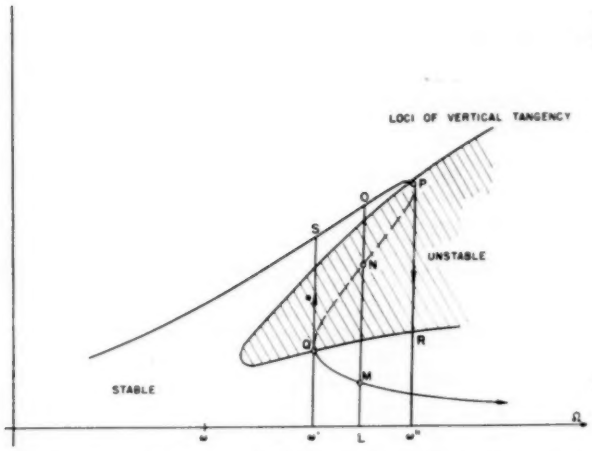

FIG. 1 TYPICAL AMPLITUDE/FREQUENCY RESPONSE FOR HARMONIC OSCILLATIONS

Such an equation has singular points at

$$\left.\begin{aligned} PA \sin \phi &= 0 \\ A(\Omega^2 - \omega^2) - \frac{3}{4}\,\mu A^3 + P \cos \phi &= 0 \end{aligned}\right\} \quad \ldots\ldots [17]$$

from which

$$\left.\begin{aligned} \sin \phi_o &= 0 \\ \left[A(\Omega^2 - \omega^2) + \frac{3}{4}\,\mu A^3\right]^2 &= P^2 \end{aligned}\right\} \quad \ldots\ldots [18]$$

If $\omega' < \Omega < \omega''$, then Fig. 1 shows that there are three singular points (Table 1).

TABLE 1 CLASSIFICATION OF SINGULAR POINTS

No.	Amplitude A_o	Phase ϕ_o	Classification
1	LM	π	center–stable
2	LN	π	saddle point –unstable
3	LO	0	center–stable

In the case where $K = 0$, Equation [15] can be integrated to give the integral curve

$$A^2(\Omega^2 - \omega^2) - \frac{3}{8}\,\mu A^4 + 2PA \cos \phi = \text{const.} \quad \ldots\ldots [19]$$

Fig. 2 shows some typical integral curves for the case of harmonic oscillations with three singular points.

For stable harmonic oscillations, the initial conditions must be inside region *A-B-C-D*. If the initial conditions lie inside region *A-E-F-G*, oscillation will be about center No. 1, and if inside *A-B-C-D-G-F-E*, the oscillations will be about center No. 3.

From this simple example it will be seen that the amplitude is determined completely once the initial conditions have been specified.

Effect of Damping. Qualitatively, the effect of introducing a small amount of damping into the system will be to convert the centers into stable focal points and to prevent closure of the separatrix. If the initial conditions lie within the region *A-E-F-G*, the oscillations will spiral down to focal point No. 1, and if they lie within the other region the oscillations will spiral down to focal point No. 3.

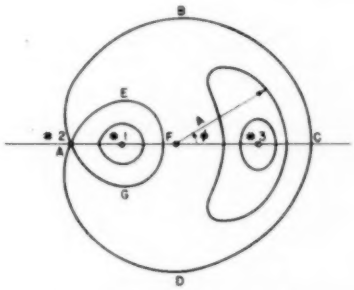

FIG. 2 TYPICAL INTEGRAL CURVES FOR HARMONIC OSCILLATOR WITH THREE SINGULARITIES
(Polar plot of amplitude and phase.)

For a qualitative treatment of the effect of damping on a system with a cubic nonlinearity with $\omega = 0$, refer to (5).

ULTRAHARMONIC OSCILLATIONS

Under suitable conditions, a nonlinear system may exhibit marked ultraharmonic oscillations in which the main component of motion has a frequency which is an integral multiple of the frequency of the driving force. In the case of a cubic nonlinearity, marked ultraharmonic behavior has been observed experimentally when the frequency of the driving force is reduced to about one third of the natural frequency of the system.

In the spirit of Trefftz, one is led to try a solution of the form

$$\left.\begin{aligned} y = A \cos \Omega t + U \cos (3\Omega t + \beta) \\ \alpha \neq 0 \end{aligned}\right\} \quad \ldots\ldots [20]$$

We may prescribe the phase of the harmonic oscillation since the phase of the forcing function was left undetermined.

Substituting into Equation [1], equating separately to zero the coefficients of $\cos \Omega t$, $\sin \Omega t$, $\cos (3\Omega t + \beta)$, $\sin (3\Omega t + \beta)$, gives

$$\text{letting } 3\Omega = \Omega', \text{ then } \Omega' \doteq \omega \quad \ldots\ldots [21]$$

$$\therefore 2\Omega' \frac{dU}{dt} + K\Omega' U = \mu \frac{A^3}{4} \sin \beta \quad \ldots\ldots [22]$$

$$2\Omega' U \frac{d\beta}{dt} = (\omega^2 - \Omega'^2)\, U + \mu \times \left(\frac{3}{2} A^2 U + \frac{3}{4} U^3 + \frac{A^3}{4} \cos \beta\right) \quad \ldots\ldots [23]$$

$$(\omega^2 - \Omega^2)A + \mu \left(\frac{3}{4} A^3 + \frac{3}{4} A^2 U \cos \beta + \frac{3}{2} A U^2\right) = P \cos \alpha \quad \ldots\ldots [24]$$

$$\Omega K A + \mu \frac{3}{4} A^2 U \sin \beta = P \sin \alpha \quad \ldots\ldots [25]$$

Considering Equations [24] and [25], eliminating α

$$P^2 = A^2 \left\{\left[(\omega^2 - \Omega^2) + \mu \frac{3}{4} (A^2 + AU \cos \beta + 2U^2)\right]^2 + \left(\Omega K + \mu \frac{3}{4} AU \sin \beta\right)^2\right\} \quad \ldots\ldots [26]$$

and using Equation [25]

$$\sin\alpha = \frac{\Omega K + \mu\frac{3}{4}AU\sin\beta}{\sqrt{\left\{\left[(\omega^2-\Omega^2)+\frac{3}{4}(A^2+AU\cos\beta+2U^2)\right]^2+\left[\Omega K+\mu\frac{3}{4}AU\sin\beta\right]^2\right\}}} \quad \ldots [27]$$

$$\leqslant \frac{\Omega K + \mu\frac{3}{4}AU\sin\beta}{(\omega^2-\Omega^2)+0(\mu)} \leqslant 0(\mu)$$

Thus the phase angle α is a quantity of first order in μ at most.

Considering Equation [26]

$$P^2 = A^2[(\omega^2-\Omega^2)+0(\mu)]^2$$

$$\therefore A = \frac{P}{\omega^2-\Omega^2}+0(\mu^2) \quad \ldots [28]$$

Thus to the first order of small quantities

$$A \doteq \frac{P}{\omega^2-\Omega^2},\ \alpha \doteq 0$$

Steady-State Solutions. The steady-state ultraharmonic solution corresponds with

$$\frac{dU}{dt} = \frac{d\beta}{dt} = 0$$

which leads to

$$\left.\begin{aligned} K\Omega' U_o &= \mu\frac{A_o^3}{4}\sin\beta_o \\ U_o(\omega^2-\Omega'^2)+\mu\left(\frac{3}{2}A_o^2U_o+\frac{3}{4}U_o^3\right) &= -\mu\frac{A_o^3}{4}\cos\beta_o \end{aligned}\right\} \quad \ldots [29]$$

Eliminating β_o

$$\left(\mu\frac{A_o^3}{4}\right)^2 = (K\Omega')^2U_o^2+\left[(\omega^2-\Omega'^2)U_o+\mu\left(\frac{3}{2}A_o^2U_o+\frac{3}{4}U_o^3\right)\right]^2 \quad \ldots [30]$$

and if $U_o \neq 0$

$$\sin\beta_o = \frac{\pm K\Omega'}{\sqrt{\left\{(K\Omega')^2+\left[\omega^2-\Omega'^2+\mu\left(\frac{3}{2}A_o^2+\frac{3}{4}U_o^2\right)\right]^2\right\}}} \quad \ldots [31]$$

Loci of Vertical Tangency. Viewed as a function of U_o, the loci of vertical tangency can be obtained from Equation [30]; they are

$$(K\Omega')^2+\left[\omega^2-\Omega'^2+\mu\left(\frac{3}{2}A_o^2+\frac{3}{4}U_o^2\right)\right]\times\left[\omega^2-\Omega'^2+\mu\left(\frac{3}{2}A_o^2+\frac{9}{4}U_o^2\right)\right]=0 \quad \ldots [32]$$

If $\Omega' K \ll \omega^2$

the loci are given approximately by

$$\left.\begin{aligned} \omega^2-\Omega'^2+\mu\left(\frac{3}{2}A_o^2+\frac{3}{4}U_o^2\right)&=0 \\ \omega^2-\Omega'^2+\mu\left(\frac{3}{2}A_o^2+\frac{9}{4}U_o^2\right)&=0 \end{aligned}\right\} \quad \ldots [33]$$

As in the case of harmonic oscillations, it will be observed that on the upper loci

$$\sin\beta_o \doteq \pm 1;\ \text{i.e.,}\quad \beta_o \doteq \frac{\pi}{2}, \frac{3\pi}{2}, \text{etc.}$$

Stability of Steady State. Let

$$\left.\begin{aligned} U &= U_o+\xi \\ \beta &= \beta_o+\eta \end{aligned}\right\} \quad \ldots [34]$$

Writing perturbations on Equations [22] and [23]

$$\left.\begin{aligned} 2\Omega'\frac{d\xi}{dt}+K\Omega'\xi &= \mu\frac{U_o^2}{4}\cos\beta_o\eta \\ 2\Omega' U_o\frac{d\eta}{dt} &= \left[\omega^2-\Omega'^2+\mu\left(\frac{3}{2}A_o^2+\frac{9}{4}U_o^2\right)\right]\xi \\ &\quad -\mu\frac{A_o^3}{4}\sin\beta_o\eta \end{aligned}\right\} \quad \ldots [35]$$

Assuming solutions of the form $e^{\lambda t}$, and substituting for $\cos\beta_o$ and $\sin\beta_o$ from Equation [29]

$$\left.\begin{aligned} (2\Omega'\lambda+K\Omega')\xi &= \left[(\Omega'^2-\omega^2)U_o-\mu U_o\left(\frac{3}{2}A_o^2+\frac{3}{4}U_o^2\right)\right]\eta \\ \left[(\omega^2-\Omega'^2)+\mu\left(\frac{3}{2}A_o^2+\frac{9}{4}U_o^2\right)\right]\xi &= U_o(2\Omega'\lambda+K\Omega')\eta \end{aligned}\right\} \quad \ldots [36]$$

which leads to the characteristic equation

$$(2\Omega'\lambda)^2+(2\Omega'\lambda)(K\Omega')+\left\{(K\Omega')^2+\left[\omega^2-\Omega'^2+\mu\left(\frac{3}{2}A_o^2+\frac{9}{4}U^2\right)\right]\times\left[\omega^2-\Omega'^2+\mu\left(\frac{3}{2}A_o^2+\frac{3}{4}U_o^2\right)\right]\right\}=0 \quad \ldots [37]$$

For stability $K \geqslant 0$ and

$$(K\Omega')^2+\left[(\omega^2-\Omega'^2)+\mu\left(\frac{3}{2}A_o^2+\frac{9}{4}U_o^2\right)\right]\times\left[(\omega^2-\Omega'^2)+\mu\left(\frac{3}{2}A_o^2+\frac{3}{4}U_o^2\right)\right]\geqslant 0 \quad \ldots [38]$$

Comparison with Equation [32] shows that the second condition is simply the requirement that U_o lie outside the region enclosed by the loci of vertical tangency. If $\Omega K \ll \omega^2$ it will be observed from Equation [33] that the system cannot have vertical tangents unless

$$\Omega'^2 \geqslant \omega^2+\mu\frac{3}{2}A_o^2$$

that is

$$\Omega^2 \geqslant \frac{1}{9}\left(\omega^2+\mu\frac{3}{2}A_o^2\right) \quad \ldots [39]$$

Thus marked ultraharmonic behavior cannot occur unless the frequency of the exciting force is slightly above one third of the natural frequency of the system.

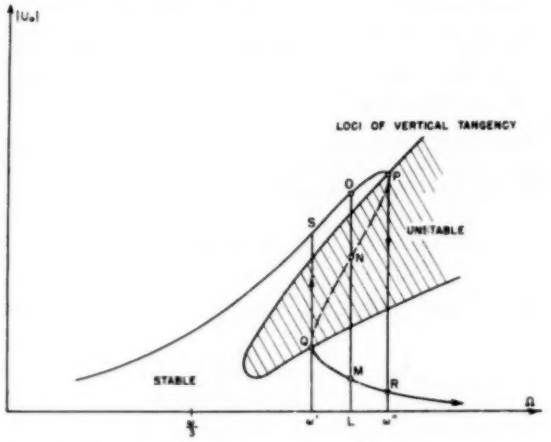

FIG. 3 TYPICAL AMPLITUDE/FREQUENCY RESPONSE FOR ULTRAHARMONIC MOTION OF ORDER THREE

Fig. 3 shows a typical amplitude/frequency-response curve for an ultraharmonic of order three. The general features of ultraharmonics are similar to those for harmonic oscillations. As frequencies below one third of the natural linear frequency, the amplitude is single-valued and small compared to A_o, the amplitude of the harmonic motion. In a small region close to one third of the linear natural frequency the amplitude becomes triple-valued, two values being stable and one unstable; in this region the ultraharmonic becomes quite large compared with the harmonic motion. At points P and Q where $|U_o|$ enters the unstable region, vertical jumps occur, exactly as in the harmonic case. As the frequency is raised further, the amplitude again becomes single-valued, and small compared with the harmonic amplitude. Only in the neighborhood of one third of the linear natural frequency does the amplitude of the ultraharmonic become comparable with that of the harmonic motion and hence, with the exception of this small region, ultraharmonic motion may be neglected in a first-order theory.

Effect of Initial Conditions on Ultraharmonic Solutions. The effect of the initial conditions on the ultraharmonic motion can best be studied by means of the integral curves for the motion. To obtain the integral curves for the motion, time can be eliminated between Equations [22] and [23] giving

$$\frac{dU}{d\beta} = \frac{\mu \frac{A^3}{4} U \sin\beta - K\Omega' U^3}{(\omega^2 - \Omega^2) U + \mu \left(\frac{3}{2} A^2 U + \frac{3}{4} U^3 + \frac{A^3}{4} \cos\beta \right)} \quad \ldots\ldots [40]$$

If damping is neglected Equation [40] becomes

$$\frac{dU}{d\beta} = \frac{\mu \frac{A^3}{4} U \sin\beta}{\left(\omega^2 + \frac{3}{2} A^2 - \Omega'^2\right) U + \mu \frac{3}{4} U^3 + \mu \frac{A^3}{4} \cos\beta} \quad \ldots\ldots [41]$$

Comparison of Equation [41] with Equation [34] shows that if

$$\left.\begin{array}{l} U \text{ is replaced by } A \\ \beta \text{ is replaced by } \phi \\ \mu \frac{A^3}{4} \text{ is replaced by } P \\ \omega^2 + \mu \frac{3}{2} A^2 \text{ is replaced by } \omega^2 \\ \Omega'^2 \text{ is replaced by } \Omega^2 \end{array}\right\} \quad \ldots\ldots [42]$$

then the two equations are identical in form, and the remarks made about harmonic motion will be equally true for ultraharmonic motion.

If the forcing frequency Ω lies in the range $\omega' < \Omega < \omega''$ (see Fig. 3) the amplitude Equation [30] has three solutions and if damping is neglected the singular points are as follows:

Number	Amplitude	Phase	Classification
1	LM	π	center–stable
2	LN	π	saddle point–unstable
3	LO	0	center–stable

[43]

Equation [41] can be integrated directly, to give

$$U^2\left(\omega^2 + \mu \frac{3}{2} A^2 - \Omega'^2\right) + \mu \frac{3}{8} U^4 + \mu \frac{UA^3}{2} \cos\beta = \text{const} \quad \ldots\ldots [44]$$

Fig. 4 shows some typical integral curves for the case of ultraharmonic motion with three singularities.

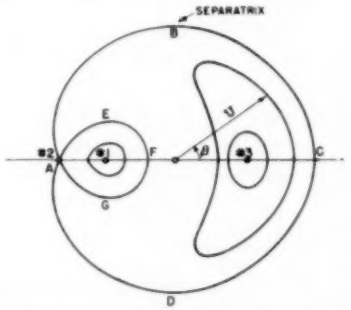

FIG. 4 TYPICAL INTEGRAL CURVES FOR ULTRAHARMONIC MOTION WITH THREE SINGULARITIES
(Polar plot of amplitude and phase.)

For stable ultraharmonic oscillations, the initial conditions must lie inside region *A-B-C-D*. If the initial conditions lie inside region *A-E-F-G*, oscillations will be about center No. 1, and if the initial conditions lie inside *A-B-C-D-F-G-E*, the oscillations will be about center No. 3. The effect of introducing a small amount of damping into the problem will be to change the centers into stable focal points and to prevent closure of the separatrix. It will still be true, however, that the separatrix will define two regions such that, if the inital conditions lie within one region the oscillations will spiral down to focal point No. 1, and if they lie inside the other region the oscillations will spiral down to focal point No. 3.

Thus the particular value of the steady-state ultraharmonic will be determined completely once the initial conditions have been specified.

Subharmonic Motion

Under suitable conditions a nonlinear system may exhibit subharmonic oscillations, in which the main component of the motion has a period which is an integral multiple of the period of the forcing function. In the case of a cubic nonlinearity, marked subharmonic behavior has been observed experimentally when the frequency of the forcing function is increased to about three times the linear natural frequency of the system.

Following Mandelstam and Papalexi (6), one is led to try a solution of the form

$$y = A \cos \Omega t + S \cos \left(\frac{\Omega}{3} t + \gamma \right) \quad \ldots\ldots [45]$$

$\alpha \neq 0$, S and γ are slowly varying functions of time. We may prescribe the phase of the harmonic solution since the phase of the exciting force is left undetermined. Let

$$\Omega'' = \frac{\Omega}{3} \doteq \omega \quad \ldots\ldots [46]$$

Substituting Equations [45] and [46] into Equation [1] and equating separately to zero the coefficients of $\sin (\Omega'' t + \gamma)$, $\cos (\Omega'' t + \gamma)$, $\sin \Omega t$ and $\cos \Omega t$, gives the first-order terms

$$\left.\begin{aligned} 2\Omega'' \frac{dS}{dt} + K\Omega'' S &= \mu \frac{3}{4} S^2 A \sin 3\gamma \\ 2\Omega'' S \frac{d\gamma}{dt} &= \left(\omega^2 + \frac{3}{2} \mu A^2 - \Omega''^2 \right) S \\ &\quad + \mu \frac{3}{4} (S^3 + S^2 A \cos 3\gamma) \end{aligned}\right\} \quad \ldots [47]$$

$$\left.\begin{aligned} (\omega^2 - \Omega^2) A + \mu \left(\frac{3}{4} A^3 + \frac{3}{2} A S^2 \right. \\ \left. + \frac{S^2}{4} \cos 3\gamma \right) &= P \cos \alpha \\ K\Omega A + \mu \frac{S^3}{4} \sin 3\gamma &= P \sin \alpha \end{aligned}\right\} \quad \ldots [48]$$

Eliminating α

$$\left.\begin{aligned} A^2 \left[\omega^2 - \Omega^2 + \frac{\mu}{4} (3A^2 + 6S^2) \right]^2 \\ + \mu \frac{A}{2} S^3 \cos 3\gamma \left[\omega^2 - \Omega^2 + \frac{\mu}{4} (3A^2 + 6S^2) \right] \\ + (K\Omega A)^2 + \mu \frac{A}{2} S^3 K\Omega \sin 3\gamma \end{aligned}\right\} = P^2 - \left(\frac{\mu S^3}{4} \right)^2 \quad \ldots [49]$$

Thus

$$A^2 [\omega^2 - \Omega^2 + 0(\mu)]^2 = P^2 - \left(\frac{\mu S^2}{4} \right)^2$$

$$\therefore A = \frac{\sqrt{\left[P^2 - \left(\frac{\mu S^3}{4} \right)^2 \right]}}{\omega^2 - \Omega^2} + 0(\mu^2) \quad \ldots\ldots [50]$$

and

$$\sin \alpha = \frac{K\Omega A + \mu \frac{S^3}{4} \sin 3\gamma}{\sqrt{\left[(\omega^2 - \Omega^2 + 0(\mu))^2 A^2 + \left(\frac{\mu S^3}{4} \right)^2 \right]}}$$

If $A \neq 0$

$$\sin \alpha = 0(\mu) \quad \ldots\ldots [51]$$

From Equation [50] it will be observed that A, the amplitude of the harmonic motion, is a quantity of first order in μ and hence the approximations made in deriving Equations [48] are justified on the grounds that the time derivative of A is a quantity of the second order in μ. In similar manner it can be shown that the variation of μA with respect to $S (A \neq 0)$ is a quantity of at most second order in μ; hence, in the stability equations, such a variation may be neglected.

Steady-State Subharmonic Motion. The steady-state subharmonic motion will be obtained from Equation [47] by setting $(dS)/(dt) = (d\gamma)/(dt) = 0$, whence

$$\left.\begin{aligned} K\Omega'' S_o &= \mu \frac{3}{4} S_o^2 A_o \sin 3\gamma_o \\ \left(\omega^2 + \frac{3}{2} \mu A_o^2 - \Omega''^2 \right) S_o + \mu \frac{3}{4} S_o^3 \\ = -\mu \frac{3}{4} S_o^2 A_o \cos 3\gamma_o \end{aligned}\right\} \quad \ldots [52]$$

where

$$A_o = \sqrt{P^2 - \left(\frac{\mu S^3}{4} \right)^2} \Big/ (\omega^2 - \Omega^2) \quad \ldots\ldots [53]$$

Eliminating γ_o from Equations [52]

$$\left(\frac{3}{4} \mu S_o^2 A_o \right)^2 = \left[\left(\omega^2 + \frac{3}{2} \mu A_o^2 - \Omega''^2 \right) S_o + \mu \frac{3}{4} S_o^3 \right]^2 + [K\Omega'' S_o]^2 \quad \ldots\ldots [54]$$

and if $S_o \neq 0$

$$\sin 3\gamma_o = \frac{\pm K\Omega''}{\sqrt{(K\Omega'')^2 + \left[\left(\omega^2 + \frac{3}{2} \mu A_o^2 - \Omega''^2 \right) + \mu \frac{3}{4} S_o^2 \right]^2}} \quad \ldots [55]$$

Loci of Vertical Tangency. Viewed as a function of S_o, the loci of vertical tangency are obtained from Equation [54] by differentiation; they are

$$S_o \left\{ \left[\omega^2 + \frac{3}{2} \mu A_o^2 - \Omega''^2 + \mu \frac{3}{4} S_o^2 \right] \times \left[\omega^2 + \frac{3}{2} \mu A_o^2 - \Omega''^2 + \mu \frac{9}{4} S_o^2 \right] + [K\Omega'']^2 - 2 \left(\frac{3}{4} \mu S_o A_o^2 \right) \right\} = 0$$

Making use of Equation [54], either

$$\left.\begin{aligned} S_o &= 0 \\ \text{or} \\ (K\Omega'')^2 + \left(\omega^2 + \frac{3}{2} \mu A_o^2 - \Omega''^2 \right)^2 \\ - \left(\mu \frac{3}{4} S_o^2 \right)^2 &= 0 \end{aligned}\right\} \quad \ldots [56]$$

If $\Omega K \ll \omega^2$ the second locus is given approximately by

$$\mu \frac{3}{4} S_o^2 = \left(\Omega''^2 - \omega^2 - \frac{3}{2} \mu A_o^2 \right)$$

It will be observed that if S_o lies on this locus then Equation [55] shows that

$$\sin 3\gamma_o = \pm 1;\ \text{i.e.,}\ 3\gamma_o = \frac{\pi}{2}, \frac{3\pi}{2}, \text{ etc.} \quad [57]$$

Stability of Steady-State Solutions. Let $S = S_o + \xi$ and $\gamma = \gamma_o + \eta$, then writing perturbations on Equation [47]

$$2\Omega'' \frac{d\xi}{dt} + K\Omega''\xi = \frac{3}{2}\mu S_o A_o \sin 3\gamma_o \xi + \frac{9}{4} S_o^2 A_o \cos 3\gamma_o \eta \quad [58]$$

$$2\Omega'' S_o \frac{d\eta}{dt} = \left(\omega^2 - \Omega''^2 + \frac{3}{2}\mu A_o^2\right)\xi - \mu\frac{9}{4} S_o^2 A_o \sin 3\gamma_o \eta + \mu\frac{3}{4}(3S_o^2 + 2S_o A_o \cos 3\gamma_o)\xi \quad [59]$$

Assuming solutions of the form $e^{\lambda t}$ and substituting for $\sin 3\gamma_o$ and $\cos 3\gamma_o$ from Equations [48] leads to the characteristic equation, $S_o \neq 0$

$$(2\Omega''\lambda)^2 + (2\Omega''\lambda)(2K\Omega'') - 3(K\Omega'')^2 + 3\left[\left(\frac{3}{4}\mu S_o^2\right)^2 - \left(\omega^2 - \Omega''^2 + \frac{3}{2}\mu A_o^2\right)^2\right] = 0 \quad [60]$$

For stability $K \geqslant 0$ and

$$\left(\frac{3}{4}\mu S_o^2\right)^2 - \left(\omega^2 - \Omega''^2 + \frac{3}{2}\mu A_o^2\right)^2 - (K\Omega'')^2 \geqslant 0 \quad [61]$$

It will be observed that this condition is simply the requirement that S_o lie outside the region enclosed by the loci of vertical tangency, as defined by Equation [56].

From Equations [58] and [59] it also can be shown that for stability $A_o S_o \cos 3\gamma_o \leqslant 0$, but since A_o is negative and S_o is positive, it follows that $\cos 3\gamma_o$ is positive. Thus those values of γ_o are admissible, for stable subharmonics, for which $\sin 3\gamma_o$ is given by Equation [55] and for which $\cos 3\gamma_o$ is positive.

If the damping is small, then except close to points of instability $\sin 3\gamma_o \doteq 0$, from which

$$\gamma_o = 0, \frac{\pi}{3}, \frac{2\pi}{3}, \pi, \frac{4\pi}{3}, \frac{5\pi}{3}$$

Since $\cos 3\gamma_o$ also must be positive, γ_o may take on only the values

$$\gamma_o = 0, \frac{2\pi}{3}, \frac{4\pi}{3} \quad [62]$$

Thus there exists three subharmonics with amplitude S_o but differing in phase by 120 deg.

From Equation [54] it will be observed that if $S_o \neq 0$

$$\left(\frac{3}{4}\mu S_o A_o\right)^2 = (K\Omega'')^2 + \left[\left(\omega^2 + \frac{3}{2}\mu A_o^2 - \Omega''^2\right) + \mu\frac{3}{4}S_o^2\right]^2$$

from which, regarding A_o as constant

$$\frac{3}{4}\mu S_o^2 = \left(\Omega''^2 - \omega^2 - \frac{9}{8}\mu A_o^2\right) \pm \sqrt{\left\{\frac{3}{4}\mu A_o^2\left(\Omega''^2 - \omega^2 - \frac{21}{16}\mu A_o^2\right) - (K\Omega'')^2\right\}} \quad [63]$$

For real values of S_o, Equation [63] requires that

$$\Omega''^2 = \frac{\Omega^2}{9} \geqslant \frac{\omega^2 + \mu\frac{21}{16}A_o^2}{1 - \frac{4}{3\mu}\frac{K^2}{A_o^2}} \quad [64]$$

This places both a lower and an upper bound on the frequency; if $\Omega K \ll \omega^2$, the lower bound is

$$\Omega^2 \geqslant 9\left(\omega^2 + \mu\frac{21}{16}A_o^2\right) \quad [65]$$

As the frequency increases beyond the value given by Equation [65], the denominator of Equation [64] decreases due to reduction of A_o, arising both from the increase in S_o and also from the rise in frequency, until a point is reached at which the equation cannot be satisfied. At this point S_o enters the unstable region and a vertical jump downward occurs.

The general features of the amplitude/frequency response for subharmonics of order one third are indicated in Fig. 5. For frequencies between ω' and ω'' three solutions of the amplitude equation exist, the two solutions corresponding to $|S_o|$ equal to zero, and $|S_o|$ equal to LN being stable, while the third solution $|S_o|$ equal to LM is unstable. At points A and B, where the upper branch of the amplitude curve intersects the upper locus of

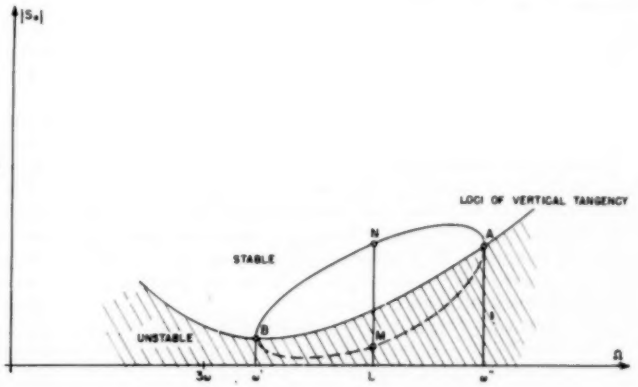

FIG. 5 (*right*) TYPICAL AMPLITUDE/FREQUENCY RESPONSE FOR SUBHARMONIC MOTION OF ORDER ONE THIRD

vertical tangency, vertical jumps occur, both downward. It will be observed that the general nature of subharmonic motion differs considerably from either harmonic or ultraharmonic motion.

Effect of Initial Conditions on Subharmonics of Order One Third. To get a more complete picture of subharmonics it is necessary to examine the dependence of the steady-state amplitude on the initial conditions. The easiest way to do this is by studying the integral curves for the motion; to this end time is eliminated between Equations [47] giving

$$\frac{dS}{d\gamma} = \frac{\mu \frac{3}{4} S^3 A \sin 3\gamma - K\Omega S^2}{\left(\omega^2 + \frac{3}{2}\mu A^2 - \Omega''^2\right) S + \frac{3}{4}\mu(S^3 + AS^2 \cos 3\gamma)} \quad \ldots\ldots [66]$$

If $K = 0$, then

$$\frac{dS}{d\gamma} = \frac{\mu \frac{3}{4} S^3 A \sin 3\gamma}{\left(\omega^2 + \frac{3}{2}\mu A^2 - \Omega''^2\right) S + \mu \frac{3}{4}(S^3 + AS^2 \cos 3\gamma)} \quad \ldots\ldots [67]$$

The singular points of Equation [67] are given by

$$\left.\begin{aligned} \mu \frac{3}{4} S^2 A \sin 3\gamma &= 0 \\ \left(\omega^2 + \frac{3}{2}\mu A^2 - \Omega''^2\right) S & \\ + \mu \frac{3}{4}(S^3 + S^2 A \cos 3\gamma) &= 0 \end{aligned}\right\} \ldots [68]$$

If $\omega' < \Omega < \omega''$ in Fig. 5, then the amplitude S_0 has three solutions 0, LM, and LN, while γ_0 has the values $0, \pi/3, 2\pi/3, \pi, 4\pi/3, 5\pi/3$. The nature of the singular points can be determined from Equations [56] and [57] (Table 2).

TABLE 2 CLASSIFICATION OF SINGULAR POINTS

No.	Amplitude	Phase	Classification
1	LN	0	center–stable
2	LM	π	saddle point–unstable
3	LM	$\pi/3$	saddle point–unstable
4	LN	$4\pi/3$	center–stable
5	LN	$2\pi/3$	center–stable
6	LM	$5\pi/3$	saddle point–unstable
7	0	indeterminate	center

Singularity No. 7 is phase unstable, but amplitude stable. If damping is neglected Equation [67] can be integrated to give

$$\left(\omega^2 + \mu \frac{3}{2} A^2 - \Omega''^2\right) \frac{1}{2} S^2 + \mu \frac{3}{4}\left(\frac{1}{4} S^4 + \frac{1}{3} S^3 A \cos 3\gamma\right) = \text{const} \ldots\ldots [69]$$

Fig. 6 shows the general features of the integral curves for subharmonic of order one third, when damping is neglected. If the initial conditions lie inside the shaded regions, stable subharmonic motion will result; outside these regions stable subharmonics cannot be obtained. This is quite different in nature from the case of harmonic and ultraharmonic motion in the fact that the second zone has shrunk down to zero.

Effect of Damping. Qualitatively, the effect of adding a small amount of damping to the system will be to transform the centers into stable focal points and to prevent closure of the separatrix. However, it will still be true that the separatrix will divide the plane into four regions, inside three of which stable harmonics will be obtained. For a quantitative discussion of the integral curves for subharmonic motion with damping, refer to (5) in which Dr. Hayashi discusses a system with a cubic nonlinearity but with the linear term omitted.

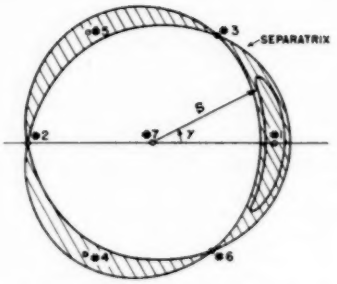

FIG. 6 TYPICAL INTEGRAL CURVES FOR SUBHARMONIC OSCILLATION OF ORDER ONE THIRD
(Polar plot of amplitude and phase.)

CONCLUSIONS

1 By a simple approximate nonlinear theory one is able to predict or verify phenomena in nonlinear systems which have no parallel in linear systems.

2 For the simple cubic nonlinearity considered here, the following conclusions can be made:

(*a*) Close to the linear natural frequency, predominantly harmonic motion exists.

(*b*) Slightly above one third of the linear natural frequency ultraharmonic motion of order three will predominate.

(*c*) Under suitable conditions, at frequencies slightly greater than three times the natural frequency, subharmonic motion may exist, of order one third.

(*d*) Cases (*a*), (*b*), and (*c*) exhibit jump phenomena, (*a*) and (*b*) being similar in behavior, case (*c*) being somewhat different in nature.

(*e*) The theory of differential equations requires that solutions of Equations [1] be unique once the initial conditions are specified, the property of uniqueness being retained by even the simple approximate method used in this paper.

3 Although the analysis presented was restricted to a cubic nonlinearity it can be shown that the results are true for any odd order polynomial nonlinearity. If a nonlinearity y^{2n+1} had been used in place of a cubic then it can be shown that stable ultraharmonics of orders $(2r + 1)$, $r = 1, 2, 3 \ldots$ exist and that subharmonics of order $1/(2r + 1)$ also exist.

The case of predominantly harmonic motion has been examined in some detail by Klotter and Pinney (7) and they have shown that similar results to those presented in the foregoing are obtained for any small antisymmetrical nonlinear function of the displacement.

The results of this analysis have been verified experimentally, using a simple analog computer. The dependence of the amplitude and phase on the various parameters was found to be in qualitative agreement with the theory. In particular, the occurrence of ultraharmonic, harmonic, and subharmonic motion, their jump behavior, and their phase relationship to the forcing function were found to be exactly as predicted.

ACKNOWLEDGMENTS

The author would like to express his thanks to Prof. D. E. Hudson of the Department of Engineering, California Institute of Technology, for his encouragement and for his many helpful suggestions in the preparation of this paper.

BIBLIOGRAPHY

1 "Ordinary Non-Linear Differential Equations," by N. W. McLachlan, Oxford University Press, Oxford, England, 1950.

2 "Non-Linear Mechanics," by N. Minorsky, Edwards Brothers, Ann Arbor, Mich., 1947.

3 "Theory of Oscillations," by A. A. Andranow and C. E. Chaikin, Princeton University Press, Princeton, N. J., 1949.

4 "Grundlagn der Schwingungstheorie," by E. Treffts, *Math. Ann.*, vol. 95, 1926, p. 307.

5 "Forced Oscillations With Non-Linear Restoring Force," by C. Hayashi, *Journal of Applied Physics*, vol. 24, 1953, pp. 198–207.

6 "Über Resonanzeracheinunger bei Frequensteilung," by L. Mandelstam and N. Papalexi, *Zeitschrift für Physik*, vol. 73, 1931, p. 227.

7 "Stability Criteria for Forced Vibrations in Non-Linear Syatems," by K. Klotter and E. Pinney, JOURNAL OF APPLIED MECHANICS, Trans. ASME, vol. 75, 1953, pp. 9–12.

Rigid-Plastic Analysis of Symmetrically Loaded Cylindrical Shells[1]

By P. G. HODGE, JR.,[2] BROOKLYN, N. Y.

A general method is presented for finding the stress and incipient velocity distribution in a symmetrically loaded cylindrical shell at collapse. The results are based upon a linearized yield surface, and a method is given for obtaining this linearized surface directly. The techniques are illustrated with reference to open and closed cylindrical shells under uniform external pressure. In each case the shell is specified completely by a single parameter c defined as the ratio of the half-length of the shell to the geometric mean of the radius and half-thickness; $c = L/\sqrt{at}$. It is found that for moderately large values of c, the limiting load is greater for the closed shell, while for small c the reverse is true.

Introduction

ALTHOUGH thin cylindrical shells now constitute a standard chapter in the theory of elasticity, only recently have they been considered from a plastic viewpoint. Schischka (1)[3] and Kempner and Salerno (2) have considered shells loaded slightly beyond the elastic limit. More recently, Drucker (3) and Onat (4) have considered fully plastic shells.

The present paper is concerned with a circular cylindrical shell under axially symmetric loading. The material of the shell is assumed to be rigid whenever the maximum shearing stress is less than the yield stress k in pure shear, and to flow plastically whenever the maximum shear stress is equal to k. It is evident that any structure made of such a rigid-plastic material will be rigid for loads below the elastic limit. For loads slightly above the elastic limit, part of the structure will carry stresses equal to the yield stress, but the structure may still remain rigid as a result of the rigid constraint of the remainder of the material. The load at which these rigid constraints are no longer sufficient to hold the rigidity of the structure is called the "collapse load."

The state of stress in a thin shell is specified by normal resultants N_x and N_φ, moment resultants M_x and M_φ, and a shear resultant Q_x. The shear can be eliminated trivially from the equilibrium equations, and it will be assumed that it may be neglected in formulating the yield condition. In the case of beams,[4] this assumption is known to give good results. The bending moment M_φ does not appear in the equilibrium equations and it is possible to formulate the yield condition independently of M_φ. Therefore, in the present problem, the state of stress in the shell is specified by the values of M_x, N_x, and N_φ. Combinations of these resultants which specify plastic behavior may be plotted in a three-dimensional stress space to form the "yield surface." This surface is always closed and convex. Its equation will be found in the next section. In the following section various methods of approximating the yield surface by a convex polyhedron will be discussed.

The defining equations of rigid-plastic cylindrical shells will be specified in the third section. In addition to the yield condition, these include the equilibrium equations and the flow rule, or stress-strain law.

The second half of the paper will apply the theoretical results to some simple examples. The fourth and fifth sections are concerned with open-ended cylindrical cylinders clamped to rigid reinforcing rings and subjected to uniform external pressure. In the final section a similar problem is considered for a closed shell.

The Yield Surface

If shear stress is to be neglected in formulating the yield condition, the state of stress at a point is specified by the values of σ_x and σ_φ. According to the Tresca (maximum shearing stress) yield condition, these stresses must satisfy

$$\max\,(|\sigma_x|,\ |\sigma_\varphi|,\ |\sigma_x - \sigma_\varphi|) - 2k \leq 0 \qquad [1]$$

The stresses σ_x will give rise to a bending moment M_x and an axial force N_x, while the stresses σ_φ produce circumferential forces and moments N_φ and M_φ, respectively.

Let the total thickness of the shell be $2t$ and let z be measured from the middle surface. At a fully plastic section of the shell, the Relation [1] will be satisfied as an equality for all $-t \leq z \leq t$. In the first octant of the stress-resultant space, the problem may be formulated as "given values of any two of the stress resultants, distribute the stresses so as to maximize the third." If positive bending moments are defined as those producing compression in the surface $z = t$, it follows that for a given N_x, the maximum value of N_φ will be independent of the particular arrangement of the positive and negative σ_x stresses, while M_x will be maximized by concentrating the negative σ_x stresses near the top surface $z = t$, and positive stresses near the bottom surface. The critical σ_x stress distribution is shown in Fig. 1(*b*). The maximum value of N_φ associated with this σ_x distribution is obtained for the σ_φ distribution shown in Fig. 1(*c*), and the minimum value of N_φ is obtained when σ_φ is given by Fig. 1(*a*). If reduced stress resultants are defined by

$$m_x = M_x/M_0, \qquad n_x = N_x/N_0, \qquad n_\varphi = N_\varphi/N_0 \qquad [2a]$$

$$M_0 = 2kt^2, \qquad N_0 = 4kt \qquad [2b]$$

the following reduced stress resultants are then obtained from Figs. 1 (*a* to *c*)

$$\left.\begin{aligned} m_x^+ &= 1 - (u^2 + v^2)/2, & n_x^+ &= (u + v)/2 \\ n_\varphi^+ &= (1 + u)/2, & n_\varphi^- &= -(1 - v)/2 \\ & -1 \leq v \leq u \leq 1 \end{aligned}\right\} \qquad [3]$$

The yield surface is then composed in part of the two quadric surfaces

---

[1] The results contained in this paper were obtained in the course of research sponsored by the Office of Naval Research under contract Nonr 267(00) with the Polytechnic Institute of Brooklyn.

[2] Associate Professor of Applied Mechanics, Polytechnic Institute of Brooklyn. Mem. ASME.

[3] Numbers in parentheses refer to the Bibliography at the end of the paper.

[4] Reference (5), chapter 2.

¶ Presented at the West Coast Conference of the Applied Mechanics Division, University of California, Berkeley, Calif., June 21–23, 1954, of The American Society of Mechanical Engineers.

Discussion of this paper should be addressed to the Secretary, ASME, 29 West 39th Street, New York, N. Y., and will be accepted until January 10, 1955, for publication at a later date. Discussion received after the closing date will be returned.

Note: Statements and opinions advanced in papers are to be understood as individual expressions of their authors and not those of the Society. Manuscript received by ASME Applied Mechanics Division, February 11, 1954. This paper was not preprinted.

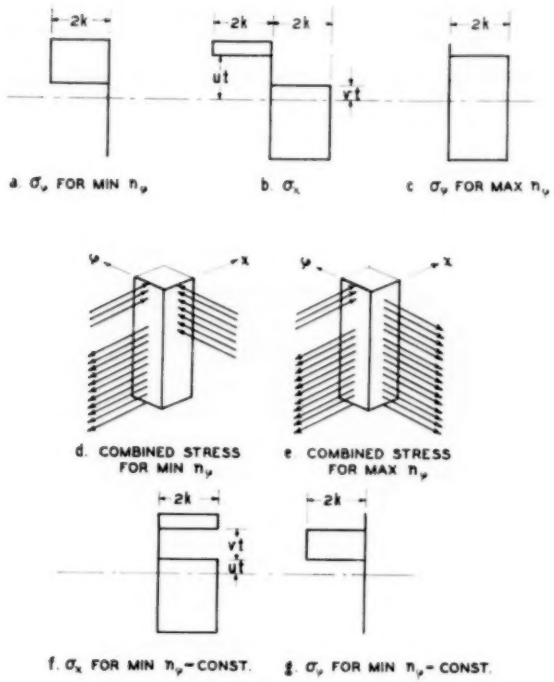

FIG. 1 CRITICAL STRESS DISTRIBUTIONS

$$m_x = m_x^+, \qquad n_x = n_x^+, \qquad n_\varphi = n_\varphi^\pm \ldots\ldots [4a, b]$$

The level curves corresponding to $n_x \geq 0$ are shown in Fig. 2.

The yield surface may be closed on "top" by observing that when $v = u$, the section is fully plastic due to the σ_x stresses alone, and n_φ may have any value between n^- and n^+. Thus the parabolic cylinder

$$m_x = 1 - u^2, \qquad n_x = u, \qquad -1 \leq u \leq 1,$$
$$-(1-u)/2 \leq n_\varphi \leq (1+u)/2 \ldots [5]$$

is part of the yield surface. To close it at the ends, one first observes that the reflection of all stresses in the center plane will change the sign of m_x but leave the membrane stresses unaffected so that the two surfaces

$$m_x = -m_x^+, \quad n_x = n_x^+, \quad n_\varphi = n_\varphi^\pm \ldots\ldots [6a, b]$$

are also part of the yield surface. The right-hand end is then obtained by setting $u = 1$ so that the section is fully plastic due to the σ_φ stresses. The resulting plane section can be defined by

$$n_\varphi = 1, \quad -2n_x(1 - n_x) \leq m_x \leq 2n_x(1 - n_x) \ldots\ldots [7]$$

The remaining section then can be closed by considering stress distributions of the type shown in Figs. 1 (*f* and *g*), leading to

$$n_x = 1 + n_\varphi, \quad -2(1 + n_\varphi)^2 \leq m_x \leq -2n_\varphi(1 + n_\varphi) \ldots [8]$$

Finally, the closure is completed by observing that if m_x, n_x, n_φ is a point on the yield surface, then the point $m_x, -n_x, -n_\varphi$ is also.

The complete level curves for $n_x \geq 0$ are shown in Fig. 2. The curves for $n_x \leq 0$ are obtained by a reflection in the origin. This yield surface is the same as that obtained by Onat (4) by a different method.

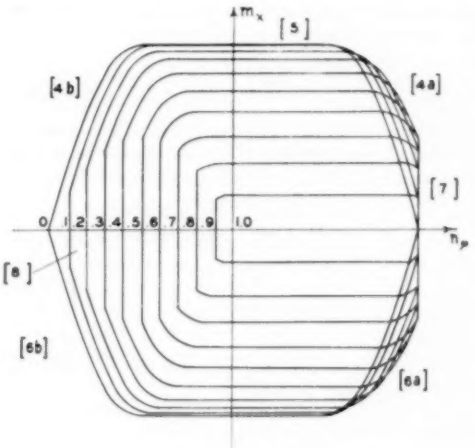

FIG. 2 YIELD SURFACE

LINEAR YIELD SURFACES

While some simple problems can be solved with the exact yield surface as obtained in the previous section by numerical integrations (3), it seems desirable to simplify the yield surface to obtain closed-form approximations, at least as a first step. In (4) a specific problem first was considered and the pertinent plane section of the yield surface was linearized. Here, the entire yield surface will be linearized. Although the resulting approximation will not be quite so accurate as that obtained in (4) it will be applicable to more general problems.

In order to fix clearly the processes involved without complicating the algebra unduly, a related two-dimensional stress problem will be considered in detail, namely, the cylindrical shell without end pressure. The axial force n_x then vanishes identically, and the yield curve is the section $n_x = 0$ of the yield surface considered previously. It consists of straight-line segments and parabolic arcs as indicated in Fig. 3. Various polygonal approximations are indicated by dashed lines in Figs. 3 (*a* to *c*). In each case the curve is symmetric with respect to the n_φ-axis.

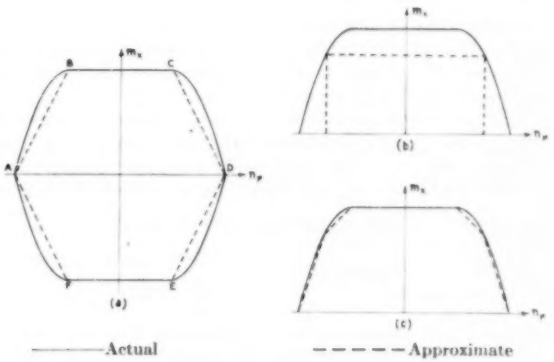

FIG. 3 TWO-DIMENSIONAL YIELD CURVES

The particular polygonal approximation indicated in Fig. 3(*a*) may be obtained directly by considering an ideal sandwich shell consisting of two faces which can carry only membrane stresses and a core which can carry only shear. Let $2H$ represent the thickness of the entire shell and T the thickness of one face. If the stresses in the top face are denoted by σ_x^1, σ_φ^1 and those in

the bottom face by σ_x^2, σ_φ^2, the resulting forces and moments for the entire shell are

$$\left.\begin{aligned} N_x &= T(\sigma_x^1 + \sigma_x^2), \quad N_\varphi = T(\sigma_\varphi^1 + \sigma_\varphi^2) \\ M_x &= HT(\sigma_x^2 - \sigma_x^1), \quad M_\varphi = HT(\sigma_\varphi^2 - \sigma_\varphi^1) \end{aligned}\right\} \quad [9]$$

The dimensions of the given constant-thickness shell and the idealized sandwich shell are chosen so that the limit moment in pure bending and limit force in pure tension are the same in each case. Thus, in view of Equations [2*b*]

$$N_0 = 4kT = 4kt, \quad M_0 = 4kHT = 2kt^2 \quad [10]$$

hence

$$T = t, \quad H = \frac{1}{2}\,t \quad [11]$$

In view of Equations [10], dimensionless stress resultants are still defined by Equations [2*a*].

For the particular problem under consideration, N_x vanishes identically. If Equations [9] are solved for σ_x^1, σ_x^2, σ_φ^1, and σ_φ^2 and substituted into Equations [1] for both the top and bottom surfaces, the resulting twelve inequalities may be written

$$-1 \leq -m_x \leq 1, \quad -1 \leq m_x \leq 1 \quad [12]$$

$$\left.\begin{aligned} &-1 + n_\varphi \\ &-1 + n_\varphi + m_x \\ &-1 - n_\varphi \\ &-1 - n_\varphi + m_x \end{aligned}\right\} \leq m_\varphi \leq \left\{\begin{aligned} &1 + n_\varphi \\ &1 + n_\varphi + m_x \\ &1 - n_\varphi \\ &1 - n_\varphi + m_x \end{aligned}\right\} \quad [13]$$

Since m_φ does not enter into the further calculations, it is only required that there exist some m_φ satisfying the eight Inequalities [13]. A necessary and sufficient condition that this be so is that each left-hand side be less than each right-hand side. If the duplications in the resulting sixteen inequalities are omitted, the following set is obtained

$$-1 \leq 1 \quad [14]$$

$$-2 \leq m_x \leq 2 \quad [15]$$

$$-1 \leq n_\varphi \leq 1 \quad [16]$$

$$-2 \leq 2n_\varphi + m_x \leq 2 \quad [17]$$

$$-2 \leq 2n_\varphi - m_x \leq 2 \quad [18]$$

To these must be adjoined the Inequalities [12]. It is readily verified that all of these inequalities are satisfied provided [12], [17], and [18] all hold. But these define precisely the domain included in the dashed curve in Fig. 3(*a*).

The same technique may now be used to find a polygonal approximation to the three-dimensional yield surface derived in the previous section. The final result is a convex polyhedron bounded by the twelve plane faces which are listed in the first two

TABLE 1 YIELD POLYHEDRON

Face	Equation	Strain-rate vector $(U^*, -W, -W^*/2c^2)$	Trace in plane $n_x = 0$
1	$-n_\varphi = 1$	$\lambda(0, -1, 0)$	...
2	$n_\varphi = 1$	$\lambda(0, 1, 0)$	...
3	$n_x - 2n_\varphi + m_x = 2$	$\lambda(1, -2, 1)$	AB
4	$-n_x + 2n_\varphi - m_x = 2$	$\lambda(-1, 2, -1)$	DE
5	$n_x - 2n_\varphi - m_x = 2$	$\lambda(1, -2, -1)$	FA
6	$-n_x + 2n_\varphi + m_x = 2$	$\lambda(-1, 2, 1)$	CD
7	$n_x - n_\varphi = 1$	$\lambda(1, -1, 0)$	...
8	$-n_x + n_\varphi = 1$	$\lambda(-1, 1, 0)$	...
9	$n_x - m_x = 1$	$\lambda(1, 0, -1)$	EF
10	$-n_x + m_x = 1$	$\lambda(-1, 0, 1)$	BC
11	$-n_x - m_x = 1$	$\lambda(-1, 0, -1)$	EF
12	$n_x + m_x = 1$	$\lambda(1, 0, 1)$	BC

columns of Table 1. The next column of Table 1 will be explained in the next section. The final column relates the general yield polyhedron to the particular case $n_x = 0$ as shown in Fig. 3(*a*).

The level curves of the yield polyhedron for positive n_x are given in Fig. 4. These may be compared with the actual level curves in

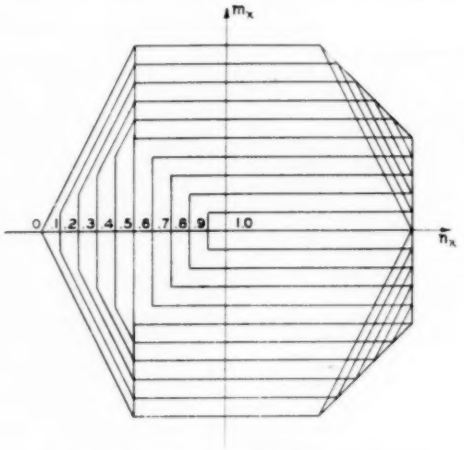

FIG. 4 LEVEL CURVES OF YIELD POLYHEDRON

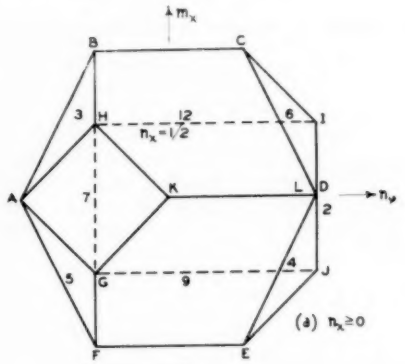

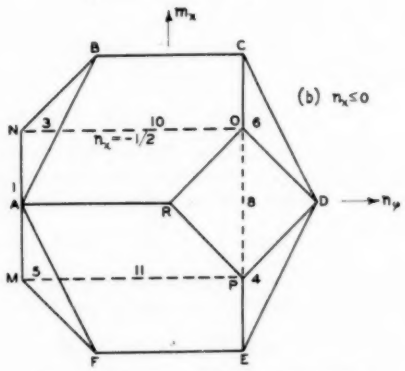

FIG. 5 SURFACES OF YIELD POLYHEDRON

Fig. 2. Fig. 5(*a*) shows the plane surfaces corresponding to positive n_x, and Fig. 5(*b*) those for negative n_x. Another convenient representation of the yield polyhedron is given in Fig. 6. The plane faces, boundary lines, and vertices are all shown in their

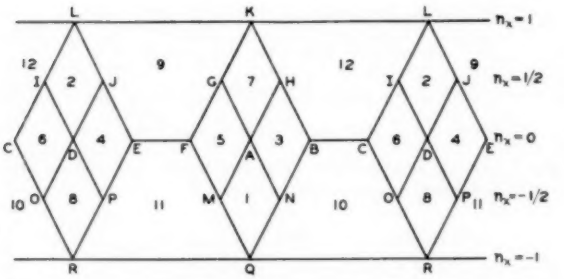

FIG. 6 TOPOLOGICAL REPRESENTATION OF YIELD POLYHEDRON

proper topological relationship by projecting the polyhedron onto a circumscribed cylinder, unrolling the cylinder, and then straightening the curved arcs. This figure proves quite useful in discussing particular problems.

EQUILIBRIUM AND FLOW RULE

The equations of equilibrium for a cylindrical shell are well known [see, for instance, reference (6)]. In terms of the present reduced variables they may be written

$$\left.\begin{array}{c} n_x = \text{const} \\ m''_x/2c^2 + n_\varphi + P = 0 \\ q_x = (L/2ac^2)m_x' \end{array}\right\} \quad \ldots\ldots\ldots\ldots [19]$$

where c, P, and y are defined by

$$c = L/\sqrt{at}, \quad P = pa/4kt, \quad y = x/L \ldots\ldots [20]$$

an l primes indicate differentiation with respect to y.

An ideal rigid plastic material often is forced to admit certain discontinuities which represent narrow regions of rapid change in real materials. Considering the equilibrium of a small element, Fig. 8, it is evident that the shear, axial moment, and axial force must be continuous but that the circumferential force and moment may be discontinuous. Thus, in view of the third Equation [19]

$$m_x] = m_x'] = n_x] = 0 \ldots\ldots\ldots\ldots [21]$$

at each surface of discontinuity where the symbol] denotes the jump in the quantity preceding.

In general, some of the boundary conditions will involve velocities so that it is necessary to consider the associated flow rule. The plastic potential-flow law can be interpreted directly in terms of the stress resultants and the extensions and curvatures of the middle surface to show that a certain strain-rate vector is normal to the yield polyhedron [4]. In terms of dimensionless velocities

$$W = w/a, \quad U = u/L \ldots\ldots\ldots\ldots [22]$$

this vector is

$$\mathbf{E} = (U', -W, -W''/2c^2) \ldots\ldots\ldots\ldots [23]$$

For each face of the yield polyhedron, the vector $\mathbf{E}$ must be normal to the yield polyhedron, and directed outward. Thus, if l_k, m_k, n_k represent direction numbers of the kth face

$$\mathbf{E} = \lambda(l_k, m_k, n_k) \ldots\ldots\ldots\ldots [24]$$

where λ is an arbitrary positive function. These vectors are listed for each face in the third column of Table 1. At the intersection of two faces the direction of the vector is partially indeterminate, but $\mathbf{E}$ must be given by

$$\mathbf{E} = \lambda(l_k, m_k, n_k) + \mu(l_p, m_p, n_p) \ldots\ldots\ldots [25]$$

where λ and μ are both nonnegative.

As regards continuity, W must be continuous since a discontinuity would correspond to an infinite shear, and the shear is assumed small. The slope W' may be discontinuous but must remain finite, since an infinite W' would imply a discontinuous W. If W' is discontinuous, then W'' is infinite. U' may be discontinuous and U' infinite. In fact, it will be shown in an example that if W' is discontinuous then the discontinuity in U is prescribed.

SHORT SHELL WITHOUT END LOAD

The general method of solution will be to use certain heuristic arguments to deduce the general nature of the stress distribution in the shell at the instant of collapse. Let the mapping of the various states of stress onto the stress resultant space be defined as the "stress profile," and the various faces and edges of the yield polyhedron identified as plastic regime 1, plastic regime A-B, and so on (7). Then the first step is to make reasonable assumptions as to which plastic regimes[b] contain the stress profile. With this information as a starting point, all equations, boundary conditions, jump conditions, and inequalities will be utilized to find the complete solution. If such a solution exists, it will of necessity be the desired solution of the problem and the heuristic arguments will have been justified. If no solution exists, then the original argument as to the proper plastic regimes was unjustified and another combination must be attempted. It should be pointed out that the original heuristic argument is unnecessary in that the exhibition of the complete mathematical solution is

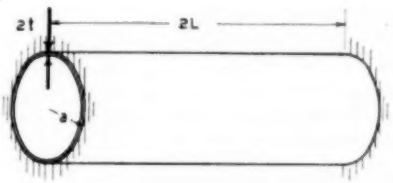

FIG. 7 CYLINDRICAL SHELL

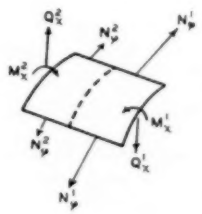

FIG. 8 (*left*) STRESS DISCONTINUITIES

sufficient. However, in view of the large number of possible plastic regime combinations, a trial-and-error procedure with no physical basis would be prohibitively lengthy.

The first example to be considered is that of an open shell, supported by rigid rings at either end, and subjected to uniform external pressure, Fig. 7. It may be observed that the solution to this problem would apply to a typical bay of a long shell with several equally spaced reinforcing rings.

Since there is no axial load, it follows immediately from the first Equation [19] that $n_x = 0$; hence the stress problem may be discussed in relation to the two-dimensional yield polygon, Fig. 3(a). If the shell is very short, it would be expected to fail in a manner similar to a uniformly loaded built-in beam, i.e., with discontinuous slopes at either end and at the center. Such a circle with discontinuous slope will be called a "hinge circle" (7). At

[b] In general, part of the stress profile may be interior to the yield polyhedron, and hence rigid, but in the examples considered the stresses are everywhere plastic.

the end $x = 0$, then, the curvature must tend to $-\infty$, while the displacement is zero. Therefore

$$W/W'' = 0, \quad W'' > 0 \qquad [26]$$

at this end. It follows from Table 1 that faces 9 and 11 of the yield surface are the only ones admitting such a velocity vector, and for $n_x = 0$ these faces both reduce to the line *E-F* in Fig. 3(*a*).

A similar analysis applied to the center $y = 1$ shows that this point must correspond to the line *B-C* if there is to be a hinge circle at the center. Finally, at all points of the shell the circumferential stress will be negative so that these points are connected along sides *F-A* and *A-B* in Fig. 3(*a*).

It is easily shown that no finite portion of the shell can be in plastic regime *E-F*. Indeed, from Table 1

$$(U', -W, -W''/2c^2) = \lambda(-1, 0, 1) + \mu(1, 0, 1)$$

along *E-F*. Thus

$$U' = -\lambda + \mu, \quad W = 0, \quad -W''/2c^2 = \lambda + \mu$$

Since λ and μ are both nonnegative, the second and third of these equations can both be satisfied only if $\lambda = \mu = 0$; i.e., there is no plastic flow. A similar argument shows that no portion of the shell is in regime *B-C*. Therefore, as y increases from zero to 1, the stress profile in Fig. 3(*a*) extends from *F* to *A* to *B*.

In plastic regime *F-A*, it follows from Table 1 and Equation [19] that

$$\left.\begin{aligned} n_\varphi &= C \cosh cy + D \sinh cy - P \\ m_x &= -2C \cosh cy - 2D \sinh cy + 2P - 2 \end{aligned}\right\} \qquad [27a]$$

The elimination of λ from the expression for the strain-rate vector on *F-A* from Table 1 leads to differential equations which are easily solved to yield

$$W = G \cosh cy + H \sinh cy, \; U = W/2 \geq 0 \qquad [27b]$$

Similarly, along *A-B*, the solution is found to be

$$\left.\begin{aligned} n_\varphi &= A \cos cy + B \sin cy - P \\ m_x &= 2A \cos cy + 2B \sin cy - 2P + 2 \end{aligned}\right\} \qquad [28a]$$

$$W = E \cos cy + F \sin cy, \quad U = W/2 \geq 0 \qquad [28b]$$

Equations [27] will hold for $0 \leq y \leq y_1$, and Equations [28] for $y_1 \leq y \leq 1$, where y_1 is to be determined. The stress-boundary conditions for the assumed profile are easily seen to be

$$\left.\begin{aligned} &m(0) = -1, \quad m(1) = +1, \quad m'(1) = 0 \\ &m(y_1^-) = 0, \quad m(y_1^+) = 0, \quad m'(y_1^-) = m'(y_1^+) \end{aligned}\right\} \qquad [29]$$

Equations [29*a*, *b*, *c*, *d*] are sufficient to determine the four arbitrary constants in Equations [27*a*] and [28*a*], the collapse load P, and the transition point y_1. The resulting solution is

$$\left.\begin{aligned} 0 < y < y_1, \quad m &= -(2P - 1)\frac{\sinh c(y_1 - y)}{\sinh cy_1} \\ &\quad -2(P-1)\left[\frac{\sinh cy}{\sinh cy_1} - 1\right] \\ n &= (P - 1/2)\frac{\sinh c(y_1 - y)}{\sinh cy_1} \\ &\quad + (P-1)\frac{\sinh cy}{\sinh cy_1} - P \end{aligned}\right\} \qquad [30a]$$

$$\left.\begin{aligned} y_1 < y < 1, \; m &= (2P - 1)\cos c(1 - y) - 2(P - 1) \\ n &= (P - 1/2)\cos c(1 - y) - P \end{aligned}\right\} \qquad [30b]$$

$$P = 1 + \cos c(1 - y_1)/2[1 - \cos c(1 - y_1)] \qquad [31]$$

$$\cos c(1 - y_1)\cosh cy_1 + \sin c(1 - y_1)\sinh cy_1 = 1 \qquad [32]$$

Fig. 9 shows y_1 as a function of c as determined by Equation [32] and also shows P as given by Equation [31].

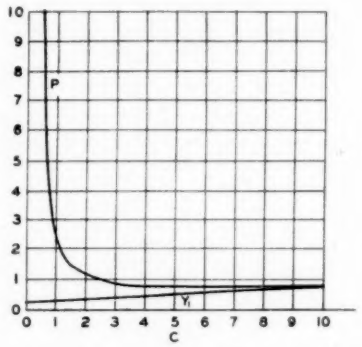

FIG. 9 ASSUMED SOLUTION WITH THREE YIELD CIRCLES

From Fig. 9 it appears that the collapse load P becomes less than 1 for c greater than about 2.5. This result is unreasonable, since for an infinitely long shell plastic flow will take place with no bending at a load $P = 1$. In order to see why the solution just given is incorrect for large c, it is necessary to consider the velocity field. If W_1 represents the velocity of the point y_1, then W must be given by Equation [27*b*] for $0 < y < y_1$, by Equation [28*b*] for $y_1 < y < 1$, and must satisfy the boundary conditions

$$\left.\begin{aligned} W(0) &= 0 & W(y_1^-) &= W_1 \\ W(y_1^+) &= W_1, & W'(y_1^+) &= W'(y_1^-) \end{aligned}\right\} \qquad [33]$$

The resulting velocity field is

$$W = W_1 \operatorname{csch} cy_1 \sinh cy, \; 0 < y < y_1 \qquad [34]$$

$$W = W_1 \operatorname{csch} cy_1[\cos c(y - y_1)\sinh cy_1 + \sin c(y - y_1)\cosh cy_1], \; y_1 < y < 1 \qquad [35]$$

It will be observed that the velocity field is determined only to within the arbitrary positive multiplier W_1 as must necessarily be the case for a perfectly plastic-rigid material.

Since the limit moment of the hinge circle at $y = 0$ is positive the discontinuity in slope (which is twice the slope, when account is taken of the other half of the shell) also must be positive. This condition can be shown to lead to the restriction

$$0 \leq c < 1.65$$

for the solution of this section to be valid.

Long Shell Without End Load

For any length shell, the solution near the clamped end must be the same as in the previous section. Indeed, since the clamped end can suffer no displacement, it must be in a state of pure negative bending under the limit load. Therefore, at least for y sufficiently small, the stress point is in plastic regime *A-F*, and the solution is still given by Equation [27]. However, it is easy to see that this solution cannot be valid for all y, since at $y = 1$ either the slope must vanish or the moment must equal $+1$. Therefore there will

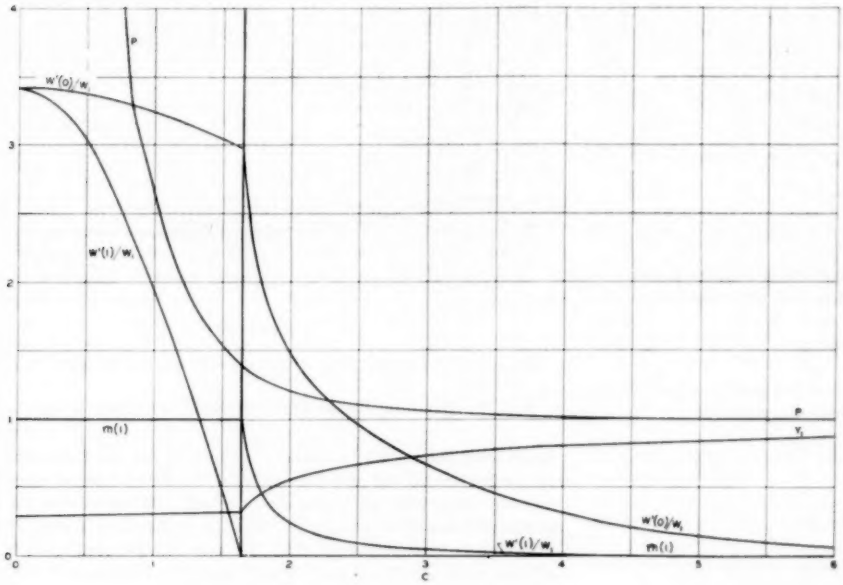

FIG. 10 (*left*) SOLUTION FOR ALL VALUES OF C

continue to be a transition point $y = y_1$ at which the stress point will move from regime *A-F* to *A-B*.

For short shells it was shown that the stress point moved all the way to *B* for $y = 1$, but for c larger than 1.65 this led to a negative slope discontinuity. Therefore for larger values of c it is evident that the stress point for $y = 1$ is some interior point of regime *A-B*. This being the case, Equations [28] are still applicable for $y_1 < y < 1$, but the proper boundary conditions are now

$$\left.\begin{aligned} &m(y_1^+) = 0, \quad W(y_1^+) = W_1 \\ &m'(y_1^+) = m'(y_1^-), \quad W'(y_1^+) = W'(y_1^-) \\ &m'(1) = 0, \quad W'(1) = 0 \end{aligned}\right\} \quad \ldots\ldots [36]$$

The complete solution is seen to be Equations [27] for $0 \leq y \leq y_1$, and

$$\left.\begin{aligned} m &= 2(P-1)\frac{\cos c(1-y)}{\cos c(1-y_1)} - 1 \\ n &= (P-1)\cos c(1-y)/\cos c(1-y_1) - P \\ W &= W_1 \cos c(1-y)/\cos c(1-y_1) \end{aligned}\right\} \quad \ldots\ldots [37a]$$

for $y_1 < y < 1$, where

$$\tan c(1-y_1) = \coth cy_1 \ldots\ldots [37b]$$

$$P = 1 + (1/2)/(2\cosh cy_1 - 1) \ldots\ldots [37c]$$

It is interesting to observe that, whereas for the short shell the entire solution could be obtained from the stress equations, Equations [37] are based on both stress and velocity.

Salient features of the complete solutions are shown in Fig. 10 as functions of the parameter c. These include the pressure P, the transition point y_1, the center moment $m(1)$, and the center and end slopes $W'(1)$ and $W'(0)$. For $0 \leq c < 1.65$ the data are obtained from the preceding section, and for $1.65 < c$ from the present section.

SHELLS WITH END LOAD

If a shell which is closed at the end by rigid plates is submersed in a hydrostatic pressure field p, there will be a compressive axial force of magnitude $\pi a^2 p$. Therefore, in view of Equations [19] and [20], the axial resultant will have the constant value

$$n_x = -P/2 \ldots\ldots [38]$$

throughout the shell. It follows that the stress point will always lie in the intersection of the plane [38] with the yield polyhedron, the height of the plane depending upon the value of P.

For very short shells, collapse will be due essentially to pure axial compression so that $P \simeq 2$. Therefore, at least for c sufficiently small the stress point will be in a plane $-1/2 < n_x < -1$, Fig. 11. From Fig. 6 it is immediately evident that only the

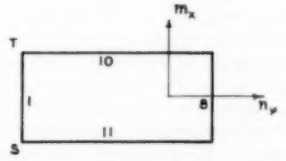

FIG. 11 TYPICAL SECTION OF YIELD POLYHEDRON ($-1 \leq n_x \leq -1/2$)

plastic regimes which need be considered are 8, 11, 1, 10. Fig. 5 then shows that plastic regime 8 corresponds to a tensile circumferential force, hence is not likely. Further, by the same argument used previously it can be shown that neither of regimes 10 nor 11 can support a strain-rate vector so the stress profile lies in regime 1.

Integration of the strain-rate vector for regime 1 from Table 1, together with the condition $W(0) = 0$ leads to

$$W = W_0 y, \quad U = C \ldots\ldots [39]$$

where W_0 is the velocity at the center. This velocity field obviously produces hinge circles at $y = 0$ and $y = 1$ so that the stress profile comprises the entire line *S-T* in regime 1, Fig. 11, with $y = 0$ corresponding to *S* and $y = 1$ to *T*.

The substitution of $n_\varphi = -1$ from Table 1 into Equation [19] together with the conditions

$$m_x(0) = -1 - n_x = -1 + P/2,$$
$$m_x(1) = 1 + n_x = 1 - P/2,\ m'_x(1) = 0 \ldots [40]$$

leads to the stress field

$$m_x = c^2(1 - P)(y^2 - 2y) - (1 - P/2),$$
$$n_x = -P/2,\ n_\varphi = -1 \ldots\ldots [41]$$

where the collapse load P is given by

$$P = (c^2 + 2)/(c^2 + 1) \ldots\ldots [42]$$

The strain-rate vector at the intersection of regimes 1 and II is obtained from Table 1 and Equation [25] and elimination of μ then furnishes

$$U' = -W''/2c^2 \ldots\ldots [43]$$

Equation [43] is to be interpreted as holding in a vanishingly narrow region, hence in the limit the jump condition

$$U] = -(1/2c^2)W'] \ldots\ldots [44]$$

is obtained. Similarly, at $y = 1$

$$U] = (1/2c^2)W'] \ldots\ldots [45]$$

If the rigid ring at $y = 0$ is arbitrarily assigned the value $U = 0$, it follows from Equations [39] and [40] that

$$U = -W_0/2c^2 \qquad 0 < y < 1 \ldots\ldots [46]$$

In the other half of the shell it then follows from Equation [45] that $U = -3W_0/2c^2$.

The heuristic thinking which led to the consideration of plastic regime 1 was based on a short shell. However, the resulting solution satisfies all conditions for any value of c and hence represents the correct solution. Fig. 12 shows the collapse pressure as a function of c for a closed shell according to Equation [42] and also shows the open shell values according to the two preceding sections. The fact that the closed shell has a higher collapse pressure than the open shell for moderately long shells may seem surprising at first glance. However, it may be explained by the following heuristic argument.

An open unsupported shell would collapse when the circumferential stress reached yield, i.e., for $P = 1$. The effect of the rigid reinforcing rings is to provide an end moment which reduces this stress slightly. For the open-end shell, the condition of zero axial force means that this moment can be produced only by equal tensile and compressive axial stresses across the height of the shell. However, the axial tensile force present reduces the compressive radial stress necessary to produce yield, see Fig. 1. Therefore the improvement due to the reinforcing ring is limited.

However, the presence of a net axial compressive force for the closed shell means that a moment up to half the yield moment can be present at the end due solely to the distribution of compressive stress with no tensile stress at all. Therefore the improvement should be greater in this case, as has been found.

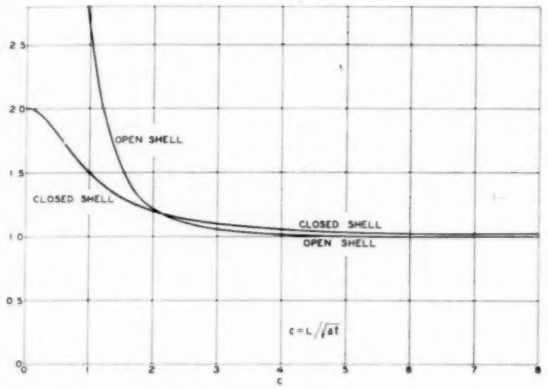

FIG. 12 COLLAPSE PRESSURES FOR OPEN AND CLOSED SHELLS

Of course, for a very short shell, the open collapse load tends to infinity while the closed shell cannot support a load greater than $P = 2$ without failing in axial compression.

In conclusion it should be pointed out that no account has been taken of the so called beam-column effect due to the end load. For the ideal material here considered there is no such effect, since there are no deformations at all until the collapse load is reached. However, in applying these results to a real material, great caution should be used if the predicted collapse load approaches the Euler buckling load of the shell.

BIBLIOGRAPHY

1 "Zur Plästizitat des Druckkörpers von U-Booten," by Ernst Schischka, *Forschungsbericht* Nr. 37, Technische Hochschule, Wien, Austria, 1945.

2 "Analysis of the Inelastic Behavior of Transversely Reinforced Cylindrical Shells Under Hydrostatic Pressure," by J. Kempner and V. L. Salerno, Pibal Report No. 172, Polytechnic Institute of Brooklyn, Brooklyn, N. Y., 1950.

3 "Limit Analysis of Cylindrical Shells Under Axially-Symmetric Loading," by D. C. Drucker, Proceedings of the First Midwest Conference on Solid Mechanics, 1953, pp. 158–163.

4 "The Plastic Collapse of Cylindrical Shells Under Axially Symmetrical Loading," by E. T. Onat, Report DA-19-020-ORD-798/-9, Brown University, Providence, R. I., 1954.

5 "Theory of Perfectly Plastic Solids," by W. Prager and P. G. Hodge, Jr., John Wiley & Sons, Inc., New York, N. Y., 1951.

6 "Theory of Plates and Shells," by S. Timoshenko, McGraw-Hill Book Company, Inc., New York, N. Y., 1940.

7 "The Load Carrying Capacities of Circular Plates," by H. G. Hopkins and W. Prager, *Journal of Mechanics of Physics and Solids*, vol. 2, 1953, pp. 1–13.

Boundary-Value Problems of the Thin-Walled Circular Cylinder[1]

By N. J. HOFF,[2] BROOKLYN, N. Y.

The homogeneous differential equations of Donnell's theory of thin cylindrical shells are integrated. Expressions are obtained in closed form for the displacements, membrane stresses, moments, and shear forces.

Nomenclature

The following nomenclature is used in the paper:

a = real number
a = radius of cylinder
A = constant of integration
b = real number
B = constant of integration
C = constant of integration
d = differential sign
D = $Eh^3/[12(1-\nu^2)]$
E = Young's modulus of elasticity
h = thickness of shell
i = imaginary unit
$4K^4$ = $12(1-\nu^2)(a/h)^2$
L = length of shell
M_x = axial bending moment per unit length
M_φ = circumferential bending moment per unit length
$M_{x\varphi}$ = torque per unit length
M_1, M_2, M_1', M_2' = constants (see Equations [93, 94])
n = integer
N_1, N_2, N_1', N_2' = constants (see Equations [95, 96])
p = complex number
Q_x = shear force per unit length in axial section
Q_φ = shear force per unit length in section perpendicular to axis
R_1, R_2, R_1', R_2' = constants (see Equations [97, 98])
S_1, S_2, S_1', S_2' = constants (see Equations [99, 100])
T_1, T_2, T_1', T_2' = constants (see Equations [101, 102])
u = u^*/a
u^* = axial displacement
v = v^*/a
v^* = circumferential displacement
w = w^*/a
w^* = radial displacement
x = x^*/a
x^* = axial co-ordinate
α = real part of p
$i\beta$ = imaginary part of p
$\gamma_{x\varphi}$ = shear strain
$\Gamma_1, \Gamma_2, \Gamma_1', \Gamma_2'$ = constants (see Equations [103, 104])
∂ = sign of partial differentiation
∇^2 = Laplace's operator
ϵ_x = axial strain
ϵ_φ = circumferential strain
$\Theta_1, \Theta_2, \Theta_1', \Theta_2'$, $\Theta_1'', \Theta_2'', \Theta_1''', \Theta_2'''$ = constants (see Equations [105, 106, 107, 108])
κ_x = curvature in axial section
κ_φ = curvature in section perpendicular to axis
Λ_1', Λ_2' = constants (see Equation [109])
ν = Poisson's ratio
σ_x = axial stress
σ_φ = circumferential stress
$\tau_{x\varphi}$ = shear stress
φ = circumferential angle
$\Phi_1, \Phi_2, \Phi_1', \Phi_2'$ = constants (see Equations [110, 111])
$\Psi_1, \Psi_2, \Psi_1', \Psi_2'$ = constants (see Equations [112, 113])
Ω = constant (see Equation [24])

Introduction

When a thin-walled cylindrical shell is subjected to arbitrary distributed surface or inertia loads, it is generally not difficult to find a particular solution satisfying the inhomogeneous equations that govern the displacements of the shell. It is much more time-consuming to solve the homogeneous equations and to adapt these solutions to the boundary conditions when the particular solution does not automatically satisfy these conditions. This statement is particularly true when the calculations are carried out with the aid of the classical theory of thin shells.

The basic equations of thin-shell theory originally were derived by Love (1)[3] in 1888 and were presented in the form most frequently used today by Flügge (2) in 1932; in this latter form they appear in the textbooks by Flügge (3), Biezeno and Grammel (4), and Timoshenko (5). A considerably simplified set of equations was derived by Donnell (6) in 1933; there are indications that, under most conditions of loading, the deformations and stresses calculated from these equations differ little from those deducible from the generally accepted set. There is even some doubt whether the classical equations are always more accurate than Donnell's equations. Eric Reissner (7) showed in two recent papers that some of the terms missing from the classical differential equations in consequence of the assumption that stresses and strains in the direction of the surface normal are small, are of the same order of magnitude as those appearing in them because the ratio of the wall thickness to the radius is not considered negligibly small as compared to unity.

The classical homogeneous equations have been solved by various authors in a form suitable for the investigation of edge effects along generators. These solutions are important in ap-

[1] This work was performed under a consulting contract with the Knolls Atomic Power Laboratory, Schenectady, N. Y., operated by the General Electric Company for the United States Atomic Energy Commission. The author is indebted to the company, to the AEC, and to Mr. Daniel R. Miller, the project supervisor, for their permission to publish this article.

[2] Head of the Department of Aeronautical Engineering and Applied Mechanics of the Polytechnic Institute of Brooklyn. Mem. ASME.

Presented at the West Coast Meeting of the Applied Mechanics Division, Berkeley, Calif., June 21–23, 1954, of The American Society of Mechanical Engineers.

Discussion of this paper should be addressed to the Secretary, ASME, 29 West 39th Street, New York, N. Y., and will be accepted until January 10, 1955, for publication at a later date. Discussion received after the closing date will be returned.

Note: Statements and opinions advanced in papers are to be understood as individual expressions of their authors and not those of the Society. Manuscript received by ASME Applied Mechanics Division, June 23, 1953. Paper No. 54—APM-4.

[3] Numbers in parentheses refer to the Bibliography at the end of the paper.

plications to reinforced-concrete shell roof structures. A detailed presentation of the problems involved can be found in a recent ASCE manual (8). A closed-form solution of the homogeneous Donnell equations was given recently in a paper published jointly by the author, Joseph Kempner, and Frederick V. Pohle (9); this solution can be employed when displacements or stresses are prescribed along generators. The solutions given by Miesel (10) and Aas Jakobsen (11) are useful when the shell is a complete cylinder of finite length and thus the free edges are circular. Such structural elements are common in mechanical-engineering practice. As the roots of the classical equations cannot be given explicitly, the Miesel and Aas Jakobsen solutions are implicit and leave a considerable amount of work to the computer.

The purpose of the present paper is to remedy this situation. Through the use of the Donnell equations all the displacement and stress quantities are given in a relatively simple explicit form. These results can be used in solving problems involving prescribed boundary conditions along circular boundaries, such as line loads and concentrated loads.

Basic Equations

In the absence of surface and body forces Donnell's equilibrium conditions of an element of a thin-walled circular cylindrical shell can be stated in the following form

$$\nabla^8 w + 4K^4 w_{,xxxx} = 0 \quad \ldots\ldots [1]$$

$$\nabla^4 u = \nu w_{,xxx} - w_{,x\varphi\varphi} \quad \ldots\ldots [2]$$

$$\nabla^4 v = (2 + \nu) w_{,xx\varphi} + w_{,\varphi\varphi\varphi} \quad \ldots\ldots [3]$$

where the subscripts following a comma indicate differentiation

$$4K^4 = 12(1 - \nu^2)(a/h)^2 \quad \ldots\ldots [4]$$

and ∇^2 is Laplace's operator

$$\nabla^2 = (\partial^2/\partial x^2) + (\partial^2/\partial \varphi^2) \quad \ldots\ldots [5]$$

The nondimensional distances and displacements are defined by the equations

$$x = (x^*/a) \quad u = (u^*/a) \quad v = (v^*/a) \quad w = (w^*/a) \quad \ldots\ldots [6]$$

and x^* is the distance measured in the axial direction along a generator, $a\varphi$ that measured around the circumference, and u^*, v^*, and w^* are the displacements in the axial, circumferential, and radial direction, respectively, as shown in Fig. 1(*a*). The remaining geometrical and physical quantities are a, the mean radius of the shell; h, the thickness of the shell; L, the length of the shell; E, Young's modulus of elasticity; and ν, Poisson's ratio.

In Donnell's approximation and with the present sign convention the strains ϵ and the curvatures κ of the median surface of the shell are defined as

$$\left.\begin{aligned} \epsilon_x &= u_{,x} & \kappa_x &= (1/a) w_{,xx} \\ \epsilon_\varphi &= v_{,\varphi} - w & \kappa_\varphi &= (1/a) w_{,\varphi\varphi} \\ \gamma_{x\varphi} &= u_{,\varphi} + v_{,x} & \kappa_{x\varphi} &= (1/a) w_{,x\varphi} \end{aligned}\right\} \quad \ldots\ldots [7]$$

The membrane stresses can be given as

$$\left.\begin{aligned} \sigma_x &= [E/(1 - \nu^2)](\epsilon_x + \nu\epsilon_\varphi) \\ &= [E/(1 - \nu^2)](u_{,x} + \nu v_{,\varphi} - \nu w) \\ \sigma_\varphi &= [E/(1 - \nu^2)](\nu\epsilon_x + \epsilon_\varphi) \\ &= [E/(1 - \nu^2)](\nu u_{,x} + v_{,\varphi} - w) \\ \tau_{x\varphi} &= [E/2(1 + \nu)]\gamma_{x\varphi} = [E/2(1 + \nu)](u_{,\varphi} + v_{,x}) \end{aligned}\right\} \quad \ldots\ldots [8]$$

The moment-resultants per unit length are indicated as right-hand vectors in Fig. 1(*b*). They are

$$\left.\begin{aligned} M_x &= -D(\kappa_x + \nu\kappa_\varphi) = -(D/a)(w_{,xx} + \nu w_{,\varphi\varphi}) \\ M_\varphi &= -D(\nu\kappa_x + \kappa_\varphi) = -(D/a)(w_{,\varphi\varphi} + \nu w_{,xx}) \\ M_{x\varphi} &= -M_{\varphi x} = (1 - \nu) D\kappa_{x\varphi} = [(1 - \nu)D/a] w_{,x\varphi} \end{aligned}\right\} \quad \ldots\ldots [9]$$

with

$$D = Eh^3/[12(1 - \nu^2)] \quad \ldots\ldots [9a]$$

The shear forces per unit length which accompany these moments and act in the radial direction are

$$\left.\begin{aligned} Q_x &= (1/a)(M_{x,x} + M_{\varphi x,\varphi}) = -(D/a^2)(w_{,xxx} + w_{,x\varphi\varphi}) \\ Q_\varphi &= (1/a)(M_{\varphi,\varphi} - M_{x\varphi,x}) = -(D/a^2)(w_{,\varphi\varphi\varphi} + w_{,xx\varphi}) \end{aligned}\right\} \quad [10]$$

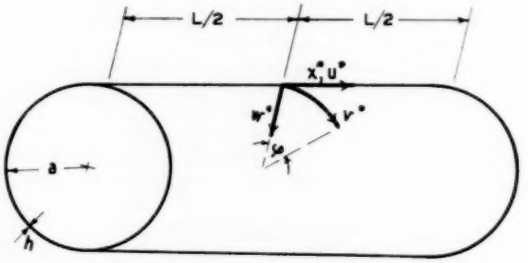

(*a*)

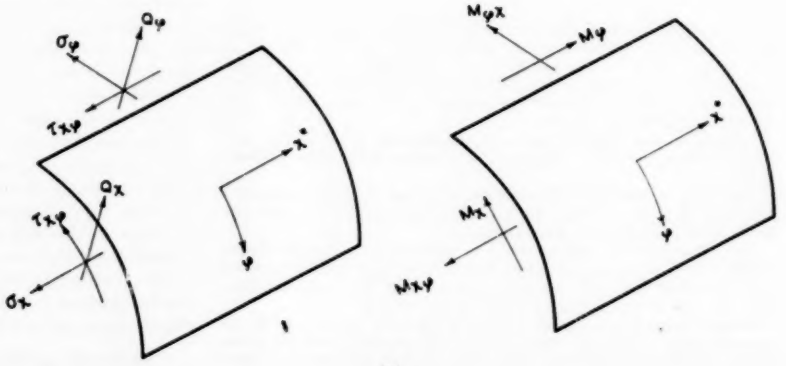

(*b*)

Fig. 1 (*a* and *b*) Sign Convention for Co-Ordinates, Displacements, Stresses, and Stress Resultants

If the equivalent shear $(1/a)M_{\varphi z,x}$ corresponding to the distributed torque is added to Q_φ in agreement with Kirchhoff's suggestion[4] the total effective shear force per unit length is

$$Q_{\varphi\text{-eff}} = -(D/a^2)[w_{,\varphi\varphi\varphi} + (2-\nu)w_{,xx\varphi}] \quad [11]$$

If the equivalent shear $(1/a)M_{x\varphi,\varphi}$ corresponding to the distributed torque is subtracted from Q_x one obtains

$$Q_{x\text{-eff}} = -(D/a^2)[w_{,xxx} + (2-\nu)w_{,x\varphi\varphi}] \quad [12]$$

Solution of the Equations

The solution is assumed in the form

$$w = Ae^{px}\cos n\varphi \quad [13a]$$

$$u = Be^{px}\cos n\varphi \quad [13b]$$

$$v = Ce^{px}\sin n\varphi \quad [13c]$$

where A and n are assumed real and B, C, and p are complex quantities. Substitution of these expressions into Equation [2] yields

$$B = \frac{\nu p^2 + n^2}{(p^2 - n^2)^2}\,pA \quad [14]$$

Substitution into Equation [3] leads to

$$C = \frac{n^2 - (2+\nu)p^2}{(p^2 - n^2)^2}\,nA \quad [15]$$

The assumption contained in Equation [13a] is correct if upon substitution in Equation [1] an identity is obtained. The condition of this is

$$(p^2 - n^2)^4 = -4K^4p^4 \quad [16]$$

This equation has eight roots for p which have to be treated individually. One root is characterized by the following choices

$$(p^2 - n^2)^2 = +i2K^2p^2 \quad [17a]$$

$$p^2 - n^2 = (1+i)Kp \quad [17b]$$

If p is represented as

$$p = \alpha + i\beta \quad [18]$$

where α and β are real quantities, Equation [17b] is equivalent to the following two equations containing only real quantities

$$ab - n^2 - Kb = 0 \quad [19a]$$

$$a^2 - b^2 - 2Ka = 0 \quad [19b]$$

where

$$a = \alpha + \beta \qquad b = \alpha - \beta \quad [20]$$

From Equation [19a]

$$a = K + (n^2/b) \quad [21]$$

and substitution into Equation [19b] yields the biquadratic

$$b^4 + K^2b^2 - n^4 = 0 \quad [22]$$

The solution is

$$b^2 = -(K^2/2) + [(K^2/2)^2 + n^4]^{1/2} \quad [23]$$

where the square root must be taken with the positive sign in order to obtain a real quantity for b. The positive square root of the right-hand member is designated by Ω

$$\Omega = +\{-(K^2/2) + [(K^2/2)^2 + n^4]^{1/2}\}^{1/2} \quad [24]$$

[4] See, for instance, reference (5), p. 90.

Both $+\Omega$ and $-\Omega$ correspond to solutions of Equation [1]. If one chooses the negative sign

$$b = -\Omega \quad [25]$$

a becomes

$$a = K - (n^2/\Omega) \quad [26]$$

and from

$$\alpha = (1/2)(a+b) \qquad \beta = (1/2)(a-b) \quad [27]$$

the real and the imaginary parts of the root are obtained as

$$\alpha = -\alpha_2 \qquad \beta = \beta_2 \quad [28]$$

where

$$\alpha_2 = (1/2)[\Omega - K + (n^2/\Omega)] \quad [29a]$$

$$\beta_2 = (1/2)[\Omega + K - (n^2/\Omega)] \quad [29b]$$

Hence the root of Equation [1] corresponding to the choice made is

$$p = -\alpha_2 + i\beta_2 \quad [30]$$

In evaluating the axial and the circumferential displacements the following expressions must be determined

$$p^2 = n^2 - K[(\alpha_2 + \beta_2) + i(\alpha_2 - \beta_2)] \quad [31a]$$

$$\frac{1}{p^2 - n^2} = \frac{-(1/2K)}{\alpha_2^2 + \beta_2^2}[(\alpha_2 + \beta_2) - i(\alpha_2 - \beta_2)] \quad [31b]$$

$$\frac{1}{(p^2 - n^2)^2} = \frac{(1/2K^2)}{(\alpha_2^2 + \beta_2^2)^2}[2\alpha_2\beta_2 - i(\alpha_2^2 - \beta_2^2)] \quad [31c]$$

$$\frac{p^2}{(p^2 - n^2)^2} = \frac{-i}{2K^2} \quad [31d]$$

$$pe^{px} = e^{-\alpha_2 x}[-\alpha_2\cos\beta_2 x - \beta_2\sin\beta_2 x + i(\beta_2\cos\beta_2 x - \alpha_2\sin\beta_2 x)] \quad [31e]$$

Substitution of these expressions in Equations [13b] and [14] results in

$$u/[Ae^{-\alpha_2 x}\cos n\varphi] = \frac{-1}{2K^2}\left\{\left[\frac{n^2}{(\alpha_2^2 + \beta_2^2)} - \nu\right]\beta_2\cos\beta_2 x + \left[\frac{n^2}{(\alpha_2^2 + \beta_2^2)} + \nu\right]\alpha_2\sin\beta_2 x\right\} + \frac{i}{2K^2}\left\{\left[\frac{n^2}{(\alpha_2^2 + \beta_2^2)} + \nu\right] \times \alpha_2\cos\beta_2 x - \left[\frac{n^2}{(\alpha_2^2 + \beta_2^2)} - \nu\right]\beta_2\sin\beta_2 x\right\} \quad [32]$$

Equation [13c] together with Equations [31] and [15] yields

$$v/[Ae^{-\alpha_2 x}\sin n\varphi] = \frac{n}{2K^2}\left\{n^2\frac{2\alpha_2\beta_2}{(\alpha_2^2 + \beta_2^2)^2}\cos\beta_2 x + \left[n^2\frac{(\alpha_2^2 - \beta_2^2)}{(\alpha_2^2 + \beta_2^2)^2} - (2+\nu)\right]\sin\beta_2 x\right\} - \frac{in}{2K^2}\left\{\left[n^2\frac{(\alpha_2^2 - \beta_2^2)}{(\alpha_2^2 + \beta_2^2)^2} - (2+\nu)\right]\cos\beta_2 x - n^2\frac{2\alpha_2\beta_2}{(\alpha_2^2 + \beta_2^2)^2}\sin\beta_2 x\right\} \quad [33]$$

Finally the radial displacement can be given as

$$w/[Ae^{-\alpha_2 x}\cos n\varphi] = \cos\beta_2 x + i\sin\beta_2 x \quad [34]$$

In Equations [32] to [34] the symbol A designates an integration constant.

If Equations [17] are replaced by the relationships

$$(p^2 - n^2)^2 = -i2K^2p^2 \quad [35a]$$

$$p^2 - n^2 = +(1 - i)Kp \quad [35b]$$

and Equation [18] is maintained unchanged, Equation [21] is replaced by

$$b = K + (n^2/a) \quad [36]$$

and Equation [23] by

$$a^2 = -(K^2/2) + [(K^2/2)^2 + n^4]^{1/2} \quad [37]$$

Let $a = -\Omega$, where Ω is defined in Equation [24]; then the root of Equation [1] is

$$p = -\alpha_2 - i\beta_2 \quad [38]$$

with α_2 and β_2 defined in Equations [29]. This is the conjugate of the root obtained earlier. Similarly the expressions resulting for u, v, and w are conjugate to those given in the foregoing. Hence the real and the imaginary parts of the solution presented are independent solutions of the system of equations.

If Equations [17] (or Equations [35]) are replaced by

$$(p^2 - n^2)^2 = i2K^2p^2 \quad [39a]$$

$$p^2 - n^2 = -(1 + i)Kp \quad [39b]$$

again Equation [23] is obtained for b^2. If b is chosen as $-\Omega$ as in Equation [25], with Ω defined in Equation [24], the root of the eighth-order equation becomes

$$p = -\alpha_1 + i\beta_1 \quad [40]$$

where

$$\alpha_1 = (1/2)[\Omega + K + (n^2/\Omega)] \quad [41a]$$

$$\beta_1 = (1/2)[\Omega - K - (n^2/\Omega)] \quad [41b]$$

Equations [31] remain unchanged except for the substitution of $-K$ for K and the subscript 1 for the subscript 2. Similarly, the new expressions for the displacements can be obtained from those presented in Equations [32] to [34] by substituting 1 for 2 in the subscripts.

Finally the choice

$$(p^2 - n^2)^2 = -i\,2K^2p^2 \quad [42a]$$

$$p^2 - n^2 = -(1 - i)Kp \quad [42b]$$

$$a = -\Omega \quad [42c]$$

yields

$$p = -\alpha_1 - i\beta_1 \quad [43]$$

and a set of expressions for the deflections which are conjugate to the preceding ones. Hence both the real and the imaginary parts of the solutions containing α_1 and β_1 are solutions of Equations [1] to [3].

This takes care of all the solutions in which the real part of the root is negative. Those for which the real part of the root is positive are obtained when the foregoing calculations are modified by using $+\Omega$ in place of $-\Omega$. This change will now be carried out for the first set of calculations. One obtains in place of Equation [30]

$$p = \alpha_1 - i\beta_1 \quad [44]$$

Equations [31] are replaced by

$$p^2 = n^2 + K[(\alpha_1 + \beta_1) + i(\alpha_1 - \beta_1)] \quad [45a]$$

$$\frac{1}{p^2 - n^2} = \frac{(1/2K)}{\alpha_1^2 + \beta_1^2}[(\alpha_1 + \beta_1) - i(\alpha_1 - \beta_1)] \quad [45b]$$

$$\frac{1}{(p^2 - n^2)^2} = \frac{(1/2K^2)}{(\alpha_1^2 + \beta_1^2)^2}[2\alpha_1\beta_1 - i(\alpha_1^2 - \beta_1^2)] \quad [45c]$$

$$\frac{p^2}{(p^2 - n^2)^2} = \frac{-i}{2K^2} \quad [45d]$$

$$pe^{pz} = e^{\alpha_1 z}[\alpha_1 \cos \beta_1 x - \beta_1 \sin \beta_1 x - i(\beta_1 \cos \beta_1 x + \alpha_1 \sin \beta_1 x)] \quad [45e]$$

Finally the displacements become

$$u/[Ae^{\alpha_1 z} \cos n\varphi] = \frac{1}{2K^2}\left\{\left[\frac{n^2}{\alpha_1^2 + \beta_1^2} - \nu\right]\beta_1 \cos \beta_1 x - \left[\frac{n^2}{\alpha_1^2 + \beta_1^2} + \nu\right] \times \alpha_1 \sin \beta_1 x\right\} - \frac{i}{2K^2}\left\{\left[\frac{n^2}{\alpha_1^2 + \beta_1^2} + \nu\right]\alpha_1 \cos \beta_1 x + \left[\frac{n^2}{\alpha_1^2 + \beta_1^2} - \nu\right]\beta_1 \sin \beta_1 x\right\} \quad [46]$$

$$v/[Ae^{\alpha_1 z} \sin n\varphi] = \frac{n}{2K^2}\left\{n^2\frac{2\alpha_1\beta_1}{(\alpha_1^2 + \beta_1^2)^2}\cos \beta_1 x - \left[n^2\frac{\alpha_1^2 - \beta_1^2}{(\alpha_1^2 + \beta_1^2)^2} - (2 + \nu)\right]\sin \beta_1 x\right\} - \frac{in}{2K^2}\left\{\left[n^2\frac{\alpha_1^2 - \beta_1^2}{(\alpha_1^2 + \beta_1^2)^2} - (2 + \nu)\right]\cos \beta_1 x + n^2\frac{2\alpha_1\beta_1}{(\alpha_1^2 + \beta_1^2)^2}\sin \beta_1 x\right\} \quad [47]$$

$$w/[Ae^{\alpha_1 z} \cos n\varphi] = \cos \beta_1 x - i \sin \beta_1 x \quad [48]$$

If a similar change is made in the second set of calculations, the root becomes

$$p = \alpha_1 + i\beta_1 \quad [49]$$

and the expressions for u, v, and w become the conjugates of those given in Equations [46] to [48]. This proves that the real and the imaginary parts of the right-hand members of Equations [46] to [48] are individual solutions of Equations [1] to [3].

Replacement of $-\Omega$ by $+\Omega$ in the remaining two sets of calculations shows that both the real and the imaginary parts of the solutions obtainable from Equations [46] to [48] through replacement of the subscript 1 by subscript 2 are individually solutions of Equations [1] to [3].

Membrane Stresses and Moment and Shear Resultants

If the expressions given for the deflections in Equations [13] are substituted in Equations [8] to [12], the following equations are obtained

$$\sigma_x = E\frac{p^2n^2}{(p^2 - n^2)^2}Ae^{pz} \cos n\varphi \quad [50]$$

$$\sigma_\varphi = -E\frac{p^4}{(p^2 - n^2)^2}Ae^{pz} \cos n\varphi \quad [51]$$

$$\tau_{x\varphi} = -E\frac{np^3}{(p^2 - n^2)^2}Ae^{pz} \sin n\varphi \quad [52]$$

$$M_x = -(D/a)(p^2 - \nu n^2)Ae^{pz} \cos n\varphi \quad [53]$$

$$M_\varphi = -(D/a)(\nu p^2 - n^2)Ae^{pz} \cos n\varphi \quad [54]$$

$$M_{x\varphi} = -(1-\nu)(D/a)npAe^{pz}\sin n\varphi \quad [55]$$

$$Q_x = -(D/a^2)(p^2-n^2)pAe^{pz}\cos n\varphi \quad [56]$$

$$Q_\varphi = (D/a^2)(p^2-n^2)nAe^{pz}\sin n\varphi \quad [57]$$

$$Q_{x\cdot eff} = -(D/a^2)[p^2-(2-\nu)n^2]pAe^{pz}\cos n\varphi \quad [58]$$

$$Q_{\varphi\cdot eff} = -(D/a^2)[n^2-(2-\nu)p^2]nAe^{pz}\sin n\varphi \quad [59]$$

When $p = -\alpha_2 + i\beta_2$ these expressions become

$$\sigma_x/[AE\,e^{-\alpha_2 z}\cos n\varphi] = (n^2/2K^2)(\sin\beta_2 x - i\cos\beta_2 x) \quad [60]$$

$$\sigma_\varphi/[AE\,e^{-\alpha_2 z}\cos n\varphi] = -(n^2/2K^2)(\sin\beta_2 x - i\cos\beta_2 x) + (1/2K)\{(\alpha_2-\beta_2)\cos\beta_2 x + (\alpha_2+\beta_2)\sin\beta_2 x - i[(\alpha_2+\beta_2)\cos\beta_2 x - (\alpha_2-\beta_2)\sin\beta_2 x]\} \quad [61]$$

$$\tau_{x\varphi}/[AEe^{-\alpha_2 z}\sin n\varphi] = -(n/2K^2)[\beta_2\cos\beta_2 x - \alpha_2\sin\beta_2 x + i(\alpha_2\cos\beta_2 x + \beta_2\sin\beta_2 x)] \quad [62]$$

$$M_x/[A(D/a)e^{-\alpha_2 z}\cos n\varphi] = -(1-\nu)n^2(\cos\beta_2 x + i\sin\beta_2 x) + K\{(\alpha_2+\beta_2)\cos\beta_2 x - (\alpha_2-\beta_2)\sin\beta_2 x + i[(\alpha_2-\beta_2)\cos\beta_2 x + (\alpha_2+\beta_2)\sin\beta_2 x]\} \quad [63]$$

$$M_\varphi/[A(D/a)e^{-\alpha_2 z}\cos n\varphi] = (1-\nu)n^2(\cos\beta_2 x + i\sin\beta_2 x) + \nu K\{(\alpha_2+\beta_2)\cos\beta_2 x - (\alpha_2-\beta_2)\sin\beta_2 x + i[(\alpha_2-\beta_2)\cos\beta_2 x + (\alpha_2+\beta_2)\sin\beta_2 x]\} \quad [64]$$

$$M_{x\varphi}/[A(D/a)e^{-\alpha_2 z}\sin n\varphi] = (1-\nu)n[\alpha_2\cos\beta_2 x + \beta_2\sin\beta_2 x - i(\beta_2\cos\beta_2 x - \alpha_2\sin\beta_2 x)] \quad [65]$$

$$Q_x/[A(D/a^2)e^{-\alpha_2 z}\cos n\varphi] = K\{-(\alpha_2^2+2\alpha_2\beta_2-\beta_2^2)\cos\beta_2 x + (\alpha_2^2-2\alpha_2\beta_2-\beta_2^2)\sin\beta_2 x + i[-(\alpha_2^2-2\alpha_2\beta_2-\beta_2^2)\times\cos\beta_2 x - (\alpha_2^2+2\alpha_2\beta_2-\beta_2^2)\sin\beta_2 x]\} \quad [66]$$

$$Q_\varphi/[A(D/a^2)e^{-\alpha_2 z}\sin n\varphi] = -nK\{(\alpha_2+\beta_2)\cos\beta_2 x - (\alpha_2-\beta_2)\sin\beta_2 x + i[(\alpha_2-\beta_2)\cos\beta_2 x + (\alpha_2+\beta_2)\sin\beta_2 x]\} \quad [67]$$

$$Q_{x\cdot eff}/[A(D/a^2)e^{-\alpha_2 z}\cos n\varphi] = (1-\nu)n^2[-\alpha_2\cos\beta_2 x - \beta_2\sin\beta_2 x + i(\beta_2\cos\beta_2 x - \alpha_2\sin\beta_2 x)] + K\{-(\alpha_2^2+2\alpha_2\beta_2-\beta_2^2)\cos\beta_2 x + (\alpha_2^2-2\alpha_2\beta_2-\beta_2^2)\sin\beta_2 x + i[-(\alpha_2^2-2\alpha_2\beta_2-\beta_2^2)\cos\beta_2 x - (\alpha_2^2+2\alpha_2\beta_2-\beta_2^2)\sin\beta_2 x]\} \quad [68]$$

$$Q_{\varphi\cdot eff}/[A(D/a^2)e^{-\alpha_2 z}\sin n\varphi] = (1-\nu)n^2(\cos\beta_2 x + i\sin\beta_2 x) - (2-\nu)Kn\{(\alpha_2+\beta_2)\cos\beta_2 x - (\alpha_2-\beta_2)\sin\beta_2 x + i[(\alpha_2-\beta_2)\cos\beta_2 x + (\alpha_2+\beta_2)\times\sin\beta_2 x]\} \quad [69]$$

When $p = \alpha_1 - i\beta_1$ one obtains

$$\sigma_x/[AEe^{\alpha_1 z}\cos n\varphi] = -(n^2/2K^2)(\sin\beta_1 x + i\cos\beta_1 x) \quad [70]$$

$$\sigma_\varphi/[AEe^{\alpha_1 z}\cos n\varphi] = (n^2/2K^2)(\sin\beta_1 x + i\cos\beta_1 x) - (1/2K)\{(\alpha_1-\beta_1)\cos\beta_1 x - (\alpha_1+\beta_1)\sin\beta_1 x - i[(\alpha_1+\beta_1)\cos\beta_1 x + (\alpha_1-\beta_1)\sin\beta_1 x]\} \quad [71]$$

$$\tau_{x\varphi}/[AEe^{\alpha_1 z}\sin n\varphi] = (n/2K^2)[\beta_1\cos\beta_1 x + \alpha_1\sin\beta_1 x + i(\alpha_1\cos\beta_1 x - \beta_1\sin\beta_1 x)] \quad [72]$$

$$M_x/[A(D/a)e^{\alpha_1 z}\cos n\varphi] = -(1-\nu)n^2(\cos\beta_1 x - i\sin\beta_1 x) - K\{(\alpha_1+\beta_1)\cos\beta_1 x + (\alpha_1-\beta_1)\sin\beta_1 x + i[(\alpha_1-\beta_1)\cos\beta_1 x - (\alpha_1+\beta_1)\sin\beta_1 x]\} \quad [73]$$

$$M_\varphi/[A(D/a)e^{\alpha_1 z}\cos n\varphi] = (1-\nu)n^2(\cos\beta_1 x - i\sin\beta_1 x) - \nu K\{(\alpha_1+\beta_1)\cos\beta_1 x + (\alpha_1-\beta_1)\sin\beta_1 x + i[(\alpha_1-\beta_1)\cos\beta_1 x - (\alpha_1+\beta_1)\sin\beta_1 x]\} \quad [74]$$

$$M_{x\varphi}/[A(D/a)e^{\alpha_1 z}\sin n\varphi] = -(1-\nu)n[\alpha_1\cos\beta_1 x - \beta_1\sin\beta_1 x - i(\beta_1\cos\beta_1 x + \alpha_1\sin\beta_1 x)] \quad [75]$$

$$Q_x/[A(D/a^2)e^{\alpha_1 z}\cos n\varphi] = -K\{(\alpha_1^2+2\alpha_1\beta_1-\beta_1^2)\times\cos\beta_1 x + (\alpha_1^2-2\alpha_1\beta_1-\beta_1^2)\sin\beta_1 x + i[(\alpha_1^2-2\alpha_1\beta_1-\beta_1^2)\cos\beta_1 x - (\alpha_1^2+2\alpha_1\beta_1-\beta_1^2)\sin\beta_1 x]\} \quad [76]$$

$$Q_\varphi/[A(D/a^2)e^{\alpha_1 z}\sin n\varphi] = nK\{(\alpha_1+\beta_1)\cos\beta_1 x + (\alpha_1-\beta_1)\sin\beta_1 x + i[(\alpha_1-\beta_1)\cos\beta_1 x - (\alpha_1+\beta_1)\sin\beta_1 x]\} \quad [77]$$

$$Q_{x\cdot eff}/[A(D/a^2)e^{\alpha_1 z}\cos n\varphi] = (1-\nu)n^2[\alpha_1\cos\beta_1 x - \beta_1\sin\beta_1 x - i(\beta_1\cos\beta_1 x + \alpha_1\sin\beta_1 x)] - K\{(\alpha_1^2+2\alpha_1\beta_1-\beta_1^2)\cos\beta_1 x + (\alpha_1^2-2\alpha_1\beta_1-\beta_1^2)\sin\beta_1 x + i[(\alpha_1^2-2\alpha_1\beta_1-\beta_1^2)\times\cos\beta_1 x - (\alpha_1^2+2\alpha_1\beta_1-\beta_1^2)\sin\beta_1 x]\} \quad [78]$$

$$Q_{\varphi\cdot eff}/[A(D/a^2)e^{\alpha_1 z}\sin n\varphi] = (1-\nu)n^2(\cos\beta_1 x - i\sin\beta_1 x) + (2-\nu)nK\{(\alpha_1+\beta_1)\cos\beta_1 x + (\alpha_1-\beta_1)\sin\beta_1 x + i[(\alpha_1-\beta_1)\cos\beta_1 x - (\alpha_1+\beta_1)\sin\beta_1 x]\} \quad [79]$$

The expressions corresponding to the remaining six roots need not be written because they follow from those given and from the remarks made earlier regarding the roots.

Final Expressions for Displacements, Membrane Stresses, Moments, and Shear Forces

When the solutions corresponding to the eight roots are multiplied by integration constants A_1 to A_8 and added up, the following final expressions result

$$u = (1/2K^2)\{e^{-\alpha_1 z}[-A_1(N_1'\cos\beta_1 x + N_1\sin\beta_1 x) + A_2(N_1\cos\beta_1 x - N_1'\sin\beta_1 x)] + e^{-\alpha_2 z}[-A_3(N_2'\cos\beta_2 x + N_2\sin\beta_2 x) + A_4(N_2\cos\beta_2 x - N_2'\sin\beta_2 x)] + e^{\alpha_1 z}[A_5(N_1'\cos\beta_1 x - N_1\sin\beta_1 x) - A_6(N_1\cos\beta_1 x + N_1'\sin\beta_1 x)] + e^{\alpha_2 z}[A_7(N_2'\cos\beta_2 x - N_2\sin\beta_2 x) - A_8(N_2\cos\beta_2 x + N_2'\sin\beta_2 x)]\}\cos n\varphi \quad [80]$$

$$v = (n/2K^2)\{e^{-\alpha_1 z}[A_1(M_1'\cos\beta_1 x + M_1\sin\beta_1 x) - A_2(M_1\cos\beta_1 x - M_1'\sin\beta_1 x)] + e^{-\alpha_2 z}[A_3(M_2'\cos\beta_2 x + M_2\sin\beta_2 x) - A_4(M_2\cos\beta_2 x - M_2'\sin\beta_2 x)] + e^{\alpha_1 z}[A_5(M_1'\cos\beta_1 x - M_1\sin\beta_1 x) - A_6(M_1\cos\beta_1 x + M_1'\sin\beta_1 x)] + e^{\alpha_2 z}[A_7(M_2'\cos\beta_2 x - M_2\sin\beta_2 x) - A_8(M_2\cos\beta_2 x + M_2'\sin\beta_2 x)]\}\sin n\varphi \quad [81]$$

$$w = \{e^{-\alpha_1 z}(A_1\cos\beta_1 x + A_2\sin\beta_1 x) + e^{-\alpha_2 z}(A_3\cos\beta_2 x + A_4\sin\beta_2 x) + e^{\alpha_1 z}(A_5\cos\beta_1 x - A_6\sin\beta_1 x) + e^{\alpha_2 z}(A_7\cos\beta_2 x - A_8\sin\beta_2 x)\}\cos n\varphi \quad [82]$$

$$\sigma_z = (En^2/2K^2)\{e^{-\alpha_1 z}(A_1\sin\beta_1 x - A_2\cos\beta_1 x) + e^{-\alpha_2 z}(A_3\sin\beta_2 x - A_4\cos\beta_2 x) - e^{\alpha_1 z}(A_5\sin\beta_1 x + A_6\cos\beta_1 x) - e^{\alpha_2 z}(A_7\sin\beta_2 x + A_8\cos\beta_2 x)\}\cos n\varphi \quad [83]$$

$$\sigma_x = E\Big\{e^{-\alpha_1 x}\Big[A_1\Big(\frac{R_1'}{2K}\cos\beta_1 x + S_1'\sin\beta_1 x\Big) + A_2\Big(-S_1'\cos\beta_1 x + \frac{R_1'}{2K}\sin\beta_1 x\Big)\Big] + e^{-\alpha_2 x}\Big[A_3\Big(\frac{R_2'}{2K}\cos\beta_2 x + S_2'\sin\beta_2 x\Big) + A_4\Big(-S_2'\cos\beta_2 x + \frac{R_2'}{2K}\sin\beta_2 x\Big)\Big] + e^{\alpha_1 x}\Big[A_5\Big(\frac{-R_1'}{2K}\cos\beta_1 x + S_1\sin\beta_1 x\Big) + A_6\Big(S_1\cos\beta_1 x + \frac{R_1'}{2K}\sin\beta_1 x\Big)\Big] + e^{\alpha_2 x}\Big[A_7\Big(\frac{-R_2'}{2K}\cos\beta_2 x + S_2\sin\beta_2 x\Big) + A_8\Big(S_2\cos\beta_2 x + \frac{R_2'}{2K}\sin\beta_2 x\Big)\Big]\Big\}\cos n\varphi \quad [84]$$

$$\tau_{x\varphi} = (En/2K^2)\{e^{-\alpha_1 x}[-A_1(\beta_1\cos\beta_1 x - \alpha_1\sin\beta_1 x) - A_2(\alpha_1\cos\beta_1 x + \beta_1\sin\beta_1 x)] + e^{-\alpha_2 x}[-A_3(\beta_2\cos\beta_2 x - \alpha_2\sin\beta_2 x) - A_4(\alpha_2\cos\beta_2 x + \beta_2\sin\beta_2 x)] + e^{\alpha_1 x}[A_5(\beta_1\cos\beta_1 x + \alpha_1\sin\beta_1 x) + A_6(\alpha_1\cos\beta_1 x - \beta_1\sin\beta_1 x)] + e^{\alpha_2 x}[A_7(\beta_2\cos\beta_2 x + \alpha_2\sin\beta_2 x) + A_8(\alpha_2\cos\beta_2 x - \beta_2\sin\beta_2 x)]\}\sin n\varphi \quad [85]$$

$$M_x = (D/a)\{e^{-\alpha_1 x}[A_1(\Psi_1'\cos\beta_1 x - KR_1'\sin\beta_1 x) + A_2(KR_1'\cos\beta_1 x + \Psi_1'\sin\beta_1 x)] + e^{-\alpha_2 x}[A_3(\Psi_2'\cos\beta_2 x - KR_2'\sin\beta_2 x) + A_4(KR_2'\cos\beta_2 x + \Psi_2'\sin\beta_2 x)] + e^{\alpha_1 x}[A_5(-\Psi_1\cos\beta_1 x - KR_1'\sin\beta_1 x) + A_6(-KR_1'\cos\beta_1 x + \Psi_1\sin\beta_1 x)] + e^{\alpha_2 x}[A_7(-\Psi_2\cos\beta_2 x - KR_2'\sin\beta_2 x) + A_8(-KR_2'\cos\beta_2 x + \Psi_2\sin\beta_2 x)]\}\cos n\varphi \quad [86]$$

$$M_\varphi = (D/a)\{e^{-\alpha_1 x}[A_1(\Gamma_1\cos\beta_1 x - \nu KR_1'\sin\beta_1 x) + A_2(\nu KR_1'\cos\beta_1 x + \Gamma_1\sin\beta_1 x)] + e^{-\alpha_2 x}[A_3(\Gamma_2\cos\beta_2 x - \nu KR_2'\sin\beta_2 x) + A_4(\nu KR_2'\cos\beta_2 x + \Gamma_2\sin\beta_2 x)] + e^{\alpha_1 x}[A_5(-\Gamma_1'\cos\beta_1 x - \nu KR_1'\sin\beta_1 x) + A_6(-\nu KR_1'\cos\beta_1 x + \Gamma_1'\sin\beta_1 x)] + e^{\alpha_2 x}[A_7(-\Gamma_2'\cos\beta_2 x - \nu KR_2'\sin\beta_2 x) + A_8(-\nu KR_2'\cos\beta_2 x + \Gamma_2'\sin\beta_2 x)]\}\cos n\varphi \quad [87]$$

$$M_{x\varphi} = (D/a)(1-\nu)n\{e^{-\alpha_1 x}[A_1(\alpha_1\cos\beta_1 x + \beta_1\sin\beta_1 x) - A_2(\beta_1\cos\beta_1 x - \alpha_1\sin\beta_1 x)] + e^{-\alpha_2 x}[A_3(\alpha_2\cos\beta_2 x + \beta_2\sin\beta_2 x) - A_4(\beta_2\cos\beta_2 x - \alpha_2\sin\beta_2 x)] + e^{\alpha_1 x}[-A_5(\alpha_1\cos\beta_1 x - \beta_1\sin\beta_1 x) + A_6(\beta_1\cos\beta_1 x + \alpha_1\sin\beta_1 x)] + e^{\alpha_2 x}[-A_7(\alpha_2\cos\beta_2 x - \beta_2\sin\beta_2 x) + A_8(\beta_2\cos\beta_2 x + \alpha_2\sin\beta_2 x)]\}\sin n\varphi \quad [88]$$

$$Q_x = K(D/a^2)\{e^{-\alpha_1 x}[A_1(-T_1\cos\beta_1 x + T_1'\sin\beta_1 x) - A_2(T_1'\cos\beta_1 x + T_1\sin\beta_1 x)] + e^{-\alpha_2 x}[A_3(-T_2\cos\beta_2 x + T_2'\sin\beta_2 x) - A_4(T_2'\cos\beta_2 x + T_2\sin\beta_2 x)] - e^{\alpha_1 x}[A_5(T_1\cos\beta_1 x + T_1'\sin\beta_1 x) + A_6(T_1'\cos\beta_1 x - T_1\sin\beta_1 x)] - e^{\alpha_2 x}[A_7(T_2\cos\beta_2 x + T_2'\sin\beta_2 x) + A_8(T_2'\cos\beta_2 x - T_2\sin\beta_2 x)]\}\cos n\varphi \quad [89]$$

$$Q_\varphi = nK(D/a^2)\{e^{-\alpha_1 x}[A_1(-R_1\cos\beta_1 x + R_1'\sin\beta_1 x) - A_2(R_1'\cos\beta_1 x + R_1\sin\beta_1 x)] + e^{-\alpha_2 x}[A_3(-R_2\cos\beta_2 x + R_2'\sin\beta_2 x) - A_4(R_2'\cos\beta_2 x + R_2\sin\beta_2 x)] + e^{\alpha_1 x}[A_5(R_1\cos\beta_1 x + R_1'\sin\beta_1 x) + A_6(R_1'\cos\beta_1 x - R_1\sin\beta_1 x)] + e^{\alpha_2 x}[A_7(R_2\cos\beta_2 x + R_2'\sin\beta_2 x) + A_8(R_2'\cos\beta_2 x - R_2\sin\beta_2 x)]\}\sin n\varphi \quad [90]$$

$$Q_{x\text{-eff}} = -(D/a^2)\{e^{-\alpha_1 x}[A_1(\Theta_1\cos\beta_1 x - \Theta_1'''\sin\beta_1 x) + A_2(\Theta_1'''\cos\beta_1 x + \Theta_1\sin\beta_1 x)] + e^{-\alpha_2 x}[A_3(\Theta_2\cos\beta_2 x - \Theta_2'''\sin\beta_2 x) + A_4(\Theta_2'''\cos\beta_2 x + \Theta_2\sin\beta_2 x)] + e^{\alpha_1 x}[A_5(\Theta_1'\cos\beta_1 x + \Theta_1''\sin\beta_1 x) + A_6(\Theta_1''\cos\beta_1 x - \Theta_1'\sin\beta_1 x)] + e^{\alpha_2 x}[A_7(\Theta_2'\cos\beta_2 x + \Theta_2''\sin\beta_2 x) + A_8(\Theta_2''\cos\beta_2 x - \Theta_2'\sin\beta_2 x)]\}\cos n\varphi \quad [91]$$

$$Q_{\varphi\text{-eff}} = (D/a^2)\{e^{-\alpha_1 x}[A_1(\Phi_1'\cos\beta_1 x + \Lambda_1'\sin\beta_1 x) + A_2(-\Lambda_1'\cos\beta_1 x + \Phi_1'\sin\beta_1 x)] + e^{-\alpha_2 x}[A_3(\Phi_2'\cos\beta_2 x + \Lambda_2'\sin\beta_2 x) + A_4(-\Lambda_2'\cos\beta_2 x + \Phi_2'\sin\beta_2 x)] + e^{\alpha_1 x}[A_5(\Phi_1\cos\beta_1 x + \Lambda_1'\sin\beta_1 x) + A_6(\Lambda_1'\cos\beta_1 x - \Phi_1\sin\beta_1 x)] + e^{\alpha_2 x}[A_7(\Phi_2\cos\beta_2 x + \Lambda_2'\sin\beta_2 x) + A_8(\Lambda_2'\cos\beta_2 x - \Phi_2\sin\beta_2 x)]\}\sin n\varphi \quad [92]$$

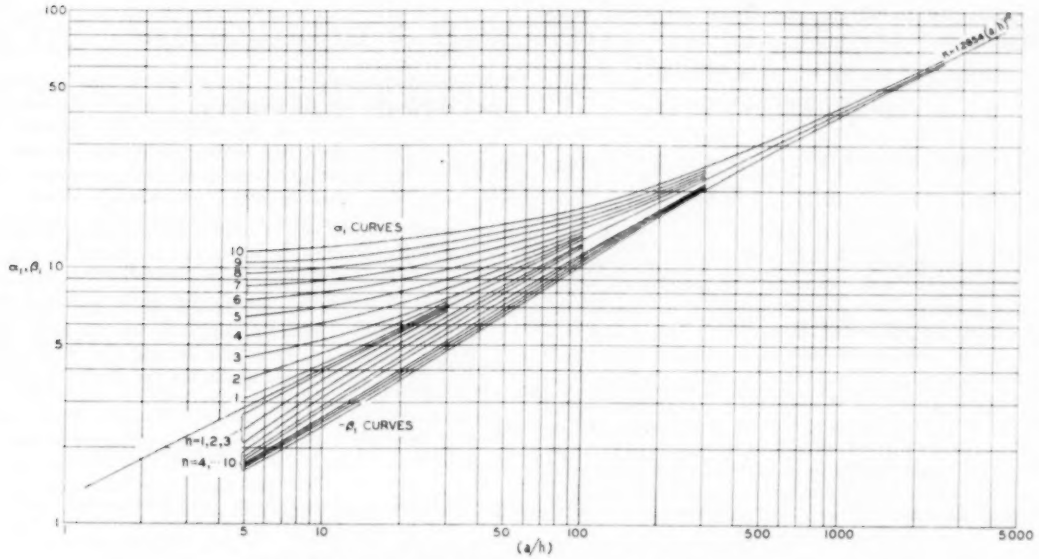

FIG. 2 REAL AND IMAGINARY PARTS α_1 AND β_1 OF FIRST ROOT

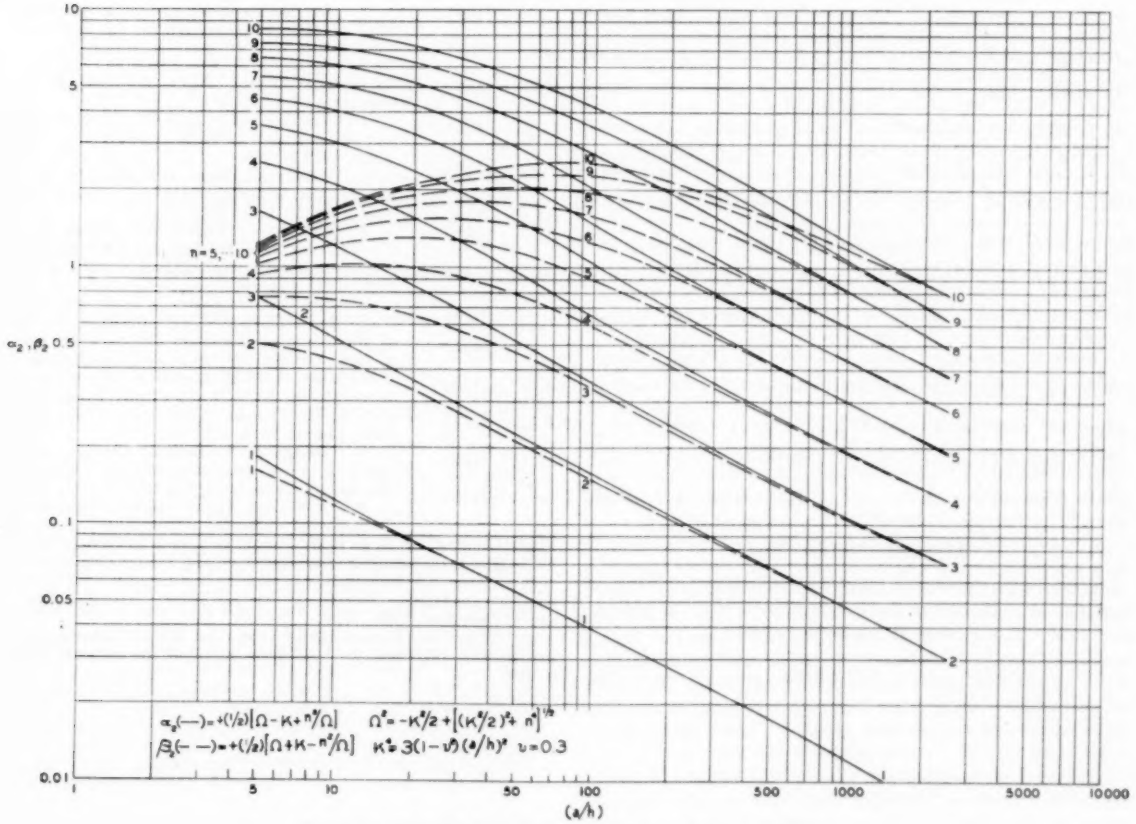

FIG. 3 REAL AND IMAGINARY PARTS α_2 AND β_2 OF SECOND ROOT

In Equations [80] to [92] the symbols used are defined in the following manner

$$K = +[3(1-\nu^2)]^{1/4}(a/h)^{1/2} \qquad D = Eh^3/[12(1-\nu^2)]$$

$$\Omega = +\left\{-(K^2/2) + [(K^2/2)^2 + n^4]^{1/2}\right\}^{1/2}$$

$$\alpha_1 = (1/2)[\Omega + K + (n^2/\Omega)] \qquad \beta_1 = (1/2)[\Omega - K - (n^2/\Omega)]$$

$$\alpha_2 = (1/2)[\Omega - K + (n^2/\Omega)] \qquad \beta_2 = (1/2)[\Omega + K - (n^2/\Omega)]$$

$$M_1 = n^2\frac{\alpha_1^2 - \beta_1^2}{(\alpha_1^2+\beta_1^2)^2} - (2+\nu) \qquad M_1' = n^2\frac{2\alpha_1\beta_1}{(\alpha_1^2+\beta_1^2)^2} \quad [93]$$

$$M_2 = n^2\frac{\alpha_2^2 - \beta_2^2}{(\alpha_2^2+\beta_2^2)^2} - (2+\nu) \qquad M_2' = n^2\frac{2\alpha_2\beta_2}{(\alpha_2^2+\beta_2^2)^2} \quad [94]$$

$$N_1 = \left[\frac{n^2}{\alpha_1^2+\beta_1^2} + \nu\right]\alpha_1 \qquad N_1' = \left[\frac{n^2}{\alpha_1^2+\beta_1^2} - \nu\right]\beta_1 \quad [95]$$

$$N_2 = \left[\frac{n^2}{\alpha_2^2+\beta_2^2} + \nu\right]\alpha_2 \qquad N_2' = \left[\frac{n^2}{\alpha_2^2+\beta_2^2} - \nu\right]\beta_2 \quad [96]$$

$$R_1 = \alpha_1 + \beta_1 = \Omega \qquad R_1' = \alpha_1 - \beta_1 = K + (n^2/\Omega) \quad [97]$$

$$R_2 = \alpha_2 + \beta_2 = \Omega \qquad R_2' = \alpha_2 - \beta_2 = -K + (n^2/\Omega) \quad [98]$$

$$S_1 = (R_1/2K) + (n^2/2K^2) \qquad S_1' = (R_1/2K) - (n^2/2K^2) \quad [99]$$

$$S_2 = (R_2/2K) + (n^2/2K^2) \qquad S_2' = (R_2/2K) - (n^2/2K^2) \quad [100]$$

$$T_1 = \alpha_1^2 - \beta_1^2 + 2\alpha_1\beta_1 \qquad T_1' = \alpha_1^2 - \beta_1^2 - 2\alpha_1\beta_1 \quad [101]$$

$$T_2 = \alpha_2^2 - \beta_2^2 + 2\alpha_2\beta_2 \qquad T_2' = \alpha_2^2 - \beta_2^2 - 2\alpha_2\beta_2 \quad [102]$$

$$\Gamma_1 = \nu KR_1 + (1-\nu)n^2 \qquad \Gamma_1' = \nu KR_1 - (1-\nu)n^2 \quad [103]$$

$$\Gamma_2 = \nu KR_2 + (1-\nu)n^2 \qquad \Gamma_2' = \nu KR_2 - (1-\nu)n^2 \quad [104]$$

$$\Theta_1 = T_1K + (1-\nu)n^2\alpha_1 \qquad \Theta_1' = T_1K - (1-\nu)n^2\alpha_1 \quad [105]$$

$$\Theta_2 = T_2K + (1-\nu)n^2\alpha_2 \qquad \Theta_2' = T_2K - (1-\nu)n^2\alpha_2 \quad [106]$$

$$\Theta_1'' = T_1'K + (1-\nu)n^2\beta_1 \qquad \Theta_1''' = T_1'K - (1-\nu)n^2\beta_1 \quad [107]$$

$$\Theta_2'' = T_2'K + (1-\nu)n^2\beta_2 \qquad \Theta_2''' = T_2'K - (1-\nu)n^2\beta_2 \quad [108]$$

$$\Lambda_1' = (2-\nu)nKR_1' \quad [109a]$$

$$\Lambda_2' = (2-\nu)nKR_2' \quad [109b]$$

$$\Phi_1 = (1-\nu)n^3 + (2-\nu)nKR_1 \qquad \Phi_1' = (1-\nu)n^3 - (2-\nu)nKR_1 \quad [110]$$

$$\Phi_2 = (1-\nu)n^3 + (2-\nu)nKR_2 \qquad \Phi_2' = (1-\nu)n^3 - (2-\nu)nKR_2 \quad [111]$$

$$\Psi_1 = KR_1 + (1-\nu)n^2 \qquad \Psi_1' = KR_1 - (1-\nu)n^2 \quad [112]$$

$$\Psi_2 = KR_2 + (1-\nu)n^2 \qquad \Psi_2' = KR_2 - (1-\nu)n^2 \quad [113]$$

Antisymmetric Loading

The derivations presented refer to conditions symmetric with respect to $\varphi = 0$. When the system is antisymmetric with respect to $\varphi = 0$, Equations [13] must be replaced by

$$w = Ae^{pz}\sin n\varphi \quad [114a]$$

$$u = Be^{pz}\sin n\varphi \quad [114b]$$

$$v = Ce^{pz}\cos n\varphi \quad [114c]$$

The expression derived for B in terms of A, Equation [14], remains unchanged but the right-hand member of Equation [15] must be multiplied by -1. All the equations representing deflections, stresses, and moment and shear-force resultants retain their validity if $\cos n\varphi$ is replaced by $\sin n\varphi$, and $\sin n\varphi$ is replaced by $-\cos n\varphi$.

Chart of Roots

For the convenience of the analyst two plots of the roots have been prepared. Fig. 2 contains α_1 and β_1, and Fig. 3, α_2 and β_2. All these quantities are plotted against the ratio (a/h).

BIBLIOGRAPHY

1 "The Small Free Vibrations and Deformations of a Thin Elastic Shell," by A. E. H. Love, Philosophical Transactions of the Royal Society, London, England, series A, vol. 179, 1888, p. 491.

"A Treatise on the Mathematical Theory of Elasticity," fourth edition. Reprinted in the U. S. A. by Dover Publications, New York, N. Y., 1944, first edition in 1892, p. 545.

2 "Die Stabilität der Kreiszylinderschale," by W. Flügge, *Ingenieur-Archiv*, vol. 3, December, 1932, p. 463.

3 "Statik und Dynamik der Schalen," by Wilhelm Flügge, Julius Springer, Berlin, Germany, 1934, p. 118.

4 "Technische Dynamik," by C. B. Biezeno and R. Grammel, Julius Springer, Berlin, Germany, 1939, p. 469.

5 "Theory of Plates and Shells," by S. Timoshenko, McGraw-Hill Book Company, Inc., New York, N. Y., 1940, p. 440.

6 "Stability of Thin-Walled Tubes Under Torsion," by L. H. Donnell, National Advisory Committee for Aeronautics, Rep. No. 479, Washington, D. C., 1933.

7 "Stress Strain Relations in the Theory of Thin Elastic Shells," by Eric Reissner, *Journal of Mathematics and Physics*, vol. 31, July, 1952, p. 109. See also "Notes on the Foundations of the Theory of Small Displacements of Orthotropic Shells," by F. B. Hildebrand, E. Reissner, and G. B. Thomas, NACA Tech. Note No. 1833, March, 1949.

8 "Design of Cylindrical Concrete Shell Roofs," American Society of Civil Engineers, Manuals of Engineering Practice, No. 31, 1952.

9 "Line Load Applied Along Generators of Thin-Walled Circular Cylindrical Shells of Finite Length," by N. J. Hoff, Joseph Kempner, and Frederick V. Pohle, *Quarterly of Applied Mathematics*, vol. 11, January, 1954, p. 411.

10 "Über die Festigkeit von Kreiszylinderschalen mit nichtachsensymmetrischer Belastung," by K. Miesel, *Ingenieur-Archiv*, vol. 1, December, 1930, p. 22.

11 "Über das Randstörungsproblem an Kreiszylinderschalen," by A. Aas Jakobsen, *Der Bauingenieur*, vol. 20, July 28, 1939, p. 394.

The Anticlastic Curvature of a Strip With Lateral Thickness Variation

By Y. C. FUNG[1] and W. H. WITTRICK,[2] PASADENA, CALIF.

The large deflection equations of von Kármán have been extended to apply to plates of variable thickness with initial deviations of the middle surface from a plane. These are used to determine the distortion of the cross section of a strip with lateral thickness variation, when bent uniformly in the longitudinal direction. Numerical calculations are made for the case of a strip whose cross section is of double-wedge shape and it is shown that when the longitudinal curvature becomes large the distortion of the cross section is quite different from that of a strip of uniform thickness.

Nomenclature

The following nomenclature is used in the paper:

b = semiwidth of plate
k = a parameter specifying initial deflection w_0, defined in Equation [34]
t = plate thickness
t_0 = average thickness
x, y, z = rectangular Cartesian co-ordinates
$w(x, y)$ = final deviation of middle surface from x-y plane
$w_0(x, y)$ = initial deviation of middle surface from x-y plane
$w^*(x, y)$ = $w - w_0$
D = flexural rigidity = $Et^3/12(1 - \mu^2)$
F = stress function defined by Equation [8]
M_x, M_y, M_{xy} = bending and twisting moments per unit length in plate
N_x, N_y, N_{xy} = tensions and shearing force per unit length in the plate
R = longitudinal radius of curvature
α = λ/b
ϕ = y/b
λ = $\frac{b}{\sqrt{Rt_0}}[3(1-\mu^2)]^{1/4}$, a nondimensional parameter
μ = Poisson's ratio, taken as 0.32 in numerical examples
ρ = t/t_0
ξ = $1 - \phi$
$\zeta(y)$ = distortion of the middle line of a cross section

[1] Assistant Professor of Aeronautical Engineering, California Institute of Technology.

[2] Visiting Research Fellow, California Institute of Technology, on leave from the University of Sydney, Australia.

Presented at the West Coast Meeting of the Applied Mechanics Division, University of California, Berkeley, Calif., June 21–23, 1954, of The American Society of Mechanical Engineers.

Discussion of this paper should be addressed to the Secretary, ASME, 29 West 39th Street, New York, N. Y., and will be accepted until January 10, 1955, for publication at a later date. Discussion received after the closing date will be returned.

Note: Statements and opinions advanced in papers are to be understood as individual expressions of their authors and not those of the Society. Manuscript received by ASME Applied Mechanics Division, February 8, 1954. Paper No. 54—APM-7.

Introduction

Consider the problem of a long flat strip of uniform thickness bent uniformly in the longitudinal direction. The simple theory of bending predicts that, if the longitudinal curvature is $1/R$, the cross section assumes a constant anticlastic curvature equal to $-\mu/R$, where μ is Poisson's ratio. It has long been known, however, that if the width $2b$ of the strip is large in comparison with its thickness t, simple bending theory does not give a true picture and that, in fact, the cross section appears to be quite flat. This problem was recognized by Searle (1)[3] in 1908, who concluded that the cross-sectional distortion depends upon the value of a parameter b^2/Rt. This conclusion recently has been confirmed by Ashwell (2) who, in 1950, gave a complete solution to the problem. He showed that if $b^2/Rt \ll 1$ the picture given by simple bending theory is correct. If however b^2/Rt is large (> 100, say) the cross-sectional distortion is confined to narrow regions, or boundary layers, near the two edges of the strip and over the remainder the cross section is substantially flat. It is evident from plate theory that over this flat portion of the cross section a lateral bending moment equal to μ times the longitudinal bending moment must exist in the plate. At the edges, this lateral bending moment is obviously zero so that the function of the boundary layer is to build up the lateral bending moment from zero at the edge to its value in the middle of the plate. The mechanism by which the boundary layer fulfills this function is quite clear. Because of the distortion in the boundary layer there exist longitudinal stresses in the middle surface of the plate which are confined to the boundary layer. These membrane stresses, combined with the longitudinal curvature, effectively provide forces normal to the surface of the plate and it is easy to show that, when integrated through the boundary layer, their resultant is a pure couple equal to μ times the longitudinal bending moment.

This paper is concerned with the effect of lateral-thickness variation on the problem described. In order to include this effect it is first necessary to extend the large deflection equations of von Kármán to apply to plates of variable thickness with initial deviations of the middle surface from a plane. The equations for uniform bending of a strip with arbitrary lateral-thickness variation are then derived and numerical solutions worked out for the particular case of a strip whose cross section is of symmetrical double-wedge shape. These solutions show that the type of cross-sectional distortion which appears is dependent upon a parameter b^2/Rt_0, where again $2b$ is the width and $1/R$ the longitudinal curvature, but t_0 is now the mean thickness of the plate. If $b^2/Rt_0 \ll 1$, the lateral curvature is constant and equal to $-\mu/R$, as given by simple bending theory.

As b^2/Rt_0 becomes large, however, the asymptotic behavior is exactly the reverse of that of a corresponding uniform plate. The cross section is now very nearly flat except for a region near the middle of the plate. There is, however, another essential difference between the flat regions in the two cases, namely, that in a plate of uniform thickness the membrane stress is zero in the flat region, whereas in the tapered plate the longitudinal membrane stress is finite and constant. This result is explainable by a con-

[3] Numbers in parentheses refer to the Bibliography at the end of the paper.

sideration of the lateral bending moment required to eliminate the lateral curvature produced by the longitudinal bending moment.[4]

Large Deflection Equations for Plates of Variable Thickness With Initial Curvatures

Consider a thin plate of variable thickness whose middle surface initially deviates from the x-y plane by a small amount $w_0(x, y)$ and that the plate is then free from internal stresses. Suppose that the plate is bent by means of forces applied on its edges and by a lateral pressure $q(x, y)$ applied on its surface in a direction perpendicular to the (x, y)-plane. Let $w(x, y)$ represent the final shape of the middle surface. It will be assumed that the deflections w_0 and w are everywhere small enough to satisfy the following inequalities

$$(\partial\omega_0/\partial x)^2 \ll 1,\ (\partial\omega_0/\partial y)^2 \ll 1,\ (\partial\omega/\partial x)^2 \ll 1,\ (\partial\omega/\partial y)^2 \ll 1 \quad [1]$$

Further, let u and v be the movements in the x and y-directions of a point on the middle surface during the application of the load. Then the strains e_x, e_y, and e_{xy} at a point (x, y, z) where z is the distance from the middle surface are given to our order of approximation by

$$\left.\begin{aligned} e_x &= \frac{\partial u}{\partial x} + \frac{1}{2}\left(\frac{\partial \omega}{\partial x}\right)^2 - \frac{1}{2}\left(\frac{\partial \omega_0}{\partial x}\right)^2 - z\,\frac{\partial^2 \omega^*}{\partial x^2} \\ e_y &= \frac{\partial v}{\partial y} + \frac{1}{2}\left(\frac{\partial \omega}{\partial y}\right)^2 - \frac{1}{2}\left(\frac{\partial \omega_0}{\partial y}\right)^2 - z\,\frac{\partial^2 \omega^*}{\partial y^2} \\ e_{xy} &= \frac{\partial u}{\partial y} + \frac{\partial v}{\partial x} + \frac{\partial \omega}{\partial x}\frac{\partial \omega}{\partial y} - \frac{\partial \omega_0}{\partial x}\frac{\partial \omega_0}{\partial y} - 2z\,\frac{\partial^2 \omega^*}{\partial x \partial y} \end{aligned}\right\} \quad [2]$$

where $w^* = w - w_0$.

If the corresponding stresses are σ_x, σ_y, and τ_{xy} the stress-strain relations give

$$\left.\begin{aligned} Ee_x &= \sigma_x - \mu\sigma_y \\ Ee_y &= \sigma_y - \mu\sigma_x \\ Ee_{xy} &= 2(1+\mu)\tau_{xy} \end{aligned}\right\} \quad [3]$$

where E is Young's modulus and μ is Poisson's ratio. Let the tensions and shearing force per unit length in the plate be N_x, N_y, and N_{xy}, so that

$$N_x = \int_{-t/2}^{t/2} \sigma_x dz, \quad N_y = \int_{-t/2}^{t/2} \sigma_y\, dz, \quad N_{xy} = \int_{-t/2}^{t/2} \tau_{xy}\, dz \quad [4]$$

where $t(x, y)$ is the thickness of the plate.

Also, let the bending moments and twisting moment per unit length be M_x, M_y, and M_{xy} so that

$$M_x = \int_{-t/2}^{t/2} \sigma_x\, z\, dz, \quad M_y = \int_{-t/2}^{t/2} \sigma_y z\, dz, \quad M_{xy} = \int_{-t/2}^{t/2} \tau_{xy} z\, dz \quad [5]$$

The equations of equilibrium of an element of the plate in the x, y, and z-directions, respectively, are

$$\left.\begin{aligned} \frac{\partial N_x}{\partial x} + \frac{\partial N_{xy}}{\partial y} &= 0 \\ \frac{\partial N_{xy}}{\partial x} + \frac{\partial N_y}{\partial y} &= 0 \end{aligned}\right\} \quad [6]$$

$$\frac{\partial^2 M_x}{\partial x^2} + 2\frac{\partial^2 M_{xy}}{\partial x \partial y} + \frac{\partial^2 M_y}{\partial y^2} + q + N_x\frac{\partial^2 w}{\partial x^2} + 2N_{xy}\frac{\partial^2 w}{\partial x \partial y} + N_y\frac{\partial^2 w}{\partial y^2} = 0 \quad [7]$$

Equations [6] are satisfied by a stress function F defined so that

$$N_x = \frac{\partial^2 F}{\partial y^2}, \quad N_{xy} = -\frac{\partial^2 F}{\partial x \partial y}, \quad N_y = \frac{\partial^2 F}{\partial x^2} \quad [8]$$

Now, using Equations [2], [3], [4], and [8] we obtain the equations

$$\left.\begin{aligned} \frac{\partial u}{\partial x} + \frac{1}{2}\left(\frac{\partial w}{\partial x}\right)^2 - \frac{1}{2}\left(\frac{\partial w_0}{\partial x}\right)^2 &= \frac{1}{Et}\left(\frac{\partial^2 F}{\partial y^2} - \mu\,\frac{\partial^2 F}{\partial x^2}\right) \\ \frac{\partial v}{\partial y} + \frac{1}{2}\left(\frac{\partial w}{\partial y}\right)^2 - \frac{1}{2}\left(\frac{\partial w_0}{\partial y}\right)^2 &= \frac{1}{Et}\left(\frac{\partial^2 F}{\partial x^2} - \mu\,\frac{\partial^2 F}{\partial y^2}\right) \\ \frac{\partial u}{\partial y} + \frac{\partial v}{\partial x} + \frac{\partial w}{\partial x}\frac{\partial w}{\partial y} - \frac{\partial w_0}{\partial x}\frac{\partial w_0}{\partial y} &= -\frac{2(1+\mu)}{Et}\,\frac{\partial^2 F}{\partial x \partial y} \end{aligned}\right\} \quad [9]$$

Also, from Equations [2], [3], and [5] we have

$$\left.\begin{aligned} M_x &= -D\left(\frac{\partial^2 w^*}{\partial x^2} + \mu\,\frac{\partial^2 w^*}{\partial y^2}\right) \\ M_y &= -D\left(\frac{\partial^2 w^*}{\partial y^2} + \mu\,\frac{\partial^2 w^*}{\partial x^2}\right) \\ M_{xy} &= -D(1-\mu)\,\frac{\partial^2 w^*}{\partial x \partial y} \end{aligned}\right\} \quad [10]$$

where

$$D = Et^3/12(1-\mu^2) \quad [11]$$

On eliminating u and v between Equations [9] we obtain the equation

$$\left.\begin{aligned} &\left[\frac{\partial^2}{\partial x^2}\left(\frac{1}{t}\,\frac{\partial^2 F}{\partial x^2}\right) + 2\,\frac{\partial^2}{\partial x \partial y}\left(\frac{1}{t}\,\frac{\partial^2 F}{\partial x \partial y}\right) + \frac{\partial^2}{\partial y^2}\left(\frac{1}{t}\,\frac{\partial^2 F}{\partial y^2}\right)\right] \\ &- \mu\left[\frac{\partial^2}{\partial x^2}\left(\frac{1}{t}\,\frac{\partial^2 F}{\partial y^2}\right) - 2\,\frac{\partial^2}{\partial x \partial y}\left(\frac{1}{t}\,\frac{\partial^2 F}{\partial x \partial y}\right) + \frac{\partial^2}{\partial y^2}\left(\frac{1}{t}\,\frac{\partial^2 F}{\partial x^2}\right)\right] \\ &= E\left[\left(\frac{\partial^2 w}{\partial x \partial y}\right)^2 - \frac{\partial^2 w}{\partial x^2}\,\frac{\partial^2 w}{\partial y^2}\right] - E\left[\left(\frac{\partial^2 w_0}{\partial x \partial y}\right)^2 - \frac{\partial^2 w_0}{\partial x^2}\,\frac{\partial^2 w_0}{\partial y^2}\right] \end{aligned}\right\} \quad [12]$$

Also, substitution of Equations [8] and [10] into Equation [7] gives

$$\left.\begin{aligned} &\left[\frac{\partial^2}{\partial x^2}\left(D\,\frac{\partial^2 w^*}{\partial x^2}\right) + 2\,\frac{\partial^2}{\partial x \partial y}\left(D\,\frac{\partial^2 w^*}{\partial x \partial y}\right) + \frac{\partial^2}{\partial y^2}\left(D\,\frac{\partial^2 w^*}{\partial y^2}\right)\right] \\ &+ \mu\left[\frac{\partial^2}{\partial x^2}\left(D\,\frac{\partial^2 w^*}{\partial y^2}\right) - 2\,\frac{\partial^2}{\partial x \partial y}\left(D\,\frac{\partial^2 w^*}{\partial x \partial y}\right) + \frac{\partial^2}{\partial y^2}\left(D\,\frac{\partial^2 w^*}{\partial x^2}\right)\right] \\ &= q + \frac{\partial^2 F}{\partial y^2}\,\frac{\partial^2 w}{\partial x^2} - 2\,\frac{\partial^2 F}{\partial x \partial y}\,\frac{\partial^2 w}{\partial x \partial y} + \frac{\partial^2 F}{\partial x^2}\,\frac{\partial^2 w}{\partial y^2} \end{aligned}\right\} \quad [13]$$

If t, and therefore D, is constant the left-hand sides of Equations [12] and [13] become $\nabla^4 F/t$ and $D\nabla^4 w^*$, respectively, where ∇^4 is the biharmonic operator. If, in addition, the middle surface is

[4] Upon completion of the present paper the authors were informed that the same problem was solved by Flügge (7) and by Murray and Niles (8) in 1949. Their derivations of the basic differential equation are different from that of the present paper. Their attention was drawn to relatively small values of the parameter b^2/Rt_0. The asymptotic behavior of the anticlastic curvature at large values of b^2/Rt_0 was not investigated by them.

initially flat so that $w_0 = 0$ and $w^* = w$ the equations become identical with those derived by von Kármán in 1910.

Uniform Bending of a Long Strip

Consider a long strip, Fig. 1, which is uniform in the x-direction but of variable thickness $t(y)$ in the y-direction. Suppose also that the initial deviation w_0 of the middle surface from a plane is a

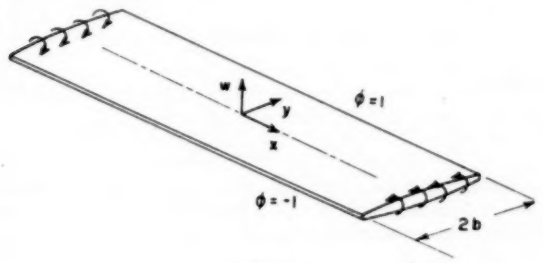

Fig. 1

function of y only, so that the strip is initially straight in the x-direction but the middle line of the cross section is cambered. In order to simplify the problem we shall also assume that the strip is symmetrical about the x-axis so that $t(y)$ and $w_0(y)$ are even functions of y. Now suppose that the strip is bent longitudinally by bending moments applied at its ends so that the curvature in the x-direction is $1/R$. It is clear that every cross section of the strip will distort identically so that we may write

$$w = \frac{x^2}{2R} + w_0(y) + \zeta(y) \quad [14]$$

where $\zeta(y)$ represents the distortion of the middle line of the cross section. In order to satisfy the inequality $(\partial w/\partial x)^2 \ll 1$, Equation [14] is valid only if $x^2 \ll R^2$. However, this is no restriction on the subsequent analysis since all sections behave identically and we therefore can confine our attention to the section $x = 0$.

Because of the identical conditions at all sections it is also evident that the stress function F is a function of y only. Hence, on substituting Equation [14] into the large deflection Equations [12] and [13], we obtain

$$\frac{d^2}{dy^2}\left(\frac{1}{t}\frac{d^2F}{dy^2}\right) = -\frac{E}{R}\frac{d^2}{dy^2}(w_0 + \zeta) \quad [15]$$

$$\frac{d^2}{dy^2}\left(D\frac{d^2\zeta}{dy^2}\right) + \frac{\mu}{R}\frac{d^2D}{dy^2} = \frac{1}{R}\frac{d^2F}{dy^2} \quad [16]$$

Equation [15] can be integrated to give

$$N_x = \frac{d^2F}{dy^2} = -t\left[\frac{E}{R}(w_0 + \zeta) + ay + c\right]$$

Since N_x, t, w_0, and ζ are even functions of y it follows that $a = 0$. Furthermore, since the total tension in the x-direction is zero we have

$$\frac{E}{R}\int_{-b}^{b}(w_0 + \zeta)t\,dy + c\int_{-b}^{b} t\,dy = 0$$

We shall now define the position of the x-y plane in such a way that

$$\int_{-b}^{b}(w_0 + \zeta)t\,dy = 0 \quad [17]$$

This means that at the section $x = 0$ the y-axis passes through the centroid of the distorted cross section. It now follows that $c = 0$ and therefore

$$N_x = \frac{d^2F}{dy^2} = -\frac{Et}{R}(w_0 + \zeta) \quad [18]$$

The membrane stress N_x/t is therefore proportional to the distance of the middle line from the axis through the centroid of the distorted cross section.

Without loss of generality we may stipulate that

$$\int_{-b}^{b} w_0 t\,dy = 0 \quad [19]$$

which is to say that the x-y plane initially passes through the centroid of the cross section $x = 0$. This can be done by giving the whole strip a rigid body movement in a direction perpendicular to the x-y plane while the bending moment is applied, so that at every instant the centroid of the cross section at $x = 0$ lies on the y-axis. It then follows from Equations [17] and [19] that

$$\int_{-b}^{b} \zeta t\,dy = 0 \quad [20]$$

We now substitute Equations [11] and [18] into Equations [16] giving

$$\frac{d^2}{dy^2}\left(t^3\frac{d^2\zeta}{dy^2}\right) + \frac{12(1-\mu^2)t}{R^2}(\zeta + w_0) + \frac{\mu}{R}\frac{d^2}{dy^2}(t^3) = 0$$

It is now convenient to transform the variables t and y into nondimensional form ρ and ϕ by the equations

$$\rho = t/t_0, \quad \phi = y/b \quad [21]$$

where t_0 is the mean thickness. The equations of the edges of the strip are now given by $\phi = \pm 1$. The foregoing differential equation then becomes

$$\frac{d^2}{d\phi^2}\left(\rho^3\frac{d^2\zeta}{d\phi^2}\right) + 4\lambda^4\rho\zeta = -4\lambda^4\rho w_0 - \frac{\mu b^2}{R}\frac{d^2}{d\phi^2}(\rho^3) \quad [22]$$

where λ is a nondimensional constant defined by

$$\lambda^2 = \frac{b^2}{Rt_0}[3(1-\mu^2)]^{1/2} \quad [23]$$

Distortion of Cross Section When the Longitudinal Curvature Is Small

Using Equations [22] we can investigate how the cross section distorts when the longitudinal curvature is small enough to satisfy the inequality $\lambda^2 \ll 1$.

The second term on the right-hand side of Equation [22] is equal to

$$-\lambda^2\mu[3(1-\mu^2)]^{-1/2}t_0\frac{d^2}{d\phi^2}(\rho^3)$$

Hence if $\lambda^2 \ll 1$ we may neglect the two terms involving λ^4 in Equation [22], giving

$$\frac{d^2}{d\phi^2}\left(\rho^3\frac{d^2\zeta}{d\phi^2}\right) = -\frac{\mu b^2}{R}\frac{d^2}{d\phi^2}(\rho^3)$$

On integrating twice we obtain the equation

$$\frac{d^2\zeta}{d\phi^2} = \frac{c_1}{\rho^3} + \frac{c_2\phi}{\rho^3} - \frac{\mu b^2}{R} \quad [24]$$

But ρ and ζ are even functions of ϕ so that $c_2 = 0$.

At the edges $\phi = \pm 1$ the lateral bending moment M_y must be zero, so that

$$D\left(\frac{\partial^2 w^*}{\partial y^2} + \mu\frac{\partial^2 w^*}{\partial x^2}\right) = 0$$

On using Equations [11], [14], and [21] this condition becomes

$$\rho^3\left(\frac{d^2\zeta}{d\phi^2} + \frac{\mu b^2}{R}\right) = 0 \quad \text{at} \quad \phi = \pm 1$$

Hence from Equation [24] we have $c_1 = 0$. It therefore follows that, whatever the variation of thickness, the distortion of the cross section involves a constant curvature in the y-direction given by

$$\frac{d^2\zeta}{dy^2} = -\frac{\mu}{R}$$

This agrees exactly with the anticlastic curvature given by simple bending theory, which is valid if $\lambda^2 \ll 1$.

Strip of Constant Thickness

Although the case of a strip of constant thickness has been fully worked out by Ashwell (2) it will be convenient, for comparison with the tapered case, to derive the results again here.

If ρ is constant Equation [22] becomes

$$\frac{d^4\zeta}{d\phi^4} + 4\lambda^4\zeta = -4\lambda^4 w_0$$

Suppose that initially the strip has a constant lateral curvature, so that

$$w_0 = kt_0\left(\frac{1}{3} - \phi^2\right)$$

which satisfies Equation [19]. The constant k defines the central rise of the plate relative to the two edges.

Then the solution of the foregoing differential equation which is an even function of ϕ is

$$\zeta = -w_0 + A\sin\lambda\phi\sinh\lambda\phi + B\cos\lambda\phi\cosh\lambda\phi$$

The conditions for determining the constants A and B are that $M_y = 0$ at the edge and that Equation [20] is satisfied. These reduce to

$$\int_0^1 \zeta\, d\phi = 0; \quad \left(\frac{d^2\zeta}{d\phi^2}\right)_{\phi=1} = -\frac{\mu b^2}{R}$$

It is easy to see from the differential equation for ζ that if the first of these two conditions is satisfied, then so is the condition that the shear force is zero on the edges.

On solving for A and B we obtain

$$\left.\begin{matrix}A\\B\end{matrix}\right\} = -t_0\left(\frac{\mu}{\sqrt{12(1-\mu^2)}} + \frac{k}{\lambda^2}\right)\frac{\cos\lambda\sinh\lambda \pm \sin\lambda\cosh\lambda}{\sin\lambda\cos\lambda + \sinh\lambda\cosh\lambda}$$

The behavior when λ is small has already been discussed and we now consider the asymptotic behavior as λ becomes large. In this case we have approximately

$$\sinh\lambda = \cosh\lambda = \frac{1}{2}e^{\lambda}$$

so that

$$\left.\begin{matrix}A\\B\end{matrix}\right\} \to -\frac{2\mu t_0}{\sqrt{12(1-\mu^2)}}e^{-\lambda}(\cos\lambda \pm \sin\lambda)$$

Now the *total* distorted shape of the cross section (not the departure from the initial shape) is defined by $(\zeta + w_0)$. At the middle of the plate, $\phi = 0$, we have

$$\zeta + w_0 = B$$

which goes to zero like $e^{-\lambda}$.

Near the edge $\phi = 1$, where $\lambda\phi$ is large enough to make the approximation

$$\sinh\lambda\phi = \cosh\lambda\phi = \frac{1}{2}e^{\lambda\phi}$$

we have

$$\zeta + w_0 = \frac{1}{2}e^{\lambda\phi}(A\sin\lambda\phi + B\cos\lambda\phi)$$

On substituting the asymptotic expressions for A and B and collecting terms together this becomes

$$\zeta + w_0 = -\frac{\mu t_0}{\sqrt{12(1-\mu^2)}}e^{-\alpha Y}(\cos\alpha Y - \sin\alpha Y) \quad [25]$$

where $Y = b(1-\phi)$ is the distance from the edge, and $\alpha = \lambda/b$ so that

$$\alpha^2 = \frac{\sqrt{3(1-\mu^2)}}{Rt_0} \quad [26]$$

The shape represented by Equation [25] is shown plotted in Fig. 2, where μ has been taken as 0.32. It will be seen that if the curvature is large, so that λ is also large, the ultimate shape of the section only deviates from the flat form near the edges. The maximum deviation occurs at the edges and is about one tenth of the

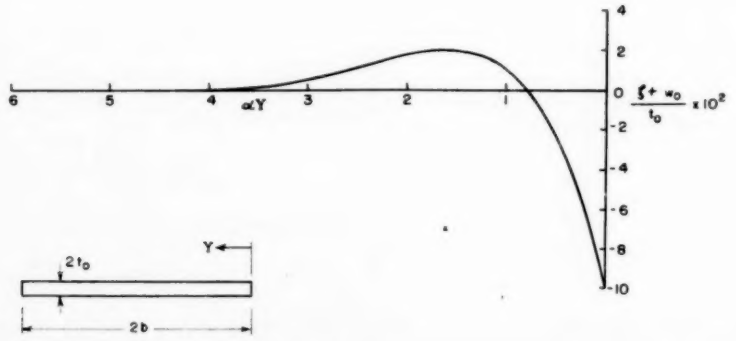

Fig. 2

thickness. Once this stage is reached, increasing the longitudinal curvature has no effect on the maximum deviation from flatness; its only effect is to decrease the width of the "boundary layer" in which the deviation occurs. Furthermore, the shape of the cross section in this boundary layer is quite independent of the width of the cross section; the only effect of increasing the width is to increase the portion which remains flat while the boundary layers remain unchanged.

Strip With Linear Thickness Variation

We now consider the case of a strip in which the thickness tapers linearly from a maximum of $2l_0$ at $y = 0$ to zero at $y = \pm b$. We still admit the possibility of having a middle line of the cross section which is not straight so that the term in w_0 is still included in the differential Equation [22]. If we now substitute

$$\xi = 1 - \phi \quad \ldots\ldots [27]$$

so that $\xi = 0$ at one edge and $\xi = 1$ at the middle of the cross section the thickness ratio is given by $\rho = 2\xi$. Then Equation [22] becomes

$$\frac{d^2}{d\xi^2}\left(\xi^3 \frac{d^2\zeta}{d\xi^2}\right) + \lambda^4\xi\zeta = -\lambda^4\xi w_0 - \frac{6\mu b^2}{R}\xi \quad \ldots\ldots [28]$$

Let ζ_0 be the particular integral of this equation corresponding to the term in w_0 so that

$$\frac{d^2}{d\xi^2}\left(\xi^3 \frac{d^2\zeta_0}{d\xi^2}\right) + \lambda^4\xi\zeta_0 = -\lambda^4\xi w_0 \quad \ldots\ldots [29]$$

Further, let

$$\zeta = \zeta^* + \zeta_0 - \frac{6\mu b^2}{\lambda^4 R}$$

Then

$$\frac{d^2}{d\xi^2}\left(\xi^3 \frac{d^2\zeta^*}{d\xi^2}\right) + \lambda^4\xi\zeta^* = 0$$

Now put

$$\eta = 2\lambda\xi^{1/2} \quad \ldots\ldots [30]$$

Then

$$\frac{d^4\zeta^*}{d\eta^4} + \frac{6}{\eta}\frac{d^3\zeta^*}{d\eta^3} + \frac{3}{\eta^2}\frac{d^2\zeta^*}{d\eta^2} - \frac{3}{\eta^3}\frac{d\zeta^*}{d\eta} + \zeta^* = 0$$

The solution of this equation is

$$\zeta^* = \frac{1}{\eta}\left(S\,\mathrm{ber}'\,\eta + T\,\mathrm{bei}'\,\eta + U\,\mathrm{ker}'\,\eta + V\,\mathrm{kei}'\,\eta\right)$$

where a prime denotes differentiation with respect to η and the *ber*, *bei*, *ker*, and *kei* functions are defined in terms of Bessel functions of complex argument (4) by the equations

$$\mathrm{ber}\,\eta + i\,\mathrm{bei}\,\eta = J_0(\eta i^{3/2})$$

$$\mathrm{ker}\,\eta + i\,\mathrm{kei}\,\eta = I_0(\eta i^{3/2})$$

The *ker'* and *kei'* functions are infinite at the edge $\eta = 0$ so that we must have $U = V = 0$. Hence we are left with

$$\zeta = \frac{1}{\eta}\left(S\,\mathrm{ber}'\,\eta + T\,\mathrm{bei}'\,\eta\right) + \zeta_0 - \frac{6\mu b^2}{\lambda^4 R} \quad \ldots\ldots [31]$$

The series expansions for *ber* η and *bei* η are

$$\mathrm{ber}\,\eta = 1 - \frac{1}{(2!)^2}\left(\frac{\eta}{2}\right)^4 + \frac{1}{(4!)^2}\left(\frac{\eta}{2}\right)^8 - \ldots\ldots$$

$$\mathrm{bei}\,\eta = \left(\frac{\eta}{2}\right)^2 - \frac{1}{(3!)^2}\left(\frac{\eta}{2}\right)^6 + \frac{1}{(5!)^2}\left(\frac{\eta}{2}\right)^{10} - \ldots$$

On differentiating these we obtain

$$\mathrm{ber}'\,\eta = -\left(\frac{\eta}{2}\right)^3\left[\frac{1}{1!2!} - \frac{1}{3!4!}\left(\frac{\eta}{2}\right)^4 + \frac{1}{5!6!}\left(\frac{\eta}{2}\right)^8 - \ldots\right]$$

$$\mathrm{bei}'\,\eta = \left(\frac{\eta}{2}\right)\left[1 - \frac{1}{2!3!}\left(\frac{\eta}{2}\right)^4 + \frac{1}{4!5!}\left(\frac{\eta}{2}\right)^8 - \ldots\right]$$

It is easy to verify that

$$\mathrm{ber}'\,\eta = -\frac{1}{\eta}\int_0^\eta \eta\,\mathrm{bei}\,\eta\,d\eta$$

$$\mathrm{bei}'\,\eta = \frac{1}{\eta}\int_0^\eta \eta\,\mathrm{ber}\,\eta\,d\eta$$

Hence, on differentiating,

$$\mathrm{ber}''\,\eta = -\mathrm{bei}\,\eta - \frac{1}{\eta}\mathrm{ber}'\,\eta$$

$$\mathrm{bei}''\,\eta = \mathrm{ber}\,\eta - \frac{1}{\eta}\mathrm{bei}'\,\eta$$

Tables of the *ber*, *bei*, and *ber'* and *bei'* functions are to be found in reference (5).

To determine the constants of integration S and T we have Equation [20] and the condition that $d\zeta/dy$ is zero at $y = 0$. These conditions become

$$\int_0^1 \xi\zeta\,d\xi = 0$$

and

$$\left(\frac{d\zeta}{d\xi}\right)_{\xi=1} = 0$$

On using these two conditions in conjunction with Equation [30] and the relations between the *ber* and *bei* functions just given, we finally obtain the expressions

$$\left.\begin{aligned} S &= \frac{P(\lambda\,\mathrm{ber}\,2\lambda - \mathrm{bei}'\,2\lambda) + Q(\lambda\,\mathrm{bei}\,2\lambda + \mathrm{ber}'\,2\lambda)}{(\lambda\,\mathrm{ber}\,2\lambda - \mathrm{bei}'\,2\lambda)^2 + (\lambda\,\mathrm{bei}\,2\lambda + \mathrm{ber}'\,2\lambda)^2} \\ T &= \frac{P(\lambda\,\mathrm{bei}\,2\lambda + \mathrm{ber}'\,2\lambda) - Q(\lambda\,\mathrm{ber}\,2\lambda - \mathrm{bei}'\,2\lambda)}{(\lambda\,\mathrm{ber}\,2\lambda - \mathrm{bei}'\,2\lambda)^2 + (\lambda\,\mathrm{bei}\,2\lambda + \mathrm{ber}'\,2\lambda)^2} \end{aligned}\right\} \quad \ldots [32]$$

where

$$\left.\begin{aligned} P &= \frac{6\mu l_0\lambda}{\sqrt{3(1-\mu^2)}} - 2\lambda^3\int_0^1 \xi\zeta_0 d\xi \\ Q &= 2\lambda\left(\frac{d\zeta_0}{d\xi}\right)_{\xi=1} \end{aligned}\right\} \quad \ldots\ldots [33]$$

Thus the solution is now complete in so far as it is only necessary to determine the particular integral ζ_0 of Equation [29] corresponding to any particular initial shape w_0.

The particular section in which we shall be interested is shown in Fig. 3 where the middle line consists initially of two straight lines. In this case

$$w_0 = kl_0\left(\xi - \frac{2}{3}\right) \quad \ldots\ldots [34]$$

the constant 2/3 being introduced in order to satisfy Equation [19]. It is easy to see that the particular integral of Equation [29] is simply $\zeta_0 = -w_0$. Equations [33] then give

$$P = \frac{6\mu\lambda t_0}{\sqrt{3(1-\mu^2)}}, \quad Q = -2k\lambda t_0$$

The shape of the middle line has been computed for five different cases, corresponding to $k = 0, \pm 1$, and ± 5. In each case values of λ equal to 1, 2, 3, 5, 7.5, and 10 were considered and the

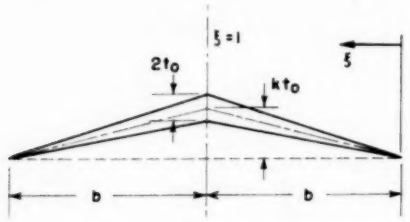

FIG. 3

results are shown plotted in Figs. 4, 5, 6, 7, and 8. The value of μ was assumed to be 0.32. Fig. 4 corresponds to $k = 0$ so that the section is initially of symmetrical double-wedge shape. It will be seen that as λ increases from zero the middle line first of all distorts in the manner predicted by simple bending theory. This, however, induces membrane stresses in the plate which tend to straighten the middle line, and by the time that λ reaches the value 10 about half the cross section is quite flat. In contrast to the plate of uniform thickness, this flat region develops first at the two edges of the plate and spreads inward toward the center as λ increases.

An exactly similar behavior is shown by Figs. 5, 6, 7, and 8. In these cases, because of the initial shape of the section, membrane stresses are induced immediately after bending starts so that there is a progressive tendency for the middle line to straighten as λ increases. In each case a considerable portion of the cross section has become flat when $\lambda = 10$. Because of the different scales to which Figs. 4 to 8 are drawn it is difficult to compare the shapes corresponding to a given value of λ but varying values of k. Consequently, Fig. 9 has been included to show the shape of the various cross sections when $\lambda = 10$. It is impossible to distinguish between them in the region of the edge; in fact, for all the values of k considered, the computation showed that when $\lambda = 10$ the displacement of the edge from the ξ-axis (which passes through the centroid of the distorted cross section) is given by

$$(w_0 + \zeta)_{\xi=1} = -0.0117t_0$$

It is easy to derive this value directly from Equation [28] since over the flat region we must have $d^2\zeta/d\xi^2 = 0$ approximately. Equation [28] then gives

$$(w_0 + \zeta) = -\frac{6\mu b^2}{\lambda^4 R} = -\frac{6\mu}{\sqrt{3(1-\mu^2)}}\frac{t_0}{\lambda^2}$$

If $\mu = 0.32$ this becomes

$$w_0 + \zeta = -\frac{1.17t_0}{\lambda^2} \qquad [35]$$

When $\lambda = 10$ this agrees with the value computed from the analytical expressions involving the *ber* and *bei* functions.

It is interesting to note the reason for the difference between the

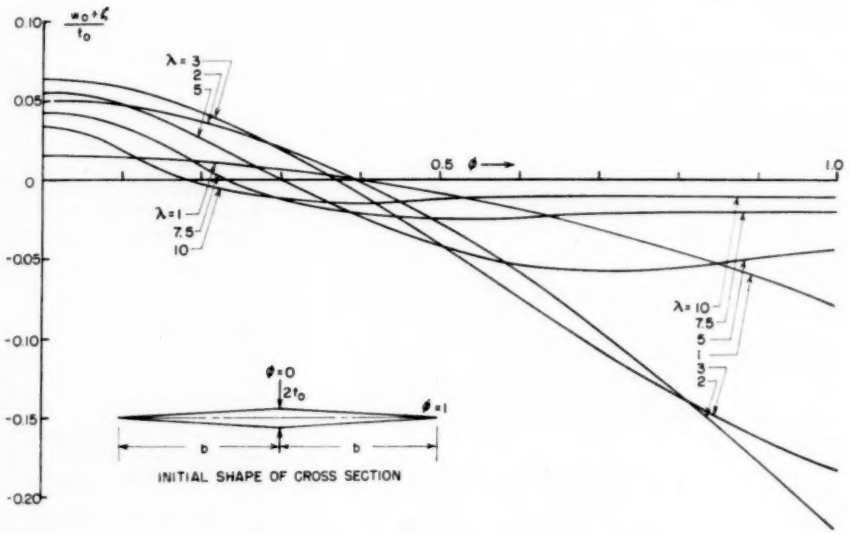

FIG. 4

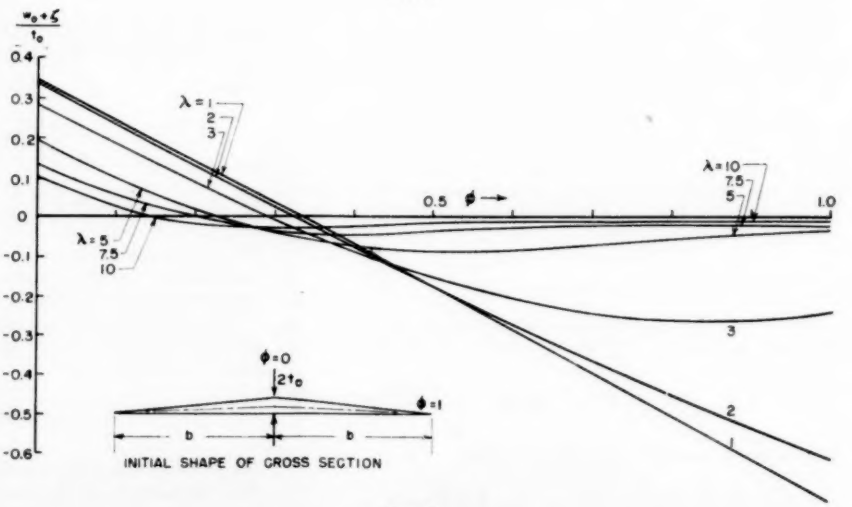

FIG. 5

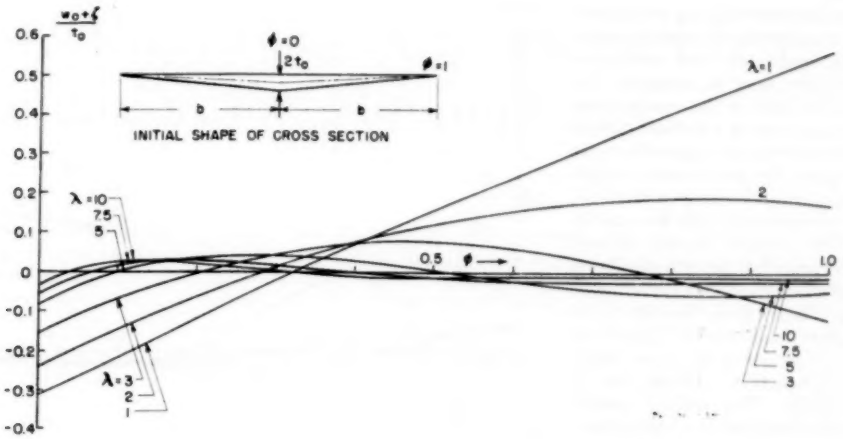

FIG. 6

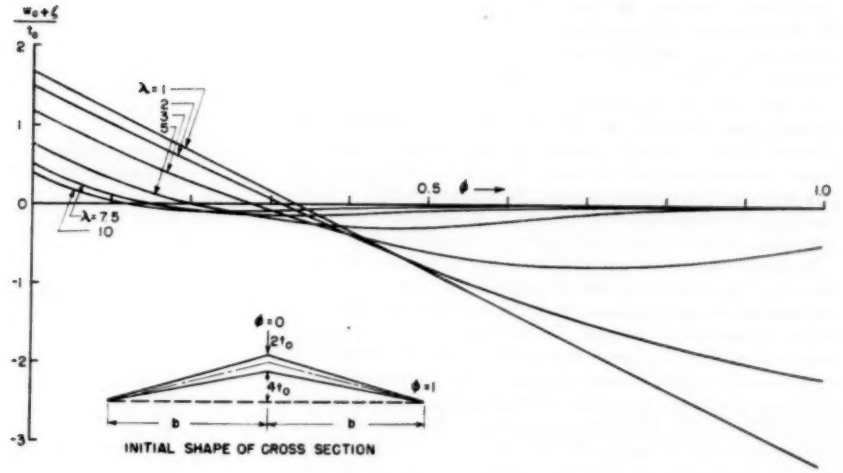

FIG. 7

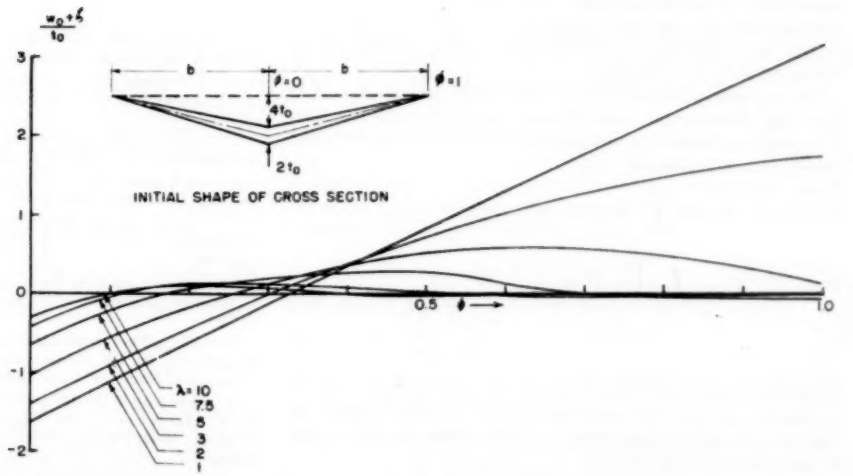

FIG. 8

asymptotic behavior of a tapered plate and that of a uniform plate. In both cases the membrane stresses tend to straighten the middle line of the cross section. In the case of a uniform plate it is clear that in a region where the middle line has become straight the lateral bending moment M_y *is constant* and equal to $-\mu D/R$. This constant bending moment is provided by the membrane stresses which exist in the boundary layers along the edges of the plate; and over the straight central portion of the cross section no membrane stresses are required. The straight portion then coincides, to a high order of approximation, with the axis through the centroid of the distorted cross section. It is easy to see from Equation [25] that the displacement of the straight portion from the centroidal axis is of the order of $t_0 e^{-\lambda}$.

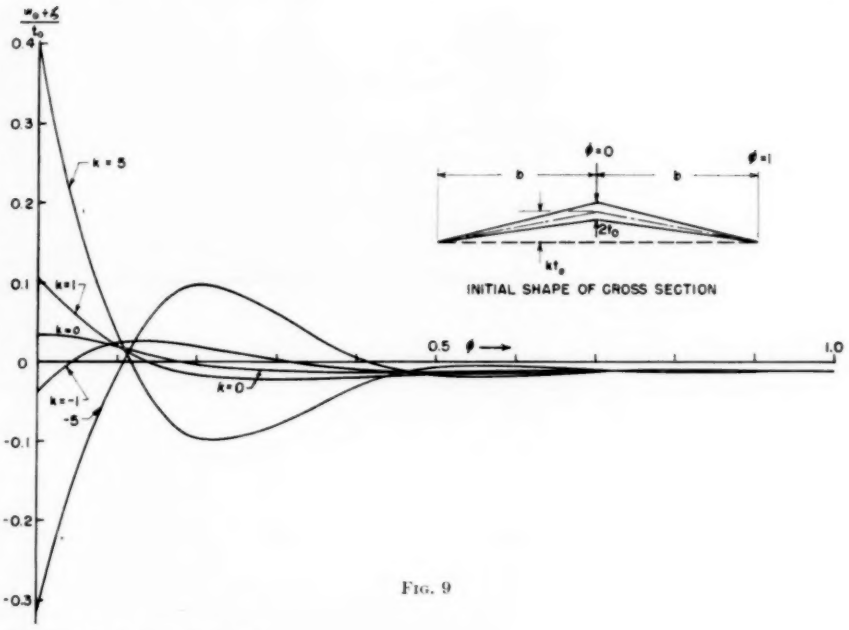

FIG. 9

In the case of the linearly tapered plate, however, the very fact that it is tapered means that in a region where the middle line has become straight the lateral bending moment M_y *must be varying* continuously and this demands a membrane stress in the straight portion. This is provided by a displacement between the straight portion and the centroidal axis of the order t_0/λ^2, given by Equation [35].

It should be pointed out that some of the equilibrium states shown in Figs. 5 to 8 may not be stable. The type of instability envisaged is exactly similar to that of a steel tape measure which has an initial lateral curvature. If the tape is bent the cross section progressively flattens and its moment of inertia therefore decreases as the bending moment increases. For the case of uniform thickness this phenomenon was investigated by Ashwell (6) who showed that if the initial lateral curvature is sufficiently large the relation between longitudinal bending moment and curvature is of the type shown in Fig. 10. The initial slope of the curve corresponds to the flexural rigidity associated with the initial cross section while the asymptotic value when the curvature is large corresponds to the flexural rigidity of a flat cross section. As the bending moment is increased from zero a sudden jump occurs from A to B, the cross section suddenly flattening and the longitudinal curvature suddenly increasing.

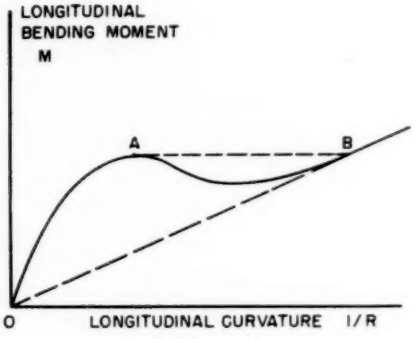

FIG. 10

For the tapered cross sections with which we are concerned here this phenomenon could be investigated in a similar way. The total longitudinal bending moment M required to produce a curvature $1/R$ is given by

$$M = 2\int_0^b M_x dy + 2\int_0^b N_x(w_0 + \zeta)dy$$

$$= -\frac{E}{6(1-\mu^2)}\int_0^b \left(\frac{1}{R} + \mu\frac{d^2\zeta}{dy^2}\right) t^3 dy - \frac{2E}{R}\int_0^b (w_0 + \zeta)^2 t dy$$

Using the expressions derived previously this integral could be evaluated, and it is to be expected that if k is large enough, the relation between bending moment and curvature would be similar to that shown in Fig. 10.

BIBLIOGRAPHY

1 "Experimental Elasticity," by G. F. C. Searle, Cambridge University Press, London, England, 1908, p. 40.

2 "The Anticlastic Curvature of Rectangular Beams and Plates," by D. G. Ashwell, *Journal of the Royal Aeronautical Society*, vol. 54, 1950, p. 708.

3 "Encyklopädie der mathematischen Wissenschaften," by Th. von Kármán, vol. 4, 1910, p. 349.

4 "A Treatise on the Theory of Bessel Functions," by G. N. Watson, Cambridge University Press, London, England, 1922.

5 "Values of the Bessel Functions ber x and bei x and Their Derivatives," by H. B. Dwight, Trans. AIEE, vol. 58, 1939, pp. 787–790.

6 "The Stability in Bending of Slightly Corrugated Plates," by D. G. Ashwell, *Journal of the Royal Aeronautical Society*, vol. 56, 1952, p. 782.

7 "Large Deflections of Thin Wings," by W. Flügge, Technical Report No. 3, Air Forces Contract W33-038, AC-16697, Stanford University, Stanford, Calif., 1949.

8 "Bending of Wide Beams of Doubly Symmetrical Section," by T. R. Murray and A. S. Niles, Technical Report No. 4, Air Forces Contract W33-038, AC-16697, Stanford University, Stanford, Calif., 1949.

Steady-State Vibrations of Beam on Elastic Foundation for Moving Load

By J. T. KENNEY, JR.,[1] PASADENA, CALIF.

This paper presents an analytic solution and resonance diagrams for a constant-velocity moving load on a beam on an elastic foundation including the effect of viscous damping. The limiting cases of no damping and critical damping are investigated. The possible velocities for the propagation of free bending waves are found and their relation to the critical velocity of the beam is studied.

Nomenclature

The following nomenclature is used in the paper:

E = modulus of elasticity of beam, psi
I = moment of inertia of beam, in.^{4}
M = bending moment, in-lb
P = applied loads, lb
a = characteristic length of a free wave, 1/in.
c = coefficient of viscous damping/unit length, lb-sec/sq in.
$c_{cr} = 2(k\rho)^{1/2}$ = coefficient of critical damping
C_{cr} = coefficient of viscous damping for which wave length is infinite
k = spring constant per unit length of beam, lb/in.^{2}
v = velocity of load, in/sec
v_{cr} = critical velocity, in/sec
w = load per unit length of beam, lb/in.
x = distance along beam, in.
y = vertical displacement of beam, in.
$\beta = c/c_{cr}$ = ratio of damping coefficients
β_{cr} = critical damping coefficient
λ = static wave characteristic, 1/in.
η = numerical coefficient
$\theta = v/v_{cr}$ = velocity ratio
ρ = mass per unit length of beam, lb sec^2/in.^{2}

Primes denote differentiation with respect to distance
Dots denote differentiation with respect to time

Introduction

In the design of modern rocket test tracks it has become desirable to learn something of the dynamics of a rapidly moving load on beam on an elastic foundation. This problem has been treated previously by several authors, (1, 2, 3, 4)[2] but only the solution of the undamped case has been attempted analytically. Except for reference (4) this investigation has been restricted to determination of critical velocity and amplification factors at speeds less than critical. A recent paper (5) has shown the results obtained with an analog computer which verify some of the results set forth here. This paper will develop further the theory to include the effect of damping and to provide amplification factors for use in designing actual beams.

Since the solutions for the static case are well known, it is presumed that interested readers may verify statements made here about the static case in one of the pertinent books, for instance, reference (6).

The differential equation of a moving load on a beam may be obtained by considering the bending of an elemental segment

$$-M = EI\frac{\partial^2 y}{\partial x^2} \qquad [1a]$$

Differentiating twice

$$\frac{\partial^2}{\partial x^2}\left(EI\frac{\partial^2 y}{\partial x^2}\right) = -\frac{\partial^2 M}{\partial x^2} = w \qquad [1b]$$

where w is load intensity.

The loads applied if the beam rests on an elastic foundation are

$$\left.\begin{aligned} &\text{Inertia: } \rho\frac{\partial^2 y}{\partial t^2}\\ &\text{Viscous damping: } c\frac{\partial y}{\partial t}\\ &\text{Spring force: } ky\\ &\text{Applied forces: } P(x,t)\end{aligned}\right\} \qquad [1c]$$

Substituting the loading [1c] into [1b] produces the differential equation of the beam with uniform cross section

$$EI\frac{\partial^4 y}{\partial x^4} + \rho\frac{\partial^2 y}{\partial t^2} + c\frac{\partial y}{\partial t} + ky = P(x,t)$$

Velocity of Free Waves

Before proceeding with the solution of Equation [1] let us digress and consider the possibility of traveling-wave shapes in the beam. For this purpose consider an undamped beam

$$EI\frac{\partial^4 y}{\partial x^4} + \rho\frac{\partial^2 y}{\partial t^2} + ky = 0$$

From the form of the equation it can be seen that any waves traveling in the beam must be harmonic functions. As a simple example assume a traveling-wave train

$$y = \sin a(x - vt)$$

Substituting this into the differential equation

$$EIa^4 - \rho a^2 v^2 + k = 0 \qquad [2]$$

Examination of this equation shows that the simplest form the terms can have is

$$a = \left(\frac{nk}{EI}\right)^{1/4} \qquad v = \left(\frac{mkEI}{\rho^2}\right)^{1/4} \qquad [3]$$

---

[1] Project Engineer, Sandberg-Serrell Corporation. Assoc. Mem. ASME.

[2] Numbers in parentheses refer to the Bibliography at the end of the paper.

Presented at the West Coast Meeting of the Applied Mechanics Division, University of California, Berkeley, Calif., June 21–23, 1954, of The American Society of Mechanical Engineers.

Discussion of this paper should be addressed to the Secretary, ASME, 29 West 39th Street, New York, N. Y., and will be accepted until January 10, 1955, for publication at a later date. Discussion received after the closing date will be returned.

Note: Statements and opinions advanced in papers are to be understood as individual expressions of their authors and not those of the Society. Manuscript received by ASME Applied Mechanics Division, August 28, 1953. Paper No. 54—APM-8.

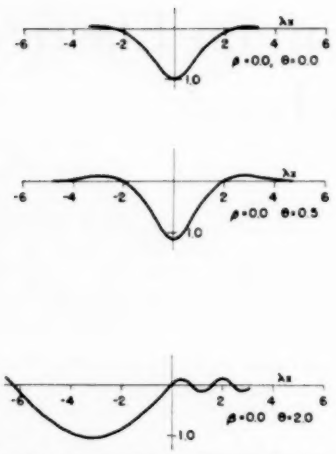

FIG. 1(a) WAVE SHAPES VERSUS VELOCITY FOR A CONCENTRATED LOAD AT ORIGIN MOVING WITH CONSTANT VELOCITY OVER AN INFINITE BEAM ON AN UNDAMPED ELASTIC FOUNDATION

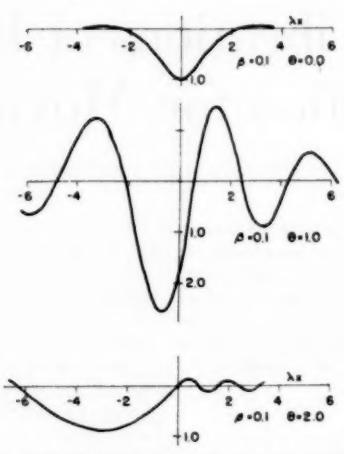

FIG. 1(b) WAVE SHAPES VERSUS VELOCITY FOR A CONCENTRATED LOAD AT ORIGIN MOVING WITH CONSTANT VELOCITY OVER AN INFINITE BEAM ON AN ELASTIC FOUNDATION WITH 10 PER CENT OF CRITICAL DAMPING

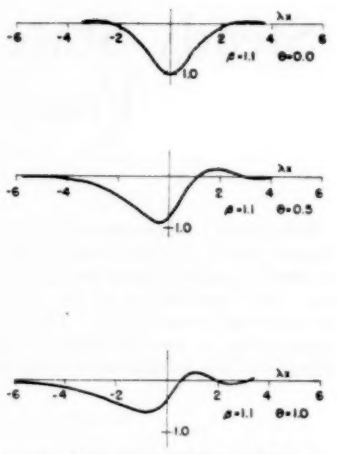

FIG. 1(c) WAVE SHAPES VERSUS VELOCITY FOR A CONCENTRATED LOAD AT THE ORIGIN MOVING WITH CONSTANT VELOCITY OVER AN INFINITE BEAM ON AN ELASTIC FOUNDATION WITH 110 PER CENT OF CRITICAL DAMPING

Utilizing these definitions and doing some rearrangement in Equation [2]

$$m = n + \frac{1}{n} + 2 \quad \ldots\ldots [4]$$

By elementary differentiation it is easy to see that the minimum value of m is 4 for $n = 1$ (negative values of n are excluded since a is then complex and the wave train disappears).

The meaning of this minimum n is that the lowest velocity at which a free wave might propagate is

$$v_{cr} = \left(\frac{4kEI}{\rho^2}\right)^{1/4} \quad \ldots\ldots [5]$$

This velocity has been given the name "critical velocity." Further, it is possible to find two particular wave trains that will propagate with any arbitrary velocity providing that this velocity is greater than critical velocity. Define θ as the ratio of velocity to critical velocity and λ as the coefficient defining static wave length. Then as a direct result of Equations [2], [3], [5] these wave trains may be written

$$y = \sin \lambda\,[(\theta^2 + 1)^{1/2} \pm (\theta^2 - 1)^{1/2}](x - vt) \quad \ldots\ldots [6]$$

with a wave length

$$(x - vt)_0 = \frac{2\pi}{a} = \frac{2\pi}{\lambda[(\theta^2 + 1)^{1/2} \pm (\theta^2 - 1)^{1/2}]} \quad \ldots\ldots [7]$$

where

$$\theta = v/v_{cr}$$

$$\lambda = \left(\frac{k}{4EI}\right)^{1/4}$$

The wave length of these waves as a ratio with static wave length $(2\pi/\lambda)$ has been plotted in Fig. 2.

From the foregoing behavior it would be expected that the system will reach a point of resonance when a load traveling at critical velocity passes over it. In fact, it might well be expected that the amplitude will be very large for all velocities equal to or greater than critical. It will be shown later, however, that the amplitude will be defined for all velocities except critical velocity. If an observer were to stand at a station x = const and watch the wave train pass, it would appear to have a circular frequency

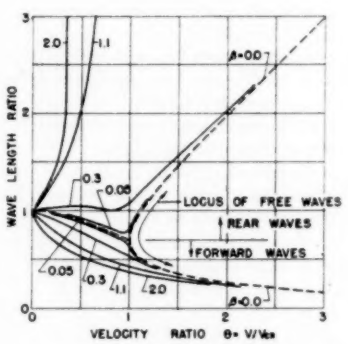

FIG. 2 RATIO OF DYNAMIC TO STATIC WAVE LENGTH VERSUS VELOCITY FOR VARIOUS VALUES OF DAMPING
(In region of $\theta = 1$ dotted line represents both possible free wave lengths and undamped forced wave lengths.)

$$\omega = av = \left[n\left(n + \frac{1}{n} + 2\right)\right]^{1/4} (k/\rho)^{1/2}$$

Inspection of this equation will show that

$$\lim_{n \to 0} \omega = (k/\rho)^{1/2}$$

In other words, the system vibrates with a higher frequency than a simple spring-mass system except in the limit of infinite wave length.

CONSTANT-VELOCITY MOVING LOAD

Return now to a consideration of a damped beam on an elastic foundation carrying a moving load, i.e., Equation [1]. Solution to this equation may be found without further manipulation. However, for the purpose of comparison of the solutions with the static solution it is more desirable to transpose the co-ordinate

system so that it is attached to the moving load. Analytically the change may be accomplished by letting

$$x_1 = x - vt \qquad y_1 = y(x - vt) = y(x_1) \ldots\ldots [8]$$

Then Equation [1] becomes

$$EI\frac{\partial^4 y}{\partial x^4} + \rho v^2\frac{\partial^2 y}{\partial x^2} - cv\frac{\partial y}{\partial x} + ky - 2\rho v\frac{\partial^2 x}{\partial x \partial t} + \rho\frac{\partial^2 y}{\partial t^2} + c\frac{\partial y}{\partial t} = P(x, t) \ldots [9]$$

Since the remainder of the paper will be concerned with the load and velocity invariant in time, all partial derivatives with respect to time become equal to zero and the homogeneous form of Equation [9] simplifies to

$$EIy^{iv} + \rho v^2 y'' - cvy' + ky = 0 \ldots\ldots\ldots\ldots [9a]$$

It is convenient to define the following terms: The coefficient defining the wave length for the static case is

$$\lambda = (k/4EI)^{1/4} \ldots\ldots\ldots\ldots\ldots\ldots [10]$$

Just as in the simple spring mass system critical damping may be defined by

$$c_{cr} = 2(k\rho)^{1/2} \ldots\ldots\ldots\ldots\ldots\ldots [11]$$

For economy of writing let

$$\theta = v/v_{cr} \qquad \beta = c/c_{cr} \ldots\ldots\ldots\ldots\ldots [12]$$

Substituting Equations [10] and [12] into [9a] gives

$$y^{iv} + 4(\theta\lambda)^2 y'' - 8\theta\beta\lambda^2 y' + 4\lambda^4 y = 0 \ldots\ldots [13]$$

If a concentrated load is assumed at the origin, Equation [13] may be solved by use of Green's function with assumed zero deflection and slope at infinity and zero change in deflection, slope, and moment across the origin. A discontinuity in shear across the origin of value $-\frac{P}{EI}$ is used as the last boundary condition. The solution to Equation [13] is developed in the Appendix with the aid of these boundary conditions and found to be

$$\left.\begin{array}{l} x < 0 \\ y = \dfrac{P\lambda}{2k}\left[\dfrac{\eta e^{\eta\lambda x}}{\eta^4 + (\eta\theta)^2 + \frac{1}{2}(\theta\beta/\eta)^2}\right]\left\{\dfrac{-(\theta\beta/\eta + \eta^2)\sin(2\theta^2 + \eta^2 - 2\theta\beta/\eta)^{1/2}\lambda x}{\eta(2\theta^2 + \eta^2 - 2\theta\beta/\eta)^{1/2}} + \cos(2\theta^2 + \eta^2 - 2\theta\beta/\eta)^{1/2}\lambda x\right\} \\ x > 0 \\ y = \dfrac{P\lambda}{2k}\left[\dfrac{\eta e^{-\eta\lambda x}}{\eta^4 + (\eta\theta)^2 + \frac{1}{2}(\theta\beta/\eta)^2}\right]\left\{\dfrac{-(\theta\beta/\eta - \eta^2)\sin(2\theta^2 + \eta^2 + 2\theta\beta/\eta)^{1/2}\lambda x}{\eta(2\theta^2 + \eta^2 + 2\theta\beta/\eta)^{1/2}} + \cos(2\theta^2 + \eta^2 + 2\theta\beta/\eta)^{1/2}\lambda x\right\} \end{array}\right\} \ldots [14]$$

where η is the positive real root of

$$\eta^6 + 2\theta^2\eta^4 + (\theta^4 - 1)\eta^2 - \theta^2\beta^2 = 0 \ldots\ldots [15]$$

No Damping

For the particular case of no damping and velocity less than critical, Equation [15] simplifies to

$$\eta = (1 - \theta^2)^{1/2} \ldots\ldots\ldots\ldots\ldots [15a]$$

and Equation [14] may be written

$$\left.\begin{array}{l} x < 0 \quad \beta = 0 \quad \theta < 1 \\ y = \dfrac{P\lambda}{2k}\left[\dfrac{e^{(1-\theta^2)^{1/2}\lambda x}}{(1-\theta^2)}\right]\left[\dfrac{-(1-\theta^2)^{1/2}}{(1+\theta^2)^{1/2}}\sin(1+\theta^2)^{1/2}\lambda x + \cos(1+\theta^2)^{1/2}\lambda x\right] \\ x > 0 \quad \beta = 0 \quad \theta < 1 \\ y = \dfrac{P\lambda}{2k}\left[\dfrac{e^{-(1-\theta^2)^{1/2}\lambda x}}{(1-\theta)^{1/2}}\right]\left[\dfrac{+(1-\theta^2)^{1/2}}{(1+\theta^2)^{1/2}}\sin(1+\theta^2)^{1/2}\lambda x + \cos(1+\theta^2)^{1/2}\lambda x\right] \end{array}\right\} [14a]$$

From this it is obvious that as $\theta \to 1$ the amplitude increases without bound. Hence the assumed point of resonance at critical velocity actually exists.

This solution for the undamped case could have been obtained as easily by direct appeal to the differential equation with the damping terms set equal to zero. When the velocity is greater than critical, an essential difficulty develops in this method since the roots become wholly imaginary (i.e., sums of undamped sines). This invalidates the four boundary conditions which state that the deflections are zero at $\pm\infty$. Hence the result cannot be evaluated by this method. A similar difficulty develops if the solution found in Equation [15a] for η is used.

To solve this problem let us maintain the form of the solution with which the damped case was successfully solved and pass to the limit from small β. If this is to be done it is seen that the applicable real positive roots of η are 0 (for $\beta = 0$). Hence we may write the following series solution for η

$$\eta = \frac{\theta\beta}{(\theta^4 - 1)^{1/2}}\left\{1 - \frac{1}{8}\left(\frac{8\beta^2\theta^4}{[\theta^2 - 1]^2}\right) + \ldots\right\} \ldots [15b]$$

Retaining only the terms linear in β the characteristic length immediately reduces to

$$\lim_{\beta \to 0}(2\theta^2 + \eta^2 \pm 2\theta\beta/\eta)^{1/2} = (\theta^2 - 1)^{1/2} \pm (\theta^2 - 1)^{1/2}. [16]$$

which is precisely the characteristic of the "free wave."

Directly from Equation [14] the amplitude of the front and rear waves is then

$$\left.\begin{array}{l} x < 0 \quad \beta = 0 \quad \theta > 1 \\ y = \dfrac{P\lambda}{2k}\left\{\dfrac{-2\sin\lambda[(\theta^2+1)^{1/2} - (\theta^2-1)^{1/2}]x}{(\theta^4-1)^{1/2}[(\theta^2+1)^{1/2} - (\theta^2-1)^{1/2}]}\right\} \\ x > 0 \quad \beta = 0 \quad \theta > 1 \\ y = \dfrac{P\lambda}{2k}\left\{\dfrac{-2\sin\lambda[(\theta^2+1)^{1/2} + (\theta^2-1)^{1/2}]x}{(\theta^4-1)^{1/2}[(\theta^2+1)^{1/2} + (\theta^2-1)^{1/2}]}\right\} \end{array}\right\} . [14b]$$

We now have the startling result of a wave train of seemingly infinite length but finite amplitude. This is shown in Fig. 1(*a*).

The present method gives no information as to whether this result might violate energy conditions. Actually it does not as was shown in the Fourier integral solution of J. Dörr (4). He showed that the solution reaches a steady amplitude, but that the length of the front and rear wave trains each increases at a definite rate.

Critical Damping

The general solution given in Equation [14] does not contain all the possible solutions, since the wave length of the solution for

$x < 0$ may become infinite or imaginary. This will happen for β sufficiently large and represents the critically damped solution. The value of this critical damping may be found as follows: The condition for infinite wave length is

$$(2\theta^2 + \eta^2 - 2\theta\beta/\eta)^{1/2} = 0$$

from which

$$\theta\beta = (2\theta^2 + \eta^2)\eta/2$$

Substituting this into the characteristic equation for η, i.e., Equation [15], and simplifying

$$\eta^4 + 4/3\theta^2\eta^2 - 4/3 = 0$$

whence

$$\eta^2 = 2/3[-\theta^2 + (\theta^4 + 3)^{1/2}]$$

Finally, from the second of the foregoing expressions

$$\beta_{cr} = \frac{1}{3}\left\{2\left[\frac{1 + (1 + 3/\theta^4)^{1/2}}{2}\right]^{1/2} + \frac{1}{\left[\frac{1 + (1 + 3/\theta^4)^{1/2}}{2}\right]^{1/2}}\right\} \quad \ldots\ldots [17]$$

Returning now to the definition of β it is easy to see that C_{cr} may be written

$$C_{cr} = \frac{2(k\rho)^{1/2}}{3}\left\{2\left[\frac{1 + (1 + 3/\theta^4)^{1/2}}{2}\right]^{1/2} + \frac{1}{\left[\frac{1 + (1 + 3/\theta^4)^{1/2}}{2}\right]^{1/2}}\right\} \quad \ldots\ldots [18]$$

where C_{cr} is the coefficient of viscous damping for which the rear running first has infinite wave length. The explanation of this velocity dependence is fairly easy. At $\theta = 0$ or the static case there is no possible solution with an infinite wave length if k is finite. Hence the solution must be underdamped for all values of c. As the velocity increases the value of the critical damping approaches that for a simple spring-mass system. The important thing to note is that the underdamped region is everywhere more extensive than might be expected.

To demonstrate further this relationship of damping and velocity, Fig. 2 has been drawn showing wave length versus velocity.

Finally, solution for the overdamped case may be written by noting that

$$\sin ix = \sinh x$$

Hence for

$x < 0 \quad \beta > \beta_{cr}$

$$y = \frac{P\lambda}{2k}\left[\frac{\eta e^{\lambda\eta x}}{\eta^4 + \theta^2\eta^2 + \frac{1}{2}(\theta\beta/\eta)^2}\right]\left[\frac{-(\theta\beta/\eta + \eta^2)\sinh(|2\theta^2 + \eta^2 - 2\theta\beta/\eta|)^{1/2}\lambda x}{\eta(|2\theta^2 + \eta^2 - 2\theta\beta/\eta|)^{1/2}} + \cosh(2\theta^2 + \eta^2 - 2\theta\beta/\eta|)^{1/2}\lambda x\right] \quad \ldots [14c]$$

The usual resonance diagrams may now be drawn [see Figs. 3(*a*) and (*b*) for deflection amplification factors]. In both diagrams the defining static amplitude has been taken as the static deflection under the concentrated load. The resonance curves are similar except that the amplitude of the front running wave is never as large as that of the rear running wave. Moment amplification factors are presented in Figs. 4(*a*) and (*b*). Like the deflection diagrams the defining static moment is taken as the static moment under the concentrated load. The amplification factor for the maximum point ahead of the load is quite similar to the usual

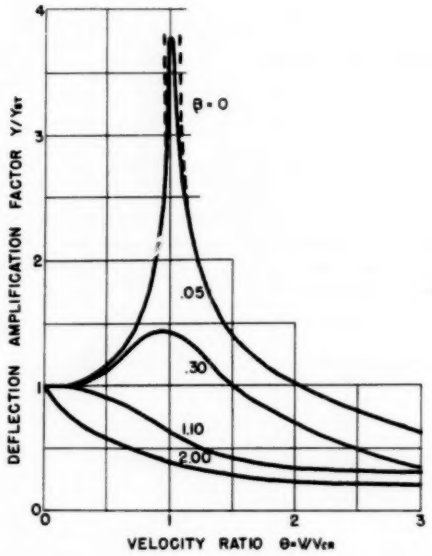

FIG. 3(*a*) RATIO OF MAXIMUM DEFLECTION BEHIND LOAD TO STATIC DEFLECTION UNDER CONCENTRATED LOAD VERSUS VELOCITY FOR A CONCENTRATED LOAD MOVING AT CONSTANT VELOCITY

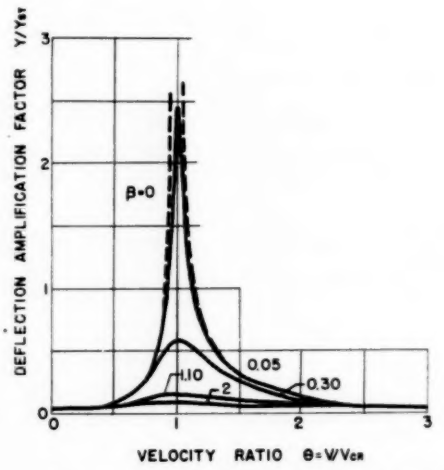

FIG. 3(*b*) RATIO OF MAXIMUM DEFLECTION AHEAD OF LOAD TO STATIC DEFLECTION UNDER CONCENTRATED LOAD VERSUS VELOCITY FOR A CONCENTRATED LOAD MOVING AT CONSTANT VELOCITY

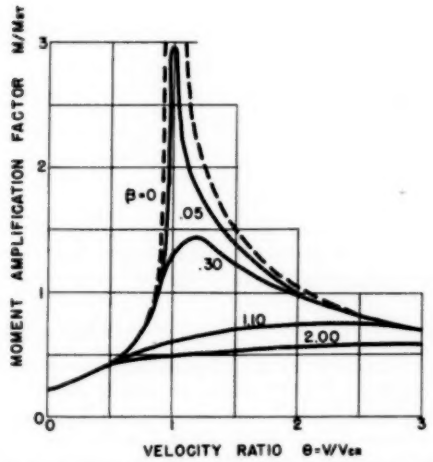

FIG. 4(*a*) RATIO OF MAXIMUM MOMENT AHEAD OF LOAD TO STATIC MOMENT UNDER A CONCENTRATED LOAD VERSUS VELOCITY FOR A CONCENTRATED LOAD MOVING AT CONSTANT VELOCITY

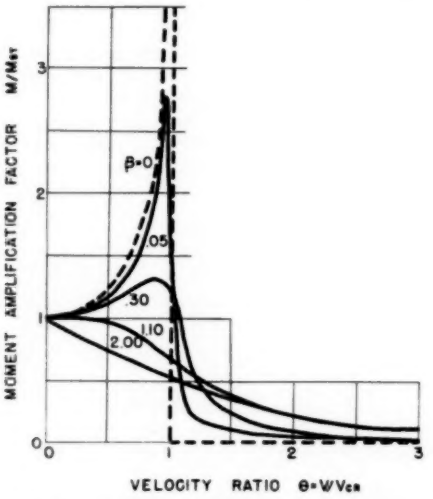

FIG. 4(*b*) RATIO OF MAXIMUM MOMENT UNDER LOAD TO STATIC MOMENT UNDER A CONCENTRATED LOAD VERSUS VELOCITY FOR A CONCENTRATED LOAD MOVING AT CONSTANT VELOCITY

resonance diagram. The maximum point one-half wave behind the load is identical with this except that the amplitudes are much smaller. At the load the amplification of moment for all velocities above critical is zero, and the damped waves give greater amplification than the undamped waves.

ACKNOWLEDGMENT

The author wishes to acknowledge the contribution of Dr. George Housner of the California Institute of Technology who developed the fundamental solutions utilized in this paper. Much of the groundwork of the paper was started during the design of a high-speed test track for Naval Ordnance Test Station at Inyokern, China Lake.

Appendix

The details of the solution of Equation [13] are as follows:

Assume the solution $y = e^{mx}$; then Equation [13] becomes

$$m^4 + 4\theta^2\lambda^2 m^2 - 8\theta\beta\lambda^3 m + 4\lambda^4 = 0 \quad \ldots\ldots [19]$$

By Descartes's rule there is not more than one pair of real roots to this equation. Since, for design purposes, interest is concentrated in the underdamped portion of the solution let us assume the following four complex roots and demand that the imaginary parts be nonzero

$$\left.\begin{aligned} m_1 &= a + ib_1 \\ m_2 &= a - ib_1 \\ m_3 &= a + ib_2 \\ m_4 &= a - ib_2 \end{aligned}\right\} \quad \ldots\ldots [20]$$

Since these are assumed to be roots they must satisfy the following identity

$$(m - m_1)(m - m_2)(m - m_3)(m - m_4) = 0 \quad \ldots\ldots [21]$$

Combining Equations [20] and [21]

$$m^4 + (-2a^2 + b_1^2 + b_2^2)m^2 - 2a(b_2^2 - b_1^2)m + (a^2 + b_1^2)(a^2 + b_2^2) \equiv 0 \quad \ldots [22]$$

Equating coefficients of Equations [19] and [22]

$$\left.\begin{aligned} -2a^2 + b_1^2 + b_2^2 &= 4\theta^2\lambda^2 \\ -2a(b_2^2 - b_1^2) &= -8\theta\beta\lambda^3 \\ (a^2 + b_1^2)(a^2 + b_2^2) &= 4\lambda^4 \end{aligned}\right\} \quad \ldots\ldots [23]$$

From the first two of these equations

$$b_1^2 = 2\theta^2\lambda^2 + a^2 - 2\theta\beta\lambda^3/a$$

$$b_2^2 = 2\theta^2\lambda^2 + a^2 + 2\theta\beta\lambda^3/a$$

Hence from the foregoing expression

$$a^6 + 2\theta^2\lambda^2 a^4 + \lambda^4(\theta^4 - 1)a^2 - \theta^2\beta^2\lambda^6 = 0$$

Finally, the coefficient may be written as $a = \lambda\eta$ where η is positive real root of

$$\left.\begin{aligned} \eta^6 + 2\theta^2\eta^4 + (\theta^4 - 1)\eta^2 - \theta^2\beta^2 &= 0 \\ b_1 &= \lambda(2\theta^2 + \eta^2 - 2\theta\beta/\eta)^{1/2} \\ b_2 &= \lambda(2\theta^2 + \eta^2 + 2\theta\beta/\eta)^{1/2} \end{aligned}\right\} \quad \ldots\ldots [24]$$

The positive real root of the auxiliary equation for η was chosen to keep the form of answers the same as assumed in Equation [20]. When written in real form the solution of the homogeneous differential equation becomes

$$y = e^{-ax}(C_1 \sin b_2 x + C_2 \cos b_2 x) + e^{ax}(C_3 \sin b_1 x + C_4 \cos b_1 x) \quad \ldots [25]$$

Now consider a concentrated load at the origin ($x = 0$). It is reasonable to assume that the deflection and slope of the beam are zero at infinity. This assumption requires

$$\left.\begin{aligned} y &= e^{-ax}(C_1 \sin b_2 x + C_2 \cos b_2 x) \quad x > 0 \\ y &= e^{ax}(C_3 \sin b_1 x + C_4 \cos b_1 x) \quad x < 0 \end{aligned}\right\} \quad \ldots\ldots [26]$$

The boundary conditions to determine the unknown coefficients are

$$\left.\begin{aligned} &(a) \lim_{\epsilon \to 0} [y(0 + \epsilon) - y(0 - \epsilon)] = 0 \\ &(b) \lim_{\epsilon \to 0} [y'(0 + \epsilon) - y'(0 - \epsilon)] = 0 \\ &(c) \lim_{\epsilon \to 0} [y''(0 + \epsilon) - y''(0 - \epsilon)] = 0 \\ &(d) \lim_{\epsilon \to 0} [y'''(0 + \epsilon) - y'''(0 - \epsilon)] = \frac{-P}{EI} \end{aligned}\right\} \quad \ldots\ldots [27]$$

The solution for the constants then gives

$$\left.\begin{aligned} C_2 = C_4 &= \frac{aP}{EI\left\{a^2[4a^2 + b_2^2 + 3b_1^2] + \frac{(b_2^2 - b_1^2)(4a^2 + b_1^2 + b_2^2)}{4}\right\}} \\ C_3 &= \frac{b_1^2 - b_2^2 - 4a^2}{4ab_1} C_2 \\ C_1 &= \frac{b_1^2 - b_2^2 - 4a^2}{4ab_2} C_2 \end{aligned}\right\} \quad \ldots [28]$$

These last equations together with Equations [24] give the final equations presented as Equations [14].

BIBLIOGRAPHY

1 "Method of Analysis of Statical and Dynamical Stresses in Rail," by S. Timoshenko, Proceedings of the Second International Congress for Applied Mechanics, Zurich, Switzerland, 1926, pp. 407–418.

2 "Beitrag zur Dynamik des geraden Eisenbahngleises," by B. K. Hovey, Dissertation, Göttingen, Germany, 1933.

3 "Deformation of a Rail Elastically Supported and of Infinite Length by Loads Moving at a Constant Horizontal Velocity," by K. Ludwig, Proceedings of the Fifth International Congress of Mechanics, 1938, p. 650.

4 "Der Unendliche, Ferund Gebettete Balken unter dem Einfluss einer Gleichformig Bewegten Last," by J. Dörr, Ingenieur-Archiv, vol. 14, 1943, pp. 167–192.

5 "Rails on Elastic Foundation Under the Influence of High-Speed Traveling Loads," by H. E. Criner and G. D. McCann, JOURNAL OF APPLIED MECHANICS, Trans. ASME, vol. 75, 1953, pp. 13–22.

6 "Beams on Elastic Foundation," by M. Hetényi, University of Michigan Press, Ann Arbor, Mich., 1945.

Vibration of Triangular Cantilever Plates by the Ritz Method

By B. W. ANDERSEN,[1] DOWNEY, CALIF.

Using the method published by Ritz in 1909, natural frequencies and corresponding node lines have been determined for two symmetric and two antisymmetric modes of vibration of isosceles triangular plates clamped at the base and having length-to-base ratios of 1, 2, 4, and 7 and for the two lowest modes of right triangular plates clamped along one leg and having ratios of the length of the free leg to that of the clamped one of 2, 4, and 7. A nonorthogonal co-ordinate system was used which gave constant limits of integration over the area of the triangle. The co-ordinate transformation made it necessary to modify the functions used by Ritz in approximating deflections and to consider cross products in the integration. The integration was done numerically, using tables compiled by Young and Felgar in 1949. To check the accuracy of results, a solution was obtained to the problem of a vibrating cantilever beam of uniform depth and triangular plan view. The results obtained were found to be consistent with those obtained for the plates by using an eight-term series to approximate the deflections of the symmetric plates (isosceles triangles) and a six-term series to approximate the deflections of the unsymmetric plates (right triangles).

Nomenclature

The following nomenclature is used in the paper:

(x, y) = rectangular co-ordinates
(u, v) = dimensionless co-ordinates related to (x, y) by $u = \frac{x}{a}$, $v = k\frac{y}{x}$
k = a dimensionless constant
a = length of plate in x-direction
$w(u, v)$ or $w(x, y)$ = transverse amplitude of vibration
E = Young's modulus
h = constant plate thickness
σ = Poisson's ratio
$D = \frac{Eh^3}{12(1-\sigma^2)}$ = plate stiffness
V = maximum potential or strain energy of plate
T = maximum kinetic energy of plate
ω = natural angular frequency of vibration
ρ = mass density of plate per unit area
$\gamma = \omega\sqrt{\frac{\rho a^4}{D}}$ = a dimensionless constant depending upon shape (not size) of plate
$\varphi_1, \varphi_2, \varphi_3$ = characteristic functions representing normal modes of vibration of a free-clamped beam
$\Psi_3, \Psi_4, \ldots$ = characteristic functions representing normal modes of vibration of a free-free beam

Introduction

Solutions to the boundary-value problem for small-amplitude vibrations of an isotropic uniform plate are known for a circular plate either free or clamped at the boundary (12)[2] and for a rectangular panel simply supported along two parallel edges with any conditions at the other two edges (simply supported, free, or clamped) (2). In 1951 Roberson (3) obtained solutions for a circular plate carrying concentrated mass and either free or clamped at the boundary.

To obtain values for the natural frequencies and mode shapes for boundary conditions which could not be handled by exact methods, approximate methods have been used. In 1909 Ritz (4, 5) published such a method which he applied to the study of a rectangular plate free at all boundaries.

In 1938 Iguchi (6) published natural frequencies for rectangular plates with a variety of boundary conditions some of which were for the known solutions mentioned previously.

Some recent investigators have been concerned with vibrations of cantilever plates which approximate short wings or missile fins.

In 1950 Young (7) applied the Ritz method to the study of vibrations of square plates with various combinations of free and fixed boundaries including the square cantilever plate. In 1951 Barton (8) extended Young's work on cantilever plates by working out some natural modes of vibration of rectangular cantilever plates with length-to-width ratios of $^1/_2$, 2, and 5. He also studied skew cantilever plates which were in the form of parallelograms with equal sides.

The results of Iguchi, Young, and Barton are summarized in a paper by Hearmon (1) (1952).

The present paper extends the work on cantilever plates to the study of both trapezoidal and triangular plates, although numerical results are given for triangular plates only.

The Ritz Method

It is assumed that the plate is vibrating with harmonic motion so that the deflection w_0 may be expressed as

$$w_0(x, y, t) = w(x, y)\cos\omega t \quad \ldots\ldots\ldots\ldots [1]$$

The maximum potential and kinetic energies of the plate will then be given by (9)

$$V = \frac{D}{2}\int\int\left\{\left(\frac{\partial^2 w}{\partial x^2}\right)^2 + \left(\frac{\partial^2 w}{\partial y^2}\right)^2 + 2\sigma\frac{\partial^2 w}{\partial x^2}\frac{\partial^2 w}{\partial y^2} + 2(1-\sigma)\left(\frac{\partial^2 w}{\partial x \partial y}\right)^2\right\}dxdy \quad \ldots [2]$$

---

[1] Research Engineer, North American Aviation, Inc.

Presented at the West Coast Meeting of the Applied Mechanics Division, University of California, Berkeley, Calif., June 21–23, 1954, of The American Society of Mechanical Engineers.

Discussion of this paper should be addressed to the Secretary, ASME, 29 West 39th Street, New York, N. Y., and will be accepted until January 10, 1955, for publication at a later date. Discussion received after the closing date will be returned.

Note: Statements and opinions advanced in papers are to be understood as individual expressions of their authors and not those of the Society. Manuscript received by ASME Applied Mechanics Division, January 25, 1954. Paper No. 54—APM-6.

[2] Numbers in parentheses refer to the Bibliography at the end of the paper.

$$T = \frac{\rho}{2}\omega^2 \int\int w^2 dxdy \quad \ldots\ldots\ldots\ldots [3]$$

the integration being extended over the entire area of the plate. By equating Expressions [2] and [3] the square of the frequency is determined as

$$\omega^2 = \frac{2}{\rho}\frac{V}{\int\int w^2 dxdy} \quad \ldots\ldots\ldots\ldots [4]$$

It can be shown that minimizing the left side of Equation [4] subject to the boundary conditions is equivalent to solving the equation of motion for plate vibrations. When no exact solution can be found, w may be determined approximately as follows

$$\text{Let} \qquad w = a_1 g_1 + a_2 g_2 + a_3 g_3 + \ldots + a_n g_n \quad \ldots\ldots\ldots [5]$$

in which each g satisfies the geometric boundary conditions of the problem and the constant coefficients are to be determined so that the left side of Equation [4] is a minimum. To do this we differentiate Equation [4] with respect to each a and equate to zero. This yields

$$\left.\begin{aligned}\frac{\partial^2\omega^2}{\partial a_i} &= \frac{2}{\rho}\frac{\dfrac{\partial V}{\partial a_i}}{\int\int w^2 dxdy} - \frac{2}{\rho}\frac{V\dfrac{\partial}{\partial a_i}\int\int w^2 dxdy}{(\int\int w^2 dxdy)^2} \\ &= \frac{\dfrac{\partial}{\partial a_i}\left(\dfrac{2}{\rho}V - \omega^2\int\int w^2 dxdy\right)}{\int\int w^2 dxdy} = 0\end{aligned}\right\} \quad \ldots\ldots [6]$$

Equating the numerator of Equation [6] to zero, substituting for V from Equation [2], and multiplying through by ρ/D gives

$$\frac{\partial}{\partial a_i}\int\int \left\{\left(\frac{\partial^2 w}{\partial x^2}\right)^2 + \left(\frac{\partial^2 w}{\partial y^2}\right)^2 + 2\sigma\frac{\partial^2 w}{\partial x^2}\frac{\partial^2 w}{\partial y^2} + 2(1-\sigma)\left(\frac{\partial^2 w}{\partial x \partial y}\right)^2 - \frac{\omega^2\rho}{D}w^2\right\} dxdy = 0 \quad [6a]$$

Equation [6a] will be a set of n linear homogeneous equations in the n-coefficients and containing the as yet undetermined frequency. In order that these equations have nontrivial solutions it is necessary that the determinant of coefficients be zero. In general, there will be n-values of w for which this determinant is zero. These will be the approximate values of the natural frequency in the problem being considered.

It should be noted that the functions used by Ritz, Young, and Barton, and in this paper, do not exactly satisfy the natural plate-boundary conditions. (In terms of second and third derivative of w on free boundaries.) However, in the case of rectangular plates in which the variation in co-ordinates was normal to the boundaries, this failing was not serious since the so-called geometric conditions were satisfied and good agreement with experimental results was obtained. In the case of skew plates the approximation became increasingly inaccurate as the skew angle increased. Barton (8) concluded, from comparison with experimental data, that the Ritz method should not be used with skew angles larger than about 30 deg.

Application to Triangular Cantilever Plates

In order to obtain constant limits of integration over the area of a triangular plate we make the co-ordinate transformation (see Fig. 1)

$$u = \frac{x}{a}, \quad v = k\frac{y}{x} \quad \ldots\ldots\ldots\ldots [7]$$

the Jacobian of which is

$$J\left(\frac{x, y}{u, v}\right) = \frac{a^2 u}{k} \quad \ldots\ldots\ldots\ldots [8]$$

In the co-ordinates u and v Equations [6] become

$$\left.\begin{aligned}\frac{\partial}{\partial a_i}\int\int \Bigg[& u\left(\frac{\partial^2 w}{\partial u^2}\right)^2 - 4v\frac{\partial^2 w}{\partial u^2}\frac{\partial^2 w}{\partial u \partial v} \\ & + \frac{2}{u}\Big\{[2v^2 + k^2(1-\sigma)]\left(\frac{\partial^2 w}{\partial u \partial v}\right)^2 \\ & + (v^2 + k^2\sigma)\frac{\partial^2 w}{\partial u^2}\frac{\partial^2 w}{\partial v^2} + 2v\frac{\partial w}{\partial v}\frac{\partial^2 w}{\partial u^2}\Big\} \\ & - \frac{4}{u^2}\Big\{[2v^2 + k^2(1-\sigma)]\frac{\partial^2 w}{\partial u \partial v}\frac{\partial w}{\partial v} \\ & + (v^3 + k^2 v)\frac{\partial^2 w}{\partial u \partial v}\frac{\partial^2 w}{\partial v^2}\Big\} \\ & + \frac{1}{u^3}\Big\{2[2v^2 + k^2(1-\sigma)]\left(\frac{\partial w}{\partial v}\right)^2 \\ & + 4(v^3 + k^2 v)\frac{\partial w}{\partial v}\frac{\partial^2 w}{\partial v^2} + (v^2 + k^2)^2\left(\frac{\partial^2 w}{\partial v^2}\right)^2\Big\} \\ & - \gamma^2 u w^2\Bigg] du dv = 0\end{aligned}\right\} \quad \ldots [9]$$

in which w is now a function of u and v and

$$\gamma = \omega\sqrt{\frac{\rho a^4}{D}}$$

It is noted that in changing co-ordinates to obtain simple boundaries the expression to be integrated has become quite complex. Furthermore, the co-ordinate transformation is not single-valued at the origin. It was necessary to multiply the free-free beam functions in v by the factor u^2 in order to obtain single-

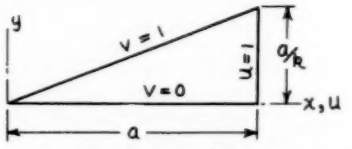

Fig. 1 Illustration of Co-Ordinates u and v

valued deflections, slopes, and moments at this point (see the next two sections). The integration is made tedious by the nonorthogonal co-ordinate system and the complex functions used to approximate w. This difficulty was resolved by integrating numerically, using Simpson's rule with eleven stations. Values for the beam functions were obtained from tables compiled by Young and Felgar (10).

First Case—Symmetric Triangle

A symmetric triangle with apex at the origin and of length a and base $2a/k$ is obtained by taking the limits

$$0 \leq u \leq 1, \quad -1 \leq v \leq +1 \quad \ldots\ldots\ldots [10]$$

The following eight-term series was used for w

$$w = [a_{11} + a_{31}u^2\Psi_3(v)]\varphi_1(u) + [a_{12} + a_{32}u^2\Psi_3(v)]\varphi_2(u) \quad \ldots [11]$$

for the symmetric modes and

$$w = [a_{21}v + a_{41}\Psi_4(v)]u^2\varphi_1(u) + [a_{22}v + a_{42}\Psi_4(v)]u^2\varphi_2(u) \ldots [12]$$

for the antisymmetric modes. φ_1 and φ_2 represent the first two modes of a cantilever beam free at $u = 0$ and clamped at $u = 1$. Ψ_3 and Ψ_4 represent the first symmetric and antisymmetric modes of a beam free at $v = \pm 1$. Substitution of Expressions [11] and [12] into Equation [9] and performance of the indicated integration and differentiation yielded two sets of four homogeneous equations. The two lowest values of γ were determined in each case for $k = 2$, 4, 8, and 14. These values of γ together with the corresponding values of the coefficients are shown in Tables 1, 2, 3, and 4.

TABLES 1 TO 4 VALUES OF γ AND CORRESPONDING VALUES OF COEFFICIENTS

TABLE 1 - First Mode Symmetric Plate

k	2	4	8	14
Γ	7.149	7.122	7.080	7.068
a_{11}	+1.000000	+1.000000	+1.000000	+1.000000
a_{12}	-0.013453	-0.018583	-0.020249	-0.020664
a_{31}	+0.000887	-0.000068	-0.000026	-0.000008
a_{32}	+0.002312	-0.001362	-0.000498	-0.000176

TABLE 2 - Second Mode Symmetric Plate

k	2	4	8	14
Γ	30.803	30.718	30.654	30.638
a_{11}	-0.77460	-0.76682	-0.76427	-0.76368
a_{12}	+1.00000	+1.00000	+1.00000	+1.00000
a_{31}	-0.02305	+0.00527	+0.00208	+0.00073
a_{32}	+0.04645	+0.01022	+0.00241	+0.00077

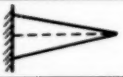

TABLE 3 - Third Mode Symmetric Plate

k	2	4	8	14
Γ	61.131	90.105	157.70	265.98
a_{21}	+1.64125	+0.60941	+0.33684	+0.27432
a_{22}	+1.00000	+1.00000	+1.00000	+1.00000
a_{41}	+0.005812	+0.001551	+0.000383	+0.000125
a_{42}	-0.003799	-0.000786	-0.000187	-0.000061

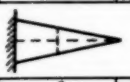

TABLE 4 - Fourth Mode Symmetric Plate

k	2	4	8	14
Γ	148.8	299.4	493.4	853.6
a_{21}	+1.00000	+1.00000	+1.00000	+1.00000
a_{22}	-0.32893	-0.31823	-0.31430	-0.31330
a_{41}	-0.008085	-0.001597	-0.000358	-0.000115
a_{42}	+0.005899	+0.001219	+0.000288	+0.000093

Second Case—Unsymmetric Triangle

An unsymmetric triangle having apex at the origin, length a, and base a/k is obtained by taking the limits

$$0 \leq u \leq 1, \quad 0 \leq v \leq 1 \ldots\ldots\ldots\ldots\ldots\ldots [13]$$

The following six-term series was used for w

$$w = [a_{11} + a_{31}u^2v + a_{51}u^2\Psi_3(v)]\,\varphi_1(u) + [a_{12} + a_{32}u^2v + a_{52}u^2\Psi_3(v)]\,\varphi_2(u) \ldots [14]$$

Substitution into Equation [9] yielded six equations from which the two lowest frequencies and corresponding coefficients were determined for values of k of 2, 4, and 7. These values are shown in Tables 5 and 6.

TABLES 5 AND 6 VALUES OF k AND CORRESPONDING VALUES OF COEFFICIENTS

TABLE 5 - First Mode Unsymmetric Plate

k	2	4	7
Γ	5.887	6.617	6.897
a_{11}	+1.00000	+1.00000	+1.00000
a_{12}	+0.02030	-0.000770	-0.012873
a_{21}	-0.31370	-0.09379	-0.03234
a_{22}	-0.14370	-0.07012	-0.02783
a_{31}	-0.000726	-0.000053	-0.000023
a_{32}	-0.005775	-0.001977	-0.000699

TABLE 6 - Second Mode Unsymmetric Plate

k	2	4	7
Γ	25.40	28.80	30.28
a_{11}	-0.81541	-0.77842	-0.77340
a_{12}	+1.00000	+1.00000	+1.00000
a_{21}	+3.1448	+1.11722	+0.40809
a_{22}	-1.25112	-0.50815	-0.19731
a_{31}	+0.052001	+0.010646	+0.003198
a_{32}	+0.018447	+0.007481	+0.000284

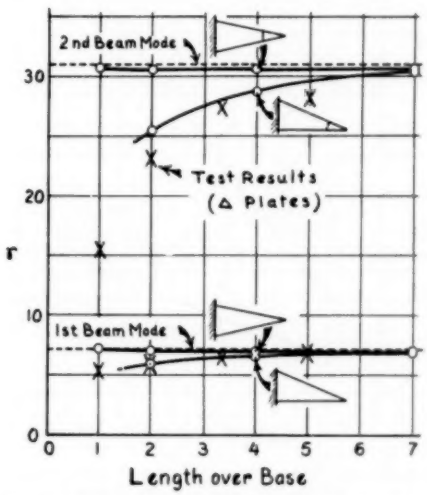

FIG. 2 COMPARISON OF 1ST AND 2ND BEAM AND PLATE-BENDING-MODE FREQUENCIES FOR TRIANGULAR PLANFORM

(Length over base is $k/2$ for symmetric plates, k for unsymmetric plates. Test values taken from reference 11.)

In the Appendix a solution is given for the free vibration of a triangular cantilever beam of uniform thickness. From this solution the first two values of γ were determined as a basis of comparison with those of the symmetric modes of vibrating plates. These values of γ are plotted in Fig. 2. Fig. 2 also shows test values obtained from reference (11) which was called to the author's attention after the present paper had been submitted for publication. To indicate the relation between beam and plate frequencies, the values of γ obtained by Barton (8) for rectangular cantilever plates are plotted against those for uniform cantilever beams in Fig. 3. Fig. 4 shows the variation of γ with the length-to-base ratio for the two lowest antisymmetric modes of triangular plates.

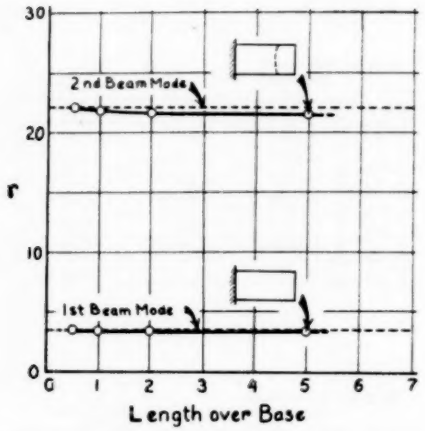

FIG. 3 COMPARISON OF BEAM AND PLATE-BENDING FREQUENCIES FOR RECTANGULAR PLANFORM

(Plate data from M. V. Barton (8); 1st and 2nd modes.)

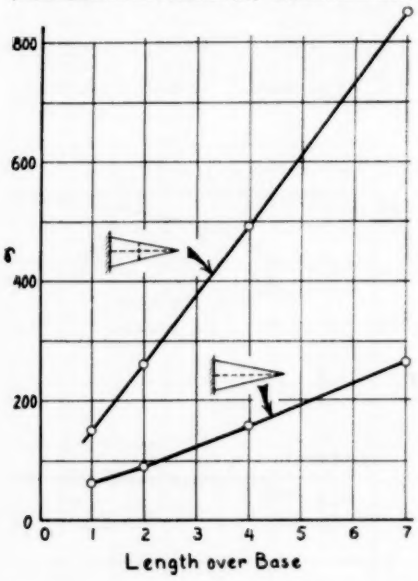

FIG. 4 ANTISYMMETRIC OR TORSION FREQUENCIES FOR SYMMETRIC PLATES, I.E., 3RD AND 4TH MODES

(Length over base equals $k/2$.)

Details of the foregoing work are given in a PhD thesis by the author in Theoretical and Applied Mechanics at the University of Illinois in 1953.

DISCUSSION OF RESULTS

It is generally known that the Ritz method yields frequencies that are higher than the actual natural frequencies. Consideration of the beam theory as compared to the plate theory indicates that the beam frequencies should be higher than the corresponding plate frequencies since the restraint of bending in one direction would tend to increase the natural frequencies. Qualitatively, the data plotted in Fig. 1 bear out this conclusion. Fig. 1 also bears out the intuitive conclusion that the behavior of very short cantilever plates should correspond closely to beam theory. It gives also an indication of the accuracy of the plate frequencies determined because if they were much in error for short plates they would be higher than the beam frequencies.

Fig. 2, which shows the magnitude of differences between the frequencies of beams and those of corresponding plates (which have been verified by tests), compares favorably with the data for symmetric triangular plates shown in Fig. 1. Again, the indication is that the frequencies determined for triangular plates are reasonable. It should be mentioned that the largest difference in the frequency of the fundamental mode between the triangular plates and the triangular beam was found to be only 1.3 per cent.

An indication of the accuracy of the frequencies obtained for unsymmetric plates is obtained from the fact that for long plates, in which the twisting is small, the frequency differs only slightly from that of the symmetric plates. Fig. 1 also shows that twisting has a marked effect upon the frequency of a short unsymmetric plate. The test values obtained by Gustafson, Stokey, and Zorowski (11) are seen to compare favorably with those obtained by the Ritz method. For long plates the test frequencies are about 5 per cent below the theoretical frequencies.

CONCLUSIONS

From the results presented and the considerations indicated in the discussion the following conclusions seem warranted:

1 The eight and six-term series used and the eleven-station numerical integration give reasonable accuracy for the frequencies of the vibration modes considered. It should be pointed out that in no case was the angle between either side of the triangle and the base less than 60 deg. This was done purposely in view of the afore-mentioned conclusion of Barton that good agreement with experiment could not be attained where the skew angle was greater than about 30 deg. More terms would be needed in the series for w if higher modes than here considered were desired.

2 The frequency of the fundamental mode of vibration of a symmetric triangular plate may be determined within 1 or 2 per cent by considering the plate as a beam, i.e., by neglecting variations in deflection across the width of the plate.

3 In short unsymmetric triangular cantilever plates, twisting is much more important than anticlastic curvature in determining the natural frequencies of vibration. The frequencies of such plates probably could be determined with sufficient accuracy by considering twisting and spanwise bending only.

4 The Ritz method as applied to triangular plates would give equally good results for trapezoidal plates which are intermediate between triangular and rectangular plates. Only changes in the integration limits in Equation [9] and in the boundaries of the approximating functions would be needed.

BIBLIOGRAPHY

1 "The Frequency of Vibration of Rectangular Isotropic Plates," by R. F. S. Hearmon, JOURNAL OF APPLIED MECHANICS, Trans. ASME, vol. 74, 1952, p. 402.

2 "Bemerkung zu dem Problem der transversalen Schwingungen rechteckiger Platten," by W. Voigt, *Göttingen Nachrichten*, 1893, p. 225.

3 "Transverse Vibrations of a Free Circular Plate Carrying Concentrated Mass," by R. E. Roberson, JOURNAL OF APPLIED MECHANICS, Trans. ASME, vol. 73, 1951, p. 280.

"Vibrations of a Clamped Circular Plate Carrying Concentrated Mass," by R. E. Roberson, ibid., p. 349.

4 "Über eine neue Methode zur Lösung gewisser Variationsprobleme der Mathematischen Physik," by W. Ritz, *Zeitschrift für Reine und Angewandte Mathematik*, vol. 135, 1909, p. 1.

5 "Theorie der Transversalschwingungen einer quadratischen Platte mit freien Rändern," by W. Ritz, *Annalen der Physik*, vol 28, 1909, p. 737.

6 "Die Eigenwertsprobleme für die Elastische Rechteckige Platte," by S. Iguchi, *Memoirs of the Faculty of Engineering, Hokkaido Imperial University*, vol. 4, 1938, p. 305.

7 "Vibration of Rectangular Plates by the Ritz Method," by

Dana Young, JOURNAL OF APPLIED MECHANICS, Trans. ASME, vol. 72, 1950, p. 448.

8 "Vibration of Rectangular and Skew Cantilever Plates," by M. V. Barton, JOURNAL OF APPLIED MECHANICS, Trans. ASME, vol. 73, 1951, p. 129.

9 "Vibration Problems in Engineering," by S. Timoshenko, D. Van Nostrand Company, Inc., New York, N. Y., 1937.

10 "Table of Characteristic Functions Representing the Normal Modes of Vibration of a Beam," by D. Young and R. P. Felgar, University of Texas, Eng. Research Series No. 4913, July, 1949.

11 "An Experimental Study of Natural Vibrations of Cantilevered Triangular Plates," by D. N. Gustafson, W. F. Stokey, and C. F. Zorowski, *Journal of the Aeronautical Sciences*, vol. 20, 1953, p. 331.

12 "Über das Gleichgewicht und die Bewegung einer elastischer Scheibe," by G. Kirchhoff, *Zeitschrift für Math. (Crelle)*, vol. 40, 1850, p. 51.

Appendix

BENDING VIBRATIONS OF A TRIANGULAR CANTILEVER BEAM OF UNIFORM DEPTH

Consider a beam free at the origin and clamped at $x = L$. Let the width for the beam be zero at the origin and b at $x = L$ and in between expressed by the equation

$$w = \frac{x}{L} b \quad [15]$$

The ordinary beam formula

$$EI \frac{\partial^2 y}{\partial x^2} = M_x \quad [16]$$

in which E is Young's modulus, I the moment of inertia, y the vertical deflection, and M_x the bending moment at a distance x from the origin, is valid in this case. In view of Equation [15] the moment of inertia I may be expressed

$$I = \frac{bh^3}{12} \frac{x}{L} \quad [17]$$

It is known that the second derivative of bending moment with respect to x is equal to the intensity of loading. The loading may be considered inertial for the purpose of writing the equation of motion. We then have

$$\frac{\partial^2 M_x}{\partial x^2} = -\rho bh \frac{x}{L} \frac{\partial^2 y}{\partial t^2} \quad [18]$$

Substituting Equation [17] in [16] and differentiating twice with respect to x and then substituting from Equation [18], we have

$$x \frac{\partial^4 y}{\partial x^4} + 2 \frac{\partial^3 y}{\partial x^3} + \frac{12\rho x}{Eh^2} \frac{\partial^2 y}{\partial t^2} = 0 \quad [19]$$

Making the substitution $n = x/L$, Equation [19] becomes

$$n \frac{\partial^4 y}{\partial n^4} + 2 \frac{\partial^3 y}{\partial n^3} + \left(\frac{12\rho L^4}{Eh^2}\right) n \frac{\partial^2 y}{\partial t^2} = 0 \quad [19a]$$

We now make the harmonic substitution $y = f(n) \cos \omega t$. The $\cos \omega t$ cancels out of each term leaving the equation in $f(n)$

$$nf''''(n) + 2f'''(n) - \frac{12\rho L^4}{Eh^2} \omega^2 nf(n) = 0 \quad [20]$$

The four boundary conditions for a cantilever beam will be

$$f'''(0) = f''(0) = 0$$

$$f(1) = f'(1) = 0$$

The solution is assumed in the form of an infinite power series

$$f(n) = \sum_{m=0}^{\infty} a_m n^{(m+s)} \quad [21]$$

Substitution into the differential equation and setting the coefficients of each power of n equal to zero give the results: For $s = 0$, a_0, a_1, and a_2 are arbitrary, and $a_3 = 0$. For arbitrary s and $m \geq 4$

$$a_m = \frac{\gamma^2}{(m+s)(m+s-1)^2(m+s-2)} a_{m-4} \quad [22]$$

for the beam

$$\gamma = \omega \sqrt{\frac{12\rho L^4}{Eh^2}}$$

and ρ is mass per unit volume. Since only three constants are arbitrary, only three terms of the general solution of Equation [20] have been found.

To obtain the fourth term the three terms already obtained are differentiated with respect to s and multiplied by the arbitrary constant b. (s is then taken as 0.) The resulting complete solution is

$$\begin{aligned} f(n) = {} & [1 + b \ln n] \left\{ a_0 \left[1 + \frac{\gamma^2 n^4}{4 \times 3^2 \times 2} + \frac{\gamma^4 n^8}{4 \times 8(3 \times 7)^2 \times 2 \times 6} + \cdots \right] \right. \\ & + a_1 n \left[1 + \frac{\gamma^2 n^4}{5 \times 4^2 \times 3} + \frac{\gamma^4 n^8}{5 \times 9 \times (4 \times 8)^2 \times 3 \times 7} + \cdots \right] \\ & \left. + a_2 n^2 \left[1 + \frac{\gamma^2 n^4}{6 \times 5^2 \times 4} + \frac{\gamma^4 n^8}{6 \times 10 \times (5 \times 9)^2 \times 4 \times 8} + \cdots \right] \right\} \\ & + b\gamma^2 n^4 \left\{ \frac{a_0}{4 \times 3^2 \times 2} \left[\left(\frac{7 \times 5}{4 \times 3 \times 2} \right) + \frac{\gamma^2 n^4}{8 \times 7^2 \times 6} \left(\frac{7 \times 5}{4 \times 3 \times 2} + \frac{15 \times 13}{8 \times 7 \times 6} \right) + \cdots \right] \right. \\ & + \frac{a_1 n}{5 \times 4^2 \times 3} \left[\left(\frac{9 \times 7}{5 \times 4 \times 3} \right) + \frac{\gamma^2 n^4}{9 \times 8^2 \times 7} \left(\frac{9 \times 7}{5 \times 4 \times 3} + \frac{17 \times 15}{9 \times 8 \times 7} \right) + \cdots \right] \\ & \left. + \frac{a_2 n^2}{6 \times 5^2 \times 4} \left[\left(\frac{11 \times 9}{5 \times 4 \times 3} \right) + \frac{\gamma^2 n^4}{10 \times 9^2 \times 8} \left(\frac{11 \times 9}{5 \times 4 \times 3} + \frac{19 \times 17}{10 \times 9 \times 8} \right) + \cdots \right] \right\} \end{aligned}$$

The first two boundary conditions are satisfied if we take $b = a_2 = 0$

The third and fourth boundary conditions become

$$a_0\left[1 + \frac{\gamma^2}{4 \times 3^2 \times 2} + \dots\right] + a_1\left[1 + \frac{\gamma^2}{5 \times 4^2 \times 3} + \dots\right] = 0$$

$$a_0\left[\frac{\gamma^2}{3^2 \times 2} + \frac{\gamma^4}{4 \times (3 \times 7^2) \times 2 \times 6} + \dots\right] + a_1\left[1 + \frac{\gamma^2}{4^2 \times 3} + \dots\right] = 0$$

By setting the determinant of coefficients of this pair of equations equal to zero, we obtain a transcendental equation in γ^2 the roots of which determine the natural frequencies of vibration. By neglecting powers of γ^2 higher than fourth the first two roots were found to be $\gamma_1 = 7.157$, and $\gamma_2 = 31.04$.

Prediction and Evaluation of Sensitivity to Transient Accelerations

By M. KORNHAUSER,[1] WHITE OAK, MD.

The determination, presentation, and interpretation of inertia-sensitivity data are discussed with application to inertia devices and to shock-resistant structures. Theoretical analysis of the single-degree-of-freedom system for response to acceleration-time pulses, amplification factors, and inertia sensitivity are used as a basis for discussion of actual devices. Effects of deviations from the ideal mass-spring system are considered. Practical use of sensitivity data is discussed with regard to the reliability of laboratory methods, the accuracy of field measurements, and variability of service conditions. Criteria are suggested for design of inertia mechanisms and design of structures for resistance to shock.

Nomenclature

The following nomenclature is used in the paper:

A = cross-sectional area of uniform beam
C_0 = speed of sound in beam material = $\sqrt{E/\gamma}$
C_1, C_2 = constants which depend upon beam geometry
E = modulus of elasticity
g = acceleration of gravity
G_0 = steady acceleration required to produce x_0 or ϵ_0
h = half-depth of uniform beam
I = moment of inertia of beam cross section
k = spring constant
l = length of beam or rod
L = free length of spring
M = mass
t = time
t_1 = duration of acceleration-time pulse
t_m = time at maximum amplitude of response
T = natural period = $2\pi\sqrt{M/k}$
V_0 = impulsive velocity change required to produce x_0 or ϵ_0
ΔV = velocity change of applied acceleration-time pulse
x = deflection of mass on spring
x_0 = specified travel of mass to actuate inertia mechanism, measured from initial position
x_m = maximum deflection
x_p = preset deflection of mass, measured from neutral position
y = deflection of free end of spring from fixed reference axis
$\ddot{y}_m$ = peak value of applied acceleration
α = dummy variable of integration
β = pulse "form factor," equal to average acceleration divided by peak acceleration
ϵ = unit strain
ϵ_0 = strain required for damage or failure
γ = density of beam material
ω = natural circular frequency = $2\pi/T = \sqrt{k/M}$

Introduction

The concepts of transient analysis, although frequently applied to electrical problems, seldom are used in the discussion of mechanical transients or "shocks." The result has been that the uninitiated are prone to make statements such as, "This structure will stand 50 g," with complete lack of regard for the fact that time is a variable in a dynamic problem. Although those familiar with the jargon of transient analysis are apt to be more cautious in their language, there does exist a general state of confusion regarding the role of duration of acceleration and natural frequency of the structure undergoing acceleration.

This paper discusses the factors which influence the response of the mechanism being subjected to shock, introduces a method of presentation of transient data which leads to a more complete description of the applied transient and the resulting response, and suggests rational criteria for design for shock resistance or for actuation of inertia mechanisms. Although the nature of the problem is such that exact design formulas may not be developed, it is possible to recommend the most probable design factors and to indicate the possible spread of performance under varied service conditions.

The mechanism or structure considered herein must move a prescribed distance against a restraining force in order to perform its function, in response to a transient forcing function. This forcing function is an acceleration-time pulse acting on a mass, and the restraining force is exerted by some elastic member. By defining the system as moving a fixed distance one not only may include many inertia-operated devices such as are common in ordnance applications (firing switches, and so on), but also shock-resistant structures, since failure is characterized by elastic or plastic strain, and strain is a travel phenomenon. Since the simplest system which fulfills the foregoing conditions is the mass-spring system, Fig. 1, the following analyses will be

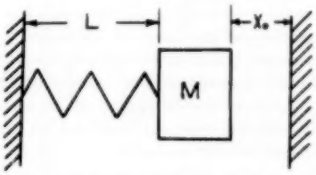

Fig. 1 A Simple Mass-Spring System

made only for the single-degree-of-freedom system. However, many of the conclusions reached for the behavior of the mass-spring system (mass-spring system will be used interchangeably with single-degree-of-freedom system hereafter) will be valid for more complex devices and structures.

When the mass-spring system of Fig. 1 is subjected to acceleration-time pulses of varying amplitude and duration, it

[1] U. S. Naval Ordnance Laboratory.

Presented at the West Coast Meeting of the Applied Mechanics Division, San Francisco, Calif., June 21–23, 1954, of The American Society of Mechanical Engineers.

Discussion of this paper should be addressed to the Secretary, ASME, 29 West 39th Street, New York, N. Y., and will be accepted until January 10, 1955, for publication at a later date. Discussion received after the closing date will be returned.

Note: Statements and opinions advanced in papers are to be understood as individual expressions of their authors and not those of the Society. Manuscript received by ASME Applied Mechanics Division, July, 27, 1953. Paper No. 54—APM-3.

is found (experimentally and theoretically) that the minimum shock values required to effect actuation (or prescribed travel) follow a curve such as Fig. 2, a typical sensitivity curve.

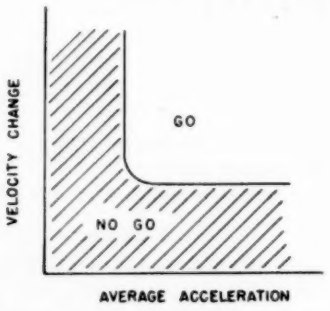

FIG. 2 A TYPICAL SENSITIVITY CURVE

The parameters of velocity change and average acceleration describe the input pulse, while the sensitivity curve defines regions of actuation or no actuation. Taking, for example, a rod with a damage level arbitrarily defined at 5 per cent elongation, its damage-sensitivity curve would predict that all pulses in the region above and to the right of the sensitivity curve produce 5 per cent or more elongation, while the pulses below and to the left are not sufficient to cause 5 per cent elongation.

In order to justify a single curve such as Fig. 2, it will be necessary to define rigidly all the conditions of impact, one of the most important being the shape of the acceleration-time pulse. These "field" conditions will be discussed further, with the aim of arriving at a single sensitivity curve which can, with reasonable accuracy, represent the behavior of a mechanism or structure in response to any single[2] acceleration transient likely to be encountered. Assuming for the moment that Fig. 2 is valid, within limits of accuracy, one can observe that it represents far more than a single number, such as 50 g. Without now going into a discussion of the full meaning or use of a sensitivity curve, one may note briefly that it predicts the minimum acceleration, at any duration, required for actuation. In other words, the curve represents sensitivity to any acceleration-time pulse.

It may be considered superfluous experimentally or analytically to obtain such extensive data on the performance of a mechanism being considered for only a single application. There are several reasons for obtaining the "whole story" on an inertia mechanism, not the least being the human tendency to employ a device in many ways other than that for which it was designed originally. Another, and overwhelmingly powerful, reason is that field conditions rarely can be defined narrowly (or if they are, it generally means that the person specifying these conditions is an optimist), laboratory methods are never exact, and there is considerable variability in manufactured products; all of which inaccuracies place the burden on the designer to determine what these variations mean in terms of performance.

The sensitivity curve will indicate whether the design will operate well with quite a spread of service conditions, or whether small variations will lead to failure—a stability criterion, as it were. For these, and many other reasons, it is worth while to consider performance under a wide range of circumstances, and experience has shown the sensitivity curve to be extremely valuable in work on mechanical transients.

[2] Multiple pulses are mentioned briefly, but this subject is extensive enough to deserve a separate treatment.

APPLICABILITY OF THE THEORY

Unfortunately, there are phenomena other than acceleration and duration which affect the performance of inertia devices, and which tend to shift or distort the sensitivity curve. One factor which makes difficult any attempt to employ a single sensitivity curve, (or narrow band) for all service conditions is the shape of the acceleration-time pulse; that is, a square pulse, a half-sine pulse, and a triangular pulse, will all produce sensitivity curves different in some regions, even though the velocity changes and average accelerations are identical. This problem represents an inherent difficulty in the accurate presentation and application of inertia-sensitivity data and is considered in detail later in this paper.

Some factors which make theoretical prediction of sensitivity curves difficult, but which do not render laboratory-determined sensitivity curves invalid, are as follows:

1 Some systems require a certain amount of kinetic energy at the end of their travel in order to perform their function. In contrast to an electrical switch which merely must make contact, many practical devices must perform mechanical work other than moving their prescribed distance against spring force. Some mechanisms are required to move mechanical parts such as detents or cams, while some firing switches must penetrate the surface of an explosive with sufficient energy to initiate detonation. In the latter case it is generally found that mere penetration of an explosive does not necessarily cause detonation and that a minimum striking velocity is needed.

2 Many systems are more complex than the single mass-spring system. For example, consider the distributed-mass system, which has an infinite number of natural periods. In this case, many of the higher modes of vibration may be excited by an input pulse and the resulting motion is far more complex and difficult to analyze than that of the mass-spring system. Compare (Fig. 3) the motions (relative to its base) of the tip of a uniform cantilever beam with those of a mass-spring system, both responding to an excitation consisting of an impulsive velocity of the base or fixed end (1).[3] The mass-spring system responds with simple harmonic motion; whereas the cantilever tip remains motionless until the disturbance traverses the length of the cantilever, begins to move in a direction opposite from that of the motion of the base, and finally executes a vibration which contains all its higher modes. Apparently, an analysis of the inertia sensitivity of the uniform cantilever would be rather difficult and laborious. However, under certain conditions of loading,[4] the cantilever will respond as a single-degree-of-freedom system, and the results of a mass-spring analysis will be directly applicable.

3 There are miscellaneous divergences from the ideal mass-spring system which influence the behavior of the mechanism or structure. Effects such as nonlinearity of the "spring," friction, preset of the spring or internal stresses in the structure, and damping may be of considerable importance in altering the shape of the sensitivity curve.

4 In complex structures there may be the possibility of internal collision of structural members, with resulting accelerations far greater than the applied loading.

It must be emphasized at this point that only when absolutely necessary should quantitative theoretical predictions be used in

[3] Numbers in parentheses refer to the Bibliography at the end of the paper.

[4] Frankland (2) suggests the following restrictions:
(*a*) The duration of impact must exceed 0.1 or more of the fundamental period. (*b*) The impact load must be distributed over the structure fairly uniformly. (*c*) The fundamental mode of the structure must be uncoupled with the higher modes; in other words, the momentary deflection profile of the structure in its extreme position must agree with its profile under static load.

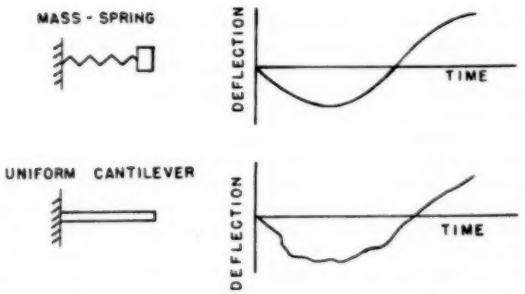

FIG. 3 COMPARISON OF MOTIONS OF MASS-SPRING SYSTEM WITH DISTRIBUTED-MASS SYSTEM

lieu of actual performance. The sources of discrepancy mentioned and possibly many others indicate that any calculated sensitivity curve should be checked in the laboratory or in the field. How closely the theoretical predictions conform to test results will depend on the skill and experience of the estimator, but even the veteran theorist occasionally will miss some "bug" in the system. However, despite the foregoing pitfalls, the qualitative theoretical conclusions will be valid; that is, the general shape of the curve will be correct, and the general conclusions as to the action of the device or structure in response to shocks of short or of long duration will also be valid.

DETERMINATION AND INTERPRETATION OF A THEORETICAL SENSITIVITY CURVE

In order to avoid being sidetracked by mathematics, it appears profitable to discuss qualitatively the response of a mass-spring system to a pulse of simple shape. After an understanding of the physical problem has been attained, the mathematical details may be examined by reference to the Appendix.

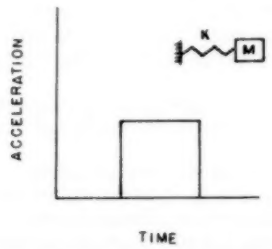

FIG. 4 MASS-SPRING SYSTEM SUBJECTED TO RECTANGULAR PULSE

Consider Fig. 4 the free end of the spring of a mass-spring system subjected to a rectangular acceleration pulse. Because of the flexibility of the spring, the mass does not follow this forcing function, but instead executes some erratic vibration, Fig. 5. The peak deflection attained by the mass is different from the deflection which could have been achieved by very slowly applying the maximum value of acceleration of the rectangular pulse. The ratio of maximum dynamic deflection to maximum static deflection is termed the amplification factor. Had the ratio of pulse duration to natural period of the mass-spring system been different, the amplification factor would have been different. A plot, Fig. 6, of amplification factors for a mass-spring system subjected to rectangular pulses shows this dependence on duration (2).

Since the mass must move a fixed distance, and a fixed deflection is equivalent to a fixed acceleration (the peak response in Fig. 5), the higher the amplification factor the lower the required

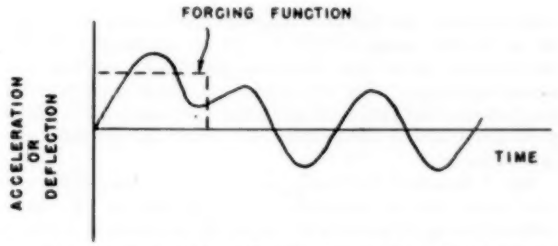

FIG. 5 RESPONSE OF MASS-SPRING SYSTEM TO A RECTANGULAR PULSE

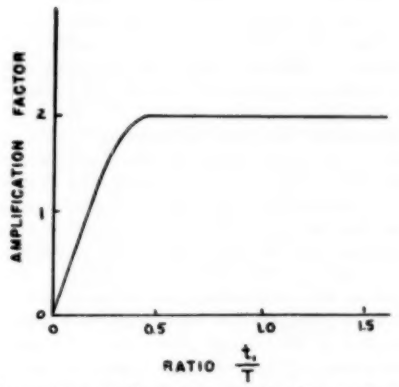

FIG. 6 AMPLIFICATION FACTORS FOR MASS-SPRING SYSTEM SUBJECTED TO RECTANGULAR PULSES

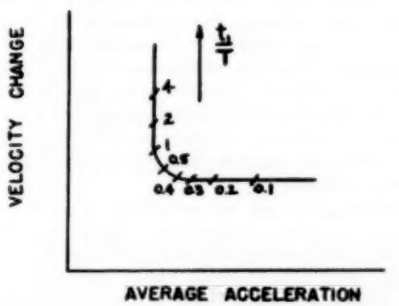

FIG. 7 INERTIA-SENSITIVITY CURVE FOR MASS-SPRING SYSTEM SUBJECTED TO RECTANGULAR PULSES

applied acceleration. For a rectangular pulse, the amplification factor increases as duration increases, soon becoming constant. With regard to velocity change, which is equal to average acceleration times duration, it appears that longer duration (higher than 0.5 in Fig. 6) signifies higher velocity change. A graphical presentation of these statements is the inertia-sensitivity curve of Fig. 7.

Exception could be taken to the choice of co-ordinates of Fig. 7 since the basic parameters are acceleration and duration. However, the use of velocity change is found to be more practical, since it leads to a curve which quickly approaches two asymptotes (the word asymptote is used loosely here, since for some shape pulses the curve crosses the "asymptote," and the rectangular pulse actually reaches its asymptote). The reason for the choice of average acceleration instead of peak accelera-

tion, aside from the fact that duration may be determined readily as velocity change divided by average acceleration, is that most service pulses have high-frequency "hash" superimposed on the main pulse. The high acceleration spikes associated with the hash have little effect on the inertia mechanism, and a plot of peak acceleration would produce very erratic and unreliable sensitivity curves.

Fig. 7 represents the inertia sensitivity of a mass-spring system to any pulse of rectangular shape. In general, for a given velocity change, it predicts the minimum acceleration necessary to actuate the mechanism. Also, for a given acceleration, it predicts the minimum velocity change necessary to actuate the mechanism.

Other conclusions may be drawn from this curve owing to the presence of the asymptotes (which also exist for other pulse shapes). Take, for example, the left-hand portion of the curve. In this region of relatively long pulse durations, the velocity change or duration may increase considerably without changing the acceleration appreciably.

The value of this fact may be illustrated by the example of the designer of an inertia mechanism which must be actuated by a catapult which attains a peak acceleration of 10 gravitational units. If he designs the mechanism with too long a natural period, the catapult pulse will act effectively as an impulsive velocity change, and the operation of the mechanism will depend on the velocity delivered by the catapult. However, by examination of the inertia-sensitivity curve, he may note that so long as the natural period of the mechanism is about $^1/_2$ or less of the duration of the catapult pulse, the mechanism operation is virtually independent of velocity. Thus, as long as he keeps that restriction on natural period in mind, he may design the mechanism solely on the basis of static deflection under 10 gravitational units.

Similar considerations apply to the right-hand portion of Fig. 7. In this region, as long as the duration of the pulse is about $^1/_3$ or less of the natural period, the velocity change remains relatively constant. Therefore the designer who is dealing with short durations (relative, of course, to the natural period of the structure or mechanism) has merely to stay below a certain duration in order to achieve a constant result. Within this region the peak acceleration may be unknown or highly variable without affecting the result.

The foregoing remarks on asymptotes apply to any sensitivity curve for a mass-spring system. The quantitative results, however, are different for different pulse shapes; that is, the asymptotes exist, but are parallel, Fig. 8. In the following paragraphs a comparison will be made of sensitivity curves for several types of pulses, in an attempt to reach some quantitative conclusions which may apply to a large number of cases.

Effect of Pulse Shape on Theoretical Sensitivity Curves

Fig. 8 presents sensitivity curves for the response of a mass-spring system to several pulse shapes. For purposes of comparison, the sensitivity curve for the rectangular pulse is repeated on each plot as a dashed curve. Fig. 8(*f*) is composed of all the sensitivity curves superimposed on one plot. It would be extremely advantageous to be able to employ a single curve, or narrow band which would be reasonably accurate in many applications. Unfortunately, Fig. 8(*f*) reveals that the low-acceleration asymptotes are spread over a considerable range. The variations, for the single pulses shown (systems which can move in either direction from the neutral position show behavior less desirable than Fig. 8, when subjected to multiple, reference (3), or complex, reference (4), pulses) is from $\pi/2$ for the triangle with very short build-up time to 4 for the half-sine pulse. Since either of these pulses is likely to be encountered in practice, it appears that the use of a single sensitivity curve should be subject to serious error.

On the brighter side of the picture, Fig. 8 shows that the high acceleration (short-duration) asymptote exhibits negligible dependence upon pulse shape. This means that any shock of duration shorter than $^1/_3$ or $^1/_4$ of the natural period, regardless of pulse shape, will require the same velocity change, or energy, to actuate the inertia mechanism.

Without going into the questions of which pulse shapes are produced in the laboratory, and which may be expected in the field, the following general conclusions may be drawn:

1 The high-acceleration asymptote is quite independent of pulse shape and therefore very reliable.

2 The low-acceleration asymptote depends a good deal upon pulse shape and is therefore unreliable for general use. Unless the use of the sensitivity curve is restricted narrowly, this asymptote is suitable for only rough estimates.

Laboratory Determination of Inertia Sensitivity

The obvious answer to the problem of pulse shape is a laboratory-determined sensitivity curve for each shape likely to be encountered with the inertia device. This, however, would lead to prohibitive expense, both in testing time and in machinery. The practical approach is to use the best equipment available and make the best attempt at interpretation.

Table 1 gives a general picture of the equipment in current use at the Naval Ordnance Laboratory for producing simple pulses.

The full practical ranges of duration, acceleration, and velocity change are covered by this equipment with some variation in pulse shape.

The general procedure in testing a specific mechanism is first to make a rough estimate of the natural frequency of the device and of the minimum velocity change to effect actuation or damage. At this stage, one may select the machines which will be used. For example, if an inertia mechanism has a natural period of 30 millisec and a minimum velocity change of 5 fps (see section on design applications for formulas for calculation of these quantities), then any machine with a duration of less than about 10 millisec would give test points out on the high-acceleration asymptote, Fig. 7. Therefore the equipment to be chosen from Table 1 would be "drop testers" for the high-acceleration region, the "square-wave tester" for the bend of the curve, and the "centrifuge" for the low-acceleration asymptote.

TABLE 1 EQUIPMENT AT NAVAL ORDNANCE LABORATORY

Equipment	Peak acceleration, g	Duration, millisec	Velocity change, fps	Pulse shape
Drop testers—steel on steel	200–25000	0.040–0.400	0–60	Half sine
Drop testers—lead pads	10–1000	0.40–20	0–60	Slow build-up, sharp drop
Sine-wave tester	20–200	3–6	0–10	Half sine
Square-wave tester	0–60	5–50	0–25	Rectangular
Air guns	5–100000	1–200	0–1000	Similar to blast pulse
Rotary accelerator	10–650	Long	...	Linear build-up, remaining constant
Centrifuges	0–30000	Long	...	...

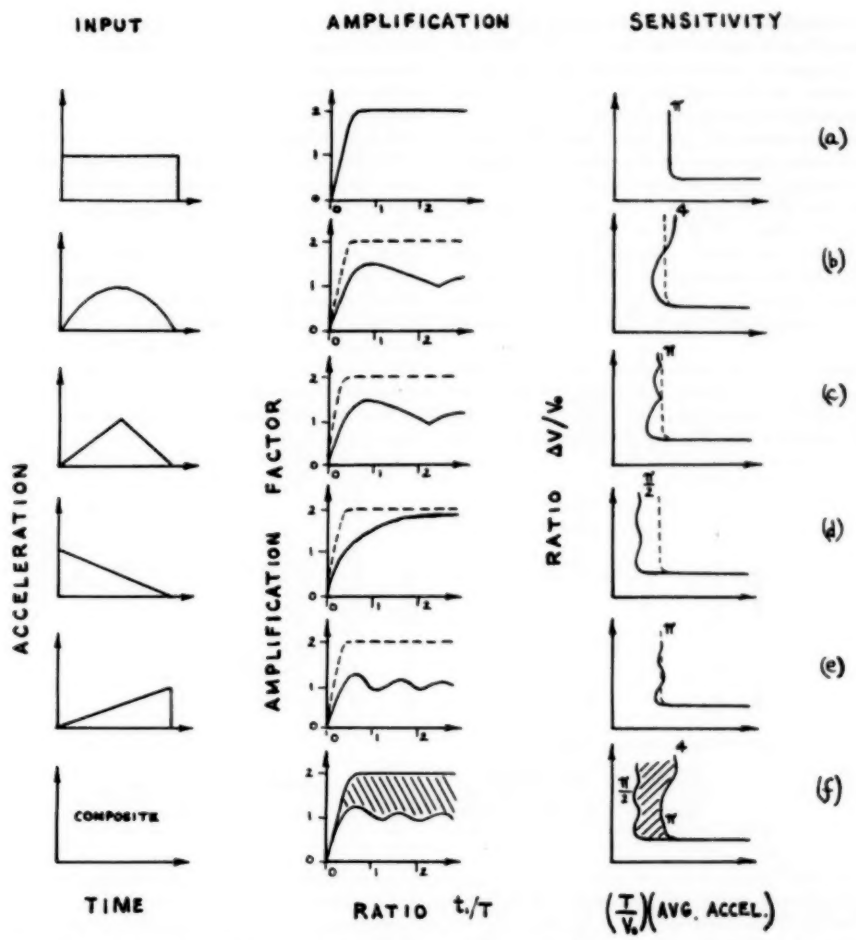

FIG. 8 AMPLIFICATION FACTORS AND SENSITIVITY CURVES FOR MASS-SPRING SYSTEM SUBJECTED TO SOME SINGLE PULSES

Proper mounting of the test specimen is most important for the sensitivity curve to have any significance. Whenever possible, the device should be mounted exactly as in the service application. In this way the only simulation involved is in the input-acceleration pulse. Unfortunately, however, many of the service vehicles carrying the inertia device are physically too large to be accommodated in the testing machines, and the question arises as to the effect of interposing a substitute elastic system between the source of shock and the component to be tested. This problem of transmission of shock through complex structures has not yet attained the stature of a science, owing to the dearth of information on even the more simple mechanical systems responding to transients. At some future date, when the literature contains the solutions of a sufficient number of classical problems, it may be practical to design an elastic mount equivalent to the actual mounting structure.

In some cases, after it has been determined that the actual mounting structure is too large, it is possible to select an intermediate mounting structure which "sees" the input pulse (in service) and is of suitable size. This method, of course, depends entirely on the judgment of the individual who decides on the relative rigidities of the structural members.

A simple, and also determinate, method of testing inertia devices is to use a relatively rigid mount which faithfully transmits the input (test) pulse. In this way, whenever the entire service mount or some intermediate mount cannot be tested as a unit, the performance of the mechanism on a determinate mount is ascertained. Although application of this information to the field-mounting condition may be difficult, the procedure is much more satisfactory than making indeterminate attempts at simulation of mounting.

After the machines have been selected and the specimen mounted, testing for sensitivity is done by finding the minimum velocity change for actuation of the device. For example, on the drop tester the method is to find the height of drop just sufficient for operation or damage. The sensitivity levels for various pulse durations are determined and the inertia-sensitivity curve plotted. (Efficient, economical testing may demand a statistical approach, such as the Bruceton or Probit methods of analysis of go or no-go data.)

PRESENTATION OF LABORATORY-SENSITIVITY DATA

Laboratory tests produce an inertia-sensitivity curve composed of points representing several pulse shapes. Unless each

point accidentally coincides with the field application as regards pulse shape, it would appear that the sensitivity curve may not be very useful. It must be recalled, however, that the high-acceleration asymptote showed negligible dependence on pulse shape, which makes half the curve quite reliable.

There are two approaches to the problem of the lack of reliability of the low-acceleration region of the curve. The generally accepted practice is to present the data "as is," based on the reasoning that the test machines yield results midway between the possible spread of values, and also based on the lack of accurate knowledge of field conditions. This approach realistically does not try to produce information on a level higher than the purpose for which it is intended. Data in the low-acceleration region are unreliable for close calculation and should be regarded as such.

In the rare instances which warrant accurate simulation, based on precise information on field shocks, it is possible to get better answers by adjusting the sensitivity data. For example, consider a set of data obtained with test equipment which gave the pulse shape and duration as indicated in Fig. 9. This curve is

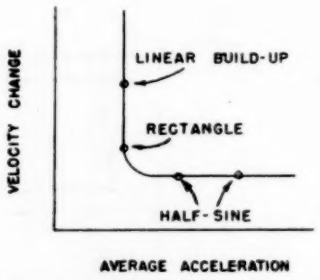

FIG. 9 SENSITIVITY CURVE OBTAINED WITH TYPICAL LABORATORY EQUIPMENT

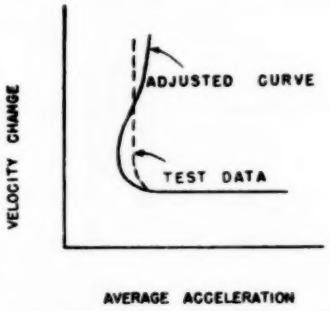

FIG. 10 ADJUSTMENT OF SENSITIVITY DATA

valid only for the pulse shapes indicated, except in the high-acceleration region where all shapes yield almost identical results. Now let us say that the mechanism tested is to be used in an application which calls for a half-sine pulse in place of the linear build-up, a symmetrical triangle instead of the rectangle, and rectangles instead of the half-sines. A rule-of-thumb approximation of the answer is to apply the theoretical values of acceleration (for each portion of the curve) to the test data of Fig. 9.

Take, for illustration, the point which was obtained with a linear build-up and which must be presented as a half-sine pulse. If the data were found as 12 gravitational units, the approximate point would be $12 \times 4/\pi = 15.3$ gravitational units, based on the theoretical value of four for the half-sine and π for the linear build-up, Fig. 8. Using this approximate method, the desired sensitivity curve would be presented as the solid curve in Fig. 10.

PRACTICAL USE OF A SENSITIVITY CURVE

There are powerful reasons for not depending too closely on inertia sensitivity in the low-acceleration region. One of the sources of difficulty lies in the statistical nature of the physical problem (7). For example, if one considers the shock on entry into water, the important factor of surface configuration leads to statistical variability of results. If it is a target-impact problem, the target structure and exact location of impact are rarely well defined. In the problems of this type any carefully reasoned estimate should be presented with a probable spread of values.

Another source of error is the lack of enough good field or service information. Gathering data in the field is an extremely expensive and time-consuming task, considering the instrumentation involved in measuring accelerations. For this reason, few measurements are made on any given field vehicle in a given service application. One or two measurements applied to a statistical problem do not lead to an answer which can be regarded with a good degree of confidence.

The designer's answer to the sources of error mentioned is to make provisions for satisfactory operation of the mechanism over a wide spread of service conditions. The mechanism must be quite flexible in its range of operation, with variability of field conditions and errors in field measurements adding up to some ± 50 per cent. This approach of recognizing and meeting the difficult design specifications is far superior to that of speculating on the probability of operation of a mechanism which operates somewhere within the spread of service conditions. An added advantage is the likelihood that a design which can cope with the spread of service requirements also will be adequate for the spread of the low-acceleration asymptotes resulting from variation in pulse shape.

Upon consideration of the variability of field conditions and the unreliability of typical field data, it becomes apparent that the laboratory-sensitivity data are probably the most carefully controlled and reliable components of the over-all problem. Therefore it is concluded that an "average" sensitivity curve (the laboratory test data) in the low-acceleration range is justified until such time as extensive and reliable field data are obtained (on each problem) to lead to solutions in terms of statistical spreads.

APPLICATION OF THEORETICAL SENSITIVITY CURVES TO DESIGN OF INERTIA MECHANISMS

The designer who must estimate a sensitivity curve has some simple formulas at his disposal. For the high-acceleration asymptote, the velocity change is close to the V_0 of Equation [17] (see Appendix). Rewriting Equation [17] to include the effect of preset of the spring (x_p)

$$V_0 = \omega x_0 \sqrt{1 + 2\frac{x_p}{x_0}} \qquad [1]$$

Since the total deflection at the point of maximum travel is equal to $x_p + x_0$, the peak acceleration applied by centrifuge $= (k/M)(x_0 + x_p) = \omega^2(x_0 + x_p)$. Using the "average" acceleration of half the centrifuge value

$$\frac{1}{2} G_0 = \frac{1}{2} \omega^2(x_p + x_0) \qquad [2]$$

Fig. 11 uses Equations [1] and [2] in estimating the sensitivity curve.

An example of the accuracy of these simple equations, when applied to a simple determinate system, is the following comparison of test results and theory for a small cantilever beam used as an inertia switch:

Measurements { centrifuge setting of switch = 4780 g; natural frequency—measured on vibrator = 2085 cps

Using Equation [18] (Appendix)

$$V_0 = \frac{G_0}{\omega} = \frac{(4780)\ (32.2)}{(2\pi)\ (2085)} = 11.78 \text{ fps}$$

The measured value of V_0, using a 50-microsec input pulse, was 11.35 fps.

The basic design parameters, Fig. 11, are velocity change, average acceleration, natural frequency, preset of the spring, and travel distance. Since, in general, the restrictions on more

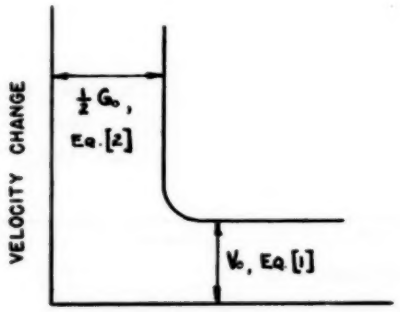

FIG. 11 AN ESTIMATED SENSITIVITY CURVE FOR THE INERTIA MECHANISM

than one or two of these quantities are not too severe, the designer has considerable latitude in his design. It is because of this freedom of design that it is possible to overcome the liability of the expected spread in operating conditions which usually characterizes the service applications of inertia devices.

APPLICATIONS TO STRUCTURAL DESIGN

It would be of value to the designer to be able to predict the shock resistance of a structure, without recourse to tedious computations of response to inertia loading. The following analysis leads to a rough approximation of "damage sensitivity" based upon the lowest natural mode of vibration, the properties of the materials, and the degree of destruction.

The structure is stated to behave as a simple mass-spring system, which assumption involves the following simplifications:

1 Failure is characterized by the amount of strain ϵ_0, which is attained by elastic action; that is, if one is dealing with some plastic deformation, an average modulus and speed of sound may be employed to simplify the problem.

2 Loading of the structure is presumed uniform, and the dynamic deflection of the structure has the same mode shape as that of the fundamental natural frequency. This allows the use of the relation $G_0 = \omega V_0$.

3 All the simplifications previously discussed, and particularly the case of internal collisions, are applicable here. For a uniform beam under a steady acceleration G_0

$$\epsilon_0 = C_1 \frac{G_0(A\gamma l^3)h}{EI} \quad [3]$$

but

$$\omega = C_2 \sqrt{\frac{EI}{\gamma A l^4}} \quad [4]$$

hence

$$G_0 = \frac{\omega\epsilon_0}{C_1C_2}\sqrt{\frac{EI}{h^2A\gamma}} = \frac{\omega\epsilon_0C_0}{C_1C_2}\sqrt{\frac{I}{h^2A}}$$

The quantity $\sqrt{I/(h^2A)}$ is equal to 0.577 for a beam of rectangular cross section, and 0.500 for the beam of circular cross section. Using an average value

$$G_0 = 0.54\frac{\omega\epsilon_0C_0}{C_1C_2} \quad [5]$$

Making use of the relationship $V_0 = G_0/\omega$, one finds that V_0 is independent of frequency

$$V_0 = 0.54\frac{\epsilon_0C_0}{C_1C_2} \quad [6]$$

but dependent on beam geometry and material properties. Examining the effects of beam geometry in Table 2, it appears that a representative value of V_0, for a system in bending

$$V_0 = 0.30\,\epsilon_0C_0 \quad [7]$$

The axially loaded rod is stronger than any of the systems mentioned:

(*a*) The rod loaded by a steady acceleration (nonuniform stress distribution)

$$\left.\begin{aligned}\epsilon_0 &= \frac{G_0\gamma l}{E}\\ \omega &= \frac{\pi}{2}\frac{C_0}{l}\end{aligned}\right\} G_0 = \frac{2}{\pi}C_0\epsilon_0\omega$$

For $G_0 = V_0\omega$

$$V_0 = \frac{2}{\pi}C_0\epsilon_0 = 0.636\,C_0\epsilon_0 \quad [8]$$

(*b*) The rod loaded with an elastic stress wave (uniform stress)

$$\epsilon_0 = \frac{\gamma C_0V_0}{E} = \frac{V_0}{C_0}$$

$$V_0 = 1.000\,C_0\epsilon_0 \quad [9]$$

TABLE 2 BEAM GEOMETRY CONSTANTS FOR STRESS AND NATURAL FREQUENCY

Beam	c_1	c_2	$\frac{0.54}{c_1c_2}$	
Cantilever	1/2	3.52	0.307	Uniform beams
Pin ends	1/8	9.87	0.438	
Both ends fixed	1/12	22.4	0.289	
One end fixed, other pinned	1/8	15.4	0.281	
Cantilever, mass at end	1	1.73	0.312	Weight of uniform beam now concentrated at one point
Both ends fixed, mass at center	1/8	13.85	0.312	
One end fixed, other pinned, mass at center	2/16	10.50	0.274	
Cantilever, mass at center	1/2	4.89	0.221	
Pin ends, mass at center	1/4	6.92	0.312	

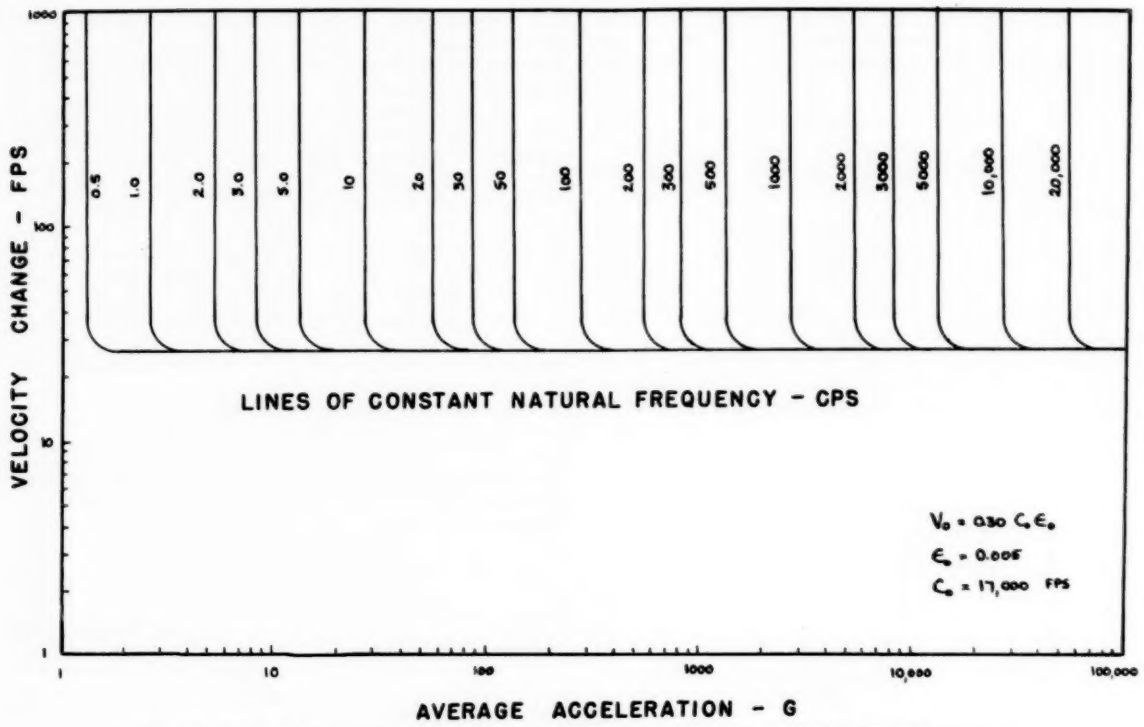

FIG. 12 DAMAGE-SENSITIVITY CURVE FOR TYPICAL STRUCTURES—FAILURE AT 1/2 PER CENT ELONGATION

In general, the bending frequencies of a structure are lower than the longitudinal mode frequencies, and therefore Equation [7] better represents most structures than Equations [8] or [9].

For steel or aluminum, with $C_0 \cong 17{,}000$ fps the strain and corresponding impulsive velocity predicted by Equation [7] are as shown in Table 3.

TABLE 3 STRESS AND STRAIN IN AN IMPULSIVELY LOADED STRUCTURE

ϵ_0, per cent	1/4	1/2	1	2
V_0, fps	12.7	25.4	51	102
Elastic stress, steel	75000	150000	300000	600000
Elastic stress, alum.	25000	50000	100000	200000

Fig. 12 is a plot of the damage-sensitivity curves for the "typical" structure of steel or aluminum, with

$$V_0 = 0.30\ C_0\epsilon_0$$
$$G_0 = \omega V_0$$
$$C_0 = 17{,}000 \text{ fps}$$
$$\epsilon_0 = \frac{1}{2} \text{ per cent}$$

The curves are drawn to represent the average sensitivity curve, or rectangular pulse, with V_0 as the short-duration asymptote and $1/2\ G_0$ as the long-duration asymptote.

These curves, and similar sets for other materials, should prove useful for preliminary design estimates.

ACKNOWLEDGMENT

The author wishes to express his thanks to Mr. J. L. Luttrell and Mr. J. H. Armstrong, both members of the staff at the Naval Ordnance Laboratory, for the many enlightening discussions which made this paper possible.

BIBLIOGRAPHY

1 "Beam-Vibration Analysis With the Electric-Analog Computer," by G. D. McCann and R. H. MacNeal, JOURNAL OF APPLIED MECHANICS, Trans. ASME, vol. 72, 1950, pp. 13–26.

2 "Effects of Impact on Simple Elastic Structures," by J. M. Frankland, David Taylor Model Basin Report 481, April, 1942.

3 "The Dynamic Response of a Simple Elastic System to Antisymmetric Forcing Functions Characteristic of Airplanes in Unsymmetric Landing Impact," by J. B. Woodson, JOURNAL OF APPLIED MECHANICS, Trans. ASME, vol. 71, 1949, pp. 310–316.

4 "The Response of a System With a Single Degree of Freedom to a Blast Load," by M. Levenson and B. Susshol, David Taylor Model Basin Report 572, December, 1947.

5 "Dynamics of Package Cushioning," by R. D. Mindlin, *Bell System Technical Journal*, vol. 25, No. 3–4, July–October, 1945.

6 "Transients in Mechanical Systems," by J. T. Muller, *Bell System Technical Journal*, vol. 27, October, 1948, p. 657.

7 "Statistical Aspects of Dynamic Loads," by Y. C. Fung, *Journal of the Aeronautical Sciences*, vol. 20, May, 1953, pp. 317–330.

Appendix

THEORETICAL SENSITIVITY OF MASS-SPRING SYSTEM

Fig. 13 shows the position of the mass-spring system relative to some fixed reference system. An analysis similar to that of

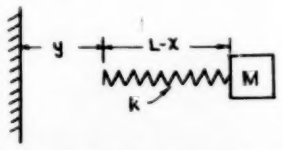

FIG. 13 THE MASS-SPRING SYSTEM

Frankland (2) is followed to derive Duhamel's integral

$$M\frac{d^2}{dt^2}[y + L - x] - kx = 0$$

$$M\ddot{x} + kx = M\ddot{y}$$

$$\ddot{x} + \omega^2 x = \ddot{y} \quad \ldots\ldots\ldots\ldots\ldots\ldots [10]$$

Multiplying by $\sin \omega t$

$$\ddot{x} \sin \omega t + \omega^2 x \sin \omega t = \ddot{y} \sin \omega t$$

$$\frac{d}{dt}(\dot{x} \sin \omega t) - \frac{d}{dt}(\omega x \cos \omega t) = \ddot{y} \sin \omega t$$

integrating

$$\dot{x} \sin \omega t - \omega x \cos \omega t = \int_0^t \frac{d^2y}{d\alpha^2} \sin \omega\alpha d\alpha \ldots\ldots [11]$$

where α is a dummy variable of integration.

Multiplying Equation [10] by $\cos \omega t$

$$\ddot{x} \cos \omega t + \omega^2 x \cos \omega t = \ddot{y} \cos \omega t$$

$$\frac{d}{dt}(\dot{x} \cos \omega t) + \frac{d}{dt}(\omega x \sin \omega t) = \ddot{y} \cos \omega t$$

integrating

$$\dot{x} \cos \omega t + \omega x \sin \omega t = \int_0^t \frac{d^2y}{d\alpha^2} \cos \omega\alpha d\alpha \ldots\ldots [12]$$

The foregoing integrations assume the boundary conditions of zero displacement and zero velocity at zero time. Eliminating terms in $\dot{x}$ from Equations [11] and [12]

$$\omega x = \sin \omega t \int_0^t \frac{d^2y}{d\alpha^2} \cos \omega\alpha d\alpha - \cos \omega t \int_0^t \frac{d^2y}{d\alpha^2} \sin \omega\alpha d\alpha$$

$$\omega x = \int_0^t \frac{d^2y}{d\alpha^2} \sin \omega (t - \alpha) d\alpha$$

Writing Duhamel's integral dimensionlessly

$$\frac{\omega^2 x}{\ddot{y}_m} = \omega \int_0^t \left(\frac{1}{\ddot{y}_m}\frac{d^2y}{d\alpha^2}\right) \sin (\omega t - \omega\alpha) d\alpha \ldots\ldots [13]$$

The procedure for determining amplification factor is to substitute

$$\frac{1}{\ddot{y}_m}\frac{d^2y}{d\alpha^2}$$

as a function of α (shape of input pulse) into Equation [13], solve for the maximum value of $\omega^2 x/\ddot{y}_m$, then

$$\text{Amplification factor} = \frac{kx_m}{M\ddot{y}_m} = \frac{\omega^2 x_m}{\ddot{y}_m} \ldots\ldots [14]$$

A sample calculation will be made for the rectangular pulse. For the rectangular pulse, Fig. 4

$$t < 0 \qquad \ddot{y}/\ddot{y}_m = 0$$

$$0 \leqq t \leqq t_1 \qquad \ddot{y}/\ddot{y}_m = 1$$

$$t > t_1 \qquad \ddot{y}/\ddot{y}_m = 0$$

Substituting into Equation [13]

$\underline{0 \leqq t \leqq t_1}$

$$\frac{\omega^2 x}{\ddot{y}_m} = \omega \int_0^t \sin(\omega t - \omega\alpha) d\alpha$$

$$= \cos (\omega t - \omega\alpha) \Big|_0^t = 1 - \cos \omega t$$

To find maximum, differentiate with respect to time and equate to zero

$$\sin \omega t_m = 0, \quad \omega t_m = 0, \pi, 2\pi \ldots\ldots$$

$$\frac{2\pi t_m}{T} = 0, \pi, 2\pi \ldots\ldots$$

$$\frac{t_m}{T} = 0, \frac{1}{2}, 1, 1\frac{1}{2} \ldots\ldots$$

and for $t_m/t_1 \leqq 1$

$$\frac{t_1}{T} \geqq \frac{1}{2}$$

Amplification factor $= 1 - (-1) = 2 \ldots\ldots [15]$

$\underline{t \geqq t_1}$

$$\frac{\omega^2 x}{\ddot{y}_m} = \omega \int_0^{t_1} \sin (\omega t - \omega\alpha) d\alpha + \omega \int_{t_1}^t 0$$

$$= \cos(\omega t - \omega\alpha) \Big|_0^{t_1} = \cos (\omega t - \omega t_1) - \cos \omega t$$

$$= \sin \omega t \sin \omega t_1 - \cos \omega t(1 - \cos \omega t_1)$$

Differentiating for maximum

$$\cos \omega t_m \sin \omega t_1 + \sin \omega t_m (1 - \cos \omega t_1) = 0$$

$$\tan \omega t_m = \frac{\sin \omega t_1}{\cos \omega t_1 - 1}$$

$$\tan \omega t_m = -\operatorname{ctn} \frac{\omega t_1}{2}$$

$$\omega t_m = \frac{\pi}{2} + \frac{\omega t_1}{2}$$

$$\frac{t_m}{T} = \frac{1}{4} + \frac{1}{2}\frac{t_1}{T}$$

and for $t_m/t_1 \geqq 1$

$$\frac{1}{4}\frac{T}{t_1} + \frac{1}{2} \geqq 1$$

or

$$\frac{t_1}{T} \leqq \frac{1}{2}$$

$$\text{Amplification factor} = \sin 2\pi\left(\frac{1}{4} + \frac{1}{2}\frac{t_1}{T}\right) \sin 2\pi \frac{t_1}{T}$$

$$- \cos 2\pi\left(\frac{1}{4} + \frac{1}{2}\frac{t_1}{T}\right)\left(1 - \cos 2\pi \frac{t_1}{T}\right)$$

$$= \cos \pi \frac{t_1}{T} \sin 2\pi \frac{t_1}{T}$$

$$+ \sin \pi \frac{t_1}{T}\left(1 - \cos 2\pi \frac{t_1}{T}\right)$$

$$= \sin\left(2\pi \frac{t_1}{T} - \pi \frac{t_1}{T}\right) + \sin \pi \frac{t_1}{T}$$

$$= 2 \sin \pi \frac{t_1}{T} \ldots\ldots [16]$$

Fig. 6 is a plot of Equation [16] for $t_1/T \leqq 1/2$ and Equation [15] for $t_1/T \geqq 1/2$. Fig. 8 shows amplification-factor curves for several pulses other than the rectangular pulse.

In order to express inertia-sensitivity parameters in dimensionless form, the quantity V_0 is introduced. This is the velocity of the mass as it passes through the neutral position (zero spring deflection) sufficient to produce x_0, which is the specified travel of the mechanism. Equating kinetic and potential energy (no preset)

$$\int_0^{x_0} kx\,dx = \frac{1}{2} M V_0^2$$

$$V_0 = \sqrt{\frac{k}{M}}\, x_0$$

$$V_0 = \omega x_0 \qquad [17]$$

Steady acceleration needed to produce x_0

$$G_0 = \frac{\text{force}}{\text{mass}} = \frac{kx_0}{M} = \omega^2 x_0$$

$$G_0 = V_0\omega \qquad [18]$$

$$\text{Peak applied acceleration} = \frac{G_0}{\text{amp factor}} = \frac{V_0\omega}{\text{amp factor}}$$

Average applied acceleration = β (peak acceleration) where β is a factor which depends on the pulse shape. For the rectangle $\beta = 1$. For the triangle $\beta = 1/2$. For the half-sine pulse $\beta = 2/\pi$

$$\text{Average acceleration} = \beta \frac{V_0\omega}{\text{amp factor}}$$

Dimensionlessly

$$\frac{\text{Avg accel}}{V_0/T} = \frac{2\pi\beta}{\text{amp factor}} \qquad [19]$$

Velocity change ΔV = avg accel $\times$ t_1

Dimensionlessly

$$\frac{\Delta V}{V_0} = \left(\frac{2\pi\beta}{\text{amp factor}}\right)\left(\frac{t_1}{T}\right) \qquad [20]$$

By selecting values of amplification factor from Fig. 8, the sensitivity plots of

$$\frac{\Delta V}{V_0} \text{ versus } \frac{\text{avg accel}}{V_0/T}$$

(also Fig. 8) were calculated easily.

At small values of t_1/T, $\Delta V/V_0$ approaches 1, or

$$\text{Amp factor} = 2\pi\beta\,\frac{t_1}{T}$$

that is, the initial slope of the amp factor versus t_1/T curve = $2\pi\beta$. Consequently

$$\text{Avg accel}\Big/\frac{V_0}{T} = \frac{T}{t_1}$$

Table 4 is applicable at large values of t_1/T, as also indicated in Fig. 8.

TABLE 4 LONG-DURATION ASYMPTOTES

Shape	Amp factor	Avg accel $/\frac{V_0}{T}$
Rectangle	2	π
Half-sine	1	4
Symmetrical triangle	1	π
Triangle, zero build-up time	2	$\frac{\pi}{2}$
Triangle, zero drop-off time	1	π
Centrifuge	1	2π

Note that half the centrifuge value of 2π would fall within the crosshatched region of Fig. 8(f), and therefore one half of the indicated centrifuge reading is used on laboratory-sensitivity curves. This is in line with the policy of using an average sensitivity curve to represent most service conditions with an accuracy warranted by such applications.

Torsional Vibrations of Beams of Thin-Walled Open Section

By J. M. GERE,[1] STANFORD, CALIF.

This analysis deals with the free torsional vibrations of bars of thin-walled open cross section for which the shear center and centroid coincide. Such sections include I-beams and Z-sections. The differential equation for torsional vibrations is derived and includes the effect of warping of the cross section. The effect of warping on the frequency of vibration and the shapes of the normal modes of vibration are determined for bars of single span with various end conditions. For a simply supported bar, a formula for the principal torsional frequencies and an expression for mode shape are derived. For other conditions of support, the frequency equations are derived and their solutions presented in graphical form. From these graphs the frequencies of vibration and the mode shapes may be obtained directly. The case of a cross section which does not warp is a limiting case of the general problem. For such shapes (for example, a cross-shaped or cruciform section) the formulas for torsional frequencies and modes of vibration are quite simple. These formulas also are valid for a circular shaft and may be used approximately for other solid sections.

Equation of Torsional Vibrations

The differential equation for the case of free vibrations is derived most easily by using D'Alembert's principle. This principle states, in effect, that the equation of motion for a dynamic system may be obtained by substituting inertia forces into the equation of static equilibrium. For the case of a thin-walled bar of open cross section, Fig. 1, the equation of static equilibrium for torsion[2] is

$$GC\frac{d\phi}{dx} - EC_w\frac{d^3\phi}{dx^3} = M_t \quad \ldots\ldots\ldots\ldots [1]$$

in which the following notation is used:

E = modulus of elasticity
G = modulus of rigidity (or shear modulus)
C = torsional constant
C_w = warping constant
M_t = total torque acting on bar at any cross section
ϕ = angle of twist of bar at any cross section
x = distance along bar

For free vibrations the static torque is replaced by the inertia torque which has an intensity (per unit length of bar) of

$$mI_p\frac{\partial^2\phi}{\partial t^2}$$

in which

I_p = polar moment of inertia of cross section about centroid
m = mass density of the material of bar
t = time

The intensity of torque is related to the total torque at any section by the expression

$$\frac{\partial M_t}{\partial x} = mI_p\frac{\partial^2\phi}{\partial t^2} \quad \ldots\ldots\ldots\ldots [2]$$

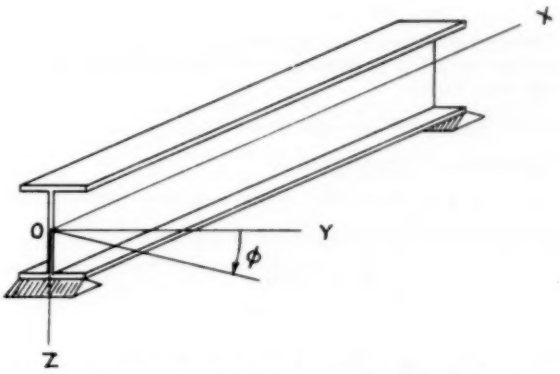

Fig. 1 I-Beam Typifying Thin-Walled Bar of Open Cross Section

which merely states that the rate of change of the total torque equals the intensity of the inertia torque.

Upon differentiating Equation [1] and combining with Equation [2], we obtain the differential equation for free torsional vibrations

$$GC\frac{\partial^2\phi}{\partial x^2} - EC_w\frac{\partial^4\phi}{\partial x^4} = mI_p\frac{\partial^2\phi}{\partial t^2} \quad \ldots\ldots\ldots [3]$$

This equation is necessarily a partial differential equation since ϕ is a function of both x and t. The equation is valid for all bars of thin-walled open cross section, provided the shear center of the cross section coincides with the centroid. If the shear center does not coincide with the centroid, the torsional vibrations will be accompanied by bending vibrations. The equations for these coupled vibrations are more complicated and in the general case

[1] Graduate student, Division of Engineering Mechanics, Stanford University.

[2] This equation was first derived for the case of an I-beam by Timoshenko, Bulletin of the Polytechnic Institute, St. Petersburg, 1905. The equation was extended to all thin-walled open cross sections by H. Wagner, "Torsion and Buckling of Open Sections," Technische Hochschule, Danzig, Germany, 25th Anniversary Publication, 1929. An English translation of this paper is given in NACA Technical Memorandum No. 807, October, 1936. The equation is valid for bars in which the length is large compared to the cross-sectional dimensions.

Presented at the West Coast Conference of the Applied Mechanics Division, University of California, Berkeley, Calif., June 21–23, 1954, of The American Society of Mechanical Engineers.

Discussion of this paper should be addressed to the Secretary, ASME, 29 West 39th Street, New York, N. Y., and will be accepted until January 10, 1955, for publication at a later date. Discussion received after closing date will be returned.

Note: Statements and opinions advanced in papers are to be understood as individual expressions of their authors and not those of the Society. Manuscript received by ASME Applied Mechanics Division, March 10, 1954. This paper was not preprinted.

the solution of three simultaneous partial differential equations is required.[3]

General Solution of Equation

To find the natural modes of vibration, the solution of Equation [3] is obtained by separation of variables. Thus, by taking ϕ in the form

$$\phi = X(x)T(t)$$

and then substituting into Equation [3], separating the variables, and setting the resulting expressions equal to $-p_n^2$, we obtain

$$T = A_n \cos p_n t + B_n \sin p_n t$$

The expression for a normal mode of vibration is then

$$\phi = X(A_n \cos p_n t + B_n \sin p_n t) \quad [4]$$

in which X is the normal function giving the shape of the mode of vibration and p_n is the natural frequency of vibration (radians per unit of time). Any actual motion of the vibrating bar can be obtained by a summation of normal modes, so that in the general case

$$\phi = \sum_{n=1}^{\infty} X_n(A_n \cos p_n t + B_n \sin p_n t)$$

in which the coefficients A_n and B_n are found from the initial conditions of the vibration.

The equation for determining the normal function X, found by substituting Equation [4] into the differential Equation [3], is then

$$EC_w \frac{d^4X}{dx^4} - GC \frac{d^2X}{dx^2} - mI_p p_n^2 X = 0 \quad [5]$$

The general solution of this equation may be found by taking the normal function X in the form $D'e^{bx}$, which yields the auxiliary algebraic equation

$$EC_w b^4 - GC\, b^2 - mI_p p_n^2 = 0$$

The four roots of this equation are

$$b_1 = +\alpha,\ b_2 = -\alpha,\ b_3 = +i\beta,\ b_4 = -i\beta$$

in which α and β are the positive, real quantities given by

$$\alpha = \sqrt{\frac{GC + \sqrt{(GC)^2 + 4EC_w mI_p p_n^2}}{2EC_w}} \quad [6]$$

$$\beta = \sqrt{\frac{-GC + \sqrt{(GC)^2 + 4EC_w mI_p p_n^2}}{2EC_w}} \quad [7]$$

The general solution of Equation [5] then becomes either

$$X = D'_1 e^{+\alpha x} + D'_2 e^{-\alpha x} + D'_3 e^{+i\beta x} + D'_4 e^{-i\beta x}$$

or

$$X = D_1 \cosh \alpha x + D_2 \sinh \alpha x + D_3 \cos \beta x + D_4 \sin \beta x \quad [8]$$

There are four arbitrary constants in this expression which must be determined so as to satisfy the particular boundary conditions of the problem. For any beam there will be two boundary conditions at each end and these four conditions determine the frequency equation and the ratios of three of the constants to the fourth constant. Solving the frequency equation then determines the principal frequencies of vibration. With the frequencies and normal functions determined, the solution is essentially complete.

The foregoing discussion is based on the assumption that C_w is not zero. The special case of $C_w = 0$, which means that the cross sections of the bar do not warp, is discussed later.

Boundary Conditions for Torsion

The supports at the ends of a bar or beam vibrating torsionally may offer restraint in two ways. There may be a restraint against rotation of the end cross section or restraint against warping of the end cross section. Warping is the displacement in the longitudinal direction of the bar of a cross section which originally was plane and at right angles to the longitudinal axis; that is, it is the distortion of a plane cross section out of its plane.

The warping displacements u in the x-direction are given by the equation[4]

$$u = \frac{\partial \phi}{\partial x}(D - \omega_s) \quad [9]$$

in which

D = constant of cross section
ω_s = quantity which varies over cross section, but is constant for any given point in cross section.

From Equation [9] we obtain the longitudinal stresses as

$$\sigma_x = E\epsilon_x = E\frac{\partial u}{\partial x} = E\frac{\partial^2 \phi}{\partial x^2}(D - \omega_s) \quad [10]$$

Thus we see from Equations [9] and [10] that the warping and the longitudinal stress at any point in the cross section of the bar are directly proportional to $\partial\phi/\partial x$ and $\partial^2\phi/\partial x^2$, respectively.

Three kinds of end support may be defined, depending on the type of restraint. A "simple support" implies restraint against rotation but not against warping; that is, the end of the bar does not rotate but is free to warp. This means the longitudinal stress σ_x is zero or, in other words, $\partial^2\phi/\partial x^2$ must be zero. Hence, for a simple support, the end conditions are

$$\phi = 0,\ \frac{\partial^2 \phi}{\partial x^2} = 0$$

A "fixed support" implies restraint not only against rotation but also against any warping of the end cross section. This means that the end of the bar is built-in rigidly so that no deformation of the end cross section can take place. Since rotation and warping are zero, the end conditions are

$$\phi = 0,\ \frac{\partial \phi}{\partial x} = 0$$

A "free end" implies no restraint of any kind at the end of the bar. This requires the stress σ_x to be zero and, in addition, the total torque acting on the end cross section must be zero. This last condition is expressed by setting $M_t = 0$ in Equation [1]. Thus the end conditions for a free end are

$$\frac{\partial^2 \phi}{\partial x^2} = 0,\ \frac{GC}{EC_w}\frac{\partial \phi}{\partial x} - \frac{\partial^3 \phi}{\partial x^3} = 0$$

By applying the foregoing end conditions to the general solution, Equation [8], a number of different types of single-span beams can be analyzed. It should be noted that the boundary

[3] This general problem is discussed in the author's doctoral dissertation, "Bending and Torsional Vibrations of Thin-Walled Bars of Open Cross Section," Stanford University, Stanford, Calif., 1954, Prof. D. H. Young, Adviser.

[4] For derivation of this equation and a further explanation of the quantities D and ω_s, see "Theory of Bending, Torsion and Buckling of Thin-Walled Members of Open Cross Section," by S. Timoshenko, *Journal of The Franklin Institute*, vol. 239, 1945, pp. 201–219, 249–268, 343–361.

conditions for the normal function X are the same as those for the angle of rotation ϕ. This is evident from Equation [4] inasmuch as the boundary conditions must hold for any time t.

Simply Supported Beam

For a beam of length l simply supported at each end, the boundary conditions are

$$\left.\begin{array}{ll} \text{BC 1 } X = 0 & \\ \text{BC 2 } \dfrac{d^2X}{dx^2} = 0 & \end{array}\right\} \text{at } x = 0 \qquad \left.\begin{array}{ll} \text{BC 3 } X = 0 & \\ \text{BC 4 } \dfrac{d^2X}{dx^2} = 0 & \end{array}\right\} \text{at } x = l$$

Applying these conditions to Equation [8], we obtain from the first boundary condition the relation $D_2 = -D_1$, and from the second condition the relation $D_1(\alpha^2 + \beta^2) = 0$. Thus either $D_1 = D_2 = 0$, or else $\alpha^2 + \beta^2 = 0$. But $\alpha^2 + \beta^2 = 0$ means that

$$(GC)^2 + 4EC_w m I_p p_n^2 = 0$$

which is impossible, since all the quantities are positive. Thus from BC 1 and BC 2, we have

$$D_1 = D_2 = 0$$

From BC 3 and BC 4 we obtain the equations

$$D_3 \sinh \alpha l + D_4 \sin \beta l = 0 \quad \ldots\ldots [11]$$

$$D_3\alpha^2 \sinh \alpha l - D_4\beta^2 \sin \beta l = 0 \quad \ldots\ldots [12]$$

For a solution other than zero, the determinant of the coefficients must be zero, which means

$$\begin{vmatrix} \sinh \alpha l, & \sin \beta l \\ \alpha^2 \sinh \alpha l, & -\beta^2 \sin \beta l \end{vmatrix} = 0$$

or

$$(\sinh \alpha l)(\sin \beta l)(\alpha^2 + \beta^2) = 0$$

Since $\alpha^2 + \beta^2 \neq 0$ and $\sinh \alpha l \neq 0$, it follows that

$$\sin \beta l = 0, \text{ or } \beta = \frac{n\pi}{l}, \; n = 1, 2, 3, \ldots\ldots [13]$$

This is the frequency equation for a simply supported beam, and upon substituting the complete expression for β, Equation [7], into this equation, we find for the fundamental frequencies of torsional vibration

$$p_n = \frac{n\pi}{l^2}\sqrt{\frac{n^2\pi^2EC_w + l^2GC}{mI_p}} \quad \ldots\ldots [14]$$

Since $\sin \beta l = 0$, we find from Equation [11] or Equation [12] that $D_3 = 0$. Hence the normal function is

$$X = D_4 \sin \frac{n\pi x}{l} \quad \ldots\ldots [15]$$

The complete expression for the angle of twist ϕ is obtained by summing up the normal modes, so that

$$\phi = \sum_{n=1}^{\infty} \sin \frac{n\pi x}{l} (A_n \cos p_n t + B_n \sin p_n t)$$

in which A_n and B_n are determined by the initial conditions.

The importance of the warping rigidity on the frequency of torsional vibration can be determined by comparing the fundamental frequencies p_n given by Equation [14] with the frequency which would be obtained if the term involving C_w were omitted. Denoting by r_1 the ratio of the frequency of vibration with warping considered, Equation [14], to the frequency with warping neglected, we obtain

$$r_1 = \frac{p_n \text{ considering warping}}{p_n \text{ neglecting warping}} = \sqrt{\frac{n^2\pi^2}{k^2} + 1}$$

where

$$k = l\sqrt{\frac{GC}{EC_w}}$$

The parameter k is a dimensionless quantity which is constant for any given beam.

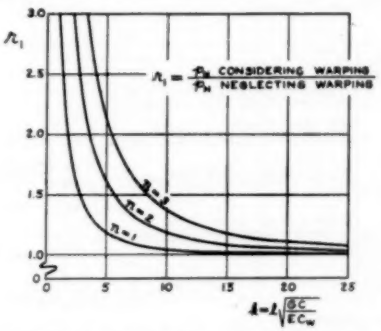

Fig. 2 Effect of Warping on Torsional Frequency—Simple Beam

Fig. 2 shows the variation of r_1 with k, for the first three modes of vibration. The effect of warping is to increase the frequency of vibration, since warping increases the stiffness of the bar against rotation. For small k, which means C_w is relatively large, the effect of warping is considerable and must be taken into account. For large k, which means C_w is relatively small, the warping effect is also small and may be neglected in many cases.

As an example, consider a standard wide-flange beam, 12WF 45, with a length of 20 ft, for which the value[5] of k (neglecting the effect of fillets) is about 4.0. From Fig. 2 we see that even for the first mode of vibration, the effect of warping is to increase the frequency about 27 per cent above the value obtained without warping.

Fixed-End Beam

In the case of a beam which is built-in rigidly at both ends, the boundary conditions are

$$\left.\begin{array}{ll} \text{BC 1 } X = 0 & \\ \text{BC 2 } \dfrac{dX}{dx} = 0 & \end{array}\right\} \text{at } x = 0 \qquad \left.\begin{array}{ll} \text{BC 3 } X = 0 & \\ \text{BC 4 } \dfrac{dX}{dx} = 0 & \end{array}\right\} \text{at } x = l$$

Applying these conditions to the general solution, Equation [8], we find from the first two boundary conditions

$$D_3 = -D_1, \quad D_4 = -D_2\frac{\alpha l}{\beta l} \quad \ldots\ldots [16]$$

Using these relations and BC 3 and BC 4, we obtain

$$\left.\begin{array}{l} D_1\beta(\cosh \alpha l - \cos \beta l) + D_2(\beta \sinh \alpha l - \alpha \sin \beta l) = 0 \\ D_1(\alpha \sinh \alpha l + \beta \sin \beta l) + D_2\alpha (\cosh \alpha l - \cos \beta l) = 0 \end{array}\right\} \quad [17]$$

Equating the determinant of the coefficients to zero, we obtain

[5] Formulas for determining C and C_w are given in the Appendix.

$$\begin{vmatrix} \beta(\cosh \alpha l - \cos \beta l), & \beta \sinh \alpha l - \alpha \sin \beta l \\ \alpha \sinh \alpha l + \beta \sin \beta l, & \alpha(\cosh \alpha l - \cos \beta l) \end{vmatrix} = 0$$

or

$$2(\alpha l)(\beta l)[1 - \cosh \alpha l \cos \beta l] + [(\alpha l)^2 - (\beta l)^2] \sinh \alpha l \sin \beta l = 0 \quad [18]$$

This is the frequency equation for a fixed-end beam. Because of the highly transcendental nature of the equation, solutions must be obtained by lengthy trial-and-error procedure. The solution of this equation for the first mode of vibration ($n = 1$) is plotted graphically in Fig. 3 for the curve labeled "Fixed Supports." Fig. 3 gives βl as a function of k, where $k = l\sqrt{(GC)/(EC_w)}$

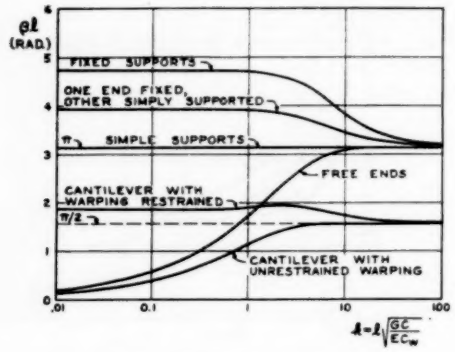

FIG. 3 VALUES OF βl—FIRST MODE ($n = 1$)

as defined previously. The procedure is to evaluate the dimensionless quantity k for any given beam, obtain βl (also dimensionless) from Fig. 3, and then compute αl from the relation

$$(\alpha l)^2 = k^2 + (\beta l)^2 \quad [19]$$

Having thus determined αl and βl, the ratios of the constants D_1, D_2, D_3, D_4 can be found from Equations [16] and [17]. The normal function X (giving the shape of the mode of vibration) is then determined completely except for an arbitrary amplitude. The mode shapes for a bar with fixed ends are shown in Fig. 5 for various values of k. In Fig. 5 the angle of rotation ϕ of any cross section is plotted as a function of distance along the beam, both co-ordinates being expressed in dimensionless ratios.

For small values of k, which means warping is relatively large, the mode shape is essentially a cosine curve with the axis shifted. As k increases, the mode shape approaches a sine curve as for the case of a simply supported bar. (In Fig. 5 the mode shape for values of k less than 1 or greater than 1000 are practically the same as for $k = 1$ and 1000, respectively.) In other words, as C_w approaches zero, k increases indefinitely, and a bar with fixed ends approaches a simply supported bar. This transition is also seen in Fig. 3 where the value of βl, which is essentially a solution of the frequency equation, approaches the case of simple supports as k increases.

It is interesting to note that whereas the angle of rotation ϕ for a bar with simple supports is the limiting case of a bar with fixed supports as k approaches infinity, this is not quite the case with regard to $\partial\phi/\partial x$. The discrepancy occurs at the ends of the bar, where $\partial\phi/\partial x$ is always zero for the fixed-end bar.

Fig. 6 is a graph of $\partial\phi/\partial x$ for a fixed-end beam, for increasing values of k. It is seen that as C_w approaches zero and k approaches infinity, the curve of $\partial\phi/\partial x$ approaches a cosine curve,

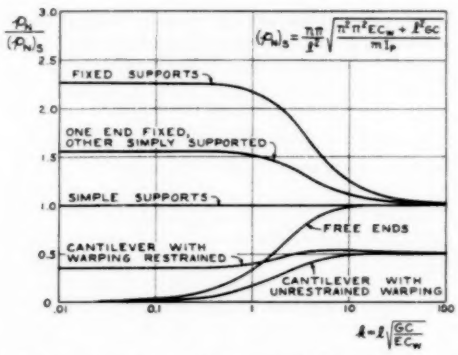

FIG. 4 VALUES OF $p_n/(p_n)_s$—FIRST MODE ($n = 1$)

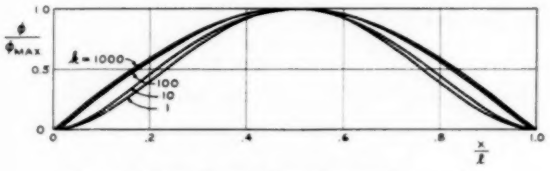

FIG. 5 MODE SHAPE—FIXED SUPPORTS ($n = 1$)

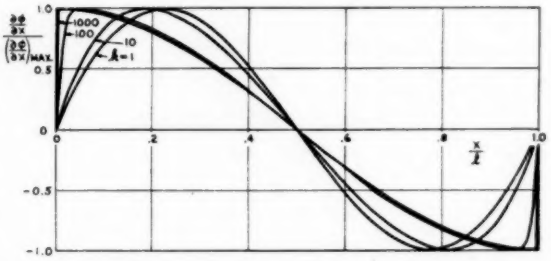

FIG. 6 GRAPH OF $(\partial\phi/\partial x)/(\partial\phi/\partial x)_{max}$—FIXED SUPPORTS ($n = 1$)

which is the case of simple supports, except at the end points where the value is always zero. This discontinuity arises because the curves for a fixed-end bar are solutions of a fourth-order differential equation, whereas the limiting case of $C_w = 0$ means that the differential equation becomes one of second order. This second-order equation is discussed later, where it is shown that for fixed supports the solution is the same as for simple supports. When the transition is made from the fourth-order to the second-order equation, a discontinuity arises in the derivative for which the boundary condition is lost, in this case $\partial\phi/\partial x$.

The frequency of vibration may be determined from the relation

$$(\alpha l)(\beta l) = p_n l^2 \sqrt{\frac{mI_p}{EC_w}} \quad [20]$$

It is more convenient, however, to express the frequency p_n by its ratio to the frequency of a simple beam of the same dimensions. The frequency of torsional vibration for a simple beam is readily obtained directly from Equation [14]. The ratio of the frequency for a fixed-end beam to the frequency of a simple beam is plotted in Fig. 4 for the curve labeled Fixed Supports.

Fig. 4 is drawn[6] for the first mode of vibration ($n = 1$) and shows that for low values of k, the warping restraint at the ends of the beam has a sizable effect on the frequency of vibration. For high values of k, which means relatively low values of C_w, the effect is very small and the frequency of a fixed-end beam approaches that of a simple beam.

Beam Fixed at One End, Simply Supported at the Other

With the end $x = 0$ taken as the simply supported end, and the end $x = l$ as the built-in end, the boundary conditions are

$$\left.\begin{aligned} &\text{BC 1 } X = 0 \\ &\text{BC 2 } \frac{d^2X}{dx^2} = 0 \end{aligned}\right\} \text{at } x = 0 \qquad \left.\begin{aligned} &\text{BC 3 } X = 0 \\ &\text{BC 4 } \frac{dX}{dx} = 0 \end{aligned}\right\} \text{at } x = l$$

From BC 1 and BC 2 we obtain $D_1 = D_3 = 0$ as for the case of a simple beam. From BC 3 and BC 4 we then obtain

$$\left.\begin{aligned} D_2 \sinh \alpha l + D_4 \sin \beta l &= 0 \\ D_2\, \alpha \cosh \alpha l + D_4\, \beta \cos \beta l &= 0 \end{aligned}\right\} \quad \ldots\ldots\ldots [21]$$

and the frequency equation is

$$\frac{\tanh \alpha l}{\alpha l} = \frac{\tan \beta l}{\beta l} \quad \ldots\ldots\ldots\ldots\ldots [22]$$

The solution of this frequency equation for βl is plotted in Fig. 3 for the first mode of vibration. When βl is thus determined, αl may be found by Equation [19], and then the ratio of the constants D_2 and D_4 found from either of Equations [21]. In this way the normal function X is determined. The ratio of the frequency p_n to the frequency of a simple beam $(p_n)_s$ is plotted in Fig. 4. For low values of k, the effect of warping is important, whereas for high values the bar approaches the case of a simple beam, both in mode shape and frequency.

Cantilever Beam With Warping Restrained

For a cantilever beam built-in rigidly at the end $x = 0$ so that warping is completely prevented, and with a free end at $x = l$, the boundary conditions are

$$\left.\begin{aligned} &\text{BC 1 } X = 0 \\ &\text{BC 2 } \frac{dX}{dx} = 0 \end{aligned}\right\} \text{at } x = 0$$

$$\left.\begin{aligned} &\text{BC 3 } \frac{d^2X}{dx^2} = 0 \\ &\text{BC 4 } \frac{GC}{EC_w}\frac{dX}{dx} - \frac{d^3X}{dx^3} = 0 \end{aligned}\right\} \text{at } x = l$$

From BC 1 and BC 2 we obtain

$$D_2 = -D_1, \quad D_4 = -D_2 \frac{\alpha l}{\beta l} \quad \ldots\ldots\ldots\ldots [23]$$

Using these relations and also Equation [19], we obtain from BC 3 and BC 4

$$\left.\begin{aligned} &D_1[(\alpha l)^2 \cosh \alpha l + (\beta l)^2 \cos \beta l] \\ &\quad + D_2[(\alpha l)^2 \sinh \alpha l + (\alpha l)(\beta l) \sin \beta l] = 0 \\ &D_1[(\beta l)^2 \sinh \alpha l - (\alpha l)(\beta l) \sin \beta l] \\ &\quad + D_2[(\beta l)^2 \cosh \alpha l + (\alpha l)^2 \cos \beta l] = 0 \end{aligned}\right\} \quad \ldots [24]$$

and the frequency equation is

$$\frac{(\alpha l)^4 + (\beta l)^4}{(\alpha l)^2(\beta l)^2} \cosh \alpha l \cos \beta l + \frac{(\alpha l)^2 - (\beta l)^2}{(\alpha l)(\beta l)} \sinh \alpha l \sin \beta l + 2 = 0 \quad \ldots [25]$$

Curves of βl and $p_n/(p_n)_s$ are given in Figs. 3 and 4, and mode shape in Fig. 7. In Fig. 7 the curves for values of k below 0.1 and

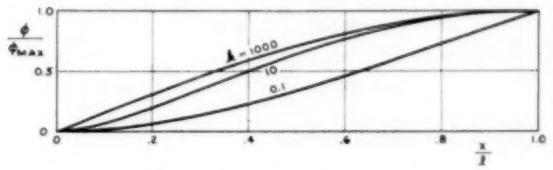

Fig. 7 Mode Shape—Cantilever With Warping Restrained ($n = 1$)

above 1000 do not vary appreciably from the curves for 0.1 and 1000, respectively. It is seen that as C_w approaches zero and hence k approaches infinity, the mode shape approaches one half of a sine wave which is the exact solution for $C_w = 0$, as shown later.

Cantilever Beam With Unrestrained Warping

In the previous case, a cantilever beam was considered in which the supported end was fixed and offered complete restraint against warping. A cantilever beam may also be supported in a manner such that warping is free to occur at the supported end. An example is a cantilever beam supported by the ordinary framing angles and moment resistant connections used in building construction. With regard to torsion, such a support offers restraint against rotation but not warping and hence is a simple support. It is, of course, a fixed support with regard to bending.

Thus, for a cantilever simply supported at one end and free at the other, the boundary conditions are

$$\left.\begin{aligned} &\text{BC 1 } X = 0 \\ &\text{BC 2 } \frac{d^2X}{dx^2} = 0 \end{aligned}\right\} \text{at } x = 0,$$

$$\left.\begin{aligned} &\text{BC 3 } \frac{d^2X}{dx^2} = 0 \\ &\text{BC 4 } \frac{GC}{EC_w}\frac{dX}{dx} - \frac{d^3X}{dx^3} = 0 \end{aligned}\right\} \text{at } x = l$$

Applying the first two conditions to Equation [8] we obtain

$$D_1 = D_3 = 0$$

From BC 3 and BC 4 and using Equation [19] we obtain

$$\left.\begin{aligned} D_2(\alpha l)^2 \sinh \alpha l - D_4(\beta l)^2 \sin \beta l &= 0 \\ D_2(\beta l) \cosh \alpha l - D_4(\alpha l) \cos \beta l &= 0 \end{aligned}\right\} \quad \ldots\ldots [26]$$

[6] Curves similar to Figs. 3 and 4, but drawn to a larger scale so that values of βl and $p_n/(p_n)_s$ may be determined accurately, are given in the reference cited in footnote 3. Similar curves for $n = 2$ and $n = 3$ also are presented. The use of these curves eliminates the laborious procedure of solving the frequency Equation [18] for each particular case.

Setting the determinant of the coefficients equal to zero, we obtain the frequency equation

$$(\alpha l)^3 \tanh \alpha l = (\beta l)^3 \tan \beta l \quad \ldots\ldots\ldots\ldots [27]$$

The results of solving this equation are shown in Figs. 3 and 4.

Beam With Free Ends

In the case of a bar which is free at both ends, the boundary conditions are

$$\left.\begin{aligned} &\text{BC 1} \quad \frac{d^2X}{dx^2} = 0 \\ &\text{BC 2} \quad \frac{GC}{EC_w}\frac{dX}{dx} - \frac{d^3X}{dx^3} = 0 \end{aligned}\right\} \text{ at } x = 0$$

$$\left.\begin{aligned} &\text{BC 3} \quad \frac{d^2X}{dx^2} = 0 \\ &\text{BC 4} \quad \frac{GC}{EC_w}\frac{dX}{dx} - \frac{d^3X}{dx^3} = 0 \end{aligned}\right\} \text{ at } x = l$$

From BC 1 and BC 2 we obtain

$$D_3 = D_1\frac{(\alpha l)^2}{(\beta l)^2}, \quad D_4 = D_2\frac{\beta l}{\alpha l} \quad \ldots\ldots\ldots\ldots [28]$$

From BC 3 and BC 4 and using Equations [19] and [28], we obtain

$$\left.\begin{aligned} &D_1(\alpha l)^3[\cosh \alpha l - \cos \beta l] \\ &\qquad + D_2[(\alpha l)^3 \sinh \alpha l - (\beta l)^3 \sin \beta l] = 0 \\ &D_1[(\beta l)^3 \sinh \alpha l + (\alpha l)^3 \sin \beta l] \\ &\qquad + D_2(\beta l)^3[\cosh \alpha l - \cos \beta l] = 0 \end{aligned}\right\} \ldots [29]$$

and the frequency equation becomes

$$[(\alpha l)^6 - (\beta l)^6] \sinh \alpha l \sin \beta l + 2(\alpha l)^3(\beta l)^3 [\cosh \alpha l \cos \beta l - 1] = 0 \ldots\ldots [30]$$

Solutions of this equation for $n = 1$ are plotted in Figs. 3 and 4 and the mode shapes are shown in Fig. 8. The curves for values of

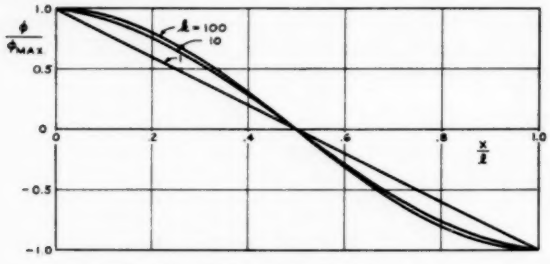

Fig. 8 Mode Shape—Free Ends ($n = 1$)

k less than 1 and larger than 100 are practically the same as the curves for 1 and 100, respectively. For very small values of k the mode shape is a straight line, and for large values of k, or C_w approaching zero, the shape approaches a cosine curve. This limiting case of $C_w = 0$ is derived in the next article.

Torsional Vibrations of Bars With $C_w = 0$

If a bar has a cross section such that $C_w = 0$, then the differential Equation [3] of free torsional vibrations becomes

$$\frac{\partial^2\phi}{\partial x^2} = \frac{mI_p}{GC}\frac{\partial^2\phi}{\partial t^2} \quad \ldots\ldots\ldots\ldots [31]$$

The expression for a normal mode of vibration is given by Equation [4] in which the normal function X is found to be

$$X = F_1 \cos p_n\sqrt{\frac{mI_p}{GC}}\,x + F_2 \sin p_n\sqrt{\frac{mI_p}{GC}}\,x \ldots\ldots [32]$$

By applying the boundary conditions at the ends of the beam, the ratio of the constants F_1 and F_2 and the frequency equation may be obtained.

The boundary conditions for torsion are somewhat simpler in this case than in the previous cases where C_w was not zero. Since C_w is zero, it follows[7] that $D - \omega_z = 0$, or, in other words, warping u and longitudinal stress σ_x are always zero (see Equations [9] and [10]). Thus it is impossible to provide end restraint against warping, and a fixed support becomes the same as a simple support, both providing restraint against rotation only ($\phi = 0$). For a free end, the only requirement is that the total torque be zero, since $\sigma_x = 0$ is automatically satisfied. From Equation [1] after substituting $C_w = 0$ and $M_t = 0$, we obtain $\partial\phi/\partial x = 0$ as the boundary condition for a free end.

For a simply supported beam, the boundary conditions are $X = 0$ at $x = 0$ and $x = l$. Applying these conditions to Equation [32], we obtain

$$F_1 = 0, \quad F_2 \sin p_n\sqrt{\frac{mI_p}{GC}}\,l = 0$$

so that

$$p_n\sqrt{\frac{mI_p}{GC}}\,l = n\pi, \quad n = 1, 2, 3 \ldots$$

Thus for a simply supported beam the frequency of vibration and the normal function are

$$p_n = \frac{n\pi}{l}\sqrt{\frac{GC}{mI_p}}, \quad X = F_2 \sin\frac{n\pi x}{l} \ldots\ldots [33]$$

These expressions are the same as Equations [14] and [15] if C_w is set equal to zero in those equations.

For a beam with fixed ends or a beam fixed at one end and simply supported at the other, the boundary conditions and hence the frequency and normal functions are the same as for a simple beam, Equation [33]. This result also can be obtained from the previous cases in which warping was taken into account, by considering the limiting case in which C_w approaches zero, or k approaches infinity. Figs. 3, 4, and 5 also show that these cases approach the simple beam case as k approaches infinity. The only exception, as previously discussed, is the discontinuity in $\partial\phi/\partial x$ at the ends of the bar. Thus, for the case when warping is considered, but for large values of k, Equations [33] can be used with considerable accuracy.

In the case of a cantilever beam with rotation prevented at the end $x = 0$, and the end $x = l$ a free end, the boundary conditions are $X = 0$ at $x = 0$, $dX/dx = 0$ at $x = l$. From these conditions we find the following expressions for the frequencies and normal modes of vibration

$$p_n = \frac{(2n-1)\pi}{2l}\sqrt{\frac{GC}{mI_p}}, \quad X = F_2 \sin\frac{(2n-1)\pi x}{2l} \ldots [34]$$

For a beam with free ends, the boundary conditions are $dX/dx = 0$ at $x = 0$ and $x = l$, from which it is found that

$$p_n = \frac{n\pi}{l}\sqrt{\frac{GC}{mI_p}}, \quad X = F_1 \cos\frac{n\pi x}{l} \ldots\ldots [35]$$

[7] See Timoshenko, footnote 4, p. 253.

Equations [34] and [35] also can be obtained by letting C_w approach zero in the previous cases where warping was considered. The frequencies and mode shapes given by Equations [34] and [35] are the limiting values obtained from Figs. 3 and 4 for the corresponding boundary conditions. Again, it is apparent that these simple expressions, derived for the case of $C_w = 0$, may be used with good accuracy if k is very large.

It is interesting to note that all these results for $C_w = 0$ also may be used for bars of solid circular cross section. It is only necessary to substitute for the torsion constant C its proper value for a circle, namely, I_p, the polar moment of inertia. Furthermore, for most solid sections, such as a square cross section, the effect of warping on the angle of twist ϕ is very small[8] if the cross sectional dimensions of the bar are small in comparison with its length. Hence an approximate expression for frequency and normal mode can be obtained from Equations [33], [34], or [35].

ACKNOWLEDGMENT

The author is indebted to Prof. Donovan H. Young, Stanford University, who offered advice and encouragement in the preparation of this paper.

[8] "Theory of Elasticity," by S. Timoshenko and J. N. Goodier, McGraw-Hill Book Company, Inc., New York, N. Y., second edition, 1951, p. 304.

Appendix

FORMULAS FOR TORSION CONSTANT C AND WARPING CONSTANT C_w

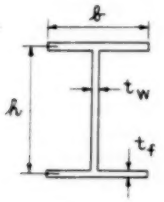

$$C = \frac{ht_w^3 + 2bt_f^3}{3}$$

$$C_w = \frac{t_f h^2 b^3}{24}$$

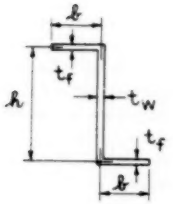

$$C = \frac{ht_w^3 + 2bt_f^3}{3}$$

$$C_w = \frac{t_f h^2 b^3}{12} \frac{2ht_w + bt_f}{ht_w + 2bt_f}$$

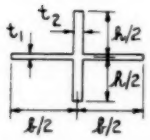

$$C = \frac{ht_2^3 + bt_1^3}{3}$$

$$C_w = 0$$

NOTE: Formulas for C_w for I and Z-sections were taken from H. N. Hill, "Torsion of Flanged Members With Cross Sections Restrained Against Warping," NACA Technical Note No. 888, 1943. Formulas for C were obtained by the formula $(1/3)\Sigma m_i t_i^3$, where m_i is the center line length and t_i is the thickness of a segment i of the cross section.

Wave Groups in the Flexural Motion of Beams Predicted by the Timoshenko Theory[1]

By R. A. ANDERSON,[2] PASADENA, CALIF.

Solutions are obtained for the wave-length distribution of the bending-moment and shear-force responses in an infinite beam to ① a concentrated transverse-force impulse; ② a concentrated bending-moment impulse. These solutions are determined with the aid of a recent classical solution (1)[3] for the flexural behavior of beams according to the Timoshenko theory. The results are used to predict the number and nature of the bending-moment and shear-force discontinuities propagating from disturbances of the type of 1 and 2.

Nomenclature

The following nomenclature is used in the paper:

y_b = lateral bending deflection
y_s = lateral shear deflection
x = index of position along beam
t = time
M = elastic bending moment
V = elastic shear force
w = arbitrary distributed transverse force
m_b = arbitrary distributed bending moment
Imp = concentrated transverse force impulse
Imp_m = concentrated bending-moment impulse
$c_1 = \sqrt{\frac{E}{\rho}}$
$c_2 = \sqrt{\frac{k'G}{\rho}}$
E = Young's modulus
G = shear modulus
k' = ratio of average shear stress to maximum shear stress over a cross section
l = length of beam
r = radius of gyration of cross section around principal axis
I = moment of inertia of cross section around principal axis
A = cross-section area
ρ = mass density
m = mass of beam
$\phi_n(x)$ = nth mode shape
$q_n(t)$ = nth generalized co-ordinate
M_n = nth generalized mass
$Q_n(t)$ = nth generalized force
ω_n = nth natural frequency
$u_n(t)$ = nth dynamic amplification factor
V = phase velocity
V_G = group velocity

Introduction

Previous papers which have discussed the Timoshenko theory of flexural beam motion (2) from a wave-group point of view have established the two sets of phase and group velocities predicted by the theory (3*a*, 3*b*, 3*c*). However, it appears that none of them has dealt quantitatively with the equally important wave-length distribution of the predicted response to a disturbance. Davies (4) discusses the wave-length distribution of the response subsequent to the relaxation of an infinitely intense deflection at a point in an infinite beam. His results cannot be considered the prediction of the Timoshenko theory since all the ensuing waves are required to travel at the lower set of phase and group velocities.

It is the purpose of this paper to determine the wave-length distribution of the bending-moment and shear-force responses for two basic cases as follows: ① a concentrated transverse-force impulse; ② a concentrated bending-moment impulse.

An infinite beam is considered since the propagation of waves from the disturbance without reflections is the topic of interest. The solutions for the wave-length distributions of the disturbances resulting from Cases ① and ② were determined from one of the recent classical solutions for the Timoshenko theory (1). The vibrations predicted by the classical solution can be converted easily to infinite trains of waves propagating in the two directions.

From the solutions obtained in the foregoing manner, the number and nature of the bending-moment and shear-force discontinuities propagating from the disturbances of Cases ① and ② were established. Recently an integral solution for the bending-moment response for Case ① due to Dengler and Goland has been evaluated numerically (5). It is noted that this solution does not agree entirely with the results of this paper.

Flexural Response of a Uniform Infinite Beam to Force and Moment Impulses

Consider the cases of ① a concentrated transverse-force impulse; ② a concentrated bending-moment impulse.

The solution for the flexural response of a finite beam to applied forces and moments is given in the Appendix. Utilizing the Appendix, the solutions for the shear-force and bending-moment responses for Cases ① and ② were obtained for a finite beam and then the beam was allowed to become infinitely long. In the limit, the series solutions assume integral form.

Since the point of interest is the propagation of elastic waves from a disturbance, the choice of end conditions is immaterial.

[1] The work reported here was supported by the U. S. Naval Ordnance Test Station as a supporting research program.

[2] Mechanical Engineer, U. S. Naval Ordnance Test Station.

[3] Numbers in parentheses refer to the Bibliography at the end of the paper.

Presented at the West Coast Conference of the Applied Mechanics Division, University of California, Berkeley, Calif., June 21–23, 1954, of The American Society of Mechanical Engineers.

Discussion of this paper should be addressed to the Secretary, ASME, 29 West 39th Street, New York, N. Y., and will be accepted until January 10, 1955, for publication at a later date. Discussion received after the closing date will be returned.

Note: Statements and opinions advanced in papers are to be understood as individual expressions of their authors and not those of the Society. Manuscript received by ASME Applied Mechanics Division, February 18, 1954. This paper was not preprinted.

For simplicity, pinned ends were chosen. In this simple case, each of the mode shapes is a single harmonic shape with nodes at the beam ends. The co-ordinate system was chosen as shown in Fig. 1 with the origin at the center of the beam and the x-axis

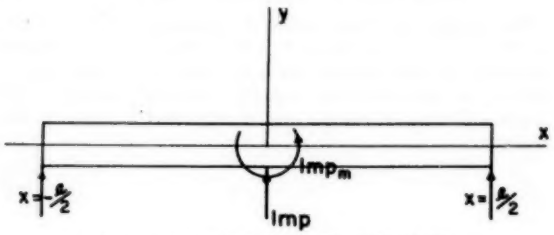

FIG. 1 FINITE PIN-ENDED BEAM PROBLEM

along the equilibrium position of the beam. The manner of application of the force and moment impulses to the beam is indicated in Fig. 1. The mode shapes are of the following form:

Odd modes

$$\phi_n^{(1)}(x),\ \phi_n^{(2)}(x),\ \psi_n^{(1)}(x),\ \psi_n^{(2)}(x) \sim \sin\frac{n\pi x}{l} \quad \ldots\ldots [1]$$

$n = 2, 4, 6, \ldots$.

Even modes

$$\phi_n^{(1)}(x),\ \phi_n^{(2)}(x),\ \psi_n^{(1)}(x),\ \psi_n^{(2)}(x) \sim \cos\frac{n\pi x}{l} \quad \ldots\ldots [2]$$

$n = 1, 3, 5, \ldots$.

① *Case of a Concentrated Force Impulse.* Utilizing the Appendix, the bending-moment and shear-force solutions for a finite beam for this simple case are, according to the Timoshenko theory

$$\frac{M(x,t)}{c_1\ \mathrm{Imp}} = \sqrt{2}\left(\frac{r}{l}\right)^2 \sum_{n=1,3,5\ldots}^{\infty} (n\pi)\left[\frac{\phi n^{(1)}(x)}{\cos\frac{n\pi x}{l}}\right]\left[\frac{m}{M_n^{(1)}}\right]\left[\frac{n\pi c_1}{\omega_n^{(1)} l}\right] \cos\frac{n\pi x}{l}\sin\omega_n^{(1)}t + \sqrt{2}\left(\frac{r}{l}\right)^2 \sum_{n=1,3,5\ldots}^{\infty} (n\pi)\left[\frac{\phi_n^{(2)}(x)}{\cos\frac{n\pi x}{l}}\right]\left[\frac{m}{M_n^{(2)}}\right]\left[\frac{n\pi c_1}{\omega_n^{(2)} l}\right]\cos\frac{n\pi x}{l}\sin\omega_n^{(2)}t \quad \ldots [3]$$

$$\frac{V(x_1 t)r}{c_1\ \mathrm{Imp}} = \sqrt{2}\left(\frac{r}{l}\right)\left(\frac{c_2}{c_1}\right)^2 \sum_{n=1,3,5\ldots}^{\infty}\left[\frac{\psi_n^{(1)}(x)}{\cos\frac{n\pi x}{l}}\right]\left[\frac{m}{M_n^{(1)}}\right]\left[\frac{n\pi c_1}{\omega_n^{(1)} l}\right] \sin\frac{n\pi x}{l}\sin\omega_n^{(1)}t + \sqrt{2}\left(\frac{r}{l}\right)\left(\frac{c_2}{c_1}\right)^2 \sum_{n=1,3,5\ldots}^{\infty}\left[\frac{\psi_n^{(2)}(x)}{\cos\frac{n\pi x}{l}}\right]\left[\frac{m}{M_n^{(2)}}\right]\left[\frac{n\pi c_1}{\omega_n^{(2)} l}\right]\sin\frac{n\pi x}{l}\sin\omega_n^{(2)}t \quad \ldots [4]$$

The wave length of the nth mode shape can be expressed as

$$\lambda_n = 2l/n \quad \ldots\ldots [5]$$

Furthermore $$\frac{1}{2l} = \frac{1}{\lambda_n} - \frac{1}{\lambda_{n-1}} = \Delta\left(\frac{1}{\lambda}\right) \quad \ldots\ldots [6]$$

Define a quantity $$k_n = 2\pi/\lambda_n = n\pi/l \quad \ldots\ldots [7]$$

Applying Equations [5], [6], and [7], Equations [3] and [4] be come

$$\frac{M(x_1 t)}{c_1\ \mathrm{Imp}} = \frac{\sqrt{2}}{\pi}\sum_{n=1,3,5\ldots}^{\infty} (k_n r)\Delta(k_n r)\left[\frac{\phi_n^{(1)}(x)}{\cos k_n x}\right]\left[\frac{m}{M_n^{(1)}}\right]\left[\frac{k_n c_1}{\omega_n^{(1)}}\right]\cos k_n x \sin\omega_n^{(1)}t + \frac{\sqrt{2}}{\pi}\sum_{n=1,3,5\ldots}^{\infty}(k_n r)\Delta(k_n r)\left[\frac{\phi_n^{(2)}(x)}{\cos k_n x}\right]\left[\frac{m}{M_n^{(2)}}\right]\left[\frac{k_n c_1}{\omega_n^{(2)}}\right]\cos k_n x \sin\omega_n^{(2)}t \quad \ldots [8]$$

$$\frac{V(x,t)r}{c_1\ \mathrm{Imp}} = \frac{\sqrt{2}}{\pi}\left(\frac{c_2}{c_1}\right)^2 \sum_{n=1,3,5\ldots,}^{\infty}\Delta(k_n r)\left[\frac{\psi_n^{(1)}(x)}{\cos k_n x}\right]\left[\frac{M}{M_n^{(1)}}\right]\left[\frac{k_n c_1}{\omega_n^{(1)}}\right]\sin k_n x \sin\omega_n^{(1)}t + \frac{\sqrt{2}}{\pi}\left(\frac{c_2}{c_1}\right)^2 \sum_{n=1,3,5\ldots}^{\infty}\Delta(k_n r)\left[\frac{\psi_n^{(2)}(x)}{\cos k_n x}\right]\left[\frac{m}{M_n^{(2)}}\right]\left[\frac{k_n c_1}{\omega_n^{(2)}}\right]\sin k_n x \sin\omega_n^{(2)}t \quad \ldots [9]$$

If $l \to \infty$, $\Delta(k_n r) \to dkr$ and the series becomes integrals

$$\left.\begin{aligned}\frac{M(x,t)}{c_1\ \mathrm{Imp}} &= \int_0^{\infty}[A_m^{(1)}(k)\sin\omega^{(1)}t + A_m^{(2)}(k)\sin\omega^{(2)}t]\cos kx\, d(kr)\\ A_m^{(1)}(k) &= \frac{\sqrt{2}}{\pi}(kr)\left[\frac{\phi^{(1)}(x)}{\cos kx}\right]\left[\frac{m}{M^{(1)}}\right]\left[\frac{kc_1}{\omega^{(1)}}\right]\\ A_m^{(2)}(k) &= \frac{\sqrt{2}}{\pi}(kr)\left[\frac{\phi^{(2)}(x)}{\cos kx}\right]\left[\frac{m}{M^{(1)}}\right]\left[\frac{kc_1}{\omega^{(2)}}\right]\end{aligned}\right\} \quad \ldots [10]$$

$$\left.\begin{aligned}\frac{V(x,t)r}{c_1\ \mathrm{Imp}} &= \int_0^{\infty}[A_v^{(1)}(k)\sin\omega^{(1)}t + A_v^{(2)}(k)\sin\omega^{(2)}t]\sin kx\, d(kr)\\ A_v^{(1)}(k) &= \frac{\sqrt{2}}{\pi}\left(\frac{c_2}{c_1}\right)^2\left[\frac{\psi^{(1)}(x)}{\cos kx}\right]\left[\frac{m}{M^{(1)}}\right]\left[\frac{kc_1}{\omega^{(1)}}\right]\\ A_v^{(2)}(k) &= \frac{\sqrt{2}}{\pi}\left(\frac{c_2}{c_1}\right)^2\left[\frac{\psi^{2}(x)}{\cos kx}\right]\left[\frac{m}{M^{(2)}}\right]\left[\frac{kc_1}{\omega^{(2)}}\right]\end{aligned}\right\} \quad \ldots [11]$$

The quantities in this solution have the form

$$\frac{\phi^{(1)}(x)}{\cos kx} = \frac{\sqrt{2}}{1 + (kr)^2\left(\frac{c_1}{c_2}\right)^2\left[1 - \left(\frac{\omega^{(1)}}{kc_1}\right)^2\right]} \quad \ldots\ldots [12]$$

$$\frac{\phi^{(2)}(x)}{\cos kx} = \frac{\sqrt{2}}{1 + (kr)^2\left(\frac{c_1}{c_2}\right)^2\left[1 - \left(\frac{\omega^{(2)}}{kc_1}\right)^2\right]} \quad \ldots\ldots [13]$$

$$\frac{\psi^{(1)}(x)}{\cos kx} = \frac{\sqrt{2}(kr)^2\left(\frac{c_1}{c_2}\right)^2\left[1 - \left(\frac{\omega^{(1)}}{kc_1}\right)^2\right]}{1 + (kr)^2\left(\frac{c_1}{c_2}\right)^2\left[1 - \left(\frac{\omega^{(1)}}{kc_1}\right)^2\right]} \quad \ldots\ldots [14]$$

$$\frac{\psi^{(2)}(x)}{\cos kx} = \frac{\sqrt{2}\,(kr)^2 \left(\frac{c_1}{c_2}\right)^2 \left[1 - \left(\frac{\omega^{(2)}}{kc_1}\right)^2\right]}{1 + (kr)^2 \left(\frac{c_1}{c_2}\right)^2 \left[1 - \left(\frac{\omega^{(2)}}{kc_1}\right)^2\right]} \quad \ldots [15]$$

$$\frac{M^{(1)}}{m} = 1 + \frac{(kr)^2}{\left\{1 + (kr)^2 \left(\frac{c_1}{c_2}\right)^2 \left[1 - \left(\frac{\omega^{(1)}}{kc_1}\right)^2\right]\right\}^2} \quad \ldots [16]$$

$$\frac{M^{(2)}}{m} = 1 + \frac{(kr)^2}{\left\{1 + (kr)^2 \left(\frac{c_1}{c_2}\right)^2 \left[1 - \left(\frac{\omega^{(2)}}{kc_1}\right)^2\right]\right\}^2} \quad \ldots [17]$$

$$\left(\frac{\omega^{(1)}}{kc_1}\right)^2 = \frac{1}{2}\left[1 + \left(\frac{c_2}{c_1}\right)^2 + \frac{1}{(kr)^2}\left(\frac{c_2}{c_1}\right)^2\right] - \sqrt{\frac{1}{4}\left[1 + \left(\frac{c_2}{c_1}\right)^2 + \frac{1}{(kr)^2}\left(\frac{c_2}{c_1}\right)^2\right]^2 - \left(\frac{c_2}{c_1}\right)^2} \quad \ldots [18]$$

$$\left(\frac{\omega^{(2)}}{kc_1}\right)^2 = \frac{1}{2}\left[1 + \left(\frac{c_2}{c_1}\right)^2 + \frac{1}{(kr)^2}\left(\frac{c_2}{c_1}\right)^2\right] + \sqrt{\frac{1}{4}\left[1 + \left(\frac{c_2}{c_1}\right)^2 + \frac{1}{(kr)^2}\left(\frac{c_2}{c_1}\right)^2\right]^2 - \left(\frac{c_2}{c_1}\right)^2} \quad \ldots [19]$$

Equations [10] through [19] are the desired solutions for the response of an infinite beam to a transverse-force impulse according to the Timoshenko theory.

② *Case of a Concentrated-Moment Impulse.* With the aid of the Appendix, and following the procedure for Case ①, the solutions for the bending-moment and shear-force responses of an infinite beam to a bending-moment impulse are, according to the Timoshenko theory

$$\left.\begin{aligned} \frac{M(x,t)r}{c_1 \operatorname{Imp}_m} &= \int_0^\infty [A_m^{(1)}(k) \sin \omega^{(1)}t + A_m^{(2)}(k) \sin \omega^{(2)}t] \sin kx\, d(kr) \\ A_m^{(1)}(k) &= \frac{1}{\pi}(kr)\left[\frac{\phi^{(1)}(x)}{\sin kx}\right]\left[\frac{m}{M^{(1)}}\right]\left[\frac{kc_1}{\omega^{(1)}}\right]\left[r\frac{d\phi^{(1)}(x)}{dx}\right]_{x=0} \\ A_m^{(2)}(k) &= \frac{1}{\pi}(kr)\left[\frac{\phi^{(2)}(x)}{\sin kx}\right]\left[\frac{m}{M^{(2)}}\right]\left[\frac{kc_1}{\omega^{(2)}}\right]\left[r\frac{d\phi^{(2)}(x)}{dx}\right]_{x=0} \end{aligned}\right\} \quad \ldots [20]$$

$$\left.\begin{aligned} \frac{V(x,t)r^2}{c_1 \operatorname{Imp}_m} &= \int_0^\infty [A_v^{(1)}(k) \sin \omega^{(1)}t + A_v^{(2)}(k) \sin \omega^{(2)}t] \cos kx\, d(kr) \\ A_v^{(1)}(k) &= \frac{1}{\pi}\left(\frac{c_2}{c_1}\right)^2\left[\frac{\psi^{(1)}(x)}{\sin kx}\right]\left[\frac{m}{M^{(1)}}\right]\left[\frac{kc_1}{\omega^{(1)}}\right]\left[r\frac{d\phi^{(1)}(x)}{dx}\right]_{x=0} \\ A_v^{(2)}(k) &= \frac{1}{\pi}\left(\frac{c_2}{c_1}\right)^2\left[\frac{\psi^{(2)}(x)}{\sin kx}\right]\left[\frac{m}{M^{(2)}}\right]\left[\frac{kc_1}{\omega^{(2)}}\right]\left[r\frac{d\phi^{(2)}(x)}{d\phi}\right]_{x=0} \end{aligned}\right\} \quad \ldots [21]$$

The quantities $\frac{\phi^{(1)}(x)}{\sin kx}$, $\frac{\phi^{(2)}(x)}{\sin kx}$, $\frac{\psi^{(1)}(x)}{\sin kx}$, and $\frac{\psi^{(2)}(x)}{\sin kx}$

have the same form as Equations [12] through [15]. The quantities $m/M^{(1)}$, $m/M^{(2)}$, $kc_1/\omega^{(1)}$, and $kc_1/\omega^{(2)}$ are given by Equations [16] through [19]. The remaining quantities in the solution are as follows

$$\left[r\frac{d\phi^{(1)}(x)}{dx}\right]_{x=0} = \frac{\sqrt{2}\,(kr)}{1 + (kr)^2\left(\frac{c_1}{c_2}\right)^2\left[1 - \left(\frac{\omega^{(1)}}{kc_1}\right)^2\right]} \quad \ldots [22]$$

$$\left[r\frac{d\phi^{(2)}(x)}{dx}\right]_{x=0} = \frac{\sqrt{2}\,(kr)}{1 + (kr)^2\left(\frac{c_1}{c_2}\right)^2\left[1 - \left(\frac{\omega^{(2)}}{kc_1}\right)^2\right]} \quad \ldots [23]$$

Application of Wave-Group Theory

The solutions for Cases ① and ②, Equations [10], [11], [20], and [21], can each be altered to a form describing a continuous spectrum of wave trains. Each of these wave trains has a velocity, termed the phase velocity, dependent on the wave length. The phase velocity can be expressed in terms of the frequency

$$V = \frac{1}{k}\,\omega \quad \ldots [24]$$

Consider the equations

$$\sin kx \sin kVt = \frac{1}{2}[-\cos k(x + Vt) + \cos k(x - Vt)] \quad \ldots [25]$$

$$\cos kx \sin kVt = \frac{1}{2}[\sin k(x + Vt) - \sin k(x - Vt)] \quad \ldots [26]$$

Utilizing Equations [25] and [26], the desired solutions for Cases ① and ② can be expressed as follows:

Case ① concentrated transverse-force impulse

$$\frac{M(x,t)}{c_1 \operatorname{Imp}} = \int_0^\infty \left\{\frac{A_m^{(1)}(k)}{2}[\sin k(x + V^{(1)}t) - \sin k(x - V^{(1)}t)] + \frac{A_m^{(2)}(k)}{2}[\sin k(x + V^{(2)}t) - \sin k(x - V^{(2)}t)]\right\} d(kr) \quad \ldots [27]$$

$$\frac{V(x,t)r}{c_1 \operatorname{Imp}} = \int_0^\infty \left\{\frac{A_v^{(1)}(k)}{2}[-\cos k(x + V^{(1)}t) + \cos k(x - V^{(1)}t)] + \frac{A_v^{(2)}(k)}{2}[-\cos k(x + V^{(2)}t) + \cos k(x - V^{(2)}t)]\right\} d(kr) \quad \ldots [28]$$

Case ② concentrated bending-moment impulse

$$\frac{M(x,t)r}{c_1 \operatorname{Imp}_m} = \int_0^\infty \left\{\frac{A_m^{(1)}(k)}{2}[-\cos k(x + V^{(1)}t) + \cos k(x - V^{(1)}t)] + \frac{A_m^{(2)}(k)}{2}[-\cos k(x + V^{(2)}t) + \cos k(x - V^{(2)}t)]\right\} d(kr) \quad [29]$$

$$\frac{V(x,t)r^2}{c_1 \operatorname{Imp}_m} = \int_0^\infty \left\{ \frac{A_v^{(1)}(k)}{2} [\sin k(x + V^{(1)}t) - \sin k(x - V^{(1)}t)] + \frac{A_v^{(2)}(k)}{2} [\sin k(x + V^{(2)}t) - \sin k(x - V^{(2)}t)] \right\} d(kr) \quad [30]$$

The functions $A_m^{(1)}(k)$, $A_m^{(2)}(k)$, $A_v^{(1)}(k)$, and $A_v^{(2)}(k)$ have been calculated for Cases ① and ② and plotted in Figs. 2 through 5. A value of $c_2/c_1 = 1/2$, corresponding to a beam of solid rectangular cross section, was chosen arbitrarily for the calculations.

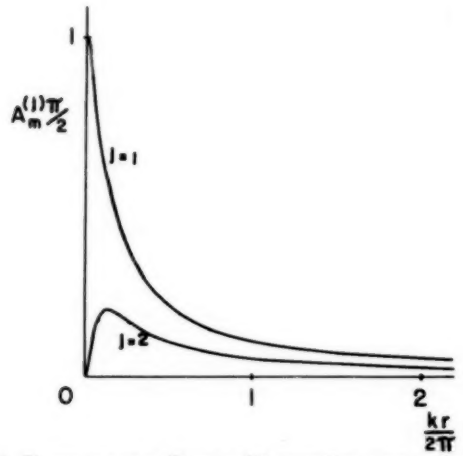

FIG. 2 DISTRIBUTION OF BENDING-MOMENT RESPONSE OF INFINITE BEAM TO TRANSVERSE CONCENTRATED IMPULSE, CASE ①

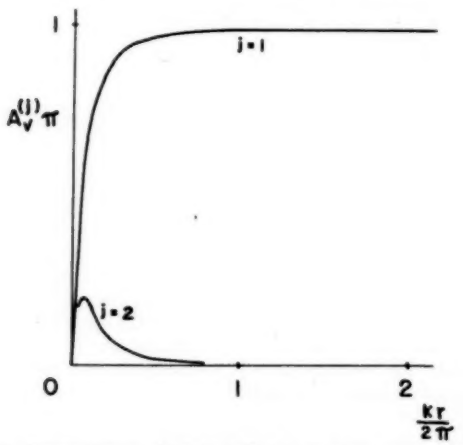

FIG. 3 DISTRIBUTION OF SHEAR-FORCE RESPONSE OF INFINITE BEAM TO TRANSVERSE CONCENTRATED IMPULSE, CASE ①

Although each train of waves travels with a phase velocity determined by its wave length, this does not reveal directly the velocity of propagation of a disturbance. In the wave-group theory, it is demonstrated that in a dispersive medium, packages of waves of nearly the same wave length travel with a velocity termed the "group" velocity, generally different from the phase velocity (6). The well-known expression for group velocity in terms of phase velocity is

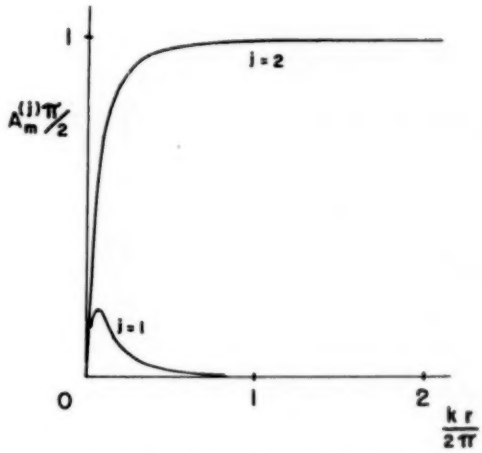

FIG. 4 DISTRIBUTION OF BENDING-MOMENT RESPONSE OF INFINITE BEAM TO CONCENTRATED MOMENT IMPULSE, CASE ②

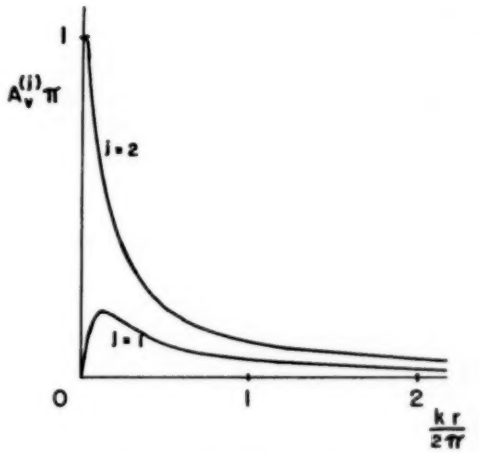

FIG. 5 DISTRIBUTION OF SHEAR-FORCE RESPONSE OF INFINITE BEAM TO CONCENTRATED MOMENT IMPULSE, CASE ②

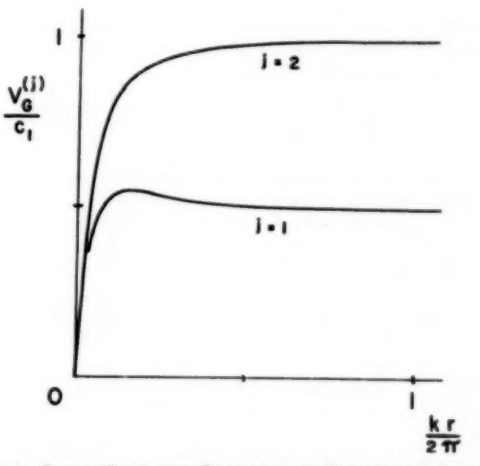

FIG. 6 GROUP VELOCITIES PREDICTED BY TIMOSHENKO THEORY

$$V_G = V - \frac{1}{kr}\frac{dV}{d\left(\frac{1}{kr}\right)} \quad \ldots\ldots [31]$$

The group velocities predicted by the Timoshenko theory were calculated for $c_2/c_1 = 1/2$ and are plotted in Fig. 6.

Discussion

A study of the wave-length distribution of the response shown in Figs. 2 through 5 reveals several interesting facts:

1 There is a reciprocal relationship existing between the wave-length distributions of the bending-moment and shear-force responses in Cases ① and ②. The roles of bending moment and shear force are interchanged in Cases ① and ②.

2 The importance of the two sets of velocities predicted by the Timoshenko theory is interchanged in Cases ① and ②. The importance of the second set of velocities in Case ② apparently has not been suspected. The second set of velocities generally has been ignored.

Further inferences can be drawn from an examination of the nature of the integrals in the solutions, Equations [27] through [30]. The presence of propagating discontinuities can be discerned from the departure from uniform convergence of the integrals (6). A study of the behavior of the part of the integral involving the shorter wave lengths will determine whether or not there is uniform convergence.

Consider Case ①. It can be established that the form of the functions involved in the solutions is, in the shorter wave lengths

$$A_m^{(1)}(k) = \frac{a_m^{(1)}}{kr} + \frac{b_m^{(1)}}{(kr)^3} + \ldots\ldots [32]$$

$$A_m^{(2)}(k) = \frac{a_m^{(2)}}{kr} + \frac{b_m^{(2)}}{(kr)^3} + \ldots\ldots [33]$$

$$A_v^{(1)}(k) = a_v^{(1)} + \frac{b_v^{(1)}}{(kr)^2} + \ldots\ldots [34]$$

$$A_v^{(2)}(k) = \frac{a_v^{(2)}}{(kr)^2} + \frac{b_v^{(2)}}{(kr)^4} + \ldots\ldots [35]$$

$$V^{(1)} = c_2 + \frac{v^{(1)}}{(kr)^2} + \ldots\ldots [36]$$

$$V^{(2)} = c_1 + \frac{v^{(2)}}{(kr)^2} + \ldots\ldots [37]$$

Consider first the propagation of the bending moment. The presence of a discontinuity in the first set of velocities can be observed by studying the integral

$$\int_0^\infty \frac{A_m^{(1)}(k)}{2} \sin k(x - V^{(1)}t)d(kr) \ldots\ldots [38]$$

If Equations [32] and [36] are utilized, the portion of the integral involving the shorter wave lengths becomes

$$\left.\begin{aligned} &\frac{a_m^{(1)}}{2}\int_a^\infty \left[\sin k(x - c_2t)\cos k\left(\frac{v^{(1)}t}{(kr)^2} + \ldots\right)\right. \\ &\qquad \left. - \cos k(x - c_2t)\sin k\left(\frac{v^{(1)}t}{(kr)^2} + \ldots\right)\right]\frac{d(kr)}{kr} \\ &+ \frac{b_m^{(1)}}{2}\int_a^\infty \left[\sin k(x - c_2t)\cos k\left(\frac{v^{(1)}t}{(kr)^2} + \ldots\right)\right. \\ &\qquad \left. - \cos k(x - c_2t)\sin k\left(\frac{v^{(1)}t}{(kr)^2} + \ldots\right)\right]\frac{d(kr)}{(kr)^3} \end{aligned}\right\} \ldots [39]$$

If $[v^{(1)}t]/(ar) \ll 1$, it can be shown that the first part of the first integral is uniformly convergent except at $x = c_2t$. The second part of the first integral and the entire second integral are uniformly convergent. With a simple transformation, $\sigma = k(x - c_2t)$, it can be seen that the first part of the first integral is the well-known complementary sine integral which has a discontinuity at $x = c_2t$. Similarly, the other integrals in the bending-moment solution can be studied. It is apparent that the bending moment in Case ① has two finite discontinuities traveling at velocities c_1 and c_2. Similarly, the shear force in Case ② has two finite discontinuities traveling at velocities c_1 and c_2. It should be noted in each case that the discontinuities at c_1 and c_2 are of opposite sign. It can be shown that the ratio of the amplitudes of the discontinuities in Case ① are indirectly proportional to the ratio of velocities c_1 and c_2 and in Case ② are directly proportional to the ratio of velocities c_1 and c_2. This is at variance with the results of Dengler and Goland (5) who for the bending moment in Case ① apparently found a relatively small discontinuity at the velocity c_1.

Consider next the propagation of shear force in Case ①. The integrals involving the second set of velocities are uniformly convergent. Hence there will be no discontinuities in the shear force in the second set of velocities. In order to detect a discontinuity in the first set of velocities, consider the integral

$$\int_0^\infty \frac{A_v^{(1)}(k)}{2} \cos k(x - V^{(1)}t)d(kr) \ldots\ldots [40]$$

If Equations [34] and [36] are utilized, the part of the integral involving the shorter wave lengths becomes

$$\left.\begin{aligned} &\frac{a_v^{(1)}}{2}\int_0^\infty \left[\cos k(x - c_2t)\cos k\left(\frac{v^{(1)}t}{(kr)^2} + \ldots\right)\right. \\ &\qquad \left. + \sin k(x - c_2t)\sin k\left(\frac{v^{(1)}t}{(kr)^2} + \ldots\right)\right]d(kr) \\ &+ \frac{b_v^{(1)}}{2}\int_0^\infty \left[\cos k(x - c_2t)\cos k\left(\frac{v^{(1)}t}{(kr)^2} + \ldots\right)\right. \\ &\qquad \left. + \sin k(x - c_2t)\sin k\left(\frac{v^{(1)}t}{(kr)^2} + \ldots\right)\right]\frac{d(kr)}{(kr)^2} + \ldots \end{aligned}\right\} \ldots [41]$$

If $[v^{(1)}t]/(ar) \ll 1$, it is evident that the second integral is uniformly convergent. The second part of the first integral is the sine-integral, having a finite discontinuity at $x = c_2t$. The first part of the first integral is divergent for all values of x and t. However, it can be recognized as the part involving the shorter wave lengths of the integral expansion of an infinitely intense disturbance at $x = c_2t$. It is apparent that the shear force in Case 1 has an infinite discontinuity propagating at velocity c_2. Similarly, the bending moment in Case 2 has an infinite discontinuity propagating at velocity c_1.

Conclusions

The propagation of elastic waves from a disturbance is considered for two types of disturbance as follows: ① a concentrated transverse-force impulse; ② a concentrated bending-moment impulse.

Conclusions reached are the following:

1 There is a reciprocal relationship existing between the wave-length distributions of the bending moment and shear force responses in Cases ① and ②. This is revealed in Figs. 2 through 5.

2 The importance of the two sets of velocities predicted by

the Timoshenko theory is interchanged in Cases ① and ②. This is revealed in Figs. 2 through 5. The importance of the second set of velocities in Case ② apparently has not been suspected.

3 Both the bending moment in Case ① and the shear force in Case ② have finite discontinuities propagating at velocities c_1 and c_2. The ratio of the amplitudes of the discontinuities in Case ① are indirectly proportional to the velocities and in Case ② are directly proportional to the velocities. This does not agree with the results of Dengler and Goland (5) who found a relatively smaller bending-moment discontinuity propagating at the velocity c_1 in Case ①.

4 The shear force in Case ① has an infinite discontinuity propagating at velocity c_2. The bending moment in Case ② has an infinite discontinuity propagating at velocity c_1.

Acknowledgment

Acknowledgment is made to the U. S. Naval Ordnance Test Station for permission to publish this paper.

Bibliography

1 "Flexural Vibrations in Uniform Beams According to the Timoshenko Theory," by R. A. Anderson, JOURNAL OF APPLIED MECHANICS, Trans. ASME, vol. 75, 1953, pp. 504–510.

2 "Vibration Problems in Engineering," by S. Timoshenko, D. Van Nostrand Company, Inc., New York, N. Y., 1937, p. 338.

3(*a*) "Elastic Waves and Vibrations of Thin Rods," by J. Prescott, *Philosophical Magazine*, series 7, vol. 33, 1942, p. 703.

3(*b*) "Die Ausbreitung von Biegungwellen in Stäben," by W. Flügge, *Zeitschrift für angewandte Mathematik und Mechanik*, vol. 22, December, 1942, pp. 312–318.

3(*c*) "Bemerkungen zur Ausbreitung von 'Biegewellen' in Stäben und Platten," by L. Cremer, *Zeitschrift für angewandte Mathematik und Mechanik*, vol. 23, October, 1943, p. 291.

4 "A Critical Study of the Hopkinson Pressure Bar," by R. M. Davies, Philosophical Transactions of the Royal Society of London, England, series A, vol. 240, 1948, pp. 375–457.

5 "Propagation of Elastic Impact Stresses," by M. Dengler, M. Goland, and P. Wickersham, ONR Progress Report No. 3, Project No. 709-E-327, October 30, 1952.

6 "The Propagation of Disturbances in Dispersive Media," by T. H. Havelock, Cambridge University Press, London, England, 1914.

Appendix

Solution for Flexural Motion of Uniform Beam According to Timoshenko Theory

According to the Timoshenko theory, the flexural vibrations in a uniform beam are described by the equations

$$EI\frac{\partial^2 y_b}{\partial x^2} + k'AG\frac{\partial y_s}{\partial x} - I_\rho\frac{\partial^3 y_b}{\partial x \partial t^2} = -m_b(x,t) \quad [42]$$

$$\rho A\left[\frac{\partial^2 y_b}{\partial t^2} + \frac{\partial^2 y_s}{\partial t^2}\right] - k'AG\frac{\partial^2 y_s}{\partial x^2} = w(x,t) \quad [43]$$

If the beam is conceived as horizontal, y_b, y_s, and $w(x,t)$ are positive in the up direction; $m_b(x,t)$ is positive in the counterclockwise direction. These equations permit bending and shear deflections, y_b and y_s. It is assumed that cross sections remain plane in bending and that bending slopes are small. The equations require that the beam be prismatic and that the force be applied in one of the principal planes.

The solution of these equations can be stated in the form (1)

$$y_b(x,t) = \sum_{n=1}^{\infty}\phi_n^{(1)}(x)q_n^{(1)}(t) + \sum_{n=1}^{\infty}\phi_n^{(2)}(x)q_n^{(2)}(t) \quad [44]$$

$$y_s(x,t) = \sum_{n=1}^{\infty}\psi_n^{(1)}(x)q_n^{(1)}(t) + \sum_{n=1}^{\infty}\psi_n^{(2)}(x)q_n^{(2)}(t) \quad [45]$$

The quantities $\phi_n^{(1)}(x)$, $\phi_n^{(2)}(x)$, $\psi_n^{(1)}(x)$, and $\psi_n^{(2)}(x)$ will be called the first and second sets of mode shapes in bending and shear. The quantities $q_n^{(1)}(t)$ and $q_n^{(2)}(t)$ will be called the first and second sets of generalized co-ordinates. Stating the solution in two series as before is somewhat arbitrary since all the terms could be included in one doubly infinite series. However, for the purposes of this paper, it is convenient to state the solution in two series.

The mode shapes have the form

$$\phi_n^{(1)}(x) = A_{bn}^{(\mathrm{I})}e^{\beta_n^{(\mathrm{I})}x} + B_{bn}^{(\mathrm{I})}e^{-\beta^{(\mathrm{I})}x} + A_{bn}^{(\mathrm{II})}e^{\beta_n^{(\mathrm{II})}x} + B_{bn}^{(\mathrm{II})}e^{-\beta_n^{(\mathrm{II})}x} \quad [46]$$

$$\phi_n^{(2)}(x) = A_{bn}^{(\mathrm{III})}e^{\beta_n^{(\mathrm{III})}x} + B_{bn}^{(\mathrm{III})}e^{-\beta_n^{(\mathrm{III})}x} + A_{bn}^{(\mathrm{IV})}e^{\beta_n^{(\mathrm{IV})}x} + B_{bn}^{(\mathrm{IV})}e^{-\beta_n^{(\mathrm{IV})}x} \quad [47]$$

$$\psi_n^{(1)}(x) = A_{sn}^{(\mathrm{I})}e^{\beta_n^{(\mathrm{I})}x} + B_{sn}^{(\mathrm{I})}e^{-\beta_n^{(\mathrm{I})}x} + A_{sn}^{(\mathrm{II})}e^{\beta_n^{(\mathrm{II})}x} + B_{sn}^{(\mathrm{II})}e^{-\beta_n^{(\mathrm{II})}x} \quad [48]$$

$$\psi_n^{(2)}(x) = A_{sn}^{(\mathrm{III})}e^{\beta_n^{(\mathrm{III})}x} + B_{sn}^{(\mathrm{III})}e^{-\beta_n^{(\mathrm{III})}x} + A_{sn}^{(\mathrm{IV})}e^{\beta_n^{(\mathrm{IV})}n} + B_{sn}^{(\mathrm{IV})}e^{-\beta_n^{(\mathrm{IV})}x} \quad [49]$$

It is usually convenient to normalize the mode shapes by the relations

$$\int_0^l [\phi_n^{(1)}(x) + \psi_n^{(1)}(x)]^2\,dx = l \quad [50]$$

$$\int_0^l [\phi_n^{(2)}(x) + \psi_n^{(2)}(x)]^2\,dx = l \quad [51]$$

The frequency equation in dimensionless terms is

$$\left[\frac{\omega_n l}{(\beta_n l)c_1}\right]^2 = -\frac{1}{2}\left[1 + \left(\frac{c_2}{c_1}\right)^2 - \frac{1}{(\beta_n l)^2}\left(\frac{l}{r}\right)^2\left(\frac{c_2}{c_1}\right)^2\right] \pm \sqrt{\frac{1}{4}\left[1 + \left(\frac{c_2}{c_1}\right)^2 - \frac{1}{(\beta_n l)^2}\left(\frac{l}{r}\right)^2\left(\frac{c_2}{c_1}\right)^2\right]^2 - \left(\frac{c^2}{c_1}\right)^2} \quad [52]$$

In general, two values of $(\beta_n l)^2$ correspond to every value of ω_n^2.

Define the generalized masses and forces as

$$M_n^{(1)} = \int_0^l \left\{\rho A[\phi_n^{(1)}(x) + \psi_n^{(1)}(x)]^2 + \rho I\left[\frac{d\phi_n^{(1)}(x)}{dx}\right]^2\right\} dx \quad [53]$$

$$M_n^{(2)} = \int_0^l \left\{\rho A[\phi_n^{(2)}(x) + \psi_n^{(2)}(x)]^2 + \rho I\left[\frac{d\phi_n^{(2)}(x)}{dx}\right]^2\right\} dx \quad [54]$$

$$Q_n^{(1)}(t) = \int_0^l \left\{w[\phi_n^{(1)}(x) + \psi_n^{(1)}(x)] + m_b\left[\frac{d\phi_n^{(1)}(x)}{dx}\right]\right\} dx \quad [55]$$

$$Q_n^{(2)}(t) = \int_0^l \left\{w[\phi_n^{(2)}(x) + \psi_n^{(2)}(x)] + m_b\left[\frac{d\phi_n^{(2)}(x)}{dx}\right]\right\} dx \quad [56]$$

Define the dynamic amplification factors as

$$u_n^{(1)}(t) = \omega_n^{(1)}\int_0^t \frac{Q_n^{(1)}(\tau)}{Q_{n\,\max}^{(1)}}\sin\omega_n^{(1)}(t-\tau)d\tau \quad [57]$$

$$u_n^{(2)}(t) = \omega_n^{(2)} \int_0^t \frac{Q_n^{(2)}(\tau)}{Q_n^{(2)}{}_{\max}} \sin \omega_n^{(2)}(t - \tau) d\tau \ldots . [58]$$

Then, by virtue of the orthogonality relation, the generalized coordinates have the form

$$q_n^{(1)}(t) = \frac{Q_n^{(1)}{}_{\max}}{M_n^{(1)}\omega_n^{(1)2}} \mu_n^{(1)}(t) \ldots\ldots\ldots\ldots [59]$$

$$q_n^{(2)}(t) = \frac{Q_n^{(2)}{}_{\max}}{M_n^{(2)}\omega_n^{(2)2}} u_n^{(2)}(t) \ldots\ldots\ldots\ldots [60]$$

The solutions for the bending moment and shear force are

$$M(x, t) = EI \frac{\partial^2 y_b}{\partial x^2} \ldots\ldots\ldots\ldots\ldots [61]$$

$$V(x, t) = k'AG \frac{\partial y_s}{\partial x} \ldots\ldots\ldots\ldots\ldots [62]$$

Fretting Corrosion[1] of Mild Steel in Air and in Nitrogen

By I-MING FENG[2] and HERBERT H. UHLIG,[3] CAMBRIDGE, MASS.

Data are presented on fretting corrosion of mild steel using weight loss as a measure of damage. Relative slip was measured both by use of stroboscopic light and strain gages. Load was applied pneumatically. Humidity of ambient air was found to be a sensitive variable requiring control, a fact first discovered through discrepancies of weight-loss data obtained in winter compared with those obtained in summer. Fretting corrosion of mild steel in moist air is only 55 to 65 per cent of the weight loss in dry air, depending on duration of test. Because of this large difference, all tests were carried out in dry air. At the same time, it was observed that fretting corrosion is appreciably greater below room temperature than above room temperature (up to 150 C). Weight losses of specimens fretted at 50 C are approximately 50 per cent losses at 0 C. Rate of fretting corrosion in air is found to be constant with time after an initial run-in period during which the rate is temporarily higher. In moist or dry nitrogen, weight losses are much less, although not zero. The greater the relative slip, the greater is fretting damage, and in complete absence of slip the data indicate that no weight loss occurs. Increased pressure or load is found to increase fretting damage. Weight loss is greater the lower the frequency for the same number of test cycles. The frequency effect increases with relative slip, and in nitrogen the frequency effect disappears.

Introduction

FRETTING corrosion is damage to a metal at the surface of contact with another metal or nonmetal, caused by relative slip. The damage is recognized by debris at the interface, which in the case of steel fretted in air is usually rust-colored, and may be accompanied by pitting. The pits often serve as stress raisers and may become nuclei of corrosion-fatigue cracks. Damage of this kind is a source of uncertainty in the operation of all machinery subject to vibration, not only because of increased susceptibility to failure by fatigue, but also because close tolerances are quickly destroyed and the corrosion debris may clog moving parts. Examples of fretting damage are frequently found in variable-pitch propellers, aircraft landing wheels, railroad tie plates, roller shafts in textile machinery, pins in gear trains, suspension springs, connecting rods, electrical contacts, and jewel bearings. Studies to reduce damage have been made using lubricants (1, 2, 3),[4] including molybdenum disulphide (4), by change in design so as to avoid slip, or by selection of materials (3, 5), but the underlying mechanism is still not known and present methods for mitigating damage are not always adequate. In this paper, fundamental studies are reported covering the factors important to fretting corrosion of mild steel. On the basis of these data a mechanism of damage is proposed, which is described in another paper. A better understanding of the mechanism, it is felt, should aid materially in advancing the present techniques for minimizing fretting damage.

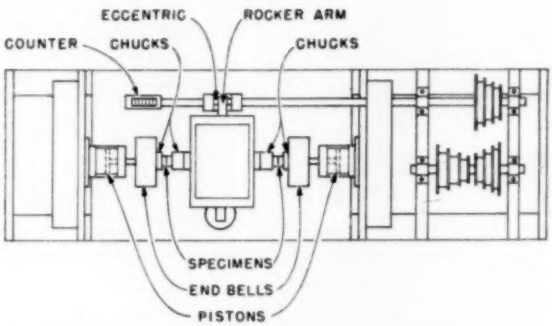

FIG. 1 SCHEMATIC PLAN OF FRETTING APPARATUS

Since quantitative data are needed to a clearer understanding of the mechanism, a machine was first designed and built to obtain reliable data of this kind. A sketch of the top view is provided in Fig. 1, further details of which have been described elsewhere (6).

Briefly, fretting corrosion was measured by weight loss of two mating cylindrical test specimens 1 in. diam and 1 in. long subject to defined oscillatory slip. The contacting cross-sectional surfaces of the test specimens were counterbored $^{7}/_{8}$-in. diam to a depth of $^{1}/_{16}$ in., with a resulting annular face equal to 0.184 sq in. on which fretting occurred. Load on this area of the specimens was applied pneumatically to a maximum pressure of 27,000 psi. Frequency of oscillation was variable between 56 and 3000 cycles per min (cpm), and relative slip was varied by means of an adjustable cam between 0 and 0.008 in. Slip was measured by two different methods. The first made use of a 40-power microscope comparator mounted on a micrometer screw which was focused on lines scribed with diamond at right angles to and across the interface of the two specimens, the latter, in turn, being illuminated by stroboscopic light at a frequency slightly different from the frequency of test. The scribed lines appeared to move slowly back and forth, making possible a measure of their extreme positions. The second method having better reproducibility made use of two strain gages mounted above and below a pointed flat spring-steel strip which pressed

[1] One of the authors, I-Ming Feng, is of the opinion that "fretting damage" or simply "fretting" would be a better name than "fretting corrosion."

[2] Department of Mechanical Engineering, Massachusetts Institute of Technology.

[3] Corrosion Laboratory, Department of Metallurgy, Massachusetts Institute of Technology.

Contributed by the Lubrication Activity Division in co-operation with the Applied Mechanics Division and presented at the Semi-Annual Meeting, Pittsburgh, Pa., June 20–24, 1954, of THE AMERICAN SOCIETY OF MECHANICAL ENGINEERS.

Discussion of this paper should be addressed to the Secretary, ASME, 29 West 39th Street, New York, N. Y., and will be accepted until January 10, 1955, for publication at a later date. Discussion received after the closing date will be returned.

NOTE: Statements and opinions advanced in papers are to be understood as individual expressions of their authors and not those of the Society. Manuscript received by ASME Headquarters, February 23, 1954. Paper No. 54—SA-6.

[4] Numbers in parentheses refer to the Bibliography at the end of the paper.

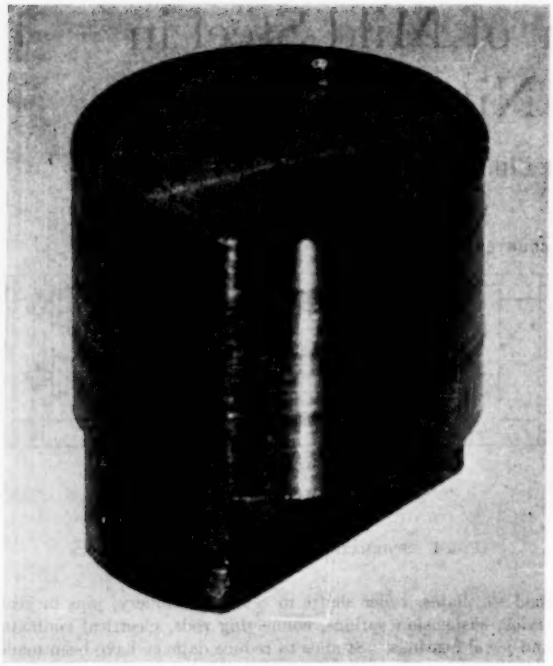

FIG. 2(*a*) TEST SPECIMEN

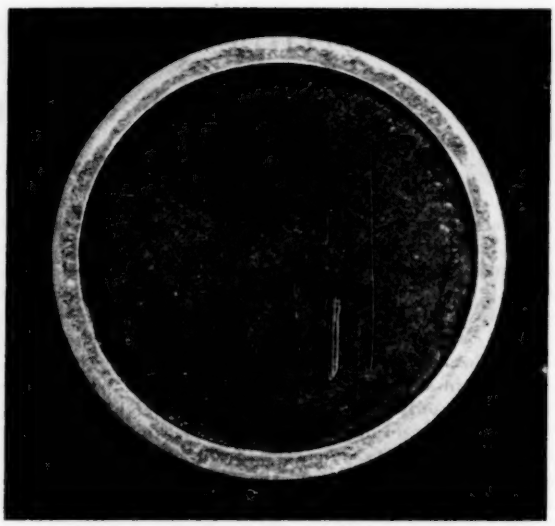

FIG. 2(*b*) TEST SPECIMEN

a, Side view. Top annular surface is tested in contact with similar surface of mating specimen.

b, Annular surface after fretting test in air, 67,800 cycles, 5300 psi, 540 cpm, 0.003-in. slip. Oxide removed by inhibited acid.

onto the surface of the moving specimen at right angles to its axis. The usual auxiliary strain-gage equipment properly calibrated was used to measure relative displacement of the steel strip.

The environment of the specimens was controlled by enclosing them with a split stainless-steel rectangular cell which was fitted with neoprene gaskets to insure a gastight seal. A glass window bolted and cemented to the top of the cell allowed measurement of slip when the stroboscopic technique was used as just described. For some measurements, especially those at high or low temperatures, the cell was redesigned so as to fit tightly to one of the specimens without use of a gasket, but with slight annular clearance around the mating specimen through which flowing gas could escape.

Specimens were degreased in boiling distilled benzene and weighed before testing. After testing, oxide was removed by pickling for 30 sec in 5 per cent sulphuric acid at 50 C (120 F) containing 0.1 weight per cent pickling inhibitor (quinolinethiodide). After pickling, the specimens were scrubbed with a stiff bristle brush in running water, rinsed in hot acetone and hot distilled benzene. Correction was made for loss of metal through pickling, amounting to 0.3 mg per specimen.

Measurements of fretting corrosion described herewith were all made using SAE 1018 cold finished steel, the certified mill analysis for which is the following: Carbon, 0.15 per cent; manganese, 0.75 per cent; phosphorus, 0.008 per cent; sulphur, 0.027 per cent. A check analysis of the carbon content gave 0.16 per cent.

The effect of various surface preparations (turning, grinding, No. 1 emery-paper polish, No. 0000 emery-paper polish, and annealing plus No. 1 emery-paper polish) was investigated, but no large differences were found. Hence abrasion by hand with No. 1 emery paper without annealing was chosen as standard procedure for all tests.

The physical appearance of a fretted 1018 steel specimen with corrosion products removed by pickling is shown in Fig. 2(*b*). Usually, in tests of sufficient duration, pitting occurred over most of the test area except for the rims at the extreme outer and inner diameters of the annular test surface. Even on the annealed specimens, the inner and outer rims showed residual bright metal, proving that the cold-worked inner and outer surfaces were not the cause. Perhaps the stress was less here than elsewhere, because the metal edges more easily deform. The visual damage appeared as shallow pits, with the deepest pits in 67,800-cycle tests, 5300-psi load, and 0.003 in. slip averaging about 0.007 in.

Numerous data were obtained in the early stages of the investigation before it was realized that atmospheric humidity is one of the important variables requiring control. The literature had not disclosed a large effect of humidity,[8] possibly because the effect was not expected and because previously reported experiments were predominantly qualitative. The importance of this factor was first indicated in our work by the disconcerting realization that weight-loss data obtained in winter were greater than similar data in summer to a degree far exceeding the experimental error. The discrepancy was opposite to that expected of normal atmospheric corrosion where attack is always more pronounced during periods of high humidity (summer). This made the cause less obvious, but the effect eventually was traced to differences in relative humidity varying from extremes of 5 per cent in winter to 100 per cent in summer.

Preliminary measurements at this time also showed that quantitative effects of temperature variation, particularly in the room-temperature range, are much larger than might have been

[8] Since the time this was written, a paper has appeared by Wright (7) emphasizing the importance of humidity to fretting corrosion of steel. He reports greater damage at 100 than at 50 per cent relative humidity, but also greater damage at 0 per cent than at 50 or 100 per cent relative humidity. We did not include results at 100 per cent RH because of extraneous rusting of the specimens caused by condensation of water.

anticipated. These facts made necessary a repetition of all earlier data but with humidity now precisely controlled, and temperature of the specimens either controlled or the weight-loss values corrected to room-temperature conditions.

Recorded weight losses reported herewith are the average of two mating specimens, except where temperature control of the specimens required that a thermocouple be attached to the stationary specimen, in which case only the moving specimen was weighed. In view of the large effect of humidity, tests usually were conducted in moving dry air, previously passed over anhydrous calcium sulphate contained in 1-in-diam tubes about 9 ft long. The relative humidity of air dried in this way measured 0 per cent, as indicated by an hygrometer at the exit end of the chamber surrounding the test specimens. Nitrogen, when used, was purified by passing through a liquid-air trap, then through 3 ft of copper turnings maintained at about 400 C, and finally through another liquid-air trap. Metal connections were used from purifier to cell in order to minimize contamination by oxygen and moisture such as otherwise would have occurred by diffusion through walls of rubber tubing.

Effect of Duration of Test

With variables of the test fixed, such as pressure, relative slip, and frequency of oscillation, weight losses of mild-steel specimens were determined for various times of test in both dry air and in purified nitrogen. Temperature recorded is the average achieved by the specimens (33 C) during test as determined by thermocouple readings of similar specimens near the interface in parallel tests. Data are reported in Fig. 3. The rate of metal loss is rapid at first, but after about 150,000 cycles of test, corresponding to a period of "run-in," the specimens reach a steady-state condition. Weight losses thereafter are linear with time, or the rate of metal loss is constant. Tests were carried out to a maximum of 1,250,000 cycles requiring about 39 hr.

In nitrogen, weight losses are much less, although not zero. At 200,000 cycles, for example, weight loss is $^1/_6$ that in air, and this fraction becomes less as the test is continued. The run-in period for nitrogen requires about 30,000 cycles compared with 150,000 cycles in air. Decrease of fretting damage in an inert atmosphere such as nitrogen or helium, or in vacuum, has been reported by several investigators (1, 8, 9, 10, 11, 12).

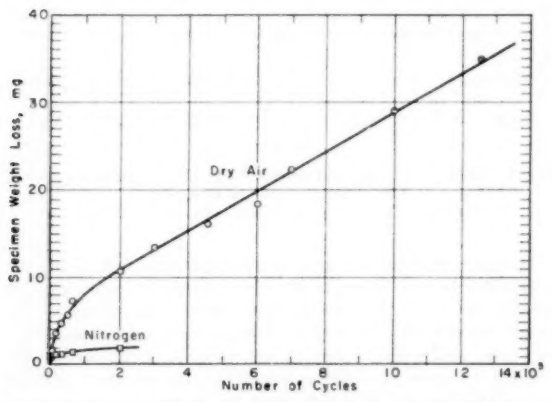

Fig. 3 Effect of Duration of Test on Fretting of Mild Steel in Dry Air and in Nitrogen

(Pressure, 5300 psi; frequency, 540 cpm; slip, 0.0036 in.; average temperature, 33 C.)

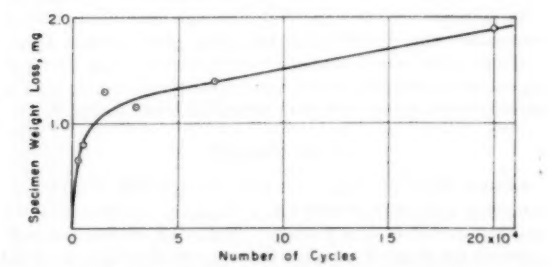

Fig. 3(a) Fretting of Mild Steel in Nitrogen

(Same data as Fig. 3, but enlarged.)

Effect of Humidity

Humidity was controlled by passing air through distilled water using submerged sintered-glass disks in order to produce a fine dispersion of gas bubbles. The flasks were submerged in a water thermostat maintained at a prescribed temperature to within 0.1 deg C. Humidity was recorded using a hygrometer manufactured by Serdex, Incorporated, located inside a gas-tight chamber at the exit system of the cell surrounding the test specimens. The hygrometer was checked at several humidities against a sling psychrometer. Although the entire range of relative humidity (RH) was possible, 100 per cent RH air was not used because rusting of the test specimens and subsequent error in weight-loss determinations occurred. Air of 90 per cent RH did not cause such rusting during the time of test and hence was the maximum extent to which air was humidified.

Data given in Fig. 4 are for two times of test—one at 67,800 cycles which brings the test short of the run-in period, and the other at 457,800 cycles, which is beyond run-in, and where weight losses of specimens become linear with number of cycles. Temperature of 33 C is the average value of the specimens near the interface throughout the test period. Values of relative humidity are based on room temperature equal to 27 C. The per cent effect of increased humidity on weight loss is appreciable and is about the same for both periods of test. At 100 per cent RH and 457,800 cycles fretting corrosion as measured by extrapolated weight loss is only 55 per cent the weight loss at 0 per cent RH, and is correspondingly 65 per cent at 67,800 cycles.

Fretting damage of mild steel in nitrogen, essentially saturated with water vapor, was found to be approximately the same as in dry nitrogen (Table 1). This fact indicates that moisture in air perhaps either decreases the abrasive properties of iron-oxide debris at the interface or alters the rate with which iron combines with oxygen (in the opposite direction to its effect in normal

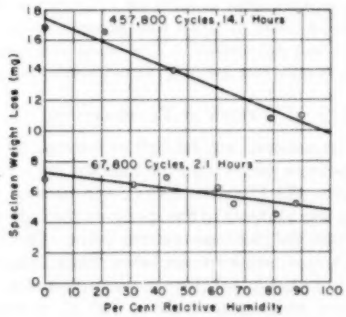

Fig. 4 Effect of Humidity on Fretting of Mild Steel for Two Test Periods in Air

(Pressure, 5300 psi; frequency, 540 cpm; slip, 0.0036 in.; average specimen temperature, 33 C; room temperature, 27 C.)

TABLE 1 EFFECT OF MOISTURE IN N_2 AND OF OXIDE AT THE INTERFACE ON FRETTING DAMAGE

Pressure, 5300 psi; slip, 0.0036 in. for air[a]

Atmosphere	Cycles/min	Total no. of cycles	Wt loss of clean spec vs clean spec, mg	Wt loss of clean spec vs oxide-coated spec, mg
Dry N_2	2000	67800	1.8	..
Moist N_2	2000	67800	1.6	..
Dry N_2	540	67800	1.4	..
Moist N_2	540	67800	2.0	..
Dry N_2	540	30000	1.2	1.3
Dry air	540	30000	4.7	4.9
Dry N_2	540	203400	1.9	1.0
Dry air	540	203400	10.7	11.4

[a] Cam displacement was same for N_2 measurements, but slip varied with number of cycles.

corrosion processes). In absence of oxygen or oxides, moisture apparently is not important.

In this connection, it was of interest to determine what effect, if any, is exercised by iron-oxide particles on fretting damage in nitrogen. Two specimens were run in dry air for about 600,000 cycles, thereby becoming covered uniformly with compacted iron oxide on the contacting surfaces. One of the specimens was then replaced by a clean specimen and the weight loss of the latter determined after 30,000 cycles, and also after 203,400 cycles. Results are listed in Table 1. For comparison, weight losses of a clean specimen run with a clean specimen are also included. The results show no certain effect of oxide, whether the specimens are run in air or in nitrogen.

Nature of Corrosion Products

Previous investigators have reported ferric oxide, αFe_2O_3, as the major component of the final debris when iron or mild steel is fretted (13, 14, 15, 16). Roll and Pulewka (17) using the Hanffstengel wear machine claimed that Fe_3O_4 also may be present depending on load and velocity of test. Fink and Hofmann (14) using the Amsler wear machine also found Fe_3O_4 in some tests. The latter authors together with Thum and Wunderlich (13) and Dies (18) reported presence of small amounts of metallic iron powder along with iron oxide. Dies reported 24 per cent ferrous oxide, FeO, as determined by chemical analysis for debris of soft iron fretted against hardened chromium steel, the remainder of the debris being 68.6 per cent Fe_2O_3 and 2.5 per cent Fe. Traces of metallic nitrides were reported by Cornelius and Bollenrath (15) and by Dies (18).

In present tests on mild steel, the major constituent of the dark-red debris, as determined by x ray,[6] was found to be αFe_2O_3. This was true for specimens run at room temperature and at —140 C and + 157 C. A small amount of metallic iron, less than perhaps 5 per cent by weight, accompanied the oxide obtained from specimens run at 5300 psi, 540 cpm, and 0.0036-in. slip. How much iron, if any, was present under other test conditions was not determined. The black powdered debris of specimens run in pure nitrogen proved to be entirely metallic iron.

Effect of Temperature

Effect of temperature was studied by heating or cooling the stationary specimen rather than the ambient air. For temperatures between —125 C and +100 C, one turn of $^3/_{16}$-in-diam copper tubing was soldered to the specimen through which liquid nitrogen was pumped (for temperatures below —50 C), or alcohol plus solid CO_2 (for temperatures below room temperature and above —50 C), or hot water (for temperatures below 100 C) was circulated. For temperatures above 100 C, a resistance-wire heating coil was wound around the specimen. The most difficult measurements were the long-time runs at low temperatures requiring large volumes of liquid nitrogen and constant manual adjustment.

Since heating or cooling one specimen of a pair produced a temperature gradient, the temperature near the interface was estimated for each condition of test. This was done in preliminary test runs maintaining conditions exactly as in regular runs. Thermocouples were soldered to each specimen near to and equidistant from the interface, and the test machine was then started. Generally, a thermocouple attached to the moving specimen gave a higher or lower reading than the stationary specimen thermocouple, depending on whether the stationary specimen was heated or cooled. The average was taken of the two temperature readings when steady-state temperature and fretting conditions were reached.

During actual runs for which weight losses were recorded, a thermocouple was attached to the stationary specimen only, the reading of which, combined with data from preliminary runs, gave the specimen temperature. Weight loss was then determined for the moving specimen alone.

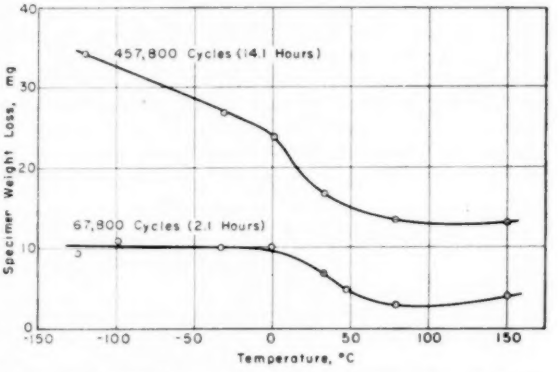

Fig. 5 Effect of Temperature on Fretting of Mild Steel for Two Test Periods in Dry Air

(Pressure, 5300 psi; frequency, 540 cpm; slip, 0.0036 in.)

Data are recorded in Fig. 5 for two periods of test, again corresponding to periods before and after run-in. Weight losses are greater the lower the temperature. Before the run-in period, weight losses at 50 C are only about 50 per cent or $^1/_2$ those at 0 C, and after the run-in, about 65 per cent. As temperatures fall below 0 C, fretting corrosion increases for long periods of test, but apparently remains relatively fixed for shorter periods. Above 50 C, and to a maximum of 150 C, the temperature coefficient of corrosion is relatively small. These data, of course, are all for unlubricated surfaces in dry air. The data may or may not correspond to observations on lubricated surfaces, where properties of the lubricant are also important, although qualitative effect of temperature should probably be the same. For example, Almen (1) found in the case of lubricated automotive bearings that fretting corrosion when it occurred was more severe in winter than in summer, which agrees with our conclusions based on Fig. 5.

Effect of Slip

Relative slip of specimens was varied from 0.0004 to 0.0091 in., employing a pressure of 5300 psi, a frequency of 540 cpm, and a total test period of 67,800 cycles. Values of relative slip were corrected for slight elastic loss between the fixed points of the transducer used to measure relative displacement. This amounted to 0.0003 in.

[6] Carried out by P. Rautala of the M.I.T. Department of Metallurgy

Whereas temperature corrections were not necessary for previous runs because the specimens were near room temperature or the temperature was controlled, corrections became of increasing importance to runs where load, slip, and frequency were increased. Temperature rise was appreciable for specimens oscillating at high frequencies or high values of slip or load, and the corresponding corrections made necessary by the higher temperatures are not small.

Ideally, a temperature-correction curve should be constructed for each condition of test. This would require considerable time, however, in view of the major effort compelled by the two temperature curves of Fig. 5 for a single set of conditions. Hence the compromise situation was to use data of Fig. 5 and assume that the effect of temperature for any condition of test was the same percentage based on weight loss. For example, the weight loss of a specimen fretted for 67,800 cycles at 5300 psi, 540 cpm, and 0.0036-in. slip is 7.8 mg at 25 C and 4.7 mg at 50 C. Correspondingly, if the temperature during a run achieved by a specimen fretted at a specified slip, load, and frequency happened to be 50 C, its weight loss was corrected by multiplying the observed value by 7.8/4.7. This order of correction is justified only in the absence of a better correction and was used in the expectation that it marks an improvement over no correction at all. However, recognizing the inherent limitations of the assumptions that are made, data recorded in the various figures include weight-loss values not temperature-corrected, as well as those corrected as described. It also should be mentioned that some scatter in the corrected results for similar test conditions comes about through variations in room temperature.

Preliminary tests were run to determine relationship of slip to average temperature rise of the specimens. A maximum temperature rise of 22 C for 0.0091-in. slip corresponded to a maximum correction in the order of 8 mg. Data are presented in Fig 6 showing that weight loss is a linear function of slip. This is true for all temperature-corrected values of weight loss, as well

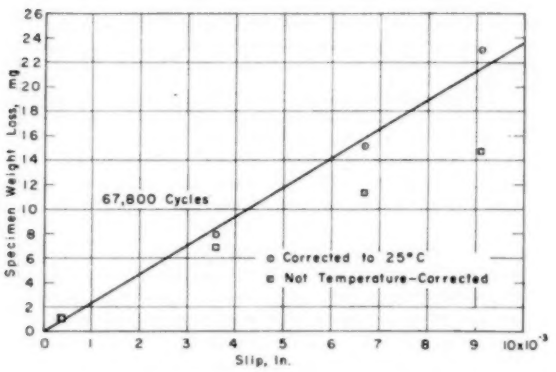

Fig. 6 Effect of Relative Slip on Fretting of Mild Steel in Dry Air
(Pressure, 5300 psi; frequency, 540 cpm.)

as for uncorrected values corresponding to the higher values of slip. The greater the amplitude of oscillatory motion, therefore, the greater is fretting corrosion. Furthermore, it appears from the extrapolated data that corrosion no longer occurs for zero slip.

Effect of Pressure

As pressure on the test specimens is increased without change of other factors, relative slip gradually decreases. Weight losses

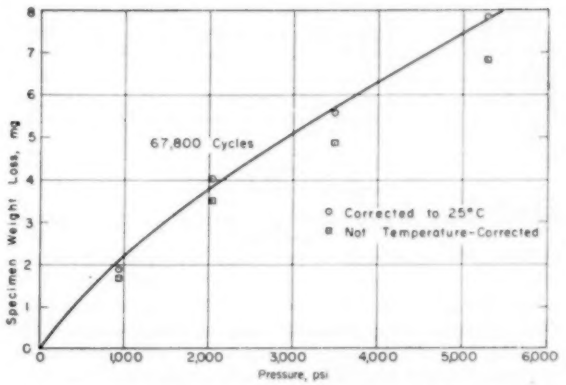

Fig. 7 Effect of Pressure (Load) on Fretting of Mild Steel in Dry Air
(Frequency, 540 cpm; slip, 0.0036 in.)

correspondingly increase at first, reach a maximum, and then decrease as more and more motion induced by the cam is taken up in elastic losses both in the machine and in the specimens. When the applied pressure is so high that relative slip of the specimens is reduced to zero, fretting corrosion also becomes nil.

It is of greater fundamental interest to know how fretting damage varies with applied pressure under conditions where the relative slip is maintained constant. This was done in a series of tests adjusting the cam after each change of pressure, so that slip was maintained at 0.0036 ± 0.0002 in. after appropriate corrections were made for elastic losses in the specimens between the fixed points of the transducer. Fig. 7 shows that weight loss increases with pressure up to the maximum pressure applied of 5300 psi.

Effect of Frequency

By means of a strain-gage transducer, relative slip between two mating specimens was found to be independent of frequency. This was checked at 5300 psi and 0.0036-in. slip.

Maximum temperature rise reached by test specimens increased appreciably with frequency, necessitating trial runs as described previously in order to establish temperature corrections. Highest value of temperature at 3000 cpm and 0.0036-in. slip, for example, was found to be 61 C. The corresponding correction re-

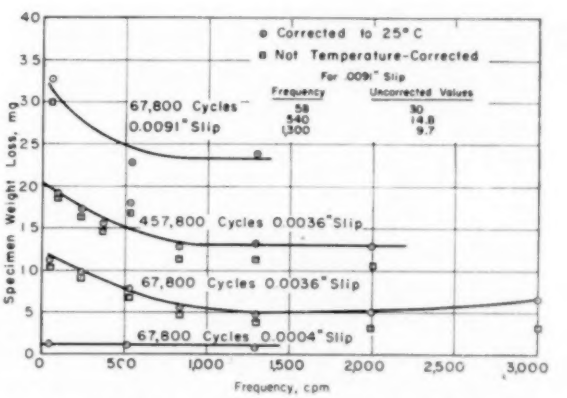

Fig. 8 Effect of Frequency on Fretting of Mild Steel in Dry Air
(Pressure 5300 psi.)

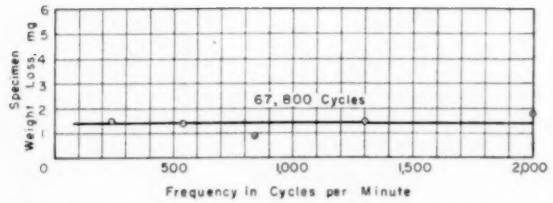

FIG. 9 EFFECT OF FREQUENCY ON FRETTING OF MILD STEEL IN NITROGEN

(Pressure, 5300 psi; slip adjusted to 0.0036 in. but was actually variable.)

quired adding 3.6 mg, or 112 per cent of the observed weight loss. Temperatures attained were still higher at 1300 cpm and 0.0091-in. slip (77 C) and the corresponding corrections greater. Great reliance, of course, cannot be placed on corrections of this order. At lower frequencies or lower values of slip, corrections were less as data of Fig. 8 show.

Temperature corrections tend to diminish the observed frequency effect of fretting corrosion, but the effect, nevertheless, remains sizable. Weight losses are definitely lower the higher the frequency for a given number of test cycles. It is also apparent that the greater the slip, the greater is the frequency effect, and for a very small value of applied slip (0.0004 in.), any applied frequency effect is within the experimental error. In nitrogen, the frequency effect also disappears, Fig. 9, even though a cam displacement of 0.08 in. was employed which produces a slip of 0.0036 in. in air, but variable slip in nitrogen. The data were not temperature-corrected.

ACKNOWLEDGMENT

The authors acknowledge helpful discussions with members of the joint Metallurgy-Mechanical Engineering Committee on Fretting Corrosion and, in particular, with M. Shaw and B. Rightmire. This investigation was supported by the National Advisory Committee for Aeronautics on contracts NAw-5789 and NAw-6128.

BIBLIOGRAPHY

1 "Lubricants and False Brinelling of Ball and Roller Bearings," by J. O. Almen, *Mechanical Engineering*, vol. 59, 1937, pp. 415–422.

2 "The Rusting of Steel Surfaces in Contact," by G. A. Tomlinson, Proceedings of the Royal Society of London, England, series A, vol. 115, 1927, pp. 472–483.

3 "Fretting Corrosion of Closely Fitting Surfaces," by S. Smith, G. Tomlinson, and R. Thurston, British Nat. Phys. Lab. Engr. Dept., June 25, 1941.

4 "Effectiveness of Molybdenum Disulfide as a Fretting-Corrosion Inhibitor," by D. Godfrey and E. E. Bisson, NACA Tech. Note 2180, September, 1950.

5 "An Investigation of the Fretting Corrosion of Closely Fitting Surfaces," by G. A. Tomlinson, P. L. Thorpe, and H. J. Gough, Proceedings of The Institution of Mechanical Engineers, vol. 141, 1939, pp. 223–237.

6 "Test Equipment for Evaluating Fretting Corrosion," by H. H. Uhlig, W. D. Tierney, and A. McClellan, Symposium on Fretting Corrosion, ASTM Tech. Publication No. 144, 1953.

7 "An Investigation of Fretting Corrosion," by K. H. R. Wright, The Institution of Mechanical Engineers, Great Britain, preprint, February, 1953.

8 "An Investigation of Fretting Corrosion Under Several Conditions of Oxidation," by B. W. Sakmann and B. G. Rightmire, NACA Tech. Note 1492, June, 1948.

9 "Wear Oxidation, a New Component of Wear," by M. Fink, Trans. American Society for Steel Treating, vol. 18, 1930, pp. 1026–1034.

10 "Consideration of the Various Phenomena of Metal Wear and Influence of Atmospheres on the Wear of Steel," by S. Saito and N. Yamamoto, Trans. Society of Mechanical Engineers, Japan, English abstract in Summary Sections, 5 pp. S88–90, original article, pp. I 76–89, 1939.

11 "Neue Ergebnisse auf dem Gebiet der Verschleissforschung," by M. Fink, *Organ für die Fortschritte des Eisenbahnwesens*, vol. 84, 1929, pp. 405–412.

12 "Die Erscheinung der Reiboxydation an Elektrolytkupfer," by M. Fink and U. Hofmann, *Zeitschrift für Metallkunde*, vol. 24, 1932, pp. 49–54.

13 "Die Reiboxydation an Festen Paarverbindungsstellen und ihre Bedeutung für den Dauerbruch," by A. Thum and F. Wunderlich, *Zeitschrift für Metallkunde*, vol. 27, 1935, pp. 277–280.

14 "Oxydation von Metallen unter dem Einfluss der Reibung," by M. Fink and U. Hofmann, *Zeitschrift für Anorganische und Allgemeine Chemie*, vol. 210, 1933, pp. 100–104.

15 "Einfluss von Einspannungen auf die Wechselfestigkeit von Unlegiertem Stahl," by H. Cornelius and F. Bollenrath, *Archiv für das Eisenhüttenwesen*, vol. 14, 1941, pp. 335–340.

16 "Investigation of Fretting Corrosion by Microscopic Observation," by D. Godfrey, NACA Tech. Note 2039, February, 1950.

17 "Beitrag zur Entstehung der Reiboxydation," by F. Roll and W. Pulewka, *Zeitschrift für Anorganische und Allgemeine Chemie*, vol. 221, 1934, pp. 177–181.

18 "Die Reiboxydation als Chemisch-Mechanischer Vorgang," by K. Dies, *Archiv für das Eisenhüttenwesen*, vol. 16, 1943, pp. 399–407.

Mechanism of Fretting Corrosion

By HERBERT H. UHLIG,[1] CAMBRIDGE, MASS.

A review of the facts suggests that the mechanism of fretting corrosion includes a chemical factor and a mechanical factor, with observed damage, in general, resulting from both. An asperity rubbing on a metal surface is considered to produce a track of clean metal which immediately oxidizes, or upon which gas rapidly adsorbs. The next asperity wipes off the oxide or initiates reaction of metal with adsorbed gas to form oxide. This is the so-called chemical factor of fretting. In addition, asperities dig below the surface to cause a certain amount of wear by welding or shearing action in which metal particles are dislodged. This is the mechanical factor of fretting. Metallic debris produced by fretting is thought not to oxidize spontaneously, as proposed by the molecular-attrition theory, but instead converts partially to iron oxide by secondary fretting action of particles rubbing against themselves or adjacent surfaces. This accounts for the fact that Fe_2O_3 is found by x ray to be the major corrosion product and metallic iron is present, if at all, in only very small amount. The quantitative expression for fretting corrosion derived on the basis of the foregoing model for relatively large values of load, frequency, and slip is

$$W\ (\text{total}) = (k_0 L^{1/3} - k_1 L)\frac{C}{f} + k_2 lLC$$

where W is the specimen weight loss, L is the load, C is the number of cycles, f is the frequency, l the slip, and k_0, k_1, and k_2 are constants. The first two terms are the chemical factor of fretting corrosion and the third term is the mechanical factor. Accordingly, the equation predicts that fretting-corrosion weight loss is a hyperbolic function of frequency, is parabolic with load and linear with number of cycles or magnitude of slip. Furthermore, the terms concerned with a frequency effect disappear when the chemical factor is suppressed, as is observed when fretting tests are conducted in nitrogen. These conclusions are confirmed by the reported data. In addition, the calculated reaction-rate constant for oxidation of a freshly formed iron surface obtained from fretting data is reasonable and falls between two independently observed values. In our experiments, the chemical or corrosion factor falls within 6 to 78 per cent of the total observed fretting damage, depending on conditions of test. Remedial measures are outlined in light of the data and the proposed mechanism.

[1] Corrosion Laboratory, Department of Metallurgy, Massachusetts Institute of Technology.

Contributed by the Lubrication Activity Division in co-operation with the Applied Mechanics Division and presented at the Semi-Annual Meeting, Pittsburgh, Pa., June 20–24, 1954, of The American Society of Mechanical Engineers.

Discussion of this paper should be addressed to the Secretary, ASME, 29 West 39th Street, New York, N. Y., and will be accepted until January 10, 1955, for publication at a later date. Discussion received after the closing date will be returned.

Note: Statements and opinions advanced in papers are to be understood as individual expressions of their authors and not those of the Society. Manuscript received by ASME Headquarters, February 23, 1954. Paper No. 54—SA-5.

Introduction

A SATISFACTORY theory of fretting corrosion should account for several facts (1)[2] among which are the following:

1 Fretting damage is reduced in vacuum or inert atmosphere.

2 Debris formed by fretting of iron is largely of the composition Fe_2O_3.

3 Greater damage occurs at low frequencies for a given number of cycles compared with high frequencies.

4 Metal loss increases with load and relative slip.

5 Greater damage occurs below room temperature compared with above room temperature.

6 Damage is greater in dry air than in moist air.

The fact that fretting corrosion involves a chemical process can hardly be doubted in view of the fact that a chemical-reaction product is formed. The process of fretting, therefore, is truly one of corrosion, a term defined as the chemical or electrochemical reaction of a metal with its environment (2). Although the terminology is reasonably clear, there is still ample room for discussion as to whether the observed chemical process accompanies or follows consumption of metal in fretting damage.

There are good reasons for believing that both situations occur in practice. The frequency effect of damage, for example, is plausibly explained as evidence of chemical reaction accompanying the fretting process, which proceeds as a function of time rather than of distance traveled during the oscillatory motion of the specimens. Accordingly, at high frequencies where time of fretting is short for a given number of oscillations, the over-all weight loss is less. On the other hand, evidence of mechanical wear comes from observed presence of iron particles in the debris. Also, photomicrographs, Fig. 1, of a fretted-specimen surface show unmistakable disturbance or cold-working of the surface, and, in some cases, there are areas where metal appears to

[2] Numbers in parentheses refer to the Bibliography at the end of the paper.

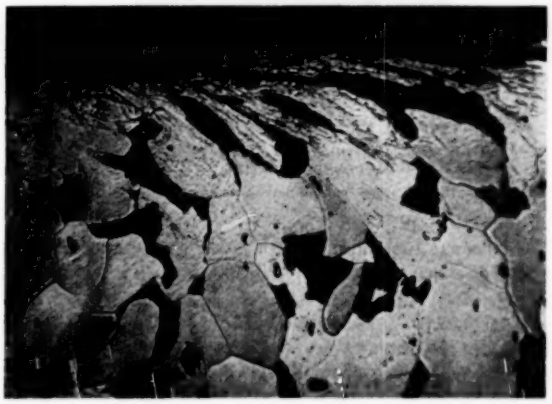

Fig. 1 Photomicrograph of Mild-Steel Surface Fretted in Air; ×500
(Pressure, 5300 psi; frequency, 1320 cpm; 0.0036-in. slip; 318,000 cycles.)

have seized and separated. Adhesion and rupture of asperities or shearing of roughened high spots is a logical source of metallic debris (3, 4). The fact that so little metallic debris is found is the result not of minor mechanical wear, but rather of conversion of metallic debris to oxide after removal of metal from the specimen surface.

It should be pointed out that typical pitting of fretted surfaces is not a result of electrochemical action such as occurs in aqueous media through operation of galvanic cells. The pits, instead, result from localized stress concentration at these areas through accumulation of oxide. Ferric oxide, Fe_2O_3, formed by fretting action, has a density of 5.12 compared with the density for iron of 7.86. This means that the oxide has greater volume than the iron from which it forms by a factor of 2.2. Therefore the metal-surface areas initially in contact and first fretted remain or become highly stress-loaded because the oxide of greater bulk than the metal tends to separate the two surfaces. Consequently, fretting corrosion is accentuated locally, in accord with data showing that damage increases with load, and the tendency is toward pitting attack rather than uniform surface wear. Fretting action thereafter between two moving surfaces is transmitted largely by compacted oxides retained in the pits. The forced separation of metal areas surrounding pits is observed in many of our test specimens, particularly before the run-in period. At these areas, marked by persistence of unattacked bright metal, original scratch lines formed during surface preparation of the specimen are still clearly seen under the microscope.

Theory of Fretting Corrosion

Facts assembled from the literature and from our test program suggest the following model for the mechanism of fretting corrosion: Assume a surface with n circular asperities or contact "points" per unit area of metal (or oxide) with average diameter c and an average distance s apart. In the fretting process, these asperities move over a plane metal surface at a linear velocity v, each asperity, in turn, plowing out a path and exposing clean metal, the area of which depends on the width of the asperity and length of travel. Behind each asperity on the track of clean metal, gas from the atmosphere will adsorb rapidly, or perhaps a thin layer of metal oxide will form. The next asperity will wipe off gas or oxide film as it traverses the path of the first asperity, and so on for all asperities, Fig. 2.

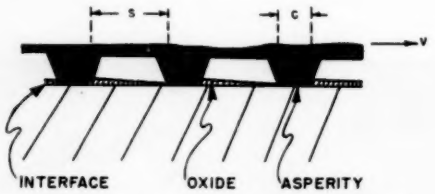

Fig. 2 Idealized Model of Fretting at a Metallic Surface
(Asperities of upper surface move over plane under surface.)

The average time during which either gas adsorbs or oxide forms is t. Then

$$t = \frac{s}{v} \quad [1]$$

The corresponding amount of oxide W removed by one asperity plowing out a path l long and c wide is dependent on the total oxidation of a clean iron surface of area cl in time t.

The empirical relation for the initial stages of oxidation of a metal is given by

$$W = clk \log_e \left(\frac{t}{\tau} + 1\right) \quad [2]$$

where τ and k are constants. This logarithmic oxidation-rate equation was first suggested by Tammann and Köster (5) as applying to oxidation of iron at low temperatures (252–385 C), as well as to oxidation of various other metals. The logarithmic equation has since been confirmed by other investigators for iron and other metals (6, 7, 8, 9, 10, 11) again for relatively low temperatures. Another relation holds when the oxide films that form are comparatively thick, but this is not the present situation.

The logarithmic equation was reported by Armbruster and Austin as applying to oxidation of iron at room temperatures (12) but after initial adsorption of oxygen on the surface too rapid to measure. Instead of oxidation, their data alternatively may represent the rate of chemisorption of oxygen on iron, where the first layer of molecules rapidly adsorbed is held by Van der Waals forces (physical adsorption), followed by less rapid conversion to dissociated atoms which become chemically bonded to the surface (chemisorption). The first layer of gas, in turn, as it becomes chemisorbed, encourages adsorption of additional gas less tightly bound. On this basis, mechanical energy of abrasion supplies the necessary activation energy immediately to convert the adsorbed gas film to a stoichiometric chemical compound of which oxide is one example. Conversion to oxide at room temperature is much slower in the absence of such an activation energy. This model for the metal surface is not essential to the present discussion, but is made here in order to include what seems to be a plausible detail of fretting action to be considered again later in an interpretation of the facts.

The final equation to be derived for rate of fretting corrosion is the same whether one assumes gas adsorption followed by formation of oxide through mechanical action, or rapid oxide formation wiped off by abrasion. Perhaps, in the general case both situations apply.

Substituting Equation [1] into Equation [2]

$$W = clk \log_e \left(\frac{s}{v\tau} + 1\right) \quad [3]$$

In the presently described fretting tests, motion of one annular ring specimen slipping with respect to a similar specimen is sinusoidal. Since $2l$ is the total length of travel in any one cycle, the linear displacement x from the mid-point of travel at time t is given by

$$x = \frac{l}{2} \cos \theta \quad [4]$$

and

$$\frac{dx}{dt} = v = -\frac{l}{2} \sin \theta \frac{d\theta}{dt} \quad [5]$$

If f represents constant linear frequency, this is related to constant angular velocity by the expression

$$\frac{d\theta}{dt} = 2\pi f \quad [6]$$

Therefore the average velocity is given by

$$\bar{V} = -\frac{\pi l f \int_0^\pi \sin \theta d\theta}{\pi} = 2lf \quad [7]$$

Hence, for n contacts or asperities per unit area of interface,

weight loss designated by W(corrosion) per single cycle caused solely by oxidation, in accord with Equation [3], is

$$W_{(\text{corrosion})} = 2\,nlck \log_e \left(\frac{s}{2lf\tau} + 1\right) \quad [8]$$

To this must be added mechanical loss of metal because each asperity, on the average, digs below the oxide layer (or adsorbed gas layer) and dissipates metal in amount proportional to the area of contact of the asperities and length of travel. The area of asperity is important now rather than width, because of the "tearing out" or welding action occurring during mechanical wear in contrast to scraping off of chemical products from the surface. A shearing off of asperities without welding also leads to wear dependent on total area of contact. For n circular asperities, weight loss per cycle is given by

$$W_{(\text{mechanical})} = 2k'n \left(\frac{c}{2}\right)^2 \pi l \quad [9]$$

But $n\pi(c/2)^2$, the total area of contact, is known to be equal to the load L divided by the yield pressure[3] p_m.

Hence

$$W_{(\text{mechanical})} = 2k' \frac{lL}{p_m} = k_2 lL \quad [10]$$

where k_2 is a constant equal to $2k'/p_m$.

The total wear or metal loss per cycle is the sum of the oxidation, or corrosion term, and the mechanical term

$$W_{(\text{total})} = W_{(\text{corrosion})} + W_{(\text{mechanical})} \quad [11]$$

Returning to Equation [8], the logarithmic term can be expanded according to the relation

$$\log_e (x + 1) = x - \frac{x^2}{2} + \frac{x^3}{3} - \ldots$$

where x is equal to $s/(2lf\tau)$. When the latter expression is much smaller than unity, the square and higher terms can be omitted. This condition applies particularly to high load (small values of s), high frequency f, and large value of slip l. The constant τ for oxidation of iron or adsorption of oxygen on iron has not been determined empirically with great precision, nor has its theoretical significance as yet been made clear. The value equals 0.06 sec for all of Tammann's data on iron (5) and is variable, but in the order of 3 sec for Winterbottom's data (11) and variable, but in the order of 60 sec for some of Armbruster and Austin's data (12).

In our experiments f is approximately 10 cps and l is about 0.01 cm. The average distance between asperities at 5000 psi after the run-in period approaches perhaps 10^{-2} to 10^{-3} cm. The quantity $\frac{s}{2lf\tau}$ therefore is approximated by

$$\frac{10^{-4}}{2 \times 0.01 \times 10 \times 0.06} = 0.008$$

Therefore, whenever experimental conditions are such that higher terms of the logarithmic expansion can be neglected

$$W_{(\text{corrosion})} = \frac{2nlcks}{2lf\tau} = \frac{ncks}{f\tau} \quad [12]$$

This expression, it will be noted, is equivalent to assuming, from the very start, a linear rate of oxidation or of gas adsorption on clean iron where k/τ is the reaction-rate constant. The linear rate reasonably approximates the actual state of affairs considering the short times of adsorption or oxidation with which we are dealing.

[3] Reference (3), p. 2.

From the fact that the number of asperities along one edge of unit area is equal to $\sqrt{n}$, it follows that $s + c$ is approximated by $1/\sqrt{n}$. Also, recalling that $n\pi(c/2)^2 = \frac{L}{p_m}$

$$W_{(\text{corrosion})} = \frac{k_0 L^{1/2}}{f} - \frac{k_1 L}{f} \quad [13]$$

where

$$k_0 = \frac{2}{\sqrt{p_m \pi}} \frac{k}{\tau} \quad \text{and} \quad k_1 = \frac{4}{p_m \pi} \frac{k}{\tau}$$

Combining Equations [10], [11], and [13], we have the final expression for fretting as measured by weight loss corresponding to a total of C-cycles

$$W_{(\text{total})} = (k_0 L^{1/2} - k_1 L) \frac{C}{f} + k_2 lLC \quad [14]$$

Note that this final equation is made up of the first two terms representing chemical reaction or corrosion, and the third term representing mechanical wear. According to this relation, total weight loss is as follows:

1 Linear with total number of cycles. This is in accord with our observations, the linear steady state being reached after a run-in period.

2 Parabolic with applied load L. This trend is also indicated by our data.

3 Hyperbolic with frequency f. Fig. 8 of reference (1) confirms this prediction except for small values of slip. Lack of frequency effect for small applied slip is explained later.

The first two terms of Equation [14] show that the corrosion factor of fretting damage:

1 Is predominant at low frequencies, but is overshadowed by mechanical wear at high frequencies.

2 Is a function of total time of test regardless of frequency, since C/f is equivalent to total time.

3 Becomes zero when $n\pi(c/2)^2$, the actual area of contact, approaches maximum area of the interface (or $s = 0$ and $1/\sqrt{n} = c$). This occurs at a load L equal to $\pi p_m/4$.

4 Is independent of total slip l, whereas the mechanical term increases linearly with slip. As l approaches zero, the term

$$2nlck \log \left(\frac{s}{2lf\tau} + 1\right)$$

approaches zero and, therefore, W_{total} also approaches zero. Zero fretting damage in absence of slip has been established by previous investigators and also by our own data.

The foregoing conclusions are in essential agreement with the experimental results.

Chemical and Mechanical Contribution to Fretting Damage

Equation [14] makes possible, furthermore, a correlation of all the reported data and an evaluation of how much fretting damage can be attributed to corrosion or chemical reaction, and how much to mechanical wear. This necessitates evaluation of the constants k_0, k_1, and k_2. An examination of weight loss versus pressure (Fig. 7 of reference 1) shows that the following equation satisfactorily describes the empirical curve

$$W = 0.038L^{1/2} + 0.0009L \quad [15]$$

TABLE 1 EFFECT OF LOAD AND FREQUENCY ON FRETTING DAMAGE OF MILD STEEL; TOTAL TEST OF 67,800 CYCLES

Pressure (Load), psi	Frequency, cps		Specimen weight loss, milligrams: Observed, Corrected	Observed, Uncorrected	Calculated, Total	Calculated, Chem. term	Calculated, Mech. term	Chem. wear, per cent	Mech. wear, per cent
500	540/60	0.0036	1.3	1.0	1.3	0.79	0.51	61	39
1000	540/60	0.0036	2.2	1.8	2.1	1.1	1.0	52	48
2000	540/60	0.0036	3.8	3.4	3.5	1.5	2.0	43	57
5000	540/60	0.0036	7.5	6.6	7.2	2.1	5.1	29	71
5300	56/60	0.0036	11.3	10.3	26.2	20.8	5.4	48	52
5300	238/60	0.0036	9.8	9.1	10.3	4.9	5.4	29	71
5300	540/60	0.0036	7.9	6.8	7.6	2.2	5.4	21	79
5300	840/60	0.0036	5.7	4.9	6.8	1.4	5.4	14	86
5300	1300/60	0.0036	5.0	4.0	6.3	0.9	5.4	10	90
5300	2000/60	0.0036	5.3	3.3	6.0	0.58	5.4	7	93
5300	3000/60	0.0036	6.6	3.2	5.8	0.4	5.4		
5300	56/60	0.0091	32.7	30.0	34.4	20.8	13.6	61	39
5300	540/60	0.0091	23.0	14.8	15.8	2.2	13.6	14	86
5300	1300/60	0.0091	24.2	9.7	14.5	0.9	13.6	6	94
5300	540/60	0.0004	1.1	1.1	2.8	2.2	0.6	78	22
5300	540/60	0.0036	7.9	6.8	7.6	2.2	5.4	29	71
5300	540/60	0.0067	15.1	11.3	12.2	2.2	10.0	18	82
5300	540/60	0.0091	23.0	14.7	15.8	2.2	13.6	14	86

Since the data are for 67,800 cycles, a frequency of 540/60 cps, and a slip of 0.0036 in., Equation [14] becomes

$$W = 7540k_0L^{1/2} + (244k_2 - 7540k_1)L \quad \ldots\ldots [16]$$

Therefore, comparing Equation [15] with [16]

$$k_0 = \frac{0.038}{7540} = 5.05 \times 10^{-6}$$

k_1 can be evaluated from k_0 employing the relation

$$k_1 = \frac{2}{\sqrt{p_m \pi}} k_0$$

where p_m, the yield pressure, is approximated by 3 times the elastic limit[4] or for mild steel equals 100 kg/mm² or 140,000 psi.

Substituting this value into the foregoing equation

$$k_1 = 1.51 + 10^{-6}$$

Finally, k_2 can be evaluated knowing k_0 and k_1 and is equal to 4.16×10^{-6}. This gives as the final expression for fretting weight loss

$$W = (5.05 \times 10^{-6}L^{1/2} - 1.51 \times 10^{-6}L)\frac{C}{f} + 4.16 \times 10^{-6} lLC \quad \ldots\ldots [17]$$

where W is in milligrams per specimen (0.184 sq in. [1.19 sq cm] surface), L is in psi, f in cps, C in cycles, and l in in.

How well this equation describes the weight-loss data for tests with variation of load (pressure), slip, and frequency can be judged by referring to Table 1. Agreement, by and large, is good.

At 56/60 cps and 0.0036-in. slip, deviation of calculated from observed value can be explained on the basis that the approximate expansion of the logarithmic term in Equation [3] no longer holds. The rate of oxide formation is not as great, in other words, as is calculated from the linear rate constant obtained from higher frequency data. It seems that deviations from the linear oxidation rate appear below 238 cpm as shown by Fig. 3, where weight losses plotted with reciprocal frequency are otherwise in good accord with predictions of Equation [14]. By increasing the slip 2.5 times from 0.0036 to 0.0091 in., thereby decreasing the value of the term $s/(2lf\tau)$ within the logarithm, agreement between calculated and observed weight loss at 56/60 cps is better (34.4 versus 32.7 mg).

Whenever increased specimen surface temperatures are generated through use of high frequencies or large values of slip or both, correspondence between theory and observation is obscured by the uncertain correction for the temperature effect. It is significant, nevertheless, that calculated values, by and large, fall between the corrected and uncorrected observed values. When test conditions are such that surface temperatures are high, the calculated values seem to agree better with uncorrected values, suggesting that the approximate temperature corrections that were used are much too large in these instances.

A frequency effect of weight loss is calculated by Equation [17] to exist for 0.0004-in. slip; however, Fig. 8 of reference (1) shows that essentially no frequency effect is found for this value of slip. The mechanical wear term is calculated to be 0.6 mg and the chemical wear term 2.2 mg. The observed weight loss value of 1.1 mg, therefore, is in between these two values and suggests that a high-frequency oscillation may have been superimposed on the applied frequency. If this extraneous frequency were constant regardless of applied frequency, the sought-for frequency effect would be masked. This consideration implies that vibration of the test machine, which despite all efforts was not entirely eliminated, interfered with weight-loss values for this low value of slip. Vibration tests confirmed that extraneous motion actually may reach a maximum of 0.0004 in. The frequency data for the lowest value of slip, therefore, are not inconsistent with the theory, but apply instead to an unspecified range of high frequencies.

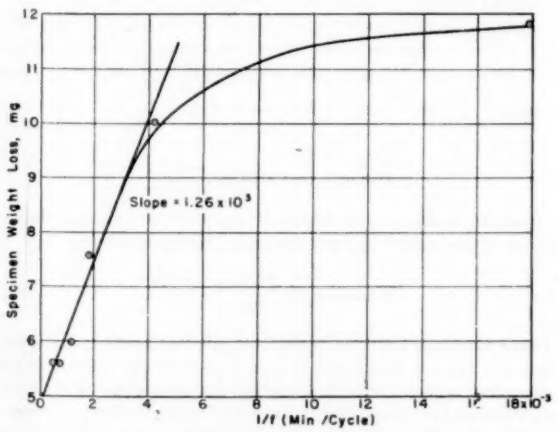

FIG. 3 DEPENDENCE OF SPECIMEN WEIGHT LOSS ON RECIPROCAL FREQUENCY
(Pressure, 5300 psi; slip, 0.0036 in.; 67,800 cycles.)

[4] Reference (3), pp. 19, 20.

The percentage of fretting damage attributable to corrosion and that part represented by mechanical wear, calculated using Equation [17], are included in Table 1. It will be noted that the chemical factor of fretting damage predominates for small values of load, slip, and frequency, but is only a small percentage of the total effect at high frequencies.

These calculations bear out Fink's statement (13) that mechanical wear predominates over chemical wear as slip increases, and that high rate of wear in nitrogen reported by Rosenberg and Jordan (14) using the Amsler wear machine, contrary to his findings, is explained in part by the larger slip employed by them.

In view of the fact that the mechanical factor at 540/60 cps, 5300 psi, and 0.0036-in. slip is relatively large (71 per cent) a significant question can be raised concerning the much smaller percentage of metallic iron actually found in debris for specimens fretted under these particular test conditions. The obvious answer is that iron particles worn off the moving surfaces are later oxidized by secondary fretting action of one particle rubbing against another or against the metal surface. Action of this kind reduces the amount of metallic iron in the debris and produces more of the same composition oxide as forms in the primary process. It seems less likely that iron particles dislodged from the metal surface should be oxidized spontaneously on contact with air as is suggested by Tomlinson (15). For one thing, the particles are probably much larger than the atomic dimensions he suggested, since the mechanism of wear appears to emphasize fracture of macroscopic asperities, rather than the tangential plucking out of atomic-size metal fragments.

Dies (16), for example, reported that the size of fretting-debris particles is about 1 micron (10^{-4} cm or about 10,000 atom diam). Furthermore, fretting debris consisting entirely of metallic-iron powder obtained from test specimens run in nitrogen displayed no observable tendency to oxidize spontaneously on exposure to air. In view of the reduced tendency of iron to oxidize at subzero temperatures, the fact that fretting action at these same low temperatures still produces predominantly an oxide debris (1, 17) is further evidence that spontaneous oxidation is not likely.

Godfrey (18) reported a change in color of iron debris from black in the center of fretting action to red at the outer rim, which he explained as spontaneous oxidation of black iron particles to red Fe_2O_3. If the change of color is truly one of continuous oxidation and not caused by change in particle size, hydration, or ratio of Fe to O in the oxide, any one of which may influence color, the observed effect can be explained by secondary fretting action as just discussed.

The weight losses of test specimens run in nitrogen are no longer frequency dependent, Fig. 9 of reference (1). The theory successfully predicts this situation because the chemical factor of fretting no longer exists, and all weight losses are accounted for by the mechanical term alone. It is noted from Equation [14] that the mechanical contribution to wear does not include a frequency factor.

Explanation is required for the fact that weight losses in nitrogen as observed are lower than corresponding calculated values of the mechanical contribution to fretting corrosion. For example, the calculated mechanical term for specimens in air at 5300 psi, 540/60 cps, 0.0036-in. slip, and 67,800 cycles is 5.4 mg, whereas the corresponding weight loss in nitrogen is 1.4 mg. This difference is explained by favorable conditions for metal transfer from one metal surface to another when test specimens are run in an inert atmosphere. In air, metal transfer occurs infrequently or not at all, because the final, if not the initial, debris is predominantly oxide rather than metal. Such metal particles as are formed become rapidly covered with oxygen or oxide, reducing the probability of their subsequent rewelding or fusing to one of the metallic surfaces. Weight-loss measurements of specimens, of course, do not include amounts of metal transferred; therefore, in nitrogen, weight losses invariably are lower than the calculated mechanical term in air, where dislodged metal particles may be lost permanently to either specimen surface.

Aluminum and stainless steels are especially damaged by fretting action, not only because hard oxide-debris particles form having the composition Al_2O_3 and Cr_2O_3, but also because the metals themselves inherently may oxidize or adsorb oxygen particularly rapidly on exposure to air. This suggests that the chemical factor of fretting damage may be more important for these metals than for metals having less affinity for oxygen. By the same reasoning, damage to noble metals must be largely or entirely mechanical.

Effect of Temperature and Humidity

Data show that fretting corrosion is greater at low than at high temperatures, Fig. 5 of reference (1), although oxidation of metals in air, on the other hand, almost always increases with temperature. One can assume, therefore, that (*a*) the mechanical factor is much greater at low temperatures, overshadowing the chemical term, or (*b*) the reaction-rate constant k/τ is greater at low temperatures despite a decreased oxidation tendency. If the latter is correct, k/τ may refer to rate of adsorption of gases on the metal surface rather than to oxidation rate, implying that the rate of adsorption of gases at low temperatures may be greater than at high temperatures.

In order to distinguish between these possibilities, further experimental data are needed. For example, data obtained at several temperatures for a variety of frequencies, slips, and loads would help evaluate the temperature coefficient of the mechanical factor as distinct from the chemical factor.[5]

Increased damage at low temperatures makes less likely any assumption that fretting occurs solely by oxidation of metal by reason of high local temperatures induced by friction. This assumption also was denied by Fink (17) who ran steel specimens in the Amsler wear machine in presence of liquid air, observing, nevertheless, rapid formation of an oxide debris. In addition, were this assumption correct, it would seem that fretting debris for steel should be mostly of mill-scale composition comparable to the high-temperature iron oxide Fe_3O_4. None of this oxide, however, was found in our tests. Wright (20) found that steel was fretted to a high degree by polymethacrylate resin melting at 80 C (176 F) and pointed out that local temperatures above the melting point would have melted the asperities and reduced frictional damage. He concluded that surface thermal effects do not affect the oxidation reactions seriously. Further evidence along the same lines comes from less observed fretting damage at high frequencies under conditions where highest interface temperatures are expected and found.

Because fretting corrosion is less in high-humidity air than in dry air, the view is supported that moisture (*a*) decreases abrasive wear of the oxide debris or (*b*) decreases rate of adsorption or of chemical reaction of oxygen with iron. Experiments in which humidified pure nitrogen was substituted for dry nitrogen showed no accelerating effect of moisture on weight loss (1). Hence water itself presumably will not react with iron in absence of oxygen,

[5] One can assume with Fink and Hofmann (19) that "lockerstellen," or chemically active surface sites, produced by mechanical disturbance of the surface, and which oxidize as rapidly as they are formed, increase in number as the temperature is lowered. Certainly, the rate of recovery of disarrayed or cold-worked metal is suppressed at low temperatures, in agreement with this premise. But were this the entire mechanism, one would expect that, for a given number of cycles, the number of active sites produced would always be the same. In other words, a frequency effect would not be expected, contrary to what is found.

even though mechanical activation energy is supplied. This fact lends support to possibility (*a*) where water is considered perhaps to hydrate the debris and thereby reduce abrasive wear. On the other hand, adsorbed water also can be considered to form a film of lubricant between the contacting surfaces,[6] which is either a hydrodynamic or a boundary film, over which asperities can move without mechanically activating the reaction between adsorbed oxygen and metal. The first assumption ascribes most of the effect to the mechanical factor of fretting damage, whereas the second possibility leans on the chemical factor. Again, more data are needed to differentiate clearly one factor from the other.

Calculation of Reaction Rate Constant for Iron

The coefficients k_0 and k_1 of Equation [14] contain the reaction rate constant k/τ for oxidation of iron, or for adsorption of oxygen on iron, whichever predominates in the fretting process. The reaction rate constant can be obtained from the value k_0 in Equation [14], or from the slope of weight loss versus reciprocal frequency in Fig. 3. In the first instance it is equal to

$$\frac{(\pi p_m)^{1/2}}{2} k_0$$

where $k_0 = 5.05 \times 10^{-6}$ (Equation [17]) and $p_m = 140{,}000$ psi. In the second instance, the rate constant is equal to

$$\frac{\text{slope}}{\sqrt{\frac{4L}{\pi p_m}} - \frac{4L}{\pi p_m}}$$

where the slope $= 1.26 \times 10^3$ mg min^{-1} or 21.0 mg sec^{-1} for 67,800 cycles, referring to a specimen having apparent contact area of 1.19 cm.^{2} After converting the value for k_0 and the slope to unit area, k/τ is calculated equal to 1.4×10^{-3} mg cm^{-2} sec^{-1} in the first instance, and 1.5×10^{-3} mg cm^{-2} sec^{-1} in the second instance. The two values are in satisfactory agreement with each other.

Precise data for the initial oxidation rate of a clean iron surface at room temperature have not been reported. Data for the rate extending over several days for hydrogen-reduced iron exposed to air at room temperature (20 C) have been presented in graphical form by Winterbottom (11) who employed an optical polarizing-light method. Tammann and Köster (5) reported data for polished specimens exposed several minutes above 250 C, using interference colors as a measure of oxide thickness. Both these data follow the equation

$$A = k \log_e \left(\frac{t}{\tau} + 1 \right)$$

where A is the thickness of the oxide film in Ångstrom units (10^{-8} cm) formed in t sec. On the basis of Winterbottom's data, k has the approximate value 3.3 Å, but τ varies with each of the three reported runs from 2.6 to 10.4 sec. For his experiment 26, data for which seem the most reliable of three runs, τ equals 2.6 sec and, therefore, k/τ is equal to 1.3 Å sec^{-1}. Tammann, whose values of τ are the same for all temperatures, reported an extrapolated value of k/τ at 15 C equal to 27,120 Å min^{-1} or 450 Å sec^{-1} for an equivalent air film. On the basis that Fe_3O_4 [index of refraction = 2.5 (reference 11) and density = 5.18] is the film substance as was assumed to be reasonable by Winterbottom, $k/\tau = 180$ Å sec^{-1}, or 6.7×10^{-3} mg Fe cm^{-2} sec^{-1} for Tammann's data, and the corresponding value for Winterbottom's data is 0.05×10^{-3} mg Fe cm^{-2} sec^{-1}. These two values are not in agreement with each other, making it more difficult to evaluate k/τ obtained from fretting data in terms of what might be expected. Since fretting action on one of two surfaces subject to relative slip occurs on the average half the time (compacted oxide slips on only one specimen surface) the calculated value of the reaction-rate constant from present fretting measurements should be multiplied by a factor in the order of 2, making the value approximately 2.9×10^{-3}. This value is roughly 0.4 of the Tammann value and 58 times the Winterbottom value.

The closer agreement with Tammann's value extrapolated from above room-temperature data suggests that a clean iron surface at room temperature oxidizes directly rather than first adsorbing gas which later reacts to oxide by mechanical activation. However, this conclusion is not certain, for one reason because of doubt introduced by the extrapolation and by some uncertainty concerning the absolute values of oxide thickness measured by the interference-color technique (21). If Winterbottom's value, which does not involve an extrapolation, is taken as correct, the lower value of k/τ compared with the fretting-data value supports the view that the mechanism of fretting actually involves gas adsorption rather than direct oxidation, since the former process is initially very rapid, as Langmuir (22) and Armbruster and Austin (12) reported. The premise is less likely that k/τ from fretting data exceeds the observed film-growth rate because of high surface temperatures of fretted specimens. This at first appears to be a distinct possibility, even if the temperatures achieved are not sufficient to produce the high-temperature oxide Fe_3O_4. But less observed fretting damage at high frequencies where interface temperatures are higher than at low frequencies is a strong argument opposing this assumption. The gas-adsorption mechanism, on the other hand, is in accord with the observed frequency effect and, furthermore, is given weight by the fact that the calculated amount of oxygen removed from the surface corresponding to the chemical factor of Equation [17] for each cycle of fretting action is less than a monolayer. The amount of iron oxidized through fretting at a load of 5300 psi is calculated as 2.7×10^{-5} mg cm^{-2} cycle^{-1} averaged over all the specimen surface, which corresponds to 1.2×10^{-5} mg oxygen cm^{-2} cycle^{-1} (assuming Fe_2O_3 as the reaction product). A close-packed monolayer of chemisorbed oxygen atoms of covalent radius 0.7 Å, on the other hand, is equivalent to 16×10^{-6} mg oxygen cm^{-2}.

It appears from these comparisons that the reaction-rate constant for iron calculated from fretting data is not an unreasonable value and, accordingly, the proposed model for fretting action is plausibly in line with the facts available so far. The proposed model and the present data do not provide support for Tomlinson's molecular-attrition theory. Oxidation of metallic particles after they are dislodged from the metal, for example, would not give rise to a frequency effect as is observed. Alternatively, the described model is in better agreement with the view of Fink and Hofmann that oxide forms on the metal surface as a result of relative slip. But the data do not indicate that formation of active chemical sites on the surface through mechanical disturbance of metal is a major condition of the fretting process, as the latter authors propose. The facts only support the view that fretting action is one of continuously removing chemical-reaction products from the metal surface, the amount of which depends mainly on time and load, combined with a purely mechanical wear factor resulting in metallic debris that forms in amount depending largely on load, slip, and number of cycles. The metallic debris, in turn, may oxidize further by secondary fretting action.

Remedial Measures

The foregoing mechanism of fretting corrosion suggests that remedial or control measures in order to be successful must depend on reduction of both the chemical and the mechanical wear factors. Excluding air from the metal interface, such as by use of special atmospheres, cements, or elastomer gaskets, will reduce the

[6] This possibility was suggested by W. E. Campbell.

chemical factor of fretting damage. The mechanical factor of fretting will persist, however, the importance of which depends on conditions under which slip occurs. But with rigid exclusion of air and other substances capable of reaction with the metal, the mechanical wear of metal also may be reduced, as our nitrogen data show. Any reduction of this kind occurs because of metal transfer in place of metal loss with formation of metallic-debris particles, the transfer being accompanied by severe cold-working of the surface metal. The factors influencing metal transfer have not yet been evaluated, other than the influence of air itself.

The proposed mechanism of fretting also suggests that interposition of a substance at the interface that can bond itself to the metal surfaces with greater strength than it is bonded to itself would reduce fretting damage. Unless the substance is metallic and a good thermal conductor, such a substance presumably must have good high-temperature characteristics because of the high local temperatures generated by friction in a poor conductor. By the same token, the internal coefficient of friction for the substance preferably should be low so as to reduce generation of heat. Perhaps molybdenum disulphide which has been shown to be beneficial (23) and is an effective high-temperature lubricant, approaches these requirements.

It has been suggested that one surface of the interface be made flexible through use of certain plastics or rubber. Fretting damage is minimized presumably by eliminating relative slip. Also, fretting debris possibly may be reduced by using a soft metal in combination with a hard metal. It would seem from the foregoing discussion that one should, in this instance, apply a load approaching the yield pressure p_m of the soft metal, since the space between asperities where oxidation occurs is thereby minimized. Should the debris particles become imbedded in the soft metal, they may, of course, continue to accelerate mechanical wear, but chemical wear will be reduced by the exclusion of air from a large fraction of the surface.

Acknowledgment

This investigation was made possible through support of the National Advisory Committee for Aeronautics on contracts NAw-5789 and NAw-6128.

BIBLIOGRAPHY

1 "Fretting Corrosion of Mild Steel in Air and in Nitrogen," by I-Ming Feng and H. H. Uhlig, published in this issue, pp. 395–400.

2 "Corrosion Handbook," edited by H. H. Uhlig, John Wiley and Sons, Inc., New York, N. Y., 1948, p. 27.

3 "The Friction and Lubrication of Solids," by F. P. Bowden and D. Tabor, Oxford University Press, New York, N. Y.; Clarendon Press, Oxford England, 1950.

4 "Metal Transfer and Wear," by I-Ming Feng, *Journal of Applied Physics*, vol. 23, 1952, pp. 1011–1019.

5 "Die Geschwindigkeit der Einwirkung von Sauerstoff, Schwefelwasserstoff und Halogenen auf Metalle," by G. Tammann and W. Köster, *Zeitschrift für Anorganische und Allgemeine Chemie*, vol. 123, 1922, pp. 196–224.

6 "A Laboratory Study of the Atmospheric Corrosion of Metals," by W. H. J. Vernon, Parts II and III, Trans. Faraday Society, vol. 31, 1935, pp. 1668–1700.

7 "Oxide Films on Iron," by R. F. Mehl and E. L. McCandless, Trans. American Institute of Mining and Metallurgical Engineers, vol. 125, 1937, pp. 531–559.

8 "The Direct Oxidation of Zinc," by W. H. J. Vernon, E. I. Akeroyd, and E. G. Stroud, *Journal of the Institute of Metals*, vol. 65, 1939, pp. 301–329.

9 "Low-Temperature Oxidation of Single Crystals of Copper," by B. Lustman and R. F. Mehl, Trans. American Institute of Mining and Metallurgical Engineers, vol. 143, 1941, pp. 246–271.

10 "The Rate of Oxidation of Copper at Room Temperature," by A. H. White and L. H. Germer, Trans. Electrochemical Society, vol. 81, 1942, pp. 305–319.

11 "Optical Studies of the Oxidation of Iron at Temperatures in the Range 20–265° C," by A. B. Winterbottom, *Journal of the Iron and Steel Institute*, vol. 165, 1950, pp. 9–22.

12 "The Adsorption of Oxygen at Low Temperature and Pressure on Smooth Iron," by M. H. Armbruster and J. B. Austin, *Journal of the American Chemical Society*, vol. 68, 1946, pp. 1347–1354.

13 Discussion Section of Reference (14).

14 "The Influence of Oxide Films on the Wear of Steels," by S. J. Rosenberg and L. Jordan, Trans. American Society for Metals, vol. 23, 1935, pp. 577–598.

15 "The Rusting of Steel Surfaces in Contact," by G. A. Tomlinson, Proceedings of the Royal Society of London, England, series A, vol. 115, 1927, pp. 472–483.

16 "Die Reiboxydation als Chemisch-Mechanischer Vorgang," by K. Dies, *Archiv für das Eisenhüttenwesen*, vol. 16, 1943, pp. 399–407.

17 "Temperaturerhöhung als Ursache der Reiboxydation," by M. Fink, *Stahl und Eisen*, vol. 52, 1932, p. 42.

18 "Investigation of Fretting Corrosion by Microscopic Observation," by D. Godfrey, NACA Tech. Note 2039, February, 1950.

19 "Zur Theorie der Reiboxydation," by M. Fink and U. Hofmann, *Archiv für das Eisenhüttenwesen*, vol. 6, 1932, pp. 161–164.

20 "An Investigation of Fretting Corrosion," by K. H. R. Wright, The Institution of Mechanical Engineers, Great Britain, preprint, February, 1953.

21 "Metallic Corrosion, Passivity and Protection," by U. R. Evans, Edward Arnold and Company, London, England, 1946, pp. 90–99; Longmans Green & Co., New York, N. Y., 1946.

22 "The Adsorption of Gases on Plane Surfaces of Glass, Mica, and Platinum," by I. Langmuir, *Journal of the American Chemical Society*, vol. 40, 1918, p. 1380.

23 "Effectiveness of Molybdenum Disulfide as a Fretting-Corrosion Inhibitor," by D. Godfrey and E. E. Bisson, NACA Tech. Note 2180, September, 1950.

Brief Notes*

On the recommendations of the Executive Committee of the ASME Applied Mechanics Division, it has been decided to initiate a section devoted to brief notes on technical matters in mechanics. These notes must not be longer than 750 words (about 2½ double-spaced typewritten pages, including figures) and will be subject to the usual review procedure prior to publication. After approval such notes will be published in the next issue of the Journal. The notes should be submitted to the Secretary of the ASME Applied Mechanics Division.

On the Signs in the Mathematical Expression of the Second Law of Thermodynamics

By S. J. KLINE,[1] STANFORD, CALIF.

THE purpose of this note is to give a proof demonstrating that in all of the mathematical statements of the "second law of thermodynamics" the equality sign applies uniquely to reversible processes and the inequality applies uniquely to irreversible processes. Since the complete proofs of the second law cannot be given in a short note, and since this discussion refers to these proofs, the presentation of Keenan[2] will be used as a basis throughout this note.

Conventional Proofs of Second Law

The conventional proofs of the second law and its corollaries start with a proof of Carnot's theorem (e.g., Keenan[3]) which is given as two theorems:

Theorem I. It is impossible to construct an engine to work between two heat reservoirs, each having a fixed and uniform temperature, which will exceed in efficiency a reversible engine working between the same reservoirs.

Theorem II. All reversible engines have the same efficiency when working between the same two reservoirs.

These two theorems are then used to give the proofs of the Clausius "inequality" and the "increase of entropy principle."

Theorems I and II deal with both equalities and inequalities. This is typical of statements of the second law of thermodynamics. In general, if two quantities are to be compared, one may be greater than, equal to, or less than, the other. In the case of the second law, one of the inequalities is impossible, the equality applies uniquely to reversible processes, and the remaining inequality applies uniquely to irreversible processes. The first part of this statement is well known but a complete proof of the last two parts does not appear to have been published.

In the case of Theorems I and II, for example, Theorem II is sufficient to show that only the equality sign can hold for a reversible process, and Theorem I rules out the possibility of creating any engine with an efficiency greater than that of a comparable reversible engine, but it does not rule out the possibility of constructing an irreversible engine with the same efficiency as the comparable reversible engine. A stronger theorem therefore is needed. The proof of such a theorem follows. It is deduced by combining statements of the first and second laws with the definition of an irreversible process. An irreversible process is here defined as: "A process in which all of the effects, in both the system and the surroundings, can never be completely undone."

Efficiency of an Irreversible Engine

Theorem III. The efficiency of any irreversible engine is less than that of any reversible engine working between the same reservoirs.

Proof: By Theorem I, the efficiency of the irreversible engine, η_I, cannot exceed that of the reversible engine, η_R; hence we need only prove that it cannot be equal.

Consider a system composed of an irreversible and a reversible engine operating between the same reservoirs as shown in Fig. 1.

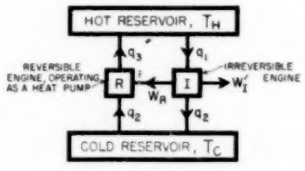

FIG. 1

Assume that the efficiencies of the two engines are equal. Turn the reversible engine around to become a heat pump. Run the engines through integer cycles in such a way that the heat rejected by the irreversible engine is equal to that absorbed by the reversible heat pump. For this process, the first law of thermodynamics applied to each engine yields

$$W_I = q_1 - q_2;\ W_R = q_3 - q_2 \quad \ldots\ldots\ldots\ldots [1]$$

and the efficiencies of the two engines, by definition are

$$\eta_I = \frac{q_1 - q_2}{q_1} = 1 - \frac{q_2}{q_1};\ \eta_R = \frac{q_3 - q_2}{q_3} = 1 - \frac{q_2}{q_3} \quad \ldots [2]$$

But by assumption $\eta_I = \eta_R$; hence Equations [2] yield $q_1 = q_3$. And from Equations [1] it follows that $W_I = W_R$, and W_I' is exactly zero. The net effect of these operations is therefore nothing, anywhere in the system or the surroundings; an irreversible process has been undone completely and all elements of the system and the surroundings have been restored to their original state. But this is a contradiction to the definition of an irreversible process given in the foregoing (for discussion see Bridgman[4]). Therefore Theorem III is proved.[5]

The use of Theorem III is sufficient to show that only the inequality sign can apply to irreversible processes in the inequality of Clausius and the principle of increase of entropy, as can be seen

[1] Assistant Professor of Mechanical Engineering, Stanford University. Mem. ASME.

[2] "Thermodynamics," by J. H. Keenan, John Wiley and Sons, Inc., New York, N. Y., 1941, pp. 73–90.

[3] Ibid., p. 73.

* Discussion of papers in Brief Notes should be addressed to the Secretary, ASME, 29 West 39th Street, New York, N. Y., and will be accepted until January 10, 1955, for publication at a later date. Discussion received after the closing date will be returned.

NOTE: Statements and opinions advanced in papers are to be understood as individual expressions of their authors and not those of the Society. Manuscript received by ASME Applied Mechanics Division, February 26, 1954.

[4] "The Nature of Thermodynamics," by P. W. Bridgman, Harvard University Press, Cambridge, Mass., second edition, 1943, p. 122.

[5] Keenan's definition of an irreversible process (see p. 69, reference 2) yields the same result but in a less straightforward manner.

readily by reference to the proofs by Keenan.[6] Or a line of argument, entirely parallel to that given here, can be applied directly to the inequality of Clausius with the same result.[7] Since the inequality of Clausius is the basis of the expression of the second law used for open systems (the control-volume expression), the same statement applies in that case.

[6] See Footnote 2, pp. 79 and 88.

[7] Such a proof has been given independently by Prof. F. O. Koenig, Chemistry Department, Stanford University, Stanford, Calif., but is unpublished.

Conclusion

We can therefore conclude that in every case the equality sign in the mathematical expressions of the second law of thermodynamics applies uniquely to reversible processes and that that inequality sign which is not impossible applies uniquely to irreversible processes. The proof given, when inserted into the normal derivations of the second-law corollaries, involves little extra work, and it not only strengthens the statements of the second law of thermodynamics but also provides a simpler interpretation in its many applications.

Discussion

Flexibility of Piping Systems Supported by Equally Spaced Rigid Hangers[1]

Rupen Eksergian[2] and F. L. Jackson.[3] This paper offers a useful approach to the analysis of multisupported pipe lines. The methods of the calculus of finite differences, particularly for linear differential equations, is a standard procedure in the calculation of symmetrically spaced discrete systems, such as distributed circuit elements, acoustic systems, and structural problems. It is intimately related in the expansion of a symmetrical determinant with constant diagonal rows. The author himself has cited previous applications to the problems of multisupported continuous beams. He deserves credit for extending this application to piping structures.

Table 1 of the paper shows the rapid convergence to a finite end slope with a given end moment, with only three supports back in a multisupported pipe. With given end moments, the moments and reactions damp down rapidly after a few span lengths which permits good approximations to be made by assuming only a few end-reaction supports and then using ordinary methods for solving.

In reviewing the author's analysis, it appears unnecessary to consider the added complication with overhanging "ears" and the several coefficients c, d, e, f, and g as listed in the nomenclature. Moreover, the m-bays shown in the author's Fig. 4 correspond, through symmetry, to an $n = 2m$ bay beam, shown in Fig. 3. Again, we note the very rapid convergence for m-bays with free and fixed ends, where $n = 2m$ in Table 1.

In the author's Equations [20] and [21], the M, Q, θ, and δ refer to the moment, shear, angular, and lateral deflections, respectively, at the end of the extended overhang length, and are not to be confused with the author's M, Q, and θ given in Equations [18] and [19] which apply at an end support.

The relations between these moments and deflections are shown in Fig. 1 of this discussion where we designate the end reactions as M_b, Q_b, and θ_b. The reactions (now internal) at the end supports, i.e., the author's M, Q, and θ, are designated as M_1, Q_1, and θ_1, respectively.

The moment at the end support is related to the external redundants M_b and Q_b

$$M_1 = M_b - bQ_b - \frac{wb^2}{2}$$

while the corresponding rotation is

$$\theta_1 = \frac{2aq_u}{EI}\left(M_1 + \frac{wa^2}{12}\right)$$

The relation between θ_b and δ_b and θ in terms of the end reactions M_b and Q_b at the end of overhang are

$$\theta_b = \theta_1 + \int_0^b \frac{M}{EI}\frac{\partial M}{\partial M_b}\,dx$$

$$\delta_b = b\theta - \int_0^b \frac{M}{EI}\frac{\partial M}{\partial Q_b}\,dx$$

which reduce to

$$EI\theta_b = [2aq_u + b]M_b - b\left[2aq_u + \frac{b}{2}\right]Q_b - w\left[b^2\left(aq_u + \frac{b}{6}\right) - \frac{a^2q_u}{6}\right]$$

$$EI\delta_b = b\left[2aq_u + \frac{b}{2}\right]M_b - b^2\left[2aq_u + \frac{b}{3}\right]Q_b - w\left[b^2\left(aq_u + \frac{b}{8}\right) - \frac{ba^2q_u}{6}\right]$$

These equations agree with the author's Equations [20] and [21].

Fig. 1 Relations Between Redundants Shown at Overhang and at First Support

Obviously, this procedure of connecting elements from one part to another becomes complicated, and offers no advantage unless additional (redundant) support reactions are encountered before reaching the terminal multiply supported end section.

In general, for coplanar pipe problems, we frequently encounter several combinations of multisupported pipes, connected to various types of configurations. The end deflections and moments of the multiple supported pipe can be considered as continuous

[1] By J. E. Brock, published in the March, 1954, issue of the Journal of Applied Mechanics, Trans. ASME, vol. 76, pp. 11–18.

[2] Consultant, Day & Zimmermann, Inc., Philadelphia, Pa.; Senior Staff Advisor, The Franklin Institute Labs. Fellow ASME.

[3] Chief Technical Service Engineer, Day & Zimmermann, Inc., Philadelphia, Pa. Assoc. Mem. ASME.

beams using the method of finite differences for arriving at the support moments and deflections.

Our procedure of analysis for combinations shown in the author's Fig. 7 is to divide the system into three parts, and equate the common deflections and rotations between parts I and III, and II and III at the outside end supports of the multi-supported pipes, respectively, which in turn connect to the common Z or U-bends. The choice of component systems should be directed to simplify the over-all analysis. There appears no advantage in increasing the component parts through the use of overhanging ears.

Fig. 2, herewith, shows a coplanar piping system divided into three systems. Systems I and II are continuous beam systems, joining system III, which is a form of any shape. For this system the origin of co-ordinates is at the outer end support reaction of system I. Thus the co-ordinates of the connection to system II, i.e., at the outer end support reaction of system II and relative to the origin of system III, are $x = L_3$ and $y = h$.

The displacements at the common connection of I and III are Δx_1, $\Delta y_1 = 0$, with the angular rotation θ_1. The displacements at the common connection of II and III are with the angular rotation θ_2. We will assume the moment reaction of system III on I to act in the direction of a positive increase of θ_1; likewise, the moment reaction of system III on II acts to increase θ_2. Q_1 and Q_2 act

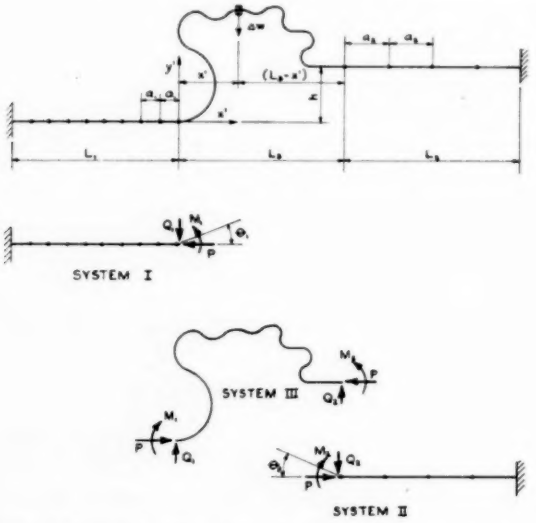

FIG. 2 DIMENSIONS AND NOTATIONS FOR GENERAL CONFIGURATION

downward on the respective outer end supports of systems I and II.

The reactions P, Q_1, and M_1 between I and III are chosen as the redundant reactions of the entire system. The reaction P, Q_2, and M_2 between II and III in terms of the redundants are

$$Q_2 = \Sigma\Delta w - Q_1$$

$$M_2 = M_1 + Q_1L_3 - Ph - \Sigma\Delta w(L_3 - x') \ldots\ldots [1]$$

The equations for the deflections in terms of the redundants, are as follows

System I

$$\theta_1 = \frac{c_1}{EI}\left(M_1 + \frac{wa_1^2}{12}\right); \quad \Delta x_1 - \alpha L_1 T = -\frac{PL_1}{EA} \ldots [2]$$

where $c_1 = 2a_1q_n$, and L_1 is the total length of system I, and T is the rise in temperature.

System II

$$\theta_2 = \frac{c_2}{EI}\left(M_2 + \frac{wa_2^2}{12}\right); \quad (\Delta x_2 + \alpha L_2 T) = \frac{PL_2}{EA} \ldots. [3]$$

where $c_2 = 2a_2q_n$ and L_2 is the total length of system II.

System III

$$\Sigma\int \frac{M}{EI}\frac{\partial M}{\partial M_1}\,ds = -\theta_1 - \theta_2 \ldots\ldots\ldots [4a]$$

$$\Sigma\int \frac{M}{EI}\frac{\partial M}{\partial P}\,ds = [(\Delta x_1 - \Delta x_2) + \alpha L_3 T + h\theta_2] \ldots [5a]$$

$$\Sigma\int \frac{M}{EI}\frac{\partial M}{\partial Q_1}\,ds = \alpha hT - L_3\theta_2 \ldots\ldots\ldots [6a]$$

Noting the origin is at the junction between I and II, with co-ordinates for system III as x and y, and noting all integral signs involve summations, i.e., $\Sigma\int yds \equiv (\int yds)$ then Equations [4a], [5a], and [6a] reduce to

$$M_1(\int ds)_{III} - P(\int yds)_{III} + Q_1(\int xds)_{III} - w(\int U_s ds)_{III} = -EI(\theta_1 + \theta_2) \ldots [4b]$$

$$-M_1(\int yds)_{III} + P(\int y^2 ds)_{III} - Q_1(\int xyds)_{III} + w(\int U_s yds)_{III} = EI[\Delta x_1 - \Delta x_2 + \alpha L_3 T + h\theta_2] \ldots [5b]$$

$$M_1(\int xds)_{III} - P(\int xyds)_{III} + Q_1(\int x^2 ds)_{III} - w(\int U_s xds)_{III} = EI(\alpha hT - L_3\theta_2) \ldots\ldots [6b]$$

where the weight coefficients are for the particular shape of system III. Other coefficients on the left side of the equation are the usual inertia shape coefficients determined by conventional methods for any shape such as system III.

Substituting for θ_1, θ_2, Δx_1, and Δx_2 from systems I and II in these equations, a solution is obtained for any general configuration as in Fig. 1. For example, choosing a typical shape such as the author's Fig. 7(a), the following general relations are obtained, omitting normal components such as $(PL)/(EA)$

$$M_1[(\int ds)_{III} + c_1 + c_2] - P[(\int yds)_{III} + c_2h] + Q_1[(\int xds)_{III} + c_2L_3] - w\overbrace{\left[(\int U_s ds)_{III} + c_2A'' - \frac{1}{12}(c_2a_2^2 + c_1a_1^2)\right]}^{A} = 0 \ldots\ldots [4c]$$

$$-M_1[(\int yds)_{III} + c_2h] + P[(\int y^2 ds) + c_2h^2] - Q_1[(\int xyds)_{III} + c_2hL_3] + w\overbrace{\left[(U_s yds)_{III} + c_2h\left(A'' - \frac{a_2^2}{12}\right)\right]}^{B} = \Delta xEI \ldots\ldots [5c]$$

$$M_1[(\int xds)_{III} + c_2L_3] - P[(\int xyds)_{III} + c_2hL_3] + Q_1[(\int x^2 ds)_{III} + c_2L_3^2] - w\overbrace{\left[(U_s xds)_{III} + c_2L_3\left(A'' - \frac{a_2^2}{12}\right)\right]}^{C} = \Delta yEI \ldots\ldots [6c]$$

where Δx now refers to the total expansion in the x-direction and Δy the total expansion in the y-direction.

It is important to note that in the foregoing equations the inertia coefficients are for the entire system. For example, with a conventional procedure the "equivalent" lengths c_1 and c_2 may

$\frac{\Sigma l_x'}{\Sigma l} = \frac{880.67}{60.926} = 14.455$ $\frac{\Sigma l_y'}{\Sigma l} = \frac{764.33}{60.926} = 12.545$

		l	x'	y'	$l_{x'}$	$l_{y'}$	$l_{x'y'}$	$l_{x'^2}$	$l_{y'^2}$	$l^3/12$	$l^3/12$
C_1	ab	3.463	–	–	–	–	–	–	–	–	–
	bc	6.	3	–	18	–	–	54	–	18	–
	cd	18	6	9	108	162	972	648	1458	–	486
	de	30	21	18	630	540	11340	13230	9720	2250	–
C_2	ef	3.463	36	18	124.67	62.33	2244.06	4488.12	1121.96	–	–
	Σ	60.926			880.67	764.33	14556	18420.12	12299.94	2268	486
								2268.00	486.00		
								20688.12	12785.94		

$I_{y'} = I_{y'} - \frac{(\Sigma l_{x'})^2}{\Sigma l} = 20688 - \frac{(880.67)^2}{60.926} = 7958.14$

$I_x = I_{x'} - \frac{(\Sigma l_{y'})^2}{\Sigma l} = 12785.94 - \frac{(764.33)^2}{60.926} = 3197.26$

$I_{xy} = I_{x'y'} - \frac{\Sigma l_{y'} \Sigma l_{x'}}{\Sigma l} = 14556 - \frac{880.67 \times 764.33}{60.926} = 3507.80$

$c_1 = c_2 = 2a_1 g_n = 3.463$

$B = \frac{\Sigma l_{x'}}{\Sigma l} A = [361341 - 12.544 \times 20231] = 107549$

$C = \frac{\Sigma l_{x'}}{\Sigma l} A = [569106 - 14.455 \times 20231] = 276684$

$\Delta_x EI = 1357983$ #/ft²

$\Delta_y EI = 226477$ #/ft²

$w = 25.37$ #/ft

P	Q_1	C	w	
+3197.26	-3507.8	-1357983	+ 107549	(1)
-1	+ 1,097127	+ 424.73	- 33.63	
	+ 7958.14	- 226477	- 276684	(2)
	- 3848.50	-1483880	+ 117994	
	+ 4109.64	- 1716357	- 158690	
	-1	+ 417.64	+ 38.61	

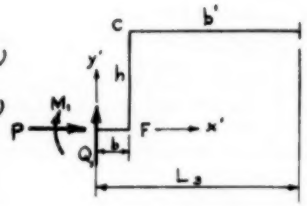

$M_1 = P\left(\frac{\Sigma l_{x'}}{\Sigma l}\right) - Q_1\left(\frac{\Sigma l_{x'}}{\Sigma l}\right) + w\left(\frac{A}{\Sigma l}\right)$

	INCLUDING WEIGHT	NEGLECTING WEIGHT
Q_1	1397 #	418 #
P	1104 #	883 #
M_1	25000 IN. #	60500 IN. #
M_2	120000 IN. #	90500 IN. #
M_3	-118,300 IN. #	-100200 IN. #

FIG. 3 AUTHOR'S EXAMPLE 2

be used to represent the effective lengths of systems I and II. The slope coefficients involving c_1 and c_2 are localized at the extremities of system III.

With this concept the foregoing equations may be restated as follows where the inertia coefficients now represent the entire system

$$M_1(\int ds) - P(\int yds) + Q_1(\int xds) - w(A) = 0 \ldots [4d]$$

$$-M_1[\int yds] + P[\int y^2 ds] - Q_1[\int xyds] + w(B) = EI\Delta x \ldots [5d]$$

$$M_1[\int xds] - P[xyds] + Q_1[\int x^2 ds] - w(C) = EI\Delta y \ldots [6d]$$

The distributed weight coefficients may be calculated for any particular system. For a Z-bend with square corners, the coefficients become, with notations as in Fig. 3 of this discussion

$$\left.\begin{aligned} A &= \left[\left(\frac{L_2^3}{6} + \frac{hL_2^2}{2} - hbb'\right) + c_2\left(\frac{L_2^2}{2} + hb'\right) - \frac{1}{12}(c_2a_2^3 + c_1a_1^3)\right] \\ B &= h\left[\left(\frac{L_2^3}{6} + \frac{hL_2^2}{2} - hbb' - \frac{hb^2}{4} - \frac{b^3}{6}\right) + c_2\left(\frac{L_2^2}{2} + hb' - \frac{a_2^2}{12}\right)\right] \\ C &= \left[\left(\frac{L_2^4}{8} + \frac{hL_2^3}{3} + \frac{2hb^3}{3} - \frac{hbL_2^2}{2}\right) + c_2L_2\left(\frac{L_2^2}{2} + hb' - \frac{a_2^2}{12}\right)\right] \end{aligned}\right\} \ldots [7]$$

$\frac{\Sigma l y'}{\Sigma l} = \frac{400}{40.77} = 9.81$

	l	y'	ly'	ly'^2	$I'/12$
C_1	5.77	0	0	0	-
	5	0	0	0	-
	20	10	200	4000	666.7
	10	20	200	2000	-
Σ	40.77		400	6000	
				666.7	
				6666.7	$= I_{x'}$

$w = 36.24$ #/ft.

$EI\Delta x = 14265046$ #ft^3

$I_x = I_{x'} - \frac{(\Sigma l y')^2}{\Sigma l} = 6666.7 - \frac{400^2}{40.77}$

$= 2742$

$\left[B' - \frac{\Sigma l y'}{\Sigma l} A'\right] = [71670 - 9.81 \times 5817]$

$= 14603$

$P = \frac{EI\Delta x}{2} \Big/ I_x + \frac{w}{I_x}\left[B' - \frac{\Sigma l y'}{\Sigma l} A'\right]$

$= 2601 + 193 = 2794$ #

$M_1 = P\left(\frac{\Sigma l y}{\Sigma l}\right) - w\left(\frac{A'}{2l}\right)$

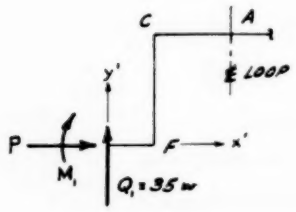

	WEIGHT COEFFICIENTS	
	NEGLECTED	INCLUDED
P	2601 #	2794 #
M_1	306200 IN.#	266900 IN.#
M_F	306200 IN.#	337500 IN.#
M_C	-318000 IN.#	-333000 IN.#
M_A	-318000 IN.#	-311300 IN.#

FIG. 4 AUTHOR'S EXAMPLE 1, CASES 3 AND 4

Equations [4d], [5d], and [6d] may be solved directly for P, Q, and M. A shorter solution is obtained by solving Equation [4d] for M and substituting in Equations [5d] and [6d]

$$P\left[\int y^2 ds - \frac{(\int y ds)^2}{\int ds}\right] - Q_1\left[\int xy ds - \frac{\int x ds \int y ds}{\int ds}\right] + w\left[B - A\frac{(\int y ds)}{\int ds}\right] = \Delta x EI \ldots\ldots [8]$$

$$-P\left[\int xy ds - \frac{(\int x ds)(\int y ds)}{\int ds}\right] + Q_1\left[\int x^2 ds - \frac{(\int x ds)^2}{\int ds}\right] - w\left[C - A\frac{(\int x ds)}{\int ds}\right] = \Delta y EI \ldots\ldots [9]$$

These coefficients may be calculated with any conventional procedure. Fig. 3 gives the solution for the author's example 2.

For the case of a U-bend, systems I, III, and II may be taken as previously, and the equations solved directly. With symmetry, however, some advantage may be obtained by choosing the redundants at the common plane of symmetry. On the other hand, we may consider system I and the symmetrical part of III, or system II and the symmetrical part of III. It is important to observe that Q_1 is not a redundant and only depends on the weight of the pipe. Using systems I and III, Equations [7], [8], and [9] become

$$P = \frac{EI\Delta x}{2\left[\int y^2 ds - \frac{(\int y ds)^2}{\int ds}\right]} + w\frac{\left[B' - A'\frac{\int y ds}{\int ds}\right]}{\left[\int y^2 ds - \frac{(\int y ds)^2}{\int ds}\right]} \ldots [10]$$

where B' and A' are the weight coefficients given previously, but modified by Q_1. Using this method, a solution of the author's example 1, cases 3 and 4, is given, Fig. 4, herewith.

By differentiating the denominator in Equation [10] with respect to the upper tangent of the loop, a criterion is obtained as to the best upper-tangent length for a given distance between the first two supports. For a given span a, and a given distance between the two supports on each side of the loop, the horizontal thrust becomes a minimum when the ratio of the length of the upper tangent is one half the sum of the distance between these two supports and the two equivalent lengths c_1 and c_2. For the author's example $c_1 = c_2 = 2aq_n = 5.774$ ft, and this ratio becomes

$$\frac{20}{30 + 11.55} \cong 0.48$$

which is a good choice.

In the author's analysis of the Z and U-bends emphasis is given to ascertaining whether contact with end supports under different expansion conditions is maintained. Our analysis of the Z-bend indicates that it is difficult to judge with small end moments toward the tapering end of a bending-moment diagram, whether a support contact is maintained.

The effect of the flexibility of the supports will considerably modify the author's analysis based on rigid supports. With flexible supports, the question of column stability of a long elastically supported pipe may be the criterion for allowable stress in the piping system. The advantage of cold-springing in improving positive support reactions should be emphasized.

A. R. C. MARKL.[4] A determination of the maximum stresses in a piping system, considering all the loadings which may be imposed upon it simultaneously, presents a problem of discouraging complexity. The loading always will include certain steady components, such as internal pressure and weight of pipe, contents and covering, upon which may be superimposed a diversity of variable loadings caused by thermal expansion, flow pulsation, wind, or earthquake effects. Neither is the piping system a simple structure; generally it is many times statically indeterminate, being restrained not only at terminal anchors or connections to pressure vessels or other equipment, but also by numerous intermediate supports and bracing members possessing load-deflection characteristics peculiar to their individual construction. In addition, piping components used for directional changes (elbows and bends), for branch take-offs (tees and laterals), and for separation into smaller units for ease of assembly and dismantlement (flanged connections, etc.) exhibit peculiar stress-strain behavior which further complicates the process of analyzing the system.

To cope with this problem, early analysts have introduced a number of simplifying assumptions which in time became accepted practice. Loadings other than thermal expansion have come to be ignored in the primary analysis and the system is usually idealized as a weightless line in space, with its freedom of

[4] Chief Research Engineer, Tube Turns, Louisville, Ky.

motion uninhibited by the supports provided. While, in principle, the use of time-saving simplifications is entirely proper for an engineering type of analysis, it has had the undesirable effect that piping-flexibility analysis has tended to degenerate to a ritual, the sense and meaning of which is often lost sight of; in other words, many of those making piping analyses today take little thought whether the customary assumptions are applicable to their specific problem and sometimes do not even realize that they are making assumptions.

In the writer's opinion, the prime merit of the present paper resides not so much in its brilliant mathematical development, but in the fact that it calls attention to the effect of one of the assumptions tacitly made in the majority of piping-flexibility calculations, which is, that the common forms of pipe support have relatively little influence on the evaluation of the expansion stress. While the author clearly demonstrates that this is not always the case, it is not to be inferred from this paper that all piping-flexibility calculations in future should include, at least approximately, the effects of nearby supports; the paper does, however, convey the lesson that the effect of simplifying assumptions should at least be mentally appraised in each instance.

Taking the expansion loop used for example 1 as an illustration, the average engineer probably would analyze this as a weightless system restrained at the two anchors only, as sketched in Fig. 11(*a*), whereas analysis as a guided loop in accordance with Fig. 11(*b*), with extraneous motions due to the straight lengths to each side is actually more nearly correct. In cases of this type it has been the writer's practice to recommend the installation of guides adjacent to the loop, even where this is located in a horizontal plane, if for no other reason than to retain control of the movement of the line.

As concerns the Z-bend used for example 2, a simple computation of the expansion of the vertical leg leads one to realize that the line will lift off support *A*, if this were to be in a fixed position; an experienced piping man will specify an ordinary spring hanger at this point if the amount of vertical expansion expected is moderate, a constant-load spring or a counterweight where a large movement is anticipated.

While this discussion has been directed primarily at indicating how the need for calculations of the type suggested by the author can be circumvented by the application of simple reasoning, it is in no way intended to detract from the merit of this development or to discourage the use of the method given. On the contrary, the writer's advice to all engaged in this field would be to make at least trial applications of the method to doubtful cases in order to build up their judgment as to when certain effects can be ignored with impunity and when they cannot, remembering in all cases that extreme mathematical accuracy is not required in this type of problem.

R. E. Newton.[5] The author is to be commended for a notable contribution to this important subject. Through an ingenious combination of conventional slope-deflection methods and analytic solutions of the difference equations he has made the solution of some highly redundant structural problems quite practical. The systematic fashion in which he has formulated his analysis makes it readily adaptable to a large variety of problems of this class. The extensive comparison of the effects of various simplifying assumptions given in example 1 will be particularly appreciated by engineers who frequently deal with problems of this kind.

The practicing engineer is of course interested in "exact" solutions. It is understandable, though, that he frequently has an even greater interest in simplifying assumptions that will yield sufficiently accurate results with appreciably less labor. Such assumptions can only be used with confidence after comparisons have been made with the results of more accurate methods in a number of representative problems. It is in this connection that the comparisons of example 1 and the detailed results of example 2 are particularly valuable. An examination of the solutions presented discloses that the large bending moments are confined to the expansion bend and the first adjacent span at either side of the bend. (When the pipe rises from the supports, the term "first adjacent span" is to be interpreted as that span between the first and second active supports.) Results also show that extreme bending moments at top and bottom of the risers are nearly equal in magnitude. These observations led the writer to conjecture that useful approximate results might be obtained by assuming the presence of hinges at the second (active) support to either side of the bend and also at mid-height of the riser (or risers).

Results have been worked out for two cases of example 2 of the paper. First of these is denoted as 2(*a*) and is based on the assumption that supports *A* and *B* (see Fig. 13 of the paper) are both active. Comparison with Brock's results is given in Table 1 of this discussion. For convenience the present method of analysis is denoted as the 3-hinge method. As may be seen, the agreement is quite close. Since the first active support reaction is negative a further trial is indicated. Using the results of the paper we skip directly to the final case in which the first active upper support is the one immediately to the right of *B*. It is seen (Case 2*b* of Table 1) that the values of horizontal thrust and bending moment at the top of the riser are still in close agreement. The fact that the reaction at the first active support is no longer in good agreement is of little practical importance. It should be noted that the results presented for the 3-hinge method were obtained on a 10-in. slide rule. Since the determination of this reaction involves the difference of two nearly equal quantities the tabulated value may be appreciably in error.

During the oral discussion of the paper a question was raised concerning the advisability of assuming the existence of a hinge at mid-height of the riser (or risers). Certainly the limited comparisons offered here are quite insufficient to warrant the use of this assumption in markedly different configurations. It is noted that the author's results show the actual displacement of the point of inflection from the mid-height of the 18-ft riser to be just 4 in. and 6 in. in cases 2(*a*) and 2(*b*), respectively. In example 1, case 1, of the paper this displacement is just 1.3 in. in 20 ft. If additional examples should show that this assumption is not generally tenable it could be abandoned with an attendant increase in the labor of the "simplified" method.

In conclusion the writer wishes again to commend the author for a genuine contribution to piping analysis. It is believed that the comparisons of this discussion justify the further investigation of the usefulness of the 3-hinge method with different choices of parameters and other configurations.

TABLE 1 COMPARISON OF RESULTS FOR EXAMPLE 2

Case	Method	Horizontal thrust, lb	Moment at top of riser (in-kips)	Reaction at first active upper support, lb
2(*a*).....	Brock	1740	−181	−2750
	3-hinge	1740	−188	−2620
2(*b*)	Brock	1020	−111	350
	3-hinge	1030	−107	60

Herbert Saunders.[6] The author has presented an elegant mathematical discussion of piping systems supported by hangers. This is one of the first attempts to solve analytically this complex

[5] Professor and Chairman, Department of Mechanical Engineering, U. S. Naval Postgraduate School, Monterey, Calif. Mem. ASME.

[6] Engineering Designer, Foster Wheeler Corporation, New York, N. Y. Mem. ASME.

problem. The writer has done a number of piping stress analyses but infrequently has had problems of such simple proportions or layout. The usual problems in practice are three-dimensional and may be multianchored layouts, resulting in much tedious calculation. The supporting steel is sometimes in such a position that equal distance between supports is impossible. The writer had occasion to solve a problem using Castigliano's method but this had only one intermediate support.

The author should be congratulated on his endeavors but much more analytical and experimental work is necessary for these types of problems which are quite prevalent in industry.

Author's Closure

The author first wishes to express his appreciation to the contributors of the preceding discussions for their kind interest and for the substantial additions their presentations make to the subject.

Dr. Eksergian and Mr. Jackson give a generalized development of the slope-deflection conjunction of a three-part configuration, the two extreme portions of which are equispan beams. They use Castigliano's Theorem to provide a generalized treatment of the center portion. The point of departure is their Equations [2] and [3] which are the same as the author's Equation [19]. The author's development is not so detailed as that they give and it does not make explicit use of energy methods. Actually, the data shown in Table 2 of the paper were obtained using a somewhat different point of view[7] but this does not affect the results.

Dr. Eksergian and Mr. Jackson question the reason for considering the "ears" as shown in Figs. 4 and 5 of the paper and are entirely correct in suggesting that it is not necessary to do so. However, one of the aims of the author's development was to make the analysis immediately applicable to practical problems without the necessity of further analytical treatment. By combining the configurations of Figs. 4 and 5 directly with those of Table 2 several interesting cases are treated at once. Of course, the ears could have been included with the "loops" in Table 2 rather than with the equispan beam, but the arrangement chosen appears to have greater adaptability.

In the first two paragraphs of his discussion, Mr. Markl concisely describes the difficulties of stress analyses in piping systems, indicates the necessity of introducing simplifying assumptions, and notes the resulting tendency to be uncritical of the applicability of the customary assumptions in particular cases. His remark that "piping-flexibility analysis has tended to degenerate to a ritual" is, unfortunately, all too true.

Mr. Markl correctly infers that it was not the author's purpose in this paper to suggest that all piping-flexibility calculations include the effect of nearby supports. To attempt to do so in general cases would simply mean that the results of the calculations would be delayed so long that they would not serve their purpose in design. (Of course the designer must, in all cases, make an approximate appraisal of the extent to which support constraints may modify the results and conclusions of a formal analysis which neglects the constraints.) The paper simply considers a class of configurations having a certain not unusual geometrical property in common and, because of the ready susceptibility of this class of problem to exact analysis, is able to obtain "exact" results with relatively little effort; this affords not only a simple exact approach to the analysis of actual configurations having the class property but also a means of getting an idea of the effect of similar constraints in configurations which cannot readily be analyzed.

As Mr. Markl suggests, practical piping-design considerations would indicate the use of appropriate guides in the systems of examples 1 and 2 and the use of spring hangers at the first one or two support points at the top of the riser in example 2. The examples were chosen, however, not to illustrate practical piping design details but instead simply to exhibit, as briefly as possible, applications of the theory developed in the paper.

Professor Newton's approach to this type of problem involves a clear-cut recognition of the rapidity with which bending moment attenuates with distance from a riser and the corresponding idealization of the configuration in a way which permits a ready analysis by conventional methods. The accuracy accompanying this idealization is much more than adequate. The labor of this analysis, although not inconsiderable, appears to be actually less than that involved in substituting in the author's formulas [39] through [58]. For the person familiar with slope-deflection type of analysis, the method suggested by Professor Newton is undoubtedly of advantage, and it appears to be applicable, possibly with modifications yet to be worked out and varying with the type of configuration, to more general systems than those considered in the paper. Simplifying idealizations must not only afford reasonable accuracy but must also signal peculiar behaviors of the configuration which might not invariably be anticipated (for example, rising off the supports in example 2 of the paper). Professor Newton's procedure seems capable of doing this, at least when applied to the general type of problem considered thus far. The approach is one which the author hopes to explore further.

Professor Newton has raised a question concerning the accuracy of his slide-rule calculations. For the sake of record, it may be noted that his results are very satisfactory. Corresponding to the six values for the three-hinge method given in Table 1 of his discussion, machine calculations give the following results: 1732,—187,—2560; 1034,—112, 52.

Mr. Saunders is, of course, quite correct in noting that the usual practical problem does not fall into the categories considered in the paper and that much more study is required before the designer can approach a typical problem with anything like peace of mind. Progress is made in steps and the present paper is only a preliminary step in an attempt to analyze piping systems in which hanger constraints are considered. Aside from the immediate applicability to the analysis of certain special but by no means unusual configurations, the analysis of the paper, or the alternate forms contributed in the discussion, provides some guide to idealizing a complicated configuration by properly recognizing how rapidly moment attenuates. If spans are unequal, an appropriately weighted "eye-average" may be used. The three-hinge approach of Professor Newton does not require any assumption of equal spans. There frequently are valid reasons for extending analytical procedures to cases where their applicability seems appropriate even though all hypotheses are not satisfied; however, the user should be aware of the difficulties and possible pitfalls involved in doing this.

[7] Cf. the author's papers "Matrix Analysis of Flexible Filaments." Proceedings of the First U. S. National Congress of Applied Mechanics, published by ASME, 1952, pp. 285–289, and "A Matrix Method for Flexibility Analysis of Piping Systems," *Journal of Applied Mechanics*, Trans. ASME, vol. 74, 1952, pp. 501–516.

The Wave Method for Solving Flexural Vibration Problems[1]

Julius Miklowitz.[2] It is important and interesting to note the author's treatment of the elementary bending equation by the Heaviside "wave method." The comparison of the normal-mode

[1] By R. P. N. Jones, published in the March, 1954, issue of the Journal of Applied Mechanics, Trans. ASME, vol. 76, pp. 75–80.

[2] Research Engineer, U. S. Naval Ordnance Test Station, Pasadena, Calif.

solution, "wave" solution, and experiment for the bending moment in a simply supported beam, subjected to a step transverse load at its mid-point, brings out quite clearly the advantage of using the wave solution for small times t in the problem treated.

The writer feels that some word of caution was needed in the paper concerning the more general use of the elementary bending equation in dynamic-loading problems. Regardless of the attack, modal analysis or the so-called wave method, it is well known that the physics of this equation restricts it from producing accurate solutions in problems where the short-wave lengths play a prominent role. The case of the simply supported beam in the paper, of course, is not seriously affected by short-wave effects since the l/d ratio is very large (576:1), and the loading, although abrupt, is of long duration. In problems involving short beams, impulsive loadings, or both, it is generally recognized that the Timoshenko bending theory, which includes the secondary effects of shear and rotatory inertia, yields more accurate transient solutions than the elementary bending theory. In problems of this type, times of much smaller magnitude than in the author's work become important.

In a present-day paper, concerned with waves in beams, it is surprising to find the author makes no mention of the role the Timoshenko theory plays in this subject. The recent literature has shown a particular interest in this theory from a standpoint of traveling-wave solutions. These physically realistic solutions, and associated characteristic velocities of propagation, cannot be derived from the elementary bending equation, which the author mentions.

Bending of Circular and Ring-Shaped Plates on an Elastic Foundation[1]

H. S. Gedizli.[2] Equation [10] of the paper is the same as Professor Klotter's Equation [80] presented in a recent publication.[3] This equation has been solved already by application of G. Kirchhoff's reduction method.[4] It also seems worth pointing out that an infinite plate on an elastic foundation, which is clamped at the circular boundary of a rigid disk with radius of length a, and a pure moment of magnitude L, is a special case which can be solved easily by reading a paper by the writer.[5] It is a simple problem but not the subject of a paper.

W. A. Nash.[6] The author has presented a very clear and concise development of a method for determining deflections and stresses in either a solid or annular circular plate supported on an elastic foundation of constant modulus. The solution of the homogeneous equation for deflections is presented in the form of Bessel functions of the first and second kind and with complex arguments. Following Kelvin's terminology, the author introduces the functions $\mathrm{ber}_n\rho$, $\mathrm{bei}_n\rho$, $\mathrm{ker}_n\rho$, and $\mathrm{kei}_n\rho$. It is true that these functions are tabulated for certain arguments.

In his study of the bending of a clamped circular plate loaded by a single concentrated force, the author finds the solution for the deflection surface in terms of sums of products of the foregoing functions. The writer would like to mention that tabulated values of most of the various combinations occurring in the solution (for certain arguments) are given in a paper by H. G. Savidge.[7] A few additional values are given in a paper by E. Reissner[8] Use of these tabulated values should render the author's solution even more valuable.

Author's Closure

The author would like to thank Professor Nash for his comments and express his appreciation for adding additional references of tabulations of those functions which are of importance in the application of the results of the paper under discussion.

As far as Mr. Gedizli's comments are concerned, the author finds them inaccurate. "Klotter's" Equation [80][3] is similar in appearance to Equation [10] of the author's paper but certainly not the same. The former arises in the theory of flexural vibrations of a thin plate, whereas the latter results from an analysis of the bending of thin plates on an elastic foundation. In addition, the comments of Mr. Gedizli tend to convey the erroneous impression that the author's paper dealt with a special case.[5] This was only one of two simple examples presented to illustrate the application of the general solution of the problem solved by the author, namely, the bending of circular and ring-shaped plates on an elastic foundation subjected to arbitrary loadings and very general boundary conditions.

---

[1] By H. Reismann, published in the March, 1954, issue of the Journal of Applied Mechanics, Trans. ASME, vol. 76, pp. 45–51.

[2] Address: Cebeci Guvey Sk. 16, Ankara, Turkey.

[3] "Neuere Festigkeitsprobleme des Ingenieurs," edited by K. Marguerre, Berlin, Germany, 1950, article by K. Klotter, p. 157.

[4] See author's reference (5), pp. 414–415; and reference (7), pp. 133–134, or reference (9), pp. 104–105.

[5] "Die Kreisplatte auf elastischer Unterlage unter einem an starrem Mittelstück angreifenden Moment," by H. S. Gedizli, *Ingenieur Archiv*, vol. 21, 1953, pp. 87–89.

[6] Associate Professor, Department of Engineering Mechanics, University of Florida, Gainesville, Fla. Mem. ASME.

[7] Report of the British Association for the Advancement of Science, 1916, pp. 109–141.

[8] "Stresses and Small Displacements of Shallow Spherical Shells, II," by E. Reissner, *Journal of Mathematics and Physics*, vol. 25, no. 4, 1947, pp. 279–300

Book Reviews

Heat Transfer

HEAT TRANSFER—A Symposium held during the summer of 1952 at the University of Michigan. University of Michigan Press, Ann Arbor, Mich., 1953. Cloth, 9 × 9 in., illus., $5.

REVIEWED BY NEWMAN A. HALL[1]

AMONG the various symposiums reported in basic fields of engineering in recent years, this will serve as one of the most useful as a general reference. While no common theme beyond that indicated by the title is apparent, each of the articles represents a well-organized critical review of the state of knowledge in the particular field covered.

The first two articles deal with the general area of thermal stresses. Alan S. Foust introduces the series with a review of conditions in heat-transfer problems which create high thermal stress. Following this, a comprehensive survey by S. S. Manson looks into most known aspects of the behavior of materials under conditions of thermal stress.

The next report by H. F. Poppendiek brings up to date the field of liquid-metal heat transfer. Also dealing with liquid heat transfer, particularly with reference to boiling of more usual fluids, is a report by Warren M. Rohsenow on heat transfer with evaporation.

The general field of convection heat transfer is covered in four papers. Martin Summerfield discusses the recent developments in convective heat transfer with special reference to high-temperature combustion chambers. In two papers E. R. G. Eckert discusses some aspects of boundary-layer behavior, first with respect to convective heat transfer at high velocities, and then the related problem of transpiration and film cooling. A somewhat more specialized discussion by Myron Tribus and John Klien considers forced convection from nonisothermal surfaces.

The program of investigation at the University of California in the transition region between continuous and free molecule flow is reported in two papers. First is given theoretical considerations in rarefied-gas dynamics, then a discussion on experimental methods and results in rarefied-gas dynamics.

The final paper by R. V. Churchill considers the comparison of temperatures in solid bodies and their scaled models.

Selected Combustion Problems

SELECTED COMBUSTION PROBLEMS: Fundamentals and Aeronautical Applications. Combustion Colloquium, Cambridge University, England, 1953. Butterworths Scientific Publications, London, England, 1954. 6 × 9¾ in., viii and 534 pp., figs.

REVIEWED BY A. J. NERAD[2]

THIS is a collection of papers from the Combustion Colloquium held at Cambridge University, Dec. 7 to 11, 1953. The papers are divided into four groups and give an excellent survey of their part of the field of combustion. In many places the unsolved problems are indicated and controversial points are discussed. Experimental and analytical approaches are both given ample treatment. The discussions at the end of each group of papers add considerably to the interest. To one looking for problems in the field of combustion, this book is strongly recommended.

The first group of seven papers on "Laminar Flame Propagation" leaves one with the feeling that the subject is exceedingly complex, e.g., J. W. Linnett, in his conclusion remarks, "However, our experimental knowledge of the composition distribution through any premixed flame is virtually nonexistent, etc." and Dorothy M. Simon, "There is no clear evidence that the diffusion of active particles controls either the process of flame propagation or the chemistry of flames in the oxidation of premixed gases. On the other hand, there is no clear evidence which contradicts the possibility that diffusion could be important in flame propagation."

The other three groups on "Turbulent Combustion, Solid and Liquid Propellants, and Technical Combustion Problems" are covered by twelve papers. These groups are so broad that even considering the very extensive bibliographies, one must realize that a somewhat limited and spotty covering of the subjects has been attained.

Because of the number and extent of survey papers this book is a valuable reference to much of this fast-growing field of combustion. It should be mentioned that four of the eighteen papers are in French.

Solid Mechanics

PROCEEDINGS OF THE FIRST MIDWESTERN CONFERENCE ON SOLID MECHANICS. Sponsored by the College of Engineering and the Panel on Fluid and Solid Mechanics of the University of Illinois, April, 1953, Urbana, Ill. The Experimental Station, Urbana, Ill., 1954. Paper, 8½ × 11 in., figs., references, 119 pp.

REVIEWED BY A. M. WAHL[3]

THIS volume comprises approximately 40 papers presented at the First Midwestern Conference on Solid Mechanics sponsored by the College of Engineering and Panel on Fluid and Solid Mechanics of the University of Illinois, Urbana, 1953. Most of these articles are concerned only with the mechanics of solids, particularly the fields of plasticity, elasticity, and vibration; however, a few papers, such as those on aeroelastic problems, also involve fluid mechanics.

Papers treating some aspect of plastic flow or inelastic action comprise the largest group presented at this Conference. Subjects in this field which will be of particular interest to stress analysts and designers include the following: Influence of axial loads on the collapse loads of frames; inelastic buckling of plates and columns; geometrical construction for plastic flow with work hardening; limit analysis of cylindrical shells under axially symmetric loading; impact effects in rods for material having a strain-rate effect; time lag in plastic deformation.

Papers dealing with elasticity include the following: Finite torsion of cylindrical shells; theory of the elastica; force at a point in a semi-infinite solid; numerical solution for notched bar in tension; thermal stresses in multiple-layer beams; circular slabs and plates on elastic foundations; torsional buckling of thin-walled columns.

Some of the papers of interest to vibration engineers are: Torsional vibration of a concentrated mass on a cantilever of

[1] Professor, Department of Mechanical Engineering, University of Minnesota, Minneapolis, Minn. Mem. ASME.

[2] General Electric Research Laboratory, Schenectady, N. Y. Mem. ASME.

[3] Advisory Engineer, Westinghouse Research Laboratories, East Pittsburgh, Pa. Fellow ASME.

rectangular tube cross section; application of integral equations to solution of beam-vibration problems; fundamental frequencies of rigid frames; forced vibrations with nonlinear restoring force; correlation of buckling and vibration of plates; problems in the dynamics of thin plates; rubber-resilient models under vibration conditions.

Summing up, this publication includes much material useful to stress analysts and designers as well as to those interested in the theoretical aspects of the mechanics of solids.

Machine Elements

DESIGN OF MACHINE ELEMENTS. By M. F. Spotts. Prentice-Hall, Inc., New York, N. Y., second edition, 1953. Cloth, 6 × 9 in., xiv and 504, illus., index. $9.65.

REVIEWED BY A. M. WAHL[4]

THIS second edition of Professor Spotts' well-known textbook on machine design (which first appeared in 1948) has been enlarged about 20 per cent both by adding new text material and by including more problems and numerical examples. Additions to the text include: Discussion of rational methods of determining working stresses under combined static and variable loading; data on wire useful in mechanical spring design; design methods for rubber springs; material for design of journal bearings with various bearing arcs. Besides this, the chapters on bevel, worm, and helical gears and on cams have been rewritten. The chapter on screws has been brought up to date by inclusion of data on the new Unified thread.

One feature of this book comprises the group of selected bibliographies which are given at the end of each chapter in order that students and others who desire more advanced information on any particular phase of machine design may know where to obtain it. In the second edition these bibliographies have been brought up to date by inclusion of additional references.

In a book of this nature, where it is necessary to cover so many subjects, all different, and yet all pertaining to the larger problem of machine design, the space limitations are very considerable. With this in mind, the reviewer feels that the author has succeeded very well in providing a maximum amount of useful information and that the book will be useful not only as a textbook but also in many cases to practical designers.

Some Basic Problems on the Mathematical Theory of Elasticity

SOME BASIC PROBLEMS OF THE MATHEMATICAL THEORY OF ELASTICITY. By N. I. Muskhelishvili. Third revised and augmented edition, Moscow, U.S.S.R., 1949. Translation from the Russian by J. R. M. Radok. P. Noordhoff Ltd., Groningen, Holland, 1953. Cloth, 6 × 9½ in., 704 pp., 66 figs., 38fl.

REVIEWED BY A. ALI KHEIRALLA[5]

ALTHOUGH the first Russian edition of this work appeared about twenty years ago, nothing comparable in scope has been published in English in the interim. The fundamental contribution of the text is a thorough exposition of the principles and applications of complex variable techniques to two-dimensional problems of the mathematical theory of elasticity. The methods have been largely developed by Soviet mathematicians, especially the members of the Tiflis Mathematical Institute of the Academy of Sciences of the Georgian S. S. R.

The text is divided into seven parts comprising a total of twenty-five chapters. Part 1 is a very lucid introduction to the fundamental equations and problems (first problem: given boundary stress, find displacements; second problem: given boundary displacements, find stresses) of the mechanics of an elastic body. Part 2 deals with the plane theory of elasticity. Here the complex representation of the solution of the equations of the plane theory of elasticity is introduced and the fundamental boundary-value problems are formulated for both simply and multiply connected regions. After a brief discussion of multivalued displacements and thermal stresses a chapter is devoted to the conformal mapping of the basic problems of plane theory. Mappings based on epitrochoidal and hypotrochoidal curves receive particular attention. The curvilinear co-ordinates associated with the conformal transformations are treated.

In Part 3 series methods are applied to regions with circular boundaries. The first and second fundamental problems for the circle and the first problem for the exterior of the circle are solved. Specific examples include the plate with circular hole under unidirectional tension and under biaxial tension, plate with circular hole under uniform pressure, concentrated force at a point (hole of zero radius) of an infinite plane, concentrated couple at a point of an infinite plane, infinite plates with elastic circular inclusions and with rigid circular inclusions. Chapter 10 is based on the solution of the first fundamental problem for the annulus. The tube under uniform internal and external pressures and the stress distribution in a rotating ring are discussed as examples. Multivalued displacements of annuli, bending of a curved beam and thermal stresses in a hollow circular cylinder end the chapter. Finally, the solution of noncircular problems by mapping onto regions bounded by circles is indicated.

Part 4 introduces the fundamental properties of Cauchy integrals (i.e., $\int_C \frac{f(w)dw}{w - z}$ which defines a holomorphic function of z except on the curve C) and presents the Plemelj formulas for their boundary values (as C is approached from one side or the other). The boundary values of holomorphic functions are then discussed and the problems characterized in terms of the properties of the Cauchy integrals.

In Part 5 the fundamental problems for a simply connected region are characterized by functional equations which are then reduced to Fredholm integral equations. In this way existence theorems for the solutions of the fundamental problems are established. Next, solutions and examples are given for regions mappable onto a circle by rational functions. Included are the circular disk under the influence of concentrated boundary forces and couples at internal points, rotating disk with attached discrete masses, plate with elliptic hole under uniaxial tension, both uniform and step pressure from hole, uniform tangential stress, various problems of plates with rigid elliptic inclusions and approximately polygonal holes. Chapter 16 deals with the solution of the fundamental problems for the half-plane and semi-infinite regions. Finally there is a chapter on the solution of boundary-value problems by integral-equation methods. The methods of S. G. Mikhlin, D. I. Sherman, G. Lauricella, and the author are discussed.

Part 6 introduces the (Riemann-Hilbert) problem of linear relationship: to find a meromorphic function F whose boundary values on the two sides of a curve C are related linearly, $F^+ = GF^- + f$, where G and f are functions given on C and G is not zero everywhere on C. It is shown how the fundamental problems for the half plane and cut plane may be obtained and the solution of the mixed fundamental problem is applied to several examples including the stamp problem with inclined, horizontal, or curved base with and without friction and the plane Hertz (contact) problem. Extensions to the cases of regions bounded by circles, infinite

[4] Advisory Engineer, Westinghouse Research Laboratories, East Pittsburgh, Pa. Fellow ASME.

[5] Lessells and Associates, Inc., Boston, Mass.

planes cut along circular arcs, and regions mappable onto the circle by rational functions are covered in two chapters.

The last four chapters of the book are devoted to problems of extension, torsion, and bending of homogeneous and compound bars. The classical results in the torsion problem of Saint Venant are presented together with the author's conformal-mapping methods and several different cross sections are treated as examples. The torsion of a circular cylinder reinforced by a longitudinal round bar of a different material is handled by mapping while that of a rectangular bar consisting of two different rectangular parts is solved by harmonic series. The two concluding chapters discuss the extension and bending of bars consisting of different materials with the same (chapter 24) and with different (chapter 25) Poisson's ratios.

The treatise not only contains much material new to that section of the Western scientific public not conversant with the Russian language but is also distinguished by its clear expository style in the presentation of classical theory. For this the translator as well as the author is to be congratulated. It can be enthusiastically recommended to all research workers in this field and it is to be hoped that it will find a place in U. S. universities as a text.

Collected Papers of Stephen P. Timoshenko

COLLECTED PAPERS. By Stephen P. Timoshenko. McGraw-Hill Book Co., Inc., New York, N. Y., 1954. Cloth, 6 × 9 in., xxv and 642 pp., illustrated, $15.

REVIEWED BY DANA YOUNG[6]

MECHANICS is one of the oldest of the physical sciences. A long line of distinguished physicists, mathematicians, and engineers has contributed to its development. In relatively recent times, historically speaking, applied mechanics has developed into a specialized field of study which is a vigorous part of modern engineering. The importance of the analytical methods of mechanics combined with laboratory experiments is widely accepted.

The success of the present renaissance in mechanics is due to the foresight and enthusiasm of a number of gifted engineers. Prominent among these is Stephen P. Timoshenko. Following his early engineering training in Russia, which was supplemented by advanced studies in Germany, he has devoted his life to teaching and research in applied mechanics. His first research publication appeared in a Bulletin of the Polytechnical Institute, St. Petersburg, in 1905. Since then, and continuing actively to the present, he has produced a remarkable list of papers and books dealing with many aspects of the mechanics of solids.

Professor Timoshenko's books are well-known classics in present-day engineering. They cover a wide range of subjects including Strength of Materials, Theory of Elasticity, Elastic Stability, Plates and Shells, Dynamics, Vibrations, and Structures. These are also the subjects in which Professor Timoshenko contributed so much in his own original research investigations. His basic scientific papers have been published in many different journals, some of which are not readily accessible. Now we are fortunate to have these papers collected together in one volume.

The volume contains 35 of Timoshenko's papers, arranged in chronological order and filling 642 pages. The first paper is "Einige Stabilitätsprobleme der Elastizitätstheorie," *Zeitschrift für Mathematik und Physik*, 1910. The last paper is "Stress Concentration and Fatigue Failures," Proceedings of The Institution of Mechanical Engineers, 1947. Eight of the papers are in German, two in French, and twenty-five in English. The author's early papers in Russian are not included directly. However, most of the material in his Russian papers is covered in the other papers; hence the volume contains virtually all of Timoshenko's basic contributions to mechanics.

In addition to the papers, the volume contains a fascinating and vivid biographical sketch of Professor Timoshenko. This was written by Donovan H. Young, a close friend and colleague of the author. There is also a spritely preface contributed by a group of his former students and colleagues.

Seven of the papers deal with important problems and methods in elastic stability. One of these, "Sur la Stabilité des Systèmes Elastiques" Annales des Ponts et Chaussées, 1913, is a virtual treatise, 133 pages in length. It is here that Timoshenko presented his versatile and powerful variational method for determining critical loads; a method which vitalized the field of elastic stability and provided solutions for many otherwise intractable problems. This paper illustrates Timoshenko's characteristic mode of presentation. After a brief and lucid statement of the principles, he proceeds to develop the details of the procedure by solving a comprehensive set of problems of increasing complexity. Specific results are obtained for many important cases in the buckling of bars, latticed struts, rings, thin plates, and in the lateral buckling of beams. The application of the results to practical design questions and the limitations of the formulas are thoroughly discussed.

In subsequent papers dealing with elastic stability, Timoshenko treats a number of more specialized problems such as the stability of stiffened plates, lateral buckling of curved bars, the stability of girder webs, and the buckling of thin-walled members.

Timoshenko's interest in vibration problems is shown by his papers in this field. In "Erzwungene Schwingungen Prismatischer Stäbe," *Zeitschrift für Mathematik und Physik*, 1911, he utilizes normal co-ordinates and Lagrange's equations to develop his powerful method for determining the behavior of bars subjected to forced vibrations. In a paper "On the Correction for Shear of the Differential Equation for Transverse Vibrations of Prismatic Bars," *Philosophical Magazine*, 1921, Timoshenko shows how the effect of the shear may be taken into account in investigating transverse vibrations and deduces the general equation of vibration. He gives an example to show that the correction for shear is several times greater than the correction for rotatory inertia. The general equation given in this paper is of great importance in vibration theory and is commonly called Timoshenko's equation. In other papers the author treats various problems including the impact of a mass on a beam, the vibration of bridges, and the vibration of an overhead trolley conductor.

In addition to his basic contribution in elastic stability and vibrations, Timoshenko has developed procedures for solving many other problems in the field of mechanics of solids. These are covered by papers which range over a wide variety of topics such as the application of trigonometric series to beam deflections, the torsion and bending of crankshafts, the bending of circular and rectangular plates, the effect of root restraint on the torsion of prismatic bars, the membrane analogy for flexure, stresses in a circular ring, bending of curved tubes, stresses in a plate with a circular hole, approximate least-work solutions for two dimensional problems in elasticity, analysis of bimetal thermostats, dynamical stresses in rails, stress concentration produced by fillets and holes, theory of suspension bridges, and the theory of thin-walled members of open cross section. The papers on suspension bridges (36 pages) and thin-walled members (51 pages) are comprehensive treatises which cover thoroughly the analytical theory in each case.

All of the papers are written in Timoshenko's characteristic

[6] Chairman, Department of Civil Engineering, Yale University, New Haven, Conn. Mem. ASME.

style and follow the same plan of presentation which he uses so successfully in his lectures. He emphasizes the physical meaning of the solutions and the practical applications. Results are carried through to numerical examples. He begins with simple particular cases, gradually introduces more complicated examples, and then the generalizations. He demonstrates very effectively the power of mathematical analysis in solving engineering problems without any unnecessary excursions into mathematical generalities.

Reading Timoshenko's papers is as stimulating as listening to him lecture. You catch his contagious enthusiasm for his beloved field of applied mechanics. Your interest is aroused by his fresh and fertile point of view. You see mathematics and engineering welded together in a friendly union. His clear and free-flowing presentation sometimes hides the greatness of his contributions.

The material in the papers is as fresh and relevant today as when written. But the volume is more than a collection of research reports. Taken together, the papers represent a philosophy and a method of attack that have inspired many others to follow along the trail which Timoshenko has blazed.

Technische Dynamik

Technische Dynamik. By C. B. Biezeno and R. Grammel. Springer-Verlag, Berlin, Göttingen, Heidelberg, Germany. Second edition, 1953, in two volumes. Volume 1, XII + 700 pp., 413 figs., and two appendixes; volume 2, VIII + 452 pp., 315 figs., and three appendixes.

Reviewed by I. Malkin[7]

THE somewhat unconventional title is explained by the authors in the preface: In line with Kirchhoff's classical definitions they generally call dynamics the part of mechanics which deals with the problem of the action of forces on mechanical systems, in particular on elastic systems, both in statical conditions and in the state of motion. The manner in which they cover this vast field is unconventional, too, and indeed unconventional in the best sense of the word. They break with certain traditions in a way which cannot fail to attract readers and to evoke their appreciation and which deserves emulation by writers of technical text and handbooks. Let us start, however, with a short outline of the contents of the set.

Each of the two volumes consists of two large parts, subdivided into chapters, sections, and divisions, which make the reading and the study of the books easier and more attractive. Part 1 of volume 1 treats of the fundamentals of the three and two-dimensional theory of elasticity, as well as of the analytical and experimental methods of solution of the elastic problem, including not only such advances as Galerkin's improvements of Ritz's method, but also the most modern numerical methods like Southwell's relaxation method. Part 2 of volume 1 deals with details of machines, like rods and shafts, springs, rings and wheels, and of plates and shells, and concludes with a presentation of the problem of buckling and of similar cases of nonstability. Part 1 of volume 2 treats of problems occurring in the design of steam turbines, namely, of stress distribution and of vibrations of various kinds in steam-turbine disks and of corresponding problems in steam-turbine blades, and finally of the critical speeds of steam-turbine shafts. Part 2 of volume 2 discusses the problems of mass balancing and energy regulation, and of the torsional vibrations of the shaft, in engines with reciprocating masses.

This mere enunciation of the chapters gives a certain idea of the scope of the contents but it does not tell much about the particular features of the volumes. In the case of a voluminous work like the one under review, the task just implied can and must be confined to such parts which have given the authors opportunity to manifest some originality of presentation. For a closer discussion we concentrate on the part of the second volume which treats of the stress distribution and bending vibrations in rotating disks. This discussion will give us a clear picture of the characteristic merits of the "Technische Dynamik." A similarly original part of the first volume will be reviewed in a more general manner.

The stress analysis can be carried out, in the case of a turbine disk of any profile, by means of the well-known (1) graphical method of Grammel. The main analytical solutions are the disks of (2) constant thickness, (3) constant strength, (4) hyperbolical, (5) conical, and (6) exponential profiles. All solutions (1) to (6) are clearly and elaborately discussed on pp. 11–29 of the second volume. Since the disks (2) and (3) are of very limited practical use, the choice of an analytical solution is restricted to (4) to (6), of which (4) again is for well-known reasons the most unfavorable one. The discussion given in the book offers the reader the possibility of judging for himself about the merits and demerits of any of the indicated solutions on the basis of concisely, but adequately, drawn characteristics. This is a fortunate deviation from a remarkable tradition, according to which all other texts prefer to give the reader a detailed presentation of the solutions (2) to (4), as far as analytical solutions are concerned, mostly without even mentioning the solution (5) and regularly ignoring solution (6), notwithstanding the fact that its very considerable practical advantages have been more than once emphasized in the Journal of Applied Mechanics and elsewhere.

The stress problem is followed by an admirable presentation of the problem of vibrations both in the disk plane and normally to it, of which the latter is "one of the most important problems in the entire field of mechanical engineering" (R. Grammel in "Neuere Festigkeitsprobleme des Ingenieurs," edited by K. Marguerre, Springer-Verlag, 1950, p. 186). On the one hand, the problem of practical determination of vibration frequencies is given a reliable foundation by explicit connection, in each particular kind of vibration, with the requirements of the Hamiltonian Principle, and on the other hand, the numerical procedure of carrying out the Rayleigh method is considerably improved by a new device, which permits determination of the influence of the profile on the vibration form (the influence of very long blades on vibration form and frequency is, however, not considered; cf. Journal of Applied Mechanics, 1946, pp. 245–246).[8] Another nonconventional item is the treatment of the influence of the centrifugal forces on the frequency of bending vibrations. The computation given in textbooks disregards the influence of the hoop stresses (see the reviewer's article in the *Schweizerische Bauzeitung* of February 15, 1936). Technische Dynamik, pp. 74–76, gives a detailed computation of the latter influence, thus correcting the error. Particular mention is deserving the detailed discussion of the transformation of the Rayleigh method into a method of successive approximations with possibilities of estimating the error incurred in Rayleigh's method (pp. 87–92). In all of these questions the presentation goes far beyond the routine and gives the reader valuable information both of a theoretical and purely practical nature, which is rather difficult or even impossible to find in other publications. Theoretical and practical sections can be read independently of each other, something which will be enjoyed by many readers.

A similarly important part of volume 1, pp. 438–561, deals with

[7] Standards and Design Engineer, Foster Wheeler Corporation, New York, N. Y.

[8] The reviewer is in a position to state that at the earliest appropriate opportunity Professor Grammel will express his approval of the conclusions arrived at by the reviewer in the reference given on p. 246 (footnote) of the Journal of Applied Mechanics of 1946.

plates and shells. Of course, only certain particular problems of this vast domain are discussed there but the studies again go far beyond the limiting lines reached in other texts on applied elasticity. An extensive and thorough study is given to the problem of the plate loaded by forces in its own plane (pp. 439–481), including the problem of plates with circular holes. The research work and the results reported there are of great interest by themselves; however, the entire section is very valuable as a preparation for the study of the still more specialized and mathematically more complicated work of the Russian mathematician, N. I. Muskhelishvili, and his pupils. The case of a plate reinforced by ribs (pp. 497–502) deserves attention in the section dealing with the plate in bending. The most important feature in the presentation of the theory of shells is the problem of the cylindrical shell of circular cross section under any load distribution and the contributions of C. B. Biezeno and J. J. Koch to the solution of this problem (pp. 518–551), as, for instance, the discussion of the case of a cylindrical shell reinforced by equidistant circular rings. On each of the subjects indicated the reader will find an abundance of practically important information, exactly as in volume 2 discussed above.

It is hardly necessary to add anything to round up the characteristics of this outstanding two-volume set. This reviewer feels fully justified in concluding with the remark that no engineer, interested in applied elasticity, can afford not to have the set in his library.

Strength and Resistance of Metals

STRENGTH AND RESISTANCE OF METALS. By John M. Lessells. John Wiley & Sons, Inc., New York, N. Y.; Chapman & Hall, Ltd., London, England, 1954. Cloth, 6 × 9 in., xiv and 450 pp., 220 illus., $10.

REVIEWED BY T. J. DOLAN[9]

THE principal purpose intended for this volume on the strength of metals was to provide advanced undergraduate and graduate students, as well as design engineers, with factual information and rational knowledge of the behavior of metals under stress. The text is liberally dispersed with references to the major source material from which the conditions and behavior patterns have been summarized by the author. Many readers will find some of these old in years, but the author has selected with care to include outstanding contributions rather than the latest references in each portion of the subject matter. The majority of the discussions center upon the behavior of steel as the primary metal used in engineering products, though mention is made of nonferrous alloys and cast iron under conditions for which their behavior is markedly different from that of steel. In expressing formulas for comparing stresses and strains with mechanical behavior, the author has limited the discussions to simple formulas in mechanics. The principal concepts are those of the observed material behavior rather than the hypothetical or analytical approach.

Particular emphasis is placed upon the subject of fatigue in metals, to which the author attributes the majority of failures of engineering components, though other types of failure such as creep and fracture at elevated temperatures, and brittle fracture at low temperature are also given due attention.

The first two chapters cover the tensile test not only as an acceptance criterion but also discuss the newer concepts of "true" stress-strain characteristics, effect of testing speed, and significance of the data to designers. The effects of overstrain, cold-working, hysteresis, and residual stresses on metals are appraised in detail. Chapter 3 covers both short-time and long-time high-temperature tests and the utilization of creep data in engineering design. Chapter 4 outlines the various types of hardness measuring equipment and its importance as an inspection tool. Chapter 5 covers the behavior of metals under impact loading with single-blow and repeated-blow tests and the development of brittle fracture below the transition temperature range. Chapters 6, 7, and 8 discuss the numerous controlling factors influencing the fatigue strength of metals such as specimen geometry, environment, types of stressing action, and range of stress. Fractures and failure phenomena are described in detail.

Chapter 9 develops the concepts of strain hysteresis and damping capacity, and chapter 10 covers the general features and nature of mechanical wear, surface fatigue, and the significance of wear testing methods. Chapter 11 includes a brief summary of the theories of strength from the viewpoint of the state of stress producing inelastic deformation and the corresponding allowable working stresses (with factors governing their selection) for various conditions met in service. Several tables of typical mechanical properties of commonly used structural materials are included as a guide in selecting working stresses. Numerous problems on all phases of the subject are placed at the end of the book for use by students.

The author has done a commendable job in attempting to summarize the state of knowledge of material behavior to enable the designer to dispense with empirical formulas and employ rational methods. The author has been careful to point out the significance to the engineer and methods of utilization of the various mechanical properties obtained from laboratory investigations. The specialist in the field may be disappointed at not finding exact methods for solution of the more complex problems such as cumulative damage in fatigue, or for creep under combined stress, and so on. In many instances for which the knowledge of material behavior is not exact, one must still rely upon a combination of theory and experiment for most reliable and economical design. The advanced engineering student or the young engineer will find the book well adapted to bringing him up to date on the facts known about the mechanical strength properties of metals.

[9] Head, Department of Theoretical and Applied Mechanics, University of Illinois, Urbana, Ill. Mem. ASME.

Third U. S. National Congress of Applied Mechanics
Preliminary Announcement

The Third U. S. National Congress of Applied Mechanics will be held at Brown University, Providence, Rhode Island, during June 11–14, 1958. It is hoped that the scheduling of conflicting meetings can be avoided by this early announcement of the date chosen for the Congress. Further announcements concerning the preparation of papers will be made as the Congress draws nearer.

Inquiries regarding the Congress should be addressed to one of the following members of the Organizing Committee at Brown University, Providence, R. I.:

Professor D. C. Drucker, *Secretary*
Professor E. H. Lee, *Treasurer*
Professor W. Prager, *Chairman*

RESOLUTION CHART

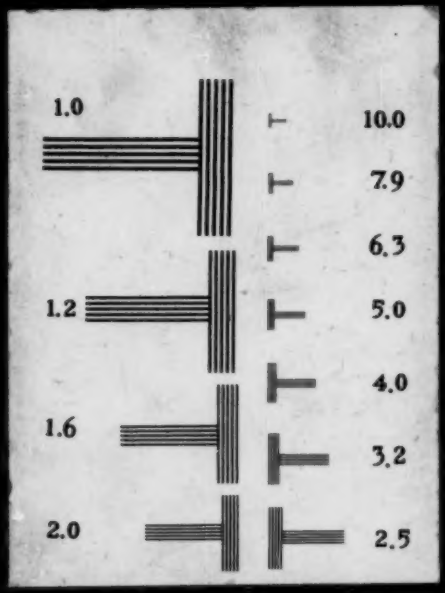

100 MILLIMETERS

INSTRUCTIONS Resolution is expressed in terms of the lines per millimeter recorded by a particular film under specified conditions. Numerals in chart indicate the number of lines per millimeter in adjacent "T-shaped" groupings.

In microfilming, it is necessary to determine the reduction ratio and multiply the number of lines in the chart by this value to find the number of lines recorded by the film. As an aid in determining the reduction ratio, the line above is 100 millimeters in length. Measuring this line in the film image and dividing the length into 100 gives the reduction ratio. Example: the line is 20 mm. long in the film image, and $100/20 = 5$.

Examine "T-shaped" line groupings in the film with microscope, and note the number adjacent to finest lines recorded sharply and distinctly. Multiply this number by the reduction factor to obtain resolving power in lines per millimeter. Example: 7.9 group of lines is clearly recorded while lines in the 10.0 group are not distinctly separated. Reduction ratio is 5, and $7.9 \times 5 = 39.5$ lines per millimeter recorded satisfactorily. $10.0 \times 5 = 50$ lines per millimeter which are not recorded satisfactorily. Under the particular conditions, maximum resolution is between 39.5 and 50 lines per millimeter.

Resolution, as measured on the film, is a test of the entire photographic system, including lens, exposure, processing, and other factors. These rarely utilize maximum resolution of the film. Vibrations during exposure, lack of critical focus, and exposures yielding very dense negatives are to be avoided.